UNIVERSITY OF CALIFORNIA

Santa Barbara

Delivery and activity of toxic effector domains from contact-dependent growth inhibition systems in *Escherichia coli*

A dissertation submitted in partial satisfaction of the

requirements for the degree Doctor of Philosophy

in Molecular, Cellular, and Developmental Biology

by

Julia Laura Elizabeth Willett

Committee in charge:

Professor Christopher S. Hayes, Chair

Professor Anthony de Tomaso

Professor David Low

Professor Denise Montell

June 2016

The dissertation of Julia Laura Elizabeth Willett is approved.

_____

Anthony de Tomaso

_____

David Low

_____

Denise Montell

_____

Christopher S. Hayes, Committee Chair

February 2016

Delivery and activity of toxic effector domains from contact-dependent growth inhibition systems in *Escherichia coli*

by

Julia Laura Elizabeth Willett

To Jason

ACKNOWLEDGEMENTS

I would first and foremost like to thank Chris for being a great advisor and for allowing me to investigate a variety of engrossing research questions throughout my graduate work in his lab. I'm appreciative of all the opportunities that I have had to grow as a scientist and writer, present my research at conferences, and interact with incredible seminar speakers and colleagues. His enthusiasm for science and research is contagious.

A number of collaborations made this work possible. I'm extremely grateful for our close (both literally and figuratively) collaboration with David Low and his research group, particularly former members Stephanie Aoki, Sanna Koskiniemi, Travis Smith, and Julia Webb. David is a tremendous scientist with whom scientific conversations are always inspiring. I am also grateful for our collaboration with Robert Morse and Celia Goulding at UC Irvine, as their crystallography expertise has provided invaluable insight into the structural world of CDI. Beatrice Ramm and Drew Endy at Stanford University provided an opportunity to work on a fun synthetic biology project well outside my microbiology comfort zone and created some really incredible videos of CDI, visualizing a process I'd been imagining for years.

Additionally, I would like to thank all past and present members of the Hayes lab – I can truthfully say I've learned something from each and every person I've worked with throughout graduate school. It's difficult to imagine these years without this camaraderie and our…shenanigans. Extra thanks goes to Fernando Garza-Sanchez for the insightful discussions, advice, and cookies. I'd also like to thank Alex Fields for making late nights spent working on the 3rd floor a little livelier.

My family and friends have been a great source of support throughout graduate school, and I'm thankful I was able to experience the eternal paradise that is Santa Barbara with such a wonderful group of people. I would especially like to thank my parents and brother for their never-ending love and encouragement and for turning everything into a teaching moment along the way. To Jason…any sentiments I could craft about reassurance, inspiration, and support would be inadequate and trite. I love you.

Last but most certainly not least, a tremendous *thank you* to my forever first years. We didn't come here to make friends, but I'd say we did a hell of a job at it. I look forward to your future coups d'état and the letters that are sure to follow.

VITA OF JULIA LAURA ELIZABETH WILLETT
February 2016

EDUCATION

PhD **Molecular, Cellular, and Developmental Biology** Exp. 2016
University of California, Santa Barbara, Santa Barbara, CA

BS **Biochemistry** 2010
University of Illinois at Urbana-Champaign, Urbana, IL
Minor in Chemistry
Distinction in the Major

BS **Food Science and Human Nutrition** 2010
University of Illinois at Urbana-Champaign, Urbana, IL
Honors in the Major

RESEARCH EXPERIENCE

Graduate Student Researcher 2010-2016
Department of Molecular, Cellular, and Developmental Biology
University of California, Santa Barbara
Advisor: Dr. Christopher S. Hayes (christopher.hayes@lifesci.ucsb.edu)

- Used genetic approaches to identify translocation pathways utilized by toxins in contact-dependent growth inhibition (CDI) systems.
- Characterized activities of nuclease and pore-forming CDI toxins from Gram-negative bacteria.
- Analyzed phenotypic responses induced by delivery and activity of CDI toxins.

Undergraduate Researcher 2008-2010
Department of Chemistry
University of Illinois at Urbana-Champaign
Advisor Dr. Yi Lu (yi-lu@illinois.edu)

- Use aptamer-based approaches to build liquid-state DNA sensors for detection of metals in complex paint and water samples.
- Developed a chelation-based approach for reducing iron interference in lead paint sensor readings.

Undergraduate Researcher 2007-2008
Department of Food Science & Human Nutrition
University of Illinois at Urbana-Champaign
Advisor Dr. Michael J. Miller (mille216@illinois.edu)

- Bioinformatic analysis of carbohydrate transporters in 11 *Lactobacillus* genomes.

TEACHING EXPERIENCE

University of California, Santa Barbara
Microbiology Laboratory Teaching Assistant 2015

- Taught two sections of the senior-level microbiology lab course
- Developed two research-based modules to integrate laboratory research and classroom learning.

Introductory Biology Laboratory Teaching Assistant 2011, 2012

- Taught weekly laboratory sections and graded assignments.
- Covered general biology concepts including marine biology, ecology, phylogenetics, computational ecology, plant and human physiology, and evolution.
- Supervised student-led experimental design projects.

University of Illinois at Urbana-Champaign
General Chemistry II Teaching Assistant 2008-2009

- Taught twice-weekly discussion sections for undergraduates in general chemistry.
- Topics included kinetics, electrochemistry, and introductory organic chemistry.
- Recognized on the "List of Teachers Recognized as Excellent" and ranked in the top 10% of chemistry teaching assistants during the Fall 2009 semester.

INDUSTRIAL EXPERIENCE

Research and Development Intern 2010
ANDalyze, Champaign, IL

- Adapted liquid-state DNA sensors for heavy metals to shelf-stable solid-state products for commercial applications.

PUBLICATIONS

1. Morse RP, **Willett JLE**, Johnson PM, Zheng M, Credali A, Iniguez A, Nowick JS, Hayes CS, Goulding CW. Diversification of β-augmentation interactions between CDI toxin/immunity proteins. *Journal of Molecular Biology*. 2015 Nov 20;427(23):3766-84. http://dx.doi.org/10.1016/j.jmb.2015.09.020.

2. **Willett JLE**, Ruhe ZC, Goulding CW, Low DA, Hayes CS. Contact-Dependent Growth Inhibition (CDI) and CdiB/CdiA Two-Partner Secretion Proteins. *Journal of Molecular Biology*. 2015 Nov 20;427(23):3754-65. http://dx.doi.org/10.1016/j.jmb.2015.09.010. Review.

3. **Willett JLE***, Gucinski GC*, Fatherree JP, Low DA, Hayes CS. Contact-dependent growth inhibition toxins exploit multiple independent cell-entry pathways. *Proceedings of the National Academy of Sciences USA*. 2015 Sep 8;112(36):11341-6. http://dx.doi.org/10.1073/pnas.1512124112. **indicates equal contribution*
    - Highlighted in *Nature Reviews Microbiology* (http://www.nature.com/nrmicro/journal/v13/n10/full/nrmicro3554.html)

4. Webb JS, Nikolakakis KC, **Willett JLE**, Aoki SK, Hayes CS, Low DA. Delivery of CdiA nuclease toxins into target cells during contact-dependent growth inhibition. *PLoS One*. 2013;8(2):e57609. http://dx.doi.org/10.1371/journal.pone.0057609.

5. Morse RP*, Nikolakakis KC*, **Willett JLE**, Gerrick E, Low DA, Hayes CS, Goulding CW. Structural basis of toxicity and immunity in contact-dependent growth inhibition (CDI) systems. *Proceedings of the National Academy of Sciences USA*. 2012 Dec 26;109(52):21480-5. http://dx.doi.org/10.1073/pnas.1216238110. **indicates equal contribution*

HONORS AND AWARDS

Graduate

2015	Doreen J. Putrah Cancer Research Foundation Conference Fellowship
2015	Best 5th year graduate student talk, MCDB Graduate Seminar Series
2015	1st place, MCDB Department Poster Competition
2014	Ellen Schamberg Burley Graduate Travel Scholarship
2013	Best 3rd year graduate student talk, MCDB Graduate Seminar Series
2012-2015	National Science Foundation Graduate Research Fellowship
2011	Charles A. Storke Award for excellence in graduate coursework

Undergraduate

2010	William H. Jackson Merit Award for outstanding thesis in Biochemistry
2009	University of Illinois List of Teachers Recognized as Excellent
2009	Top 10% of Chemistry Teaching Assistants
2009	2nd place, LIGASE Biology Poster Competition
2007	Mansperger Scholar
2005-2008	James Scholar
2005-2008	Jonathan Baldwin Turner Agriculture Scholar
2005	Chancellor's Scholar (top 5% of incoming class)

ORAL PRESENTATIONS

1. **Willett JLE**, Jones AM, Gucinski GC, Garza-Sánchez F, Low DA, and Hayes CS. EF-Tu and EF-Ts are common cofactors utilized by contact-dependent inhibition (CDI) systems. *Molecular Genetics of Bacteria and Phage Meeting*. Madison, WI. August 2015.

2. **Willett JLE**, Morse RP, Goulding CW, and Hayes CS. Structural and functional analysis of contact-dependent inhibition nuclease toxins in the EC869 superfamily. *MCDB Graduate Seminar Series*. Santa Barbara, CA. January 2015.
   - Awarded best 5th year graduate student talk by student vote

3. **Willett JLE** and Hayes CS. Rearrangement of insertion elements confers transient resistance to a contact-dependent inhibition toxin from *Escherichia coli*. *MCDB*

Graduate Seminar Series. Santa Barbara, CA. March 2014.

4. **Willett JLE**, King O, and Hayes CS. Rearrangement of insertion elements confers resistance to a contact-dependent inhibition toxin from *Escherichia coli*. *West Coast Bacterial Physiologists Meeting*. Asilomar, CA. December 2013.

5. **Willett JLE**, King O, and Hayes CS. Rearrangement of insertion elements confers resistance to a contact-dependent inhibition toxin from *Escherichia coli*. *Molecular Genetics of Bacteria and Phage Meeting*. Madison, WI. August 2013.

6. **Willett JLE**, King O, and Hayes CS. Genetic rearrangements confer resistance to a contact-dependent inhibition toxin from *Escherichia coli*. *MCDB Graduate Seminar Series*. Santa Barbara, CA. May 2013.
   - Awarded best 3rd year graduate student talk by student vote

7. **Willett JLE** and Hayes CS. The inner membrane protein YciB is required for contact-dependent inhibition in *Escherichia coli*. *West Coast Bacterial Physiologists Meeting*. Asilomar, CA. December 2012.

SELECTED POSTER PRESENTATIONS

1. **Willett JLE** and Hayes CS. Insertion element transposition provides transient resistance against contact-dependent inhibition toxins from *Escherichia coli*. Department of MCDB Poster Symposium. Santa Barbara, CA. February 2015.
   - Received best poster award as decided by faculty and student vote

2. **Willett JLE**, Morse RP, Goulding CW, and Hayes CS. Structural and functional analysis of contact-dependent inhibition nuclease toxins in the EC869 superfamily. Molecular Genetics of Bacteria and Phage Meeting. Madison, WI. August 2014.

3. **Willett JLE** and Hayes CS. Insertion element transposition provides transient resistance against contact-dependent inhibition toxins from *Escherichia coli*. Gordon Research Seminar/Gordon Research Conference. Mount Holyoke, MA. July 2014.

PROFESSIONAL CONTRIBUTIONS

Chair, Gordon Research Seminar on Microbial Stress	July 2016
President, Graduate Union of Molecular Biology Investigators	2011-2015
Department of MCDB Faculty Committee Student Representative	2012-2013

MENTORING AND OUTREACH

Graduate

Women in Science and Engineering, Mentorship Committee	2011-2015
Tech Savvy Workshop Leader	2014-2016

Graduate Student Mentor (laboratory rotation projects)

1. Sonya Donato (Winter 2013), *Characterization of toxins in the EC869 superfamily*
2. Tiffany Halvorsen (Spring 2015), *Contact-dependent inhibition systems in natural isolates of* Escherichia coli.
3. Parker Dabbs (Fall 2015), *Characterization of a predicted endonuclease contact-dependent inhibition toxin from* E. coli *STEC_O31*.

Undergraduate Student Mentor

1. Dinh Quan Nhan (November 2014-present), *Mapping the orientation of CdiA during contact-dependent growth inhibition in* Escherichia coli.
   - Presented a poster at the UCSB undergraduate research symposium and received departmental honors in the major
2. Danielle McSheery (January-June 2015), *Development of a high-throughput fluorescent screen to identify mutations in* E. coli *mutants resistant to contact-dependent inhibition.*
3. Chrissy Rouales (January-June 2014), *Mutational analysis of YciB, a putative inner membrane protein required for translocation of a contact-dependent inhibition toxin from* E. coli.
4. Oliver King (January-December 2013), *Characterization of contact-independent inhibition toxins in the EC869 superfamily*.
   - Received departmental honors in the major
5. Brandon Butterfield (July-November 2012), *Identification of* E. coli *mutants resistant to a contact-dependent inhibition toxin from* Dickeya dadantii *3937.*
6. Jeniffer Lee (August 2012-December 2013), *Transposon mutagenesis to identify novel factors required for import of contact-dependent inhibition toxins in* E. coli.
   - Presented a poster at the UCSB undergraduate research symposium and received departmental honors in the major

Undergraduate

Reaching and Educating America's Chemists of Tomorrow 2008-2010

- Directed the 4th grade outreach program on forensic science.
- Developed and updated chemistry lesson plans for grade school students.
- Participated in community outreach events such as Trick-or-Treat with Chemistry and the Holiday Demonstration Show.

American Chemical Society Student Affiliates 2007-2010

- Served as Tutoring Chair on the executive board and ran the undergraduate tutoring program, where I expanded enrollment from 25 to more than 150 students.
- Organized conference trips and presented group posters at national ACS meetings.

ABSTRACT

Delivery and activity of toxic effector domains from contact-dependent growth inhibition systems in *Escherichia coli*

by

Julia Laura Elizabeth Willett

Bacteria are ubiquitous in nature and have evolved a variety of communication and competition systems to survive in dense, complex environments. Contact-dependent growth inhibition (CDI) is a microbial competition system that is widespread throughout Gram-negative bacteria. CDI is mediated by the CdiB/CdiA two-partner secretion system, which displays the large CdiA exoprotein on the surface of CDI^+ inhibitor cells. The C-terminal domain of CdiA (CdiA-CT) is toxic and inhibits cell growth after delivery into target bacteria. CDI^+ cells are protected from auto-inhibition by expression of a cognate immunity protein (CdiI), which binds to the CdiA-CT and inactivates toxicity. CdiA-CT/CdiI pairs are highly divergent across species, indicating that CDI systems are capable of deploying a variety of toxins.

This thesis explores several aspects of CDI, including delivery of CdiA-CTs into target cells, the toxic activities that lead to growth inhibition by CdiA-CT domains, and target cell stress responses that may influence CDI populations in natural environments. In Chapter I, we provide a general introduction to both diffusible and contact-dependent bacterial

competition systems. This provides an overview of our current knowledge of CDI systems and also highlights key features of other secretion systems that contribute to population dynamics within bacterial communities. We then present a genetic study characterizing pathways of CdiA-CT translocation into target cells in Chapter II. In Chapter III, we focus on one protein, YciB, which is required for translocation of CdiA-CT_{o11}^{EC869}, a DNase toxin from *E. coli*, and examine the role of YciB in *E. coli* physiology outside of CDI. Chapter IV explores genetic responses that occur inside target cells after delivery of CdiA-CT_{o11}^{EC869}; in Chapter V, we present a study characterizing CdiA-CT/CdiI modules related to CdiA-$CT/CdiI_{o11}^{EC869}$. In Chapter VI, we discuss unpublished work examining the role of the translation factor EF-Tu as a co-factor required for activity by numerous CdiA-CT toxins. Chapter VII describes a collaborative project that utilized principle components of CDI systems as synthetic biology tools. Finally, we discuss research questions of significant interest in the field of CDI in Chapter VIII.

TABLE OF CONTENTS

I. Introduction

Bacteria are unicellular organisms that exist and thrive in complex multicellular communities. They form intricate microbial networks in the rhizosphere and in the ocean (1), have important host-associated roles on plants and in insects (2), and are commensal organisms on skin, in the nose, and in gut microbiomes (3). Historical research has appreciated a pathogenic role for these microbes in disease states in plants and animals, but recent research demonstrates that bacterial populations influence a plethora of physiological behaviors. Microbial communities can influence a variety of host behaviors and phenotypes, including gene expression and metabolism in *Drosophila* (4); light organ development in the squid *Euprymna scolopes* (5, 6); maturation, differentiation, and morphology of gut and immune cells (4, 7); vasculature remodeling (8); endocrine, neurological, and immune signaling (4, 9); brain and nervous system diseases (10-13); and social behavior and mating (14). Within these niches, microbes must communicate and compete with each other and the surrounding host environment in order to survive. A great body of work has characterized secreted factors that govern the behaviors of bacterial communication, including quorum sensing pathways involving production and recognition of *N*-acyl homoserine lactones or thiolactones (15-19); competition for nutrient acquisition using siderophores or manipulation of host machinery (20-22); and bacterial competition via killing of surrounding cells using molecular tools such as colicins and anti-microbial peptides (23-26), yet relatively little is known about systems that require direct physical contact to control neighboring cells in dense microbial environments.

This introduction will provide a review of bacterial secretion systems and inhibition mechanisms and will also introduce the contact-dependent growth inhibition (CDI) system,

the study of which is the focus of this thesis. First, colicins will be discussed as a means of providing background information on perhaps the best-studied group of bacterial toxins. An understanding of the fundamentals of colicin biology is helpful when considering the complexities of CDI systems. Next, we briefly introduce bacterial secretion systems to examine the different ways in which prokaryotes export toxins and other effector molecules to target cells. We then discuss the history of CDI and our current understanding of the mechanisms by which CDI systems deploy toxins, recognize target cells, and carry out inhibitory activities. Finally, we provide a short review of additional competition systems to contextualize CDI within a larger group of "contact-dependent" inhibition systems.

A. Colicins

In addition to being one of the best-studied Gram-negative organisms, *Escherichia coli* is a coliform and is present in the human intestinal microbiome (27). In the gut, *E. coli* is in constant competition with surrounding host cells and other microbes for space and nutrients. As such, *E. coli* has evolved many ways to gain a competitive advantage in a dense microbial environment. These competitive tools include secreted compounds that aid in nutrient acquisition, secreted proteins and nonribosomal peptides that inhibit the growth of nearby cells, or systems that require physical contact between cells and result in cell death (which will be discussed later in this chapter). Bacteriocins are secreted proteins that inhibit the growth of surrounding cells. These include the small peptide lantibiotics produced by Gram-positive bacteria, small cyclic peptides and microcins, non-ribosomal peptides, and larger ribosomally-produced toxins (23). The best studied toxins in the latter class are colicins, which are toxins produced by *E. coli* for the purpose of inhibiting other *E. coli* strains. Analogous toxins exist in other Gram-negative bacteria and are named accordingly (klebicins

are produced by *Klebsiella pneumoniae*, cloacins by *Enterobacter cloacae*, and so forth). For a comprehensive review of colicins, the 2007 review by Cascales *et al.* (23) is an excellent resource.

1. Colicin production and release

Colicins are 40-80 kDa peptides produced by strains carrying a pCol plasmid (28-31). Most colicins inhibit cells by degrading nucleic acids or forming pores in cell membranes. A smaller number have other activities, such as peptidoglycan degradation in the case of colicin M (23). Colicin operons contain two to three genes that encode the toxin, an immunity protein that inactives the peptide, and in some cases, a lysis protein required for release into the environment (32-39). Some colicin operons contain multiple immunity or lysis genes, suggesting these genetic domains can be mobile and may have evolved from common ancestors (33, 36, 40). Expression of colicin operons is typically repressed by the LexA protein, which is the canonical repressor of genes involved in the SOS response pathway induced by DNA damage (41). As such, colicin production can be induced by DNA damage from UV light or other mutagens as well as other stress or nutrient starvation conditions (23). Upon alleviation of LexA repression, colicin and immunity genes are co-transcribed and translated, although the immunity genes typically have their own promoters to prevent auto-inhibition during colicin production (42). Expression of the lysis protein ultimately leads to death of the colicinogenic cell and expulsion of the colicin-immunity dimers into the environment, where they can interact with and inhibit target cells (43, 44).

2. Structure and function of colicin domains

Colicins carry out a variety of discrete steps during the process of inhibition. After release from colicin-producing cells, the toxins first bind a receptor at the surface of target

cells. Sequence homology was used to map this to the central region of the primary sequence of colicins. The primary colicin receptors are the outer membrane proteins BtuB (utilized for uptake of vitamin B_{12}) and FepA (also involved in iron uptake via transport of siderophores), and to a lesser extent, OmpF, OmpA, Cir, and Tsx (23). Some colicins compete with the natural ligand for these outer membrane proteins, suggesting that the toxins and the natural substrate share overlapping binding sites (45, 46).

Though colicins can interact with these outer membrane receptors in an energy-independent manner, they require a source of cellular energy in order to translocate through the membrane (23). This activity is mediated by the N-terminal translocation domain of colicins, and colicins are separated into two groups based on the protein complex utilized for this process. Group A colicins utilize the Tol machinery while group B colicins hijack the Ton complex to move across the outer membrane. Translocation of group A colicins has been best studied using the DNase colicin E9. After binding BtuB at the outer membrane, a secondary outer membrane protein (OmpF) is engaged, where it interacts with the unstructured N-terminal domain of colicin E9. Part of this N-terminal domain then enters the periplasm and recruits TolB, a membrane-associated periplasmic protein involved in maintaining outer membrane integrity (47-51). Group A colicins require varying subsets of the TolABQR proteins for translocation (23, 52, 53). In contrast to group A colicins, group B colicins require just a single outer membrane protein for translocation across this barrier. Instead, it appears that the outer membrane receptor is also utilized for translocation. Instead of Tol proteins, group B colicins interact with TonB via a small motif termed the TonB box (54, 55). In normal *E. coli* physiology, TonB interacts with ExbB and ExbD to transduce energy of the proton motive force for active transport (23).

3. Cytotoxic activities of colicins

Once inside the cell, inhibitory activities are conferred by the C-terminal cytotoxic domain of colicins (23). Almost all colicins kill cells in one of two basic ways: 1) by pore formation in the inner membrane or 2) through degradation of nucleic acids. One exception is colicin M, which degrades peptidoglycan precursor molecules and blocks cell wall synthesis (56). After translocation across the outer membrane, pore-forming toxins insert themselves into the inner membrane of *E. coli* target cells, converting the 10-helix bundle it maintains as a secreted toxin into a lipid-soluble voltage-gated channel (57-62). Toxicity of these proteins is orientation-dependent, as pore-forming colicins that insert into the membrane from the intracellular compartment are not toxic and do not require the presence of immunity protein for survival. The immunity proteins associated with these toxins typically block activity by "plugging" the pore formed by these ionophoric colicins and do not block pore formation in the membrane (23).

Nucleases are the other major class of colicins. These toxins cleave a variety of nucleic acid substrates, including DNA (colicins E2, E7, E8, and E9), 16S RNA (colicins E3, E4, and E6), and tRNA (colicins D and E5) (23, 34, 63-70). DNase colicins coordinate a transition metal cofactor and stochastically make cuts in genomic DNA, eventually creating double-stranded breaks that lead to cell death (23). Studies of colicin E7, colicin E9, and related DNases show that these toxins bind the minor groove of double-stranded DNA (71, 72), distorting the phosphodiester backbone towards the coordinated metal ion. The relevant metal ion *in vivo* is unknown due to conflicting purification and activity assay results, but Zn^{2+}, Mg^{2+}, and Ca^{2+} have supported DNase activity *in vitro* (73-75). Colicins that cleave RNA target one of two sets of substrates: 16S RNA or tRNA. Colicin E3 attacks the 30S

ribosomal subunit and cleaves 16S RNA near the A site of the ribosome (69). Colicins E5 and D each cleave the anticodon loops of a different subset of tRNA molecules (68, 70). ColE5 cleaves $tRNA^{His}$, $tRNA^{Asn}$, $tRNA^{Tyr}$, and $tRNA^{Asp}$, while colicin D cleaves all 4 arginine isoacceptors. The immunity proteins that correspond to the DNase and RNase colicins physically bind the C-terminal cytotoxic domain of these toxins, as opposed to the pore-forming immunities that interact with the inner membrane of cells. ImmE5 and ImmD directly block the active site of their cognate colicins (76, 77), while the immunities for the DNase colicins as well as colicins E3, E4, and E6 bind exosite locations outside of the active site residues (71, 72, 78, 79). Mechanisms of immunity inactivation will be discussed in Chapter V of this thesis.

A fundamental difference between nuclease and pore-forming colicins is the location of the cellular compartment containing their substrates. Nucleases cleave RNA and DNA, meaning that these colicins must necessarily cross both the outer and inner membranes in order to reach the cytoplasmic compartment. This makes the delivery pathway of these toxins distinct from pore-forming colicins, which exert their toxic effect at the inner membrane. A major interest in the colicin field is elucidating how nuclease colicins carry out the nontrivial task of crossing the inner membrane. Studies have shown that the cytotoxic domains of colicins E3 and E9 associate with anionic lipid vesicles in a charge-dependent manner (80-84), suggesting that these toxins may interact with the inner membrane of cells in a similar fashion, perhaps facilitating their translocation across this barrier. This hypothesis was tested by Walker *et al*., who examined cytotoxicity in cells with variable anionic phospholipid levels (85). They utilized a cell line in which the phospholipid composition of the inner membrane could be altered by regulating the expression of *pgsA* (and thus the

production of the anionic phospholipid phosphatidylglycerol) and found a positive correlation between the levels of phosphatidylglycerol and inhibition by colicin E9 (85). Additionally, constructing mutant variants of colicin E9 with increased or reduced positive charges in the DNase domain enhanced or decreased cytotoxicity, respectively (85). Taken together, this data suggests that charge-mediated interactions with the inner membrane may be required for nuclease toxins to access the cytoplasm of cells.

4. Colicins undergo processing during translocation into target cells

A number of processing steps have been identified as essential for colicin translocation. The first involves the immunity protein, which is bound to the toxin during synthesis to prevent auto-inhibition of the colicinogenic cell. Therefore, the colicin/immunity complex is intact when producing cells lyse and release the toxins into the extracellular milieu. The immunity protein is necessarily lost during translocation into susceptible cells in order to liberate the toxin and allow it to carry out toxic function upon reaching its intended destination. Given the extremely strong binding affinities measured for colicin-immunity complexes ($K_d = 10^{-12} – 10^{-14}$ (23)), it is unlikely that they simply dissociate upon release from a lysed cell. Therefore, stripping away the immunity protein must be an active process that occurs during colicin binding or translocation instead of simply a stochastic event.

The first step at which removal of the immunity protein could occur is during interaction with the outer membrane receptor. If receptor binding induces a conformational change in the colicin, this could promote dissociation of the toxin-immunity complex upon binding. However, binding studies show that colicins do not unfold upon receptor binding and that immunity release does not occur at this step (86-88). In the case of colicin E9, which binds BtuB at the outer membrane and requires OmpF for translocation, the entire BtuB-E9-

ImmE9-OmpF complex can be isolated from the outer membrane of cells via nickel-affinity purification using His-tagged ImmE9, indicating that the immunity protein does not dissociate at this step (87). Instead, translocation across the outer membrane may be a requirement for immunity dissociation. Crystal structure analysis of colicin E3 reveals that the immunity protein interacts with both the C-terminal cytotoxic domain as well as the N-terminal translocation domain, which is required for release of ImmE3 (79, 89). Additionally, the Tol machinery involved in translocation is required for the release of ImmE2 from colicin E2 (90). Changes that occur in the toxin itself may also be important for release of the immunity. Some models suggest that colicins become unfolded as they translocate across the outer membrane. Unfolding of the domains that interact with immunity proteins would presumably facilitate dissociation of the colicin-immunity complex, liberating the toxin and enabling it to carry out toxic activity once refolded inside the cell.

Several colicins, including pore-formers and nucleases, undergo proteolytic processing events during delivery. Accordingly, only the C-terminal cytotoxic domains and not full-length toxin are detected in cells treated with both DNase and RNase colicins (91, 92). Many are processed either *in vitro* or *in vivo* by OmpT, although interpreting the relevance of this event is not always straightforward (93-97). OmpT is a surface-associated serine protease that cleaves cationic antibiotic peptides and may be involved in processing secreted proteins (98, 99). Interestingly, although OmpT processes colicin D and E3 *in vitro*, this cleavage is not required for inhibition. E3 is still processed by lysates made from cells expressing an inactive form of OmpT, suggesting that another component cleaves colicin E3 *in vivo* (23, 91). OmpT processing of colicins D and E2 may be a defense mechanism to protect the cell from inhibition, as the presence of ImmE2 blocks OmpT-dependent cleavage, and over-

expression of OmpT increases resistance to both toxins (91, 100).

Additional colicin processing steps have been found to require essential proteins. de Zamaroczy and colleages identified a single point mutation in LepB that prevents processing of colicin D and confers resistance to this toxin (101). LepB is an essential inner membrane peptidase that removes signal peptides from secreted proteins, such as OmpA (102). The mutation (N274K) is in a conserved domain that is required for activity of LepB, but this specific asparagine does not contribute to canonical peptidase function (101). It is hypothesized that the LepB-dependent processing event is not required for translocation across the outer membrane into the periplasm, but simply to remove the C-terminal cytotoxic domain such that it can continue on into the cytoplasm. Furthermore, ImmD protects against *in vitro* cleavage of colicin D by LepB (101), suggesting that the processing event takes place after the immunity protein is stripped away at the outer membrane. LepB interacts with colicin D *in vitro*, and Mora *et al.* recently identified a LepB recognition motif in colicin D and two related toxins from *Klebsiella pneumoniae* (103). However, purified LepB is insufficient to cleave colicin D, suggesting that perhaps another cellular component is required for this processing to take place (91, 101). Interestingly, OmpT processes colicin D *in vitro*, but this does not require the catalytic activity of LepB, and OmpT-dependent processing is not required for inhibition of cells *in vivo* (91). Unlike the E group colicins that contain patches of positively-charged residues that presumably interact with the inner membrane and facilitate delivery, colicin D and related klebicins do not have this charge distribution in their cytotoxic domains. Therefore, it has been proposed that a direct interaction with LepB helps bring these toxins close to the membrane, where they can be subsequently processed and translocated into the cytoplasm (103).

Early reports on colicin resistance found that cells with mutations in *tolZ* (*ftsH*) were resistant to both nuclease and pore-forming colicins (104-107). Further tests with rigorously-characterized mutant backgrounds determined that FtsH is required for inhibition by all nuclease toxins but not pore-formers or colicin M (85). The FtsH-dependent step is presumably downstream of receptor binding and translocation across the outer membrane, as both Tol- and Ton-dependent nuclease toxins require FtsH for inhibition (85). FtsH is an essential AAA+ ATPase that contains a cytoplasmic protease domain and is involved in the degradation of aberrant proteins and the heat shock response (108-111). Because FtsH typically degrades substrates into small peptides, its role in colicin processing is not immediately clear. The involvement of FtsH in processing cytotoxic fragments in other toxin-immunity systems will be discussed in Chapter II.

B. Bacterial secretion systems

Secretion of effector molecules is critical for bacteria survival. Microbes produce and export a number of secreted compounds used for nutrient acquisition, transfer of genetic materials, and inhibition of other cells. To date, seven secretion systems that accomplish these tasks have been described (T1SS through T7SS). Additional systems utilized for the biogenesis of extracellular structures like pili and curli have also been identified. Here, we will briefly introduce the seven well-described secretion systems with the exception of T6SS, which will be discussed in section D.

1. One-step transport systems (T1SS, T3SS, and T4SS)

One-step secretion pathways transport effector molecules from Gram-negative bacteria across both the inner and outer membranes, and include the type 1, type 3, and type 4 secretions systems (T1SS, T3SS, and T4SS, respectively). The best-studied T1SS effector is *E. coli* α-hemolysin (HlyA), a toxin that forms pores in plasma membranes of red blood cells

and is commonly produced by uropathogenic strains of *E. coli* (112). The suite of proteins secreted by the T1SS is broad and ranges from the 5.8kDa colicin V up to ~900 kDa RTX/MARTX toxins (113, 114). T1SS loci are regulated in a variety of ways, including cis-acting regulatory elements, mRNA structure, H-NS binding, and the Fur transcriptional regulator (115), and many T1SS substrates are involved in inhibiting the growth of surrounding cells or acquiring resources for the producing cell (116). T1SS structures are composed of an outer membrane protein, a membrane fusion protein, and an ABC transport system. Together, these span from the cytoplasm to the extracellular space of Gram-negative organisms, enabling transport of effectors across both membranes and eventual secretion from the cell. The ABC transporter permits transport across the inner membrane using energy from ATP hydrolysis, and the outer membrane factor is typically a protein pore that facilitates the final step of secretion (117). ABC transport components are highly specific for their substrates, but the outer membrane proteins involved in T1SS activity are more promiscuous. For example, HlyA secretion requires the outer membrane factor TolC, which is also involved in colicin V secretion and works with the inner membrane protein AcrB to export small cytotoxic drug molecules (116, 118, 119).

Secreted proteins are targeted for export via the T1SS in both signal peptide-dependent and signal peptide-independent manners. Low molecular weight bacteriocins (microcins) contain an N-terminal signal peptide that is cleaved by a C39-like peptidase domain in their associated ABC transporters. It is thought that the C39 peptidase domain/signal peptide interaction may help retain substrates in a conformation that permits membrane translocation (116). Interestingly, the ABC transporters required for export of signal peptide-independent T1SS effectors contain an N-terminal domain that resembles C39 peptidase in both sequence

and structure. These peptidase-like domains lack a conserved cysteine required for activity and are not involved in processing, but they are nevertheless required for the export of their T1SS effector molecules (116). Other well-studied proteins secreted by T1SS have C-terminal secretion signals that are not proteolytically cleaved during export but are required for targeting to T1SS machinery (116). T1SS substrates are exported in an unfolded state (120). The HasB iron-binding protein produced by *Serratia marcescens* interacts with the SecB chaperone to remain in an unfolded state and facilitate export, but not via interaction with the same residues involved in the canonical SecB/SecA chaperone pathway. This is the only T1SS substrate exported using this chaperone, and it hypothesized that others have intramolecular motifs that help retain them in an unfolded or secretion-competent state (120).

In contrast to the simple three-partner T1SS export machinery, type 3 secretion systems (T3SS) are composed of a complex assemblage termed the injectosome, which contains approximately 25 unique proteins and allows bacteria to deliver proteins to eukaryotic cells (121, 122). The T3SS injectosome apparatus is structurally conserved and resembles flagella. Flagella are anchored to the inner membrane by a ring composed of FliF subunits and span the periplasmic space to the outer membrane. They elaborate a curved "hook" on the cell surface, from which the filament extends away from the cell (121). Turning of the flagella is achieved by a cytosolic ATPase motor. Similarly, T3SS injectosomes are anchored to both the inner and outer membrane by ring structures and include a cytosolic ATPase required for export of effectors. The injectosome needle is analogous to the flagellar filament and is a hollow protein tube that extends away from the cell surface. Electron microscopy studies show that the width of the tube cannot accommodate folded proteins; as such, T3SS effectors are exported in an unfolded state. T3SS needles have evolved to best

deliver effector molecules to unique environments of their hosts. T3SS systems from enteropathogenic *E. coli* must move effectors across the intestinal mucosa, but plant pathogens must transport their T3SS effectors across plant cell walls. To accomplish these similar but distinct tasks, T3SS needles produced by enteropathogenic *E. coli* are more flexible than the thin pilus produced by T3SS loci in plant pathogens (123, 124). Both flagella and the T3SS injectosome have molecular "rulers" to regulate the length of these structures, which ensures that T3SS effectors are properly deployed from one cell cytoplasm to another.

Though the injectosome machinery is highly conserved, T3SS effectors are diverse (121). Numerous plant and animal pathogens employ T3SS to target their respective hosts. Many T3SS effectors from plant pathogens such as *Pseudomonas*, *Xanthomonas*, and *Erwinia* species influence host cell defense mechanisms and are involved in the transcriptional cascades that control programmed cell death, hormone signaling through jasmonic acid pathways, or morphological changes in response to an invading pathogen. Other T3SS effectors deployed against plant hosts have protease or phosphatase activities that directly degrade or alter host proteins (125, 126). Many T3SS effectors from animal pathogens interact with host GTP-binding proteins involved in regulation of cytoskeletal movement, trafficking, cell growth, and apoptosis (122). For example, the well-studied *Salmonella* effector SopE activates the Rho GTPases Cdc42 and Rac1, thus promoting invasion into host cells through cytoskeletal rearrangements. T3SS effectors from *Yersinia* have a complimentary effect and work by inactivating GTPases to prevent phagocytosis and inflammatory responses (122). Other T3SS effectors deployed against animal hosts act as proteases, phosphatases, or kinases that directly inactivate target molecules or modulate

transcriptional cascades involved in the host immune response (122). Numerous plant and animal pathogens require a functional T3SS for virulence.

Like T3SS assemblages, T4SSs resemble another bacterial macrostructure in that their extracellular filament is related to pili. T4SSs are found in Gram-positive and Gram-negative organisms and are used to transfer both DNA and protein effectors (127, 128). They carry out plasmid conjugation, transfer of conjugative elements to other bacteria, and delivery of proteins to eukaryotic cells. The well-studied conjugative T4SS encoded by the *vir* locus in *Agrobacterium tumefaciens* delivers a nucleoprotein complex into plant cells, resulting in integration of bacteria DNA into the host genome and tumor formation (128, 129). Conjugative T4SSs in Gram-negative bacteria, such as the VirB/Vir4 T4SS in *A. tumefaciens* and the well-studied F-pilus, are typically encoded on plasmids (129). T4SS structures in *Neisseria* and *Helicobacter pylori* transport DNA to and from the extracellular space instead of directly to or from a target cell. Most protein-transferring T4SS complexes are found in pathogens such as *Bordetella*, *Legionella*, and *Bartonella* (129). Both contact-dependent and contact-independent mechanisms of T4SS effector secretion and delivery have been characterized.

In Gram-negative bacteria, T4SSs are anchored to the cell by a large core complex composed of distinct inner membrane and outer membrane regions and more than a dozen Vir proteins (130). At its widest point, the diameter of this structure is 80 Å wide and can presumably accommodate large substrates. At the outer membrane face, the pore constricts to 10 Å, and conformational changes of the membrane-spanning protein VirB10 gate the release of substrates (131). Conserved pili-like structures extend outward from the surface of the cell and mediate substrate delivery to the extracellular space or target cells. F-type pili

are dynamic and can undergo cycles of extension and retraction. Conversely, P pili are not thought to retract and instead are static structures that are deposited on the target cell surface after conjugation (129, 132). F pili have an inner pore diameter of 30 Å, which can accommodate unfolded protein substrates or single-stranded DNA (131). The T4SS from *H. pylori* and *L. pneumophila* contain non-canonical surface structures that are larger than F- and P-type pili (133). Cytoplasmic coupling proteins related to VirD4 interact with substrates in the cytoplasm, and many contain ATP-binding motifs (130). Export of T4SS effectors, as with other secretion systems, depends on ATPase activity (129, 134).

Conjugative T4SSs have been identified in a number of Gram-positive organisms, including *Enterococcus faecalis*, *Streptococcus* species, and *Bacillus subtilis*, and are found on both plasmids and genomic integrative and conjugative elements (ICEs) (133, 135). Vir homologs in Gram-positive T4SSs resemble the components needed for effector translocation across the inner membrane of Gram-negative cells, and these Vir components are thought to form the core complex of Gram-positive T4SSs (133, 136). Gram-positive T4SS surface structures are similar to adhesin proteins, not the pili-like structures that extend from Gram-negative T4SSs (137). The transfer of plasmid elements via T4SS complexes in *Enterococcus* species is tightly regulated by pheromone signaling and is required for virulence (136, 138).

2. Two-step transport systems (T2SS and T5SS)

Unlike the one-step transport processes that export unfolded substrates through narrow tubes, T2SSs can secrete folded proteins (134). T2SS substrates are first transported from the cytoplasm to the periplasm via the Sec (unfolded precursors) or Tat (folded precursors) pathways and then exported across the outer membrane by the T2SS apparatus. As with

other secretion systems, T2SS machinery contains outer membrane, periplasmic, inner membrane, and cytoplasmic components, but role of these must be bridged by secretion from the cytoplasm into the periplasm by a different system before T2SS-mediated export can take place. While T2SSs do not elaborate a true extracellular pilus, they contain a pseudopilus that is anchored to the inner membrane and spans the perisplasm (134, 139). This is related to the T4SS pilus that extends outside the cell and used for transfer of protein and DNA substrates. The GspD monomer that makes up the T2SS outer membrane structure is homologous to other secretion systems and filamentous phage (139). Like other secretion systems, the inner membrane baseplate anchors the apparatus and connects to a cytoplasm ATPase, GspE, which is required for activity; the proton motive force is also required for substrate export (140).

T2SS effector molecules are diverse and include a variety of toxins, enzymes, and cytochromes (139-141). However, these substrates are specific not only for T2SS-mediated export, but the specific T2SS complexes from the organisms in which they are produced (140). Several studies support the idea of T2SS-specific motifs required for export of substrates, though these are not yet well-defined (142). The literature on T2SS export signals suggest that the residues in these domains are not co-localized in primary sequence, and that any required structural motifs may be formed by protein folding and disulfide bond formation in the periplasm prior to export across the outer membrane (140, 142).

Type V secretion systems are composed of either one or two polypeptides that enable the surface display of a large filamentous exoprotein. These surface proteins are common virulence factors and can be used for adhesion to other cells, in biofilm formation, and for the delivery of toxic effectors to neighboring bacteria (143). There are currently 5 known

subfamilies of T5SSs (Va – Ve), with the best studied being the class Va autotransporters, which consist of a single polypeptide that forms the substrate pore as well as the exported substrate, and the class Vb two-partner secretion systems, which utilize separate proteins for pore formation and substrate secretion (144). Two-partner secretion (TPS) systems utilize separate proteins for pore formation and substrate secretion. Both autotransporters and TPS systems require the Sec machinery for translocation across the inner membrane of cells, and they catalyze their own export across the outer membrane. Contact-dependent growth inhibition systems, which are the focus of this thesis, are two-partner secretion systems and will be described in detail in the following sections. Autotransporters are secreted into the periplasm in an unfolded state by the Sec machinery, where the periplasmic chaperones keep them in this conformation until they are assembled on the cell surface. Interestingly, the N-terminal signal peptide domains of autotransporters are longer than canonical Sec-dependent signal peptide sequences, and this extra sequence space seems to slow down translocation (145). The translocation domain of these systems is recognized by the Bam complex of essential proteins (BamABCDE) that is required for the biogenesis of outer membrane proteins. The C-terminal region of autotransporter polypeptides is then exported to the surface of the outer membrane. Recent evidence suggests that the final secretion steps of autotransporter proteins require the Bam complex as well as other cellular machinery. After secretion, many autotransporter proteins undergo autoproteolysis and are released from the cell surface, although some remain anchored to the outer membrane (146, 147).

TPS systems encode a β-barrel transport protein (generically called TpsB), which is responsible for the surface display of the filamentous protein TpsA (143). Most TpsB proteins are substrate-specific and only export one TpsA protein. TpsB is structurally

homologous to BamA and forms a 16-strand β-barrel in the outer membrane with two periplasmic POTRA domains. TpsA proteins interact with their cognate TpsB via a highly-conserved TPS domain near the N-terminus; this region interacts with the POTRA domains of TpsB. The N-terminal region of TpsA proteins also contains an extended signal peptide that is required for secretion into the periplasm. Once translocated to this compartment, periplasmic chaperones help keep these peptides unfolded until secretion across the outer membrane. Two models exist for the orientation of TpsA during outer membrane translocation. The first, put forth by Mazar and Cotter when studying FHA systems in *Bortadella pertussis*, posits that the N-terminus remains anchored in the periplasm, while the C-terminus loops around in a hairpin and is displayed on the cell surface, where it is processed and released (148). Conversely, the HMW1 adhesin from *Haemophilus influenzae* is oriented such that the C-terminus stays in the periplasm, where a peptide loop prevents release from HMW1B (the TpsB homolog for this system) (149). The orientation of contact-dependent growth inhibition proteins during biogenesis is unknown and will be speculated upon in the conclusion chapter.

In addition to autotransporters and two-partner secretion systems, three additional subclasses of T5SSs have been described: trimeric autotransporters (Vc), fused two-partner secretion systems (Vd), and inverted autotransporters (Ve) (143, 150). Unlike monomeric transporters, trimeric autotransporters are not cleaved at the cell surface and instead remain attached to the outer membrane. They are widespread in pathogenic bacteria and are often used to bind eukaryotic host cells, as is the case for YadA in *Yersinia enterocolitica* (151). Trimeric autotransporters are secreted across the inner membrane into the periplasm, where a combination of chaperones and internal peptide motifs keep them in an unfolded state until

secreted by their trimeric outer membrane β-barrel proteins. Members of the Vd family of fused two-partner secretion systems are autolytically processed like autotransporters but are found as a single peptide that also contains a β-barrel outer membrane protein with an associated POTRA domain (143). The intimin and invasin proteins that make up the Ve subfamily of inverted autotransporters also make contact with host cells and are important for pathogenesis, but the orientation of export is opposite that in the Va subfamily in that the N-terminus is looped outside the cells, and the C-terminal end is then transported to the surface, where it makes contact with target cells (143, 150, 152, 153).

3. The type 7 secretion systems of Gram-positive bacteria

In contrast to secretion systems in Gram-negative bacteria, Gram-positive cells must export extracellular substrates across a single membrane and a thick cell wall that undergoes constant turnover. This necessitates structural differences in comparison to the protein complexes that anchor Gram-negative secretion systems to the cell wall. Type 7 secretion systems (T7SS) are composed of a conserved protein complex that spans the plasma membrane, and they lack the pseudopili or pili-like filaments that project away from the cell surface in many Gram-negative secretion systems (134). As with other secretion systems, T7SSs contain a conserved AAA+ ATPase essential for activity. T7SS loci have been characterized in a variety of Gram-positive organisms, including *Bacillus subtilis*, *Staphylococcus aureus*, and *Listeria* species, as well as in mycobacteria (154). T7SS substrates belong to the ESAT-6/WXG100 family, named as such because these proteins are approximately 100 amino acids in size and contain a conserved WXG motif. A related family of secreted toxins, the PF04740 proteins from *Bacillus subtilis*, are related to ESAT-6/WXG100 proteins and have been characterized as toxic RNases (155).

C. Contact-dependent growth inhibition (CDI) systems

1. Discovery of contact-dependent growth inhibition

Contact-dependent growth inhibition (CDI) was first described in 2005 in *E. coli* strain EC93, an intestinal isolate from a rat colony (156). Like many natural isolates, EC93 has a significant growth advantage over domesticated *E. coli* K-12 lab strains; in co-culture, EC93 reduces the number of viable K-12 cells several thousand-fold after only a few hours (156-159). Unlike many previously-characterized natural isolates, EC93 does not inhibit bacteria solely using diffusible toxins like colicins, but instead requires direct physical contact with target cells (156, 157). Thus, this new form of bacterial competition was termed contact-dependent growth inhibition (CDI) (156). The locus responsible for CDI was identified using a genomic library from *E. coli* EC93, and the gene cluster *cdiBAI* was found to be sufficient to confer the CDI^+ phenotype to laboratory strains of *E. coli* (156).

The first two gene products from the CDI operon, CdiB and CdiA, comprise a two-partner secretion (TPS) system in which CdiB facilitates the display of CdiA on the cell surface. TPS systems are a sub-family of type V secretion systems and include a number of adhesins that are important for bacterial virulence in eukaryotic hosts (160-164). As the name indicates, TPS systems are composed of two proteins (generically known as TpsB and TpsA) that are secreted across the Gram-negative cell envelope. TpsB proteins are outer membrane β-barrels of the Omp85 family, which are responsible for secretion of the TpsA cargo across the outer membrane. TpsA proteins are often very large and are predicted to form long α-helical filaments (165, 166). CdiB corresponds to the TpsB transporter, and CdiA represents the large filamentous TpsA cargo protein. CdiA is a large exoprotein (up to 600 kDa) that is predicted to project away from the cell membrane. As discussed below,

CdiA also contains a C-terminal toxic effector domain and is responsible for the inhibition of target bacteria (156, 167, 168). The third gene of the cluster, *cdiI*, encodes an immunity protein (CdiI) that is required to protect cells from inhibition by its neighboring sibling (CDI^+) cells (167, 169).

Though CdiA proteins vary in size (180 – 640 kDa), they contain a series of conserved domains that most closely resemble the filamentous hemagglutinin adhesins from *Bordetella* (148, 160). As with many T5SS substrates, CdiA contains an N-terminal signal sequence that directs it to the Sec machinery for secretion into the periplasm. The N-terminal region of CdiA also contains a TPS domain that is recognized by CdiB when it reaches the periplasm; the TPS domain is required for surface display on the outer membrane (156, 167, 170). Data from the well-characterized TPS system from *Bordetella pertussis* shows that the TpsB outer membrane component (FhaC in *B. pertussis*, CdiB in CDI systems) threads the unfolded TpsA substrate (FhaB in *B. pertussis*, CdiA in CDI systems) through a central pore upon recognition of the TPS domain (166, 171). Dual FHA repeat domains in CdiA suggest that this exoprotein could extend up to 140 nm from the cell surface (170).

2. Genetic structure of CDI systems in gammaproteobacteria

A majority of the length of CdiA is highly conserved, but sequence homology drops off significantly towards the C-terminus. In *E. coli*, this hypervariable region is demarcated by a conserved tetrapeptide motif (VENN) located a few hundred residues from the C-terminal end of the protein (167). These C-terminal residues encode the toxin domains of CDI systems (abbreviated CdiA-CTs). CdiA-CT toxins can themselves be subdivided into distinct regions. Bioinformatic analysis of many toxins reveals the presence of two discrete domains, which we have termed the N-terminal domain and C-terminal domain (NT and CT,

respectively) (172, 173). This architecture is reminiscent of colicins, which contain three domains that carry out unique functions during the process of cell killing (23). These CdiA-CT domains function independently and can be rearranged with other CdiA-CTs or colicin domains to produce functional chimeras that are capable of inhibiting cell growth (173, 174). Work demonstrating the purpose of the N-terminal domain of CdiA-CTs will be discussed in Chapter II. Remarkably, this modularity extends across species, and CdiA-CT cytotoxic domains from *Yersinia*, *Dickeya dadantii*, and *Enterobacter cloacae* have been successfully fused to *E. coli* CdiA at the VENN motif and delivered into *E. coli* target cells (167, 175).

The discrete domain structures observed in CdiA-CT toxins may have arisen from genomic rearrangement and recombination events that could increase diversity of CDI systems. A number of CDI loci have "orphan" toxin/immunity pairs downstream of the main *cdiAI* genes (176). Orphan immunity genes are often expressed, but the associated toxins are not fused to the structural CdiA core and do not function as delivered effector molecules under normal conditions (167, 176). However, they encode functional toxins and are active when expressed intracellularly or when fused to CdiA and delivered to target cells (167, 173, 177). Many orphan *cdiA-CT*/*cdiI* genes are flanked by integrases or transposable elements, suggesting that they have undergone or are capable of undergoing genetic rearrangements (176). CDI loci are often found on pathogenicity islands, indicating that they can be exchanged via horizontal gene transfer (176, 178-180). Further evidence for horizontal transfer of CDI systems can be found by examining closely-related toxin/immunity modules across species. Recombination events that swap orphan toxin/immunity pairs may provide cells with a means to effectively load another toxin onto CdiA for deployment. These orphan loci may represent a reservoir of toxin/immunity pairs that could expand the CDI weaponry

of a given strain.

3. Genetic structure of CDI systems in other Gram-negative bacteria

All *cdi* genes in gammaproteobacteria are ordered the same way (*cdiBAI*), but this gene arrangement is not conserved in distantly-related betaproteobacteria. In *Burkholderia*, the CDI genes are ordered *cdiAIB* (170, 176). The best-studied betaproteobacteria CDI systems are from *B. thailandensis* and *B. pseudomallei*, the latter of which contains 10 distinct CDI loci (169). As in *E. coli*, CDI systems in *Burkholderia* are typically found on genomic islands (180, 181). While *Burkholderia* CDI systems do not contain typical orphan toxin/immunity modules, many contain extra genes outside of the *cdiAIB* core set (169, 170, 176). Some *Burkholderia* loci contain multiple immunity genes, and 4 of the 10 types are associated with a gene termed *bcpO* that resides between *cdiI* and *cdiB* (170, 176, 182). While the precise function of BcpO is unknown, studies from the Cotter laboratory indicate that this gene product is a lipoprotein that is required for CDI in *Burkholderia thailandensis* (182). However, our preliminary evidence suggests that the CDI systems in *B. thailandensis* E264 *bcpO* deletion strains are fully-functional (Fernando Garza-Sanchez and Christopher Hayes, unpublished work). Further work will be required to characterize the contribution of this gene product to CDI.

4. Outer membrane recognition and receptor binding

CDI requires physical contact between inhibitor and target cells (156), suggesting that a cell-surface receptor may be required to engage CdiA on the surface of target bacteria. Aoki *et al*. used a genetic approach to identify CDI-resistant mutants and isolated a strain with a transposon insertion upstream of *bamA* that was resistant to the CDI system from *E. coli* EC93 (157). This transposon insertion disrupted the promoter region of *bamA*, and this

mutant expressed approximately 5-fold less BamA than wild-type cells. BamA is an essential β-barrel outer membrane protein that is part of the Bam (β-barrel assembly machine) complex in Gram-negative bacteria, which also includes the proteins BamBCDE and is required for proper folding and insertion of proteins into the outer membrane (183-190). CDI does not require other components of the Bam complex or the POTRA-3 domain that is required for protein biogenesis (157, 188). Cell-cell binding between inhibitors and targets is influenced by BamA levels on the surface, and anti-BamA antibodies block the interaction between these cell populations (157). Furthermore, replacing the highly-conserved extracellular loops of *E. coli* BamA with the corresponding region from other bacteria such as *Salmonella* or *Enterobacter cloacae* prevents CDI inhibitory activity and disrupts interactions between cells (159). Together, this evidence indicates that BamA is a bonafide outer membrane receptor required for target cell recognition by CdiA. Interestingly, the region of CdiA that interacts with BamA varies across CDI classes, suggesting that a variety of outer membrane receptors may be required by different CDI families (Zach Ruhe, Christina Beck, David Low, and Chris Hayes, unpublished data).

With the exception of three extracellular loops, BamA is highly conserved across enterobacteria (159, 191). Given the physical interaction that must occur between BamA and CdiA in order for delivery of CDI toxins to occur, an attractive hypothesis is that the extracellular loops in BamA mediate binding, and polymorphisms in this region may restrict CDI efficacy across species. This hypothesis is supported by experiments showing that the CDI system from EC93 does not inhibit closely-related bacteria such as *Citrobacter freundii*, *Salmonella* Typhimurium LT2, *Proteus mirabilis*, or *Enterobacter* species, but some of these bacteria become CDI-sensitive when they express plasmid-borne $bamA^{E.\ coli}$ (159).

Furthermore, BamA from *Enterobacter cloacae* can be converted into a receptor for $CdiA^{EC93}$ by swapping extracellular loops 6 and 7 with the corresponding sequence from *E. coli* (159). This specificity profile dictates potential CDI interactions and restricts the inhibitory potential of the *E. coli* EC93 CDI system to other *E. coli* strains, thereby constraining the range of target bacteria that are susceptible to attack by *E. coli* CDI systems. This raises the question of what benefit is derived from only targeting sibling cells instead of different species that may be competing for space and nutrients in the same niche.

Genetic selections for *Burkholderia thailandensis* mutants resistant to the CDI system from *Burkholderia pseudomallei* 1026b produced clones with transposon insertions in BTH_I0986, a predicted lipooligosaccharide glycosyl-transferase (192). Cells lacking BTH_I0986 have altered LPS structures and show decreased binding to CDI^+ *Burkholderia* inhibitor strains, indicating that this cell surface alteration affects the ability of CDI inhibitor cells to interact with their targets (192). BamA was not identified as a binding determinant or cell-surface receptor in this study, suggesting that *E. coli* and *Burkholderia* CDI systems utilize distinct mechanisms to recognize their targets.

5. The proton motive force is required for translocation across the inner membrane

Many CDI toxins are nucleases that target intracellular substrates such as DNA or RNA (167, 169, 172, 175, 177, 193). Given the location of these substrates, CdiA-CTs must presumably be delivered into the cytoplasm of target cells in order to exert their toxic effects. We have previously showed that CdiA-CT fragments are transferred into target cells during CDI (194) and that delivery into target cells does not require active protein synthesis by CDI inhibitor cells (172). *E. coli* utilizes the proton motive force (pmf) for a variety of processes, including generating ATP, transporting macromolecules and nutrients, turning

flagella (195), and transporting colicins into the cell (23, 196). CDI toxin delivery also requires an active pmf, and target cells in which the pmf has been disrupted (by chemical uncoupling agents such as CCCP and DNP or by pore-forming CDI toxins) are resistant to inhibition and show no signs of toxin delivery as measured by activity assays (172). This is true for CdiA-CTs with a variety of activities, indicating that the pmf requirement is a general feature of translocation and not a toxin-specific phenomenon.

Membrane-spanning systems such as TonB-ExbB-ExbD transduce the energy of the pmf from the inner membrane to the outer membrane (197, 198), so it is possible that the pmf is required at either one of these barriers. However, cell-cell binding between CDI^+ inhibitors and target cells was not significantly altered when the target cell pmf was disrupted (172). Additionally, pmf-disrupted target cells that were mixed with CDI^+ inhibitors and treated with proteinase K to remove extracellular CdiA retained the ability to import cytotoxic CdiA fragments when the pmf was restored by removal of chemical uncouplers (172). Together, these data suggest that multiple independent steps occur during CDI, and that the pmf-dependent step that occurs during CdiA-CT delivery is downstream of the binding event that occurs at the outer membrane. This also suggests that the initial steps in CDI deliver a CdiA fragment to the periplasm of target cells which remains stable for several minutes and retains the ability to be translocated into the cytoplasm (172).

6. CdiA-CTs do not require Tol and Ton pathways to enter target cells

Of great interest in the CDI field is to determine the relationship between CdiA-CT domains and colicins. Both are, at their core, proteinaceous toxin systems that deliver folded peptides across two membranes into the cytoplasm of target cells. Colicin delivery requires either the Tol system (A group colicins) or the Ton system (B Group colicins) for

translocation (23). CDI systems face the same challenge of moving a cytotoxic protein across cellular membranes, but they accomplish this in a Tol/Ton-independent manner (172). Neither TolA nor TonB are required for inhibition by CDI systems delivering ionophore toxins, DNases, or RNases (172), indicating that this is a general feature of CdiA-CT translocation that is not specific to any one class of toxins. This may be indicative of another energy-transducing step involving CdiA. Much of the structural region upstream of CdiA-CT is uncharacterized, and it is possible that these regions are involved in harnessing the target cell pmf during delivery into cells. With limited exceptions, exogenous addition of purified CdiA-CTs does not result in inhibition (174). Conversely, colicins are small, diffusible toxins that do not need to be physically delivered to target cells in the same way as CdiA-CTs and type 6 secretion system toxins.

Although CDI toxins do not require the Tol or Ton systems to transduce energy during toxin delivery, they may share other commonalities with colicin translocation pathways. Much work has been done to determine the mechanism by which colicins are transported across the inner membrane of target cells. Colicins E3 and E9 have been shown to interact with and be destabilized by membrane phospholipids (80-82, 85), and the inner membrane AAA+ ATPase FtsH has also been implicated in colicin processing during delivery (85, 91, 105). As discussed in Chapter II, we have genetic evidence suggesting that a subset of CDI toxins also require FtsH for toxicity (173). A variety of inner membrane proteins, including ABC and PTS transporters, are required for delivery of other CdiA-CTs (173). The toxins that utilize these inner membrane proteins have diverse activities (167, 169, 175, 193). Therefore, while a pmf-dependent step may be a common feature in the delivery of these toxins across the inner membrane, the mechanistic steps and translocation partners involved

may vary.

7. Crystal structures can inform biochemical activity of CdiA-CTs

Activities for the first characterized CdiA-CTs were identified using a series of biochemical screens and sequence homology to known bacteriocins. Just as colicins have diverse functions, CdiA-CTs that act as DNases, RNases, and pore-formers have been identified (156, 167, 169, 173, 175-177). More than 20 unique families of CdiA-CTs have been identified in *E. coli* alone (170). Although bioinformatics analyses predict the existence of CdiA-CT domains with peptidase and deaminase activities (199, 200), we have yet to experimentally identify any toxins that carry out these functions. Interestingly, there are no known CdiA-CTs that have cell wall-degrading activities similar to that of colicin M (56), perhaps indicating fundamental differences in biogenesis and toxin delivery mechanisms between these toxin families. Recently, we have taken a structural approach to understand the activity of CdiA-CTs which have no significant homology to characterized proteins. The data acquired from these endeavors have provided a wealth of information about many facets of CDI biology, including biochemical activity, inactivation by immunity proteins, and potential sites for evolution and diversification of CdiA-CTs across bacteria.

The first CDI toxins for which crystal structures were resolved were CdiA-CT/$CdiI_{II}^{Bp1026b}$ from *Burkholderia pseudomallei* and CdiA-CT/$CdiI_{o11}^{EC869}$ from *E. coli* EC869 (177). These CdiA-CTs share little sequence homology (approximately 15%), but alignment of their crystal structures revealed striking similarities. Both toxins are composed of a mix of β-strands and α-helices forming a half-β-barrel and are structurally similar to known restriction endonucleases, including the nickase BspD6I and a XisH protein from *Anabaena varabilis* that controls DNA excision (177, 201). Despite this structural

conservation, these CdiA-CTs possess distinct nuclease activities. CdiA-$CT_{II}^{Bp1026b}$ is an Mg^{2+}-dependent tRNase that cleaves alanine and arginine tRNAs in the aminoacyl acceptor stem (169). Based on the nuclease homology revealed by the crystal structure, CdiA-CT_{o11}^{EC869} was found to be a Zn^{2+}-dependent DNase that degrades chromosomal DNA during cell-cell competitions as well as purified DNA *in vitro*. We expand on these results in Chapter V to show that a family of site of immunity interaction (202).

Recently, we published a crystal structure of a CdiA-CT/CdiI pair from *Enterobacter cloacae* (175). CdiA-CT^{ECL} has little sequence homology to known proteins, but the crystal structure revealed structural homology (Z-score of 4.8) to the nuclease domain of colicin E3, which cleaves 16S RNA. CdiA-CT^{ECL} and colicin E3 have a similar core structure composed of a twisted β-sheet, and potential catalytic residues in CdiA-CT^{ECL} superimpose on the known active site residues of E3. Based on this structural similarity, Beck *et al*. confirmed that CdiA-CT^{ECL} also cuts 16S RNA. HecA, a related toxin from Erwinia chrysanthemi EC16, shares a catalytic motif with colicin E3 and also cuts 16S RNA (175, 203). However, molecular modeling suggests that each toxin interacts with the ribosome in a different manner and has a distinct mechanism for RNA cleavage. Together, this illustrates how structural analysis of CdiA-CT families can reveal mechanistic differences in activity despite common core structures.

8. Mechanisms of immunity inactivation revealed by crystal structure analysis

Despite the conservation between CdiA-$CT_{II}^{Bp1026b}$ and CdiA-CT_{o11}^{EC869}, the respective CdiI proteins share little sequence or structural homology, and the mechanisms of inactivation by CdiI are markedly different (177). $CdiI_{II}^{Bp1026b}$ directly binds the active site of its cognate CdiA-CT, rendering this inaccessible to tRNA substrates. $CdiI_{o11}^{EC869}$ binds an

exosite formed by a β-hairpin that protrudes from the core of CdiA-CT_{o11}^{EC869}. β-complementation between these hairpins form a 6-stranded antiparallel β-sheet; this motif is the first β-augmentation interaction identified stable toxin/immunity complexes and resembles structural features of eukaryotic signaling pathways (204), viral capsid assembly (205), and nascent membrane protein contacts with the Bam complex during outer membrane protein biogenesis in prokaryotes (206). Both CdiA-CTs strongly associate with their cognate immunity (K_d values approximately 18-20 nM), but the non-cognate immunity does not block activity *in vitro* or *in vivo* (177).

Similiarly, CdiA-CT^{ECL} and colicin E3 share structural conservation in their nuclease domains, but the methods of inactivation by cognate CdiI proteins is distinct. The CdiA-CT/$CdiI^{ECL}$ interface is a complicated network of hydrogen bonds between residues in both proteins, hydrophobic patches, electrostatic interactions, and water molecules (175). $CdiI^{ECL}$ contains multiple β-sheets that form a compact β-sandwich and protect against cleavage of 16S RNA by directly binding the active site of CdiA-CT^{ECL} (175). In contrast, ImmE3, which inactivates colicin E3, binds an exosite on the toxin and does not directly occlude the active site (207). The immunity proteins do not cross protect against activity of the non-cognate toxin, and this is likely mediated by a structural difference between the orientation of loop 2 in these toxins, the positioning of which may sterically prevent non-cognate immunity interactions. Colicin E3 also contains a C-terminal helix that CdiA-CT^{ECL} lacks, which would likely prevent $CdiI^{ECL}$ from binding to colicin E3. While no structural data is available for the HecA toxin or immunity proteins, the HecA immunity does not protect against CdiA-CT^{ECL} or colicin E3, and neither of these immunity proteins inactivate HecA. Interestingly, colicins E3, E7, and E9 all interact with their respective immunity proteins via

exosite interactions, and it is believed that exosite immunity binding results in electrostatic repulsions between colicins and substrate molecules (78).

Another example of inactivation of CdiA-CTs by active site occlusion comes from $CdiI_{o2}^{MC58\text{-}1}$, an immunity protein from *Neisseria meningiditis* (208). All sequenced *N. meningiditis* isolates contain at least one CDI system, and some strains have multiple CDI loci or complex CDI loci that contain orphan toxin/immunity pairs. $CdiI_{o2}^{MC58\text{-}1}$ contains a helical bundle packed against a 4-strand antiparallel β-sheet and has structural homology to the eukaryotic proteins Why2, a plant ssDNA binding protein involved in DNA repair (209), and MRP1, a mitochondrial RNA binding and editing protein (210). However, $CdiI_{o2}^{MC58\text{-}1}$ lacks the structural regions Why2 and MRP1 use to bind nucleic acids. The CdiA-CT associated with $CdiI_{o2}^{MC58\text{-}1}$ is a predicted Mn^{2+}-dependent nuclease, and a related MafB toxin from *Neisseria* has RNase activity (211). Modeling suggests that $CdiI_{o2}^{MC58\text{-}1}$ blocks the active site of the cognate CdiA-CT to prevent activity. If this CdiA-CT is indeed a nuclease and immunity inactivation occurs by binding the active site, that may explain the structural homology between nucleic acid binding proteins and $CdiI_{o2}^{MC58\text{-}1}$ despite $CdiI_{o2}^{MC58\text{-}1}$ lacking the structural domains required to bind these substrates. Like $CdiI_{o2}^{MC58\text{-}1}$, $CdiI^{ECL}$ is also structurally similar to Whirly proteins (175) and binds the active site of $CdiA\text{-}CT^{ECL}$.

Riley and other colicin biologists have proposed that diversification of bacteriocins occurs at the toxin/immunity interface, where mutations in the immunity that retain high-affinity binding to the colicin are matched by mutations in the toxin (38, 39, 212). Similar evolutionary forces likely contribute to the diversity of CdiA-CT/CdiI pairs, and CdiI sequences usually diverge more than their related CdiA-CT toxins (213). Mechanistic and

evolutionary implications of immunity inactivation will be explored elsewhere in this thesis. Chapter V discusses a superfamily of toxins related to CdiA-CT_{o11}^{EC869} that have highly conserved structures but divergent CdiA-CT/CdiI interfaces (202).

9. Crystal structures contribute to delineation of distinct CdiA-CT domains

Bioinformatic analysis of CDI toxins reveals that many CdiA-CTs are divided into N-terminal and C-terminal domains that independently cluster (193). These domains are functionally interchangeable to some extent (172, 173, 194), and genetic analysis shows that N- and C-terminal domains can "mix and match" in CDI loci, resulting in N-terminal domains fused to different C-terminal sequences (and vice versa). This dual domain architecture is supported by crystal structure analysis of CDI toxins. Interestingly, N-terminal domains are often poorly resolved or completely missing in structures, suggesting that they are susceptible to proteolytic degradation to a greater degree than the compact C-terminal catalytic cores. Coupled with evidence that the C-terminal catalytic cores of many CdiA-CTs are sufficient for activity (169, 177, 193), this suggests that the N- and C-terminal domains are functionally distinct, and the structural features of each may have intrinsic importance for function. Catalytic C-terminal domains must adopt tight, carefully-folded structures to ensure that active site residues are appropriately situated for activity. Perhaps the flexible, disordered nature of N-terminal domains is also critical for their function. Colicins exploit disordered domains to facilitate translocation across membranes into target cells (49, 87). Given the intracellular location of many CDI substrates such as RNA and DNA, CdiA-CTs that target these molecules must presumably cross the outer and inner membranes to exert activity. Chapter II presents work defining the contribution of N-terminal domains to CdiA-CT delivery into the cytoplasm of target cells (173).

10. Some CdiA-CTs require the presence of a cofactor for activity

Many CdiA-CTs are active *in vitro* with only purified components and do not require the presence of other protein factors for activity (167, 169, 175-177, 193). An exception to this is a CdiA-CT from uropathogenic *E. coli* strain 536 (CdiA-CT^{Ec536}), which is a general tRNase that cuts in the anticodon loops of target tRNA (193). Initial studies showed that purified CdiA-CT^{Ec536} does not cleave tRNA *in vitro* unless whole-cell *E. coli* lysate is added to the reaction, suggesting that a cellular cofactor may be needed to activate this toxin (193). This so-called "permissive factor" was identified as CysK, an *O*-acetylserine sulfhydralase that functions with its binding partner CysE to synthesize L-cysteine from L-serine (214, 215). The other *O*-acetylserine sulfhydralase in *E. coli*, CysM (216), does not interact with CdiA-CT^{Ec536} and does not play a role in activating the toxin (193). Interestingly, the enzymatic activity of CysK is not required for its function as a permissive factor, as a K42A mutation that alters a critical pyridoxal 5'-phosphate-coordinating residue (217) still supports CdiA-CT^{Ec536} activity *in vitro* and during CDI in co-culture experiments (193).

The CysK-CysE interaction is mediated by the C-terminal four residues of CysE (sequence GDGI), which bind the active site of CysK (218-220). This motif is nearly identical to the C-terminal residues of CdiA-CT^{Ec536} (sequence GYGI), which are required for binding to CysK and for activation of nuclease activity (193). Preliminary work indicates that CdiI^{Ec536} and CysK do not bind overlapping sites, as ternary complexes with CdiA-CT^{Ec536}, CdiI^{Ec536}, and CysK can be formed from purified proteins (Robert Morse, Celia Goulding, Christina Beck, and Christopher Hayes, unpublished data). CysK enzymes found in Gram-positive organisms can interact with CymR, a transcription factor that controls expression of cysteine biosynthesis genes (221). If the CysK/CdiA-CT^{Ec536} complex has an

additional function such as transcriptional control, cellular communication, or signaling, it could potentially exert this activity even in immune cells that are not susceptible to CdiA-CT^{Ec536}-induced toxicity. Toxicity of CdiA-CT^{Ec536} may also be influenced by environmental conditions that regulate the expression of *cysK*. Expanding our knowledge of CDI systems will determine whether CdiA-CTs utilize additional permissive factors and whether these CdiA-CT/co-factor complexes have biological roles other than inhibition. Chapter VI presents work on the relationship between CdiA-CT domains from *E. coli* and *Klebsiella pneumoniae* and the translation factor EF-Tu, which may function as a co-factor for these toxins.

D. Additional inhibition systems that require physical contact between cells

1. Contact-dependent inhibition systems in Gram-positive bacteria

Other bacterial killing systems that require physical contact between inhibitor and target cells can be broadly classified as contact-dependent inhibition systems. Classical CDI systems are found in Gram-negative bacteria, and the functions of CdiB and CdiA are finely-tuned to support display of an exoprotein on the Gram-negative cell surface. Bridging the outer membrane is specifically achieved by CdiB, which resides in the outer membrane and is responsible for elaborating CdiA on the surface of CDI^+ cells. The mechanistic details of CDI systems are inherently different than protein-based inhibition systems in Gram-positive organisms because of the fundamental differences between Gram-negative and Gram-positive bacterial membranes and cell walls. Gram-negative bacteria are separated from extracellular space by an outer membrane, a periplasmic space containing peptidoglycan, and an inner membrane. The outer leaflet of the outer membrane is composed of lipidpolysaccharide molecules. Gram-positive organisms are surrounded by a single

membrane and a thick cell wall composed primarily of peptidoglycan and smaller amounts of techoic and lipotechoic acids. Though bonafide CDI systems are not present in Gram-positive bacteria, many contain a similar inhibition system composed of the abundant wall-associated protein A (WapA), which is associated with the thick peptidoglycan layer surrounding the cell (222).

WapA was first identified in *Bacillus subtilis* and shares certain characteristics with CdiA. Both are large – CdiA proteins range from 180-640 kDa, and the *Bacillus subtilis* strain 168 WapA is predicted to be approximately 250 kDa – and are associated with the cell surface (168, 170, 213, 222, 223). As with toxicity conferred by CdiA, delivery of WapA-CT domains into target bacteria is contact-dependent. The C-terminal domains of both proteins are highly variable and encode toxic peptides; several WapA-CT regions have been characterized as tRNases (167, 224). WapA-CT^{168} removes the CCA acceptor tail plus an additional nucleotide from the 3´ of tRNA molecules, WapA-CT^{natto} cleaves the anticodon loop of tRNA^{Glu}, and WapA-CT$^{T\text{-}UB\text{-}10}$ cleaves the anticodon loops of tRNA^{Ser} (224). *wapA* is also immediately followed by variable open reading frames that encode immunity proteins that bind to and inactive their cognate WapA-CT toxins. *wapAI* loci are found in a variety of Gram-positive organisms including *Bacillus*, *Geobacillus*, *Anoxybacillus*, and *Listeria* species and may be involved in kin/non-kin discrimination in a manner analogous to Gram-negative CDI systems (159, 224, 225).

2. Rearrangement hotspot systems

rhs genes were first identified as rearrangement hotspots in *E. coli* (226), but they do not mediate large-scale genome rearrangements in the same way as transposable elements or rRNA operons (227). Six families of *rhs* genes have been identified throughout

Enterobacteriaceae (227), and the genetic structure of these loci resemble those that encode CDI systems (176). Two domains consisting of a conserved core and a variable C-terminal tip were originally identified in Rhs proteins (228, 229). Recent work has refined this genetic structure to include four distinct domains: 1) an N-terminal domain that is conserved across *rhs* families, 2) a core domain with conserved secondary structure and glycine residues, 3) a DPXG repeat motif, and 4) a variable C-terminal tip that is not conserved in families, loci, or species. As in *cdi* loci, "orphan" regions are often found downstream of the main *rhs* gene. Many *rhs* tip orphans contain homology to the core domain, suggesting that they can undergo recombination to displace the native C-terminal tip of a given *rhs* loci (227). Sequence analysis reveals the existence of a large genomic reservoir of C-terminal tips in Enterobacteriaceae, suggesting that gene displacement is the primary force behind diversity of *rhs* systems as opposed to rapid evolution of new domains (227). Long-term passaging of *Salmonella* yielded cells in which orphan *rhs* genes had undergone recombination with the main structural gene, resulting in expression and delivery of these domains (230). Indeed, *rhs* elements in *Salmonella* are found on mobile regions, suggesting that they can be transferred between cells through gene transfer (227).

Rhs systems were first linked to CDI bioinformatically, when a C-terminal tip domain and the downstream nucleotides from *Waddlia chondrophila* were found to have homology to a CdiA-CT CdiI module from *Yersinia pestis* (176). As with the VENN tetrapeptide sequences that separate CdiA-CT domains from the rest of CdiA, Rhs-CT domains are demarcated by a conserved PxxxxDPxGL motif (227). Rhs-CT domains from *Dickeya dadantii*, a plant pathogen, inhibit cells via DNA degradation when expressed intracellularly and when delivered into a target cell in a contact-dependent manner. The RhsA-CT domain

from *E. coli* is thought to inhibit cell growth by preventing translation (231). Analogous to CdiI proteins, a small open reading frame downstream of the main *rhs* genes encode an immunity protein that blocks the activity of the cognate Rhs-CT toxin (176, 224). Taken together, these genetic and biochemical data indicate that Rhs proteins encode another contact-dependent bacterial competition system in which a small, variable C-terminal peptide is delivered into neighboring cells.

The C proteins of ABC toxin systems in *Yersinia entomophaga* contain RHS repeats and are predicted to have polymorphic C-terminal toxin domains that are auto-proteolytically processed during delivery (232, 233). Remarkably, these ABC toxin complexes form a cage-like structure that encapsulates the C-terminal toxic region of the C-protein. The RHS repeats in protein C form strand-turn-strand motifs and comprise part of the shell in this structure, and a plug domain orients the toxin towards the lumen of the complex (233). The repeat RHS motifs in *Yersinia* ABC toxins are structurally related to the YD-repeat peptides found throughout bacteria, fungi, and eukaryotes (224, 234). YD-repeat proteins are involved in a variety of signaling pathways in eukaryotes as well as interactions between pathogenic bacteria and host cells (224, 234). Interestingly, the C-terminal ends of some eukaryotic YD-repeat proteins are processed and function as signaling domains. It is therefore intriguing to postulate that Rhs proteins that function as bacterial competition systems and YD-repeat proteins that function in eukaryotic neural signaling pathways may form elaborate conserved cage structures and share processing mechanisms.

Like other bacterial inhibition systems, the distribution of *rhs* genes varies across species. Rhs systems in *Pseudomonas* can also produce bacteriocins (235) or target eukaryotic cells and elicit an immune response (236). These gene clusters are also widespread in clinically-

relevant pathogens such as *Rothia mucilaginosa*, which can cause infections in patients with cystic fibrosis or suppressed immune systems (237). *Salmonella* strains usually have only one full-length copy, but *E. coli* and *Shigella* contain multiple Rhs systems (227). While lab strains of *E. coli* do not contain inhibition systems such as colicins or CDI, they contain up to 5 *rhs* loci (238). In many species, *rhs* genes are associated with the *vgr* genes that are hallmarks of type 6 secretion systems (T6SS, discussed below) (227). The Rhs-CTs from *Dickeya dadantii* are deployed in a T6SS-dependent manner (224). This feature distinguishes Rhs from CDI systems, which do not require additional components outside of the *cdi* locus for activity. Rhs systems have also been implicated in social behaviors such as mobility in *Myxococcus xanthus* (239). While *rhs* genes are widely distributed, it is still unknown how they are regulated and under what conditions they are expressed (228). The role of Rhs in cellular communication and competition both as a stand-alone system and as intertwined with other inhibition mechanisms is invariably complex and remains to be elucidated.

3. Type 6 secretion systems

CDI is a relatively simple inhibition system in that the three core genes in *cdi* loci are sufficient to confer an inhibitory CDI^+ phenotype to CDI^- cells. Of greater complexity are the type 6 secretion systems (T6SS) found throughout Gram-negative bacteria that inhibit both prokaryotic and eukaryotic cells (240-242). T6SS loci encompass more than a dozen genes required for activity, stretching across 20 kilobases in some organisms (243). The number of T6SS loci in a given organism varies greatly; *Enterobacter cloacae* contains two T6SS loci (244), the well-studied T6SS model organism *Pseudomonas aeruginosa* has three (245, 246), and a whopping six distinct systems have been identified in *Burkholderia*

thailandensis (247). The existence of so many independent T6SS loci in the same organism is especially interesting considering the size of these systems.

These structures mimic inverted phage tail spikes, which may be indicative of their evolutionary history in the bacterial lineage (248-252). The T6SS core apparatus contains two proteinaceous tubes. The inner sheath is composed of Hcp homohexamer subunits, which can contain toxic effector molecules encompassed in its central pore (245, 253), and the outer sheath is made of VipA and VipB (also annotated as TssB/TssC) (252). The inner Hcp tube is required for assembly of the entire sheath, suggesting that Hcp polymerization precedes formation of the outer tube and may be important for scaffolding its assembly (254). These are attached to the cell envelope via a membrane complex containing TssL, TssM, and TssJ (252), which in turn is capped by a baseplate that resembles phage structures used to anchor viruses to the cell surface (248, 255). The baseplate anchors the T6SS assembly to the inner membrane of cells and is composed of TssE, TssK, and VgrG proteins (256, 257). Upon recognition and firing into target cells, the inner Hcp is destabilized, releasing Hcp into the extracellular milieu as well as Hcp, VgrG, and effector molecules into target cells (240, 244, 246, 253). After firing, the apparatus is disassembled by ClpV, an ATPase that unfolds VipB and destabilizes the sheath (252, 258, 259).

Though the general regulation of T6SS loci is poorly-characterized, some progress has been made towards understanding the cues that activate these systems. Work on the *P. aeruginosa* T6SS shows that this system fires into target cells in response to attack from other species expressing active T6SS, constituting a "tit-for-tat" response that ensures T6SS firing and effector delivery happens under conditions of duress (260). T6SS firing also occurs in response to detection of type 4 secretion system structures as well as membrane

disruptions by polymixin B (261). This level of control is practical considering the resources required for construction and firing.

Although many T6SS systems deploy effectors of unknown function, a variety of toxins from these systems have been characterized. These effector molecules target both periplasmic and cytoplasmic components of bacteria as well as eukaryotic cells and carry out a diverse array of activities. So far, phospholipases, $NAD(P)^+$ hydrolases, DNases, peptidases, muramidases, and peptidoglycan amidases have been identified as T6SS effectors (240, 244, 246, 253, 262). Therefore, T6SS effectors must necessarily localize to different compartments in target cells. Current T6SS models posit that delivery of effector molecules is facilitated by the sheath puncturing the outer membrane of target cells and releasing Hcp and associated proteins into the periplasm. Given the somewhat crude method of delivery, it is thought-provoking to consider T6SS effectors must necessarily localize to different cellular compartments. A recent study shows that the elongation factor EF-Tu is required for the import of a cytoplasmic-acting effector from *P. aeruginosa* (262). As discussed in Chapter VI, the requirement for this protein co-factor may be shared with other inhibition systems such as CDI. However, the exact translocation pathways for T6SS effectors that must reach the cytoplasm are unknown, as is the regulation of membrane puncture into the periplasm during delivery. As previously mentioned, a functional T6SS is required for delivery of Rhs toxins from *D. dadantii*, hinting at an even greater degree of complexity in the role of this system in bacterial physiology (224).

E. Thesis overview

Bacterial competition systems, including contact-dependent growth inhibition (CDI), are widespread throughout bacteria. Much of the early work on CDI demonstrated the scope and

complexity of *cdi* loci throughout Enterobacteriaceae and unraveled preliminary mechanistic details of target cell recognition and toxin activities (127, 156, 167, 168, 176, 194). In this thesis, we build upon this past work and also begin to address fundamental questions regarding the role of CDI in complex environments. In Chapter II, we present a recently-published study describing the translocation of CdiA-CT domains into target cells, demonstrating that different toxin families require unique delivery pathways across the inner membrane. Chapter III contains unpublished work examining the role of a specific inner membrane required for the translocation of CdiA-CT_{o11}^{EC869}, a toxin from *E. coli*. This inner membrane protein, called YciB, is uncharacterized in *E. coli*. We provide evidence that this protein is required for metal tolerance, thus complementing its role in CDI with a role in normal *E. coli* physiology. In Chapter IV, we investigate the target cell stress response to delivery of CdiA-CT_{o11}^{EC869} and the resulting DNA damage. This constitutes the first attempt to characterize an outcome other than immediate cell death that could be relevant in a natural bacterial community undergoing CDI. Chapter V characterizes the superfamily of CdiA-CT_{o11}^{EC869}-related toxins and specifically examines the CdiA-CT/CdiI interface to better understand diversification of this family of toxins throughout evolution.

In Chapter VI, we present data suggesting that the elongation factor EF-Tu interacts with multiple CdiA-CTs in different ways. In theory, this complements the recent finding from the T6SS field that EF-Tu is required for import of an effector molecule (262). Finally, we step outside of bacterial physiology in Chapter VII to adapt CDI systems for synthetic biology purposes. The conclusion chapter contains speculation on uncharacterized aspects of CDI systems, especially the regulation of these loci in natural environments.

II. CDI toxins exploit multiple independent cell-entry pathways

A majority of this work has been published in the Proceedings of the National Academy of Sciences (USA). Permission to reprint was obtained prior to inclusion in this thesis.

A. Introduction

Bacteria are constantly in competition for environmental resources and have evolved a number of systems to suppress the growth of competing cells. Research during the past decade has revealed that Gram-negative bacteria commonly use type V and type VI secretion systems to deliver protein toxins into neighboring cells (213, 243). The type V mechanism was the first to be identified and has been termed contact-dependent growth inhibition (CDI) because inhibitor cells must make direct contact with target bacteria to transfer toxins (156, 157). CDI^+ bacteria express CdiB/CdiA two-partner secretion (TPS) systems, which assemble as a complex on the cell surface. CdiB is an outer-membrane β-barrel protein required for the export and presentation of toxic CdiA effectors. CdiA proteins are very large (180–630 kDa depending on bacterial species) and are presented as individual β-helical filaments that emanate several hundred angstroms from the inhibitor-cell surface (263). CdiA binds to specific outer-membrane receptors on susceptible bacteria and transfers its C-terminal toxin domain (CdiA-CT) into the target cell (159, 167). CDI^+ bacteria also produce CdiI immunity proteins to protect themselves from toxin delivered by neighboring sibling cells. The immunity protein binds to the CdiA-CT and neutralizes its toxin activity (167, 169). Notably, CdiA-CT/CdiI sequences are highly variable between bacteria and even between different strains of the same species (167, 169). For example, isolates of *Escherichia coli* contain at least 20 CDI toxin/immunity sequence types. These toxin/immunity protein families are distinct from one another and form specific CdiA-

CT/CdiI cognate pairs. Because CdiI immunity proteins do not protect against noncognate toxins, CDI provides a mechanism for self/nonself recognition between bacteria.

A remarkable feature of CDI is the modularity of CdiA-CT toxins, which can be exchanged between different CdiA proteins to generate functional chimeras. All CdiA proteins have a similar architecture consisting of an N-terminal TPS transport domain, an extended central region of filamentous hemagglutinin peptide repeats, and the CdiA-CT toxin region (Figure 1A). In many bacteria, the variable CdiA-CT region is demarcated by the VENN peptide motif, which forms the C-terminal boundary of the pretoxin-VENN domain (Figure 1A) (167, 200). Heterologous CdiA-CTs can be delivered into *E. coli* target cells when fused to the VENN sequence of $CdiA^{EC93}$ from *E. coli* EC93 (167, 172, 175, 177, 194). Closer examination of the CdiA-CT region reveals that it is often composed of two variable domains that assort independently to form CdiA-CT composites (Figure 1B). For example, the $CdiA\text{-}CT^{EC536}$ from uropathogenic *E. coli* 536 and $CdiA\text{-}CT^{ECL}$ from *Enterobacter cloacae* American Type Culture Collection 13047 (ECL) share nearly identical N-terminal domains but carry different C-terminal nucleases (175, 193). The function of the CdiA-CT N-terminal domain has not been examined, but biochemical studies show this region is not required for nuclease activities *in vitro* (169, 177, 193). Here, we provide evidence that the N-terminal domain of the CdiA-CT region plays a critical role in toxin translocation during CDI. Using a genetic approach, we identified a collection of CDI-resistance (CDI^R) mutations that protect *E. coli* target cells from specific CDI toxins. Each CDI^R mutation disrupts expression of an inner-membrane protein (IMP) and confers resistance to CdiA-CTs that share homologous N-terminal domains. We also demonstrate that the N- and C-terminal domains of CdiA-CT regions can be recombined to produce novel hybrids that are functional

in cell-mediated CDI. We propose that the N-terminal domain of the CdiA-CT region binds to specific IMP receptors and mediates toxin transport across the inner membrane.

B. Results

1. Resistance to CdiA-CTs is conferred by mutations in genes encoding inner membrane proteins

We performed a series of selections for CDI-resistant (CDI^R) *E. coli* mutants, reasoning that protective mutations would disrupt genes required for toxin import and/or activation. Plasmid-borne chimeric CDI systems were constructed in which heterologous *cdiA-CT*/*cdiI* coding sequences were fused at the VENN encoding region of $cdiA^{EC93}$ (Figure 1A). Each chimeric fusion was functional in CDI, reducing target-cell viability between 10^3- and 10^6-fold during co-culture (Figure 1C). Moreover, target bacteria were protected when provided with the appropriate cognate *cdiI* immunity gene (Figure 1C), indicating that the grafted CdiA-CTs are responsible for growth inhibition. Inhibitor strains were then used to enrich CDI^R target cells from a pool of *mariner* transposon-insertion mutants. CDI^R mutants were selected with iterative cycles of competition co-culture until the target-cell population was fully resistant. We isolated individual target-cell clones from independent experiments and tested CDI^R phenotypes in competitions. Linkage of CDI^R to each transposon insertion was confirmed by transduction. Identification of the transposon-insertion sites revealed that resistance to a given CdiA-CT toxin was due to disruption of one or two genes. For example, CDI^{MHI813}-resistant mutants contained independent insertions in *metI*, whereas the nine CDI_1^{Dd3937}-resistant mutants had multiple insertions within *rbsC* (Figure 2A). CDI^{TTO1}-resistant mutants were disrupted in *gltK* or *gltJ*, and CDI_{o11}^{EC869}-resistant mutants carried insertions in *yciC* or *yciB* (Figure 2A). Interestingly, *ptsG* mutations were isolated from

selections for resistance to CDI^{NC101} and CDI^{EC3006} (Figure 2A). Notably, each disrupted gene encodes an integral membrane protein. MetI, RbsC, and GltJ/GltK are ABC transporter membrane permeases for D/L-methionine, D-ribose, and L-glutamate/L-aspartate, respectively (264-266). PtsG is the main phosphotransferase system permease for D-glucose (267). The functions of YciC and YciB are unknown, but both are predicted integral IMPs. In-frame deletions were constructed for each gene to confirm its role in CDI^{R} (Figure 2B). This analysis showed that Δ*yciC* mutants are not resistant to CDI_{o11}^{EC869} (Figure 3), indicating that the original *yciC* insertion exerts a polar effect on *yciB* (Figure 2A). Complementation analysis confirmed the role of *yciB* in the CDI_{o11}^{EC869} pathway, and showed the *metI, rbsC, gltK*, and *ptsG* are required for their respective CDI pathways (Figure 3). We also tested each in-frame deletion strain in competitions against other inhibitor strains and found that resistance was specific, such that Δ*metI* cells were resistant to CDI^{MHI813} but susceptible to other CDI systems (Figure 2B). Thus, each CDI system requires a specific IMP to inhibit target cells.

2. CdiA-CTs are not delivered to the cytoplasm of target cells in the absence of inner membrane proteins required for translocation

Given that CDI^{R} was invariably associated with disruption of IMPs, we hypothesized that CDI toxins exploit these proteins to enter target bacteria. We tested whether CDI toxins are delivered into CDI^{R} target cells by monitoring nuclease activities in competition co-cultures. CdiA-CT_{o11}^{EC869} toxin has a potent DNase activity that produces anucleate target cells (Figure 4A) (177). However, Δ*yciB* mutants retained normal nucleoid morphology during co-culture with CDI_{o11}^{EC869} inhibitors and appeared similar to immune target cells that express the $CdiI_{o11}^{EC869}$ immunity protein (Figure 4A). We also examined the tRNase

activity of CdiA-CT^{EC3006}, which specifically cleaves tRNA$_1^{Ile}$. Cleaved tRNA was detected in *ptsG*+ cells after 1 h incubation with CDI^{EC3006} inhibitors, but no tRNase activity was observed in co-cultures with Δ*ptsG* targets (Figure 4B). These results suggest that toxin is excluded from the cytoplasm of CDI^R target cells. Alternatively, the IMPs could function as so-called permissive factors, which activate CDI toxins after entry into target bacteria (193). This latter model predicts that CDI^R mutants should also be resistant to toxin produced internally. To test this model, we used controllable proteolysis to degrade *ssrA*(DAS)-tagged immunity proteins and thereby activate toxins inside the cell (169, 176, 268). CdiA-CT$_{o11}^{EC869}$ activation was slow in *yciB*+ cells, with growth inhibition and *in vivo* DNase activity observed after 3 h (Figure 5A). In contrast, Δ*yciB* cell growth was inhibited immediately upon toxin activation, and DNase activity was apparent within 1 h (Figure 5A). Similar results were obtained when CdiA-CT^{EC3006} was activated in *ptsG*+ and Δ*ptsG* cells, in which growth inhibition was immediate and tRNase activity was identical in both backgrounds (Figure 5B). These results show that CdiA-CT$_{o11}^{EC869}$ and CdiA-CT^{EC3006} retain full toxicity when expressed inside CDI^R mutant strains, excluding the toxin-activation model. Together, these data support a role for IMPs in the delivery of CDI toxins into the target-cell cytoplasm.

3. *The N-terminal domain of CdiA-CTs specifies translocation across the inner membrane of target cells, which does not require canonical transport function of inner membrane protein complexes*

Most of the CDI^R mutations disrupt metabolite permeases, raising the possibility that transport activity could play a general role in CDI toxin import. We tested mutants lacking the cytoplasmic ATP-binding components of the Met (Δ*metN*), Rbs (Δ*rbsA*), and Glt (Δ*gltL*)

ABC transporters and found that each strain was still sensitive to CDI (Figure 6). We also tested PtsG proteins that carry the Cys421Ser mutation and lack the entire cytoplasmic IIB domain, both of which are unable to transport D-glucose (267, 269). Each transport-defective PtsG protein rendered Δ*ptsG* cells sensitive to CDI^{EC3006} (Figure 6). Therefore, the membrane permeases are required for CDI-mediated growth inhibition, but their metabolite transport activities are not.

ptsG mutants were isolated in selections for resistance to CDI^{NC101} and CDI^{EC3006} (Figure 2A). These CdiA-CT sequences are 73.7% identical over the first 167 residues, but the C-terminal nuclease domains are unrelated (Figure 7A). The CdiI immunity proteins also share no significant homology (Figure 7B). In accord with this divergence, neither immunity protein protects against inhibition by the heterologous system (Figure 7C). Together with previous analyses of CDI toxins (169, 177, 193), these observations indicate that CdiA-CT regions are often composed of two domains, with the extreme C-terminal domain containing the actual growth inhibition activity. Moreover, the genetic interaction between PtsG and the N-terminal sequences of $CdiA\text{-}CT^{NC101}$ and $CdiA\text{-}CT^{EC3006}$ suggests that the shared domain specifies the cell-entry pathway. The CdiA-CTs from uropathogenic *E. coli* 536 (EC536) and ECL also share N-terminal domains, but carry different C-terminal RNase domains and have distinct immunity proteins (Figure 8A and B) (175, 193). Based on reports that *E. coli* Δ*ftsH* mutants are resistant to multiple colicin nucleases (85, 91, 105), we screened Δ*ftsH* cells in CDI competitions and discovered that they are resistant to CDI^{EC536} and CDI^{ECL}, but sensitive to inhibition by CDI^{EC93} (Figure 8C). FtsH is a hexameric AAA+ unfoldase/protease that is tethered to the inner membrane through two transmembrane helices, again suggesting that each CDI system exploits a specific IMP. Δ*ftsH* mutants are

also resistant to the CdiA-CT^{PestA} toxin from *Yersinia pestis* Pestoides A, which shares the N-terminal domain with CdiA-CT^{EC536} and CdiA-CT^{ECL} (Figure 8A and B). Together, these data show that CdiA-CT regions are commonly composed of two variable domains and suggest that the N-terminal domain may dictate the cell-entry pathway.

Analyses of naturally occurring CdiA-CTs suggest that the N- and C-terminal domains can be rearranged to deliver nucleases through different pathways. We tested this prediction with novel CdiA-CT hybrid constructs. We fused the N-terminal domain of CdiA-CT^{EC3006} (Val1–Leu167, numbered from Val1 of the VENN motif; Figure S3A) to the DNase domain of CdiA-CT$_{o11}$^{EC869} (Ala154–Lys297) (177) (Figure 6), and then grafted the hybrid onto CdiA^{EC93} to generate a chimeric CDI system. The resulting triple chimera reduced target-cell viability ~100-fold in co-culture, and target cells were protected when they expressed *cdiI*$_{o11}$^{EC869} but not the *cdiI*^{EC3006} immunity gene (Figure 9). We then tested the EC3006/EC869o11 hybrid against Δ*yciB* and Δ*ptsG* target cells and found that only Δ*ptsG* mutants were resistant (Figure 9). We used the same approach to deliver the CdiA-CT^{EC536} tRNase domain (Lys127–Ile227) into target cells with the CdiA-CT^{EC3006} N-terminal domain (Figure 10). As expected, CdiI^{EC536} protein protected target cells from the EC3006/EC536 hybrid, and growth inhibition required PtsG (Figure 10). These results show that the two CdiA-CT domains are modular, and nucleases can be delivered through different pathways specified by the N-terminal domain.

4. FtsH activity is required for delivery of a class of CdiA-CTs but may be via an indirect mechanism as opposed to a direct interaction

FtsH is a hexameric zinc-dependent protease that belongs to the AAA+ family of ATP-dependent proteases. It is tethered to the inner membrane by two transmembrane domains

connected by a 72-residue periplasmic loop (Figure 11) and contains cytoplasmic ATPase and protease domains (270, 271). Because Δ*ftsH* cells were resistant to inhibition by CdiA-CT^{EC536}, CdiA-CT^{ECL}, and CdiA-CT^{PestA}, we wished to determine whether the activity of FtsH is required for translocation of these toxins or whether CdiA-CTs use FtsH in a different manner.

We first asked whether the full-length FtsH protein is required for inhibition. Our previous results demonstrate that transport-deficient PtsG mutants carrying either the Cys421Ser mutation or lacking the cytoplasmic IIB domain still support CDI. Therefore, we wished to determine whether ATPase or protease function of FtsH is required for translocation of CdiA-CT domains. To test this, we constructed truncations at residues K129 (which maintains the membrane-spanning domains but removes the ATPase and protease domains) and S400 (which removes only the protease domain) and transformed these into Δ*ftsH* cells. We then mixed these with cells delivering CdiA-CT$_{o1}^{EC93}$, an orphan toxin found in the *cdi* locus first identified in *E. coli* EC93. This toxin is 76% identical to CdiA-CT^{EC536} (Figure 12A) and belongs to the same N-terminal domain family as CdiA-CT^{ECL} and CdiA-CT^{PestA}. As predicted, CdiA-CT$_{o1}^{EC93}$ is also FtsH-dependent (Figure 12A). Cells expressing the K129 or S400 truncations in place of full-length FtsH were not inhibited by CdiA-CT$_{o1}^{EC93}$, indicating that the entire protein is necessary for CDI (Figure 12B). To determine whether the specific protease or ATPase function of FtsH is required for CDI as opposed to simply the physical presence of these domains, we constructed point mutants in these regions. Phe228Ala changes a key phenylalanine inside the substrate pore, and His414Tyr mutation disrupts the first of two histidine residues found in the HEXXH zinc-coordinating motif of the FtsH protease domain; both mutations disrupt activity, as evidenced

by the ablation of proteolysis of RpoH (σ^{32}), a heat shock transcription factor (85, 272-274). Neither mutant complemented CDI resistance of Δ*ftsH* targets during co-culture with CDI_{o1}^{EC93} inhibitor cells (Figure 12B).

During translocation into target cells, CDI nuclease toxins presumably traverse the periplasmic space as they cross from outer to inner membrane. Therefore, we reasoned that if FtsH makes direct contact with CdiA-CTs, this may be facilitated by the 72-residue periplasmic loop that spans the two transmembrane domains anchoring FtsH to the inner membrane (271). This region mediates the interaction between FtsH and the membrane-anchored proteins HflKC and is also involved in substrate recognition and specificity (270). The loop is highly conserved in *E coli* and closely-related species but varies in other Gram-negative bacteria (Figure 11B). A comparison of the FtsH periplasmic domains from *E. coli* and *Proteus mirabilis* reveals that the loops are only 56% conserved, as opposed to approximately 90% homology across the rest of the protein (Figure 13A). Therefore, we constructed an FtsH chimera in which the first 196 residues from *E. coli* were replaced with the corresponding region from *Proteus mirabilis*, resulting in a protein with the *P. mirabilis* periplasmic loop. We then transformed this construct into Δ*ftsH* cells and measured survival during co-culture assays against CDI_{o1}^{EC93} and CDI^{ECL} inhibitor cells. Cells expressing $FtsH^{EC\text{-}Proteus}$ were inhibited to wild-type levels, indicating that this construct supports CDI (Figure 13B). Furthermore, we note that $FtsH^{EC\text{-}Proteus}$ rescues the severe growth defect observed with Δ*ftsH* cells (data not shown), indicating that this protein is functional.

Using CdiA-CT_{o11}^{EC869} and CdiA-CT^{3006}, we demonstrated that the IMPs required for delivery of these domains is not involved in activation of intracellular toxin (Figure 5). Because FtsH is a protease, we wondered whether this IMP is necessary for the function

FtsH-dependent toxins, or whether its role (direct or indirect) is solely part of the translocation process. To test this, we fused the CdiA-CT/CdiI^{Ec536} module (starting at the VENN tetrapeptide motif of CdiA-CT) to an *ssrA*(DAS) tag. This construct results in degradation of the immunity protein and release of intracellular toxin. We then performed a transformation assay using this construct or an empty vector plasmid control into wild-type and Δ*ftsH* cells and observed the growth of colonies on LB-agar plates supplemented with 150 μg/mL ampicillin. Both cell backgrounds grow when the empty pTrc99a plasmid is transformed, although we note that the Δ*ftsH* strain has a severe growth defect that manifests as smaller colonies (Figure 15, left panel). When the CdiA-CT/CdiI^{Ec536}-*ssrA*(DAS) construct is expressed, both strain fail to form colonies. A Δ*cysK* control grows under both conditions; CysK is a cysteine biosynthesis enzyme required for activation of CdiA-CT^{Ec536} (193). Because Δ*ftsH* cells fail to grow when intracellular toxin is produced, this suggests that this IMP is not required for activity of CdiA-CT^{Ec536} and instead functions solely in the translocation step of CDI.

5. *Expression of inner membrane proteins required for inhibition permits delivery of CdiA-CTs across species*

CDI systems are generally conserved between bacteria, but *Burkholderia* systems have an alternative gene order, and the CdiA-CT region is demarcated by a distinct ELYN peptide motif(169, 182). We found that fusion of CdiA-CT$_{II}^{Bp1026b}$ (Glu1–Asn297, numbered from Glu1 of ELYN) from *Burkholderia pseudomallei* 1026b to CdiA^{EC93} produces a nonfunctional chimera (Figure 14A). However, the C-terminal tRNase domain from CdiA-CT$_{II}^{Bp1026b}$ (Thr162–Asn297) can be delivered efficiently when fused to the N-terminal domain of CdiA-CT$_{o11}^{EC869}$ (Figure 14A). Moreover, as predicted from the delivery domain

model, *E. coli* Δ*yciB* mutants are resistant to the EC869o11/Bp1026b hybrid CdiA-CT (Figure 14A). This latter result shows that the *Burkholderia* tRNase domain can be delivered into *E. coli* target cells, raising the possibility that *E. coli* lacks the pathway required for native CdiA-$CT_{II}^{Bp1026b}$ import. We recently discovered that *Burkholderia thailandensis* ΔBTH_II0599 mutants are resistant to the $CDI_{II}^{Bp1026b}$ system (192). BTH_II0599 encodes a member of the major facilitator superfamily (MFS), which are integral membrane transporters of small metabolites and antibiotics (275). BTH_II0599 is highly conserved among *Burkholderia* species, but homologs are absent from enterobacteria. Therefore, we provided *E. coli* cells with plasmid-borne BTH_II0599 and tested them as targets in competitions against inhibitors that deploy the native CdiA-$CT_{II}^{Bp1026b}$. Remarkably, cells that express BTH_II0599 became sensitized to growth inhibition, and showed a ~15-fold decrease in viable cell counts after 3 h (Figure 14B). Moreover, sensitized target cells were protected when they expressed the cognate $cdiI_{II}^{Bp1026b}$ immunity gene (Figure 14B), indicating that the CdiA-$CT_{II}^{Bp1026b}$ tRNase domain mediated growth inhibition. Collectively, these data reveal a genetic interaction between the N-terminal domain of CdiA-$CT_{II}^{Bp1026b}$ and BTH_II0599 and suggest that this MFS protein is required for toxin translocation into target bacteria.

C. Discussion

We previously reported that variable CdiA-CT regions are often composed of two domains (169, 175, 177, 193). The extreme C-terminal domain typically has nuclease activity and is sufficient to inhibit growth when expressed inside *E. coli* cells (175, 177, 193). In contrast, the N-terminal domain of the CdiA-CT has no inhibition activity, and its function has not been explored. The findings presented here suggest that the N-terminal domain is

critical for nuclease toxin translocation during CDI. This model is based on the identification of multiple CDI^R mutations that disrupt integral membrane proteins and concomitantly protect target bacteria from specific CdiA-CT toxins. In principle, these membrane proteins could function as permissive factors that bind and activate CdiA-CT toxins after delivery (193). However, CdiA-CT_{o11}^{EC869} and CdiA-CT^{EC3006} nuclease domains have full activity when expressed inside CDI^R mutants, excluding permissive factor function (Figure 4). Moreover, *ptsG*, *yciB*, and *ftsH* mutants are resistant to CdiA-CTs based on the identity of the nontoxic N-terminal domains. These genetic interactions suggest that N-terminal domains use specific IMPs as receptors during CDI. Although our data do not demonstrate direct toxin–IMP interactions, this model is supported by experiments showing that BTH_II0599 expression sensitizes *E. coli* to the native CdiA-$CT_{II}^{Bp1026b}$ toxin. Because BTH_II0599 is completely heterologous, with no homologs in γ-proteobacteria, the simplest explanation is that CdiA-$CT_{II}^{Bp1026b}$ binds directly to this IMP to translocate into the cytoplasm. Moreover, the N-terminal domain of CdiA-$CT_{II}^{Bp1026b}$ is limited to *B. pseudomallei* systems, arguing that these effectors target only other *Burkholderia* that contain BTH_II0599 homologs.

Crystal structures are available for three CDI toxin/immunity protein complexes, but the N-terminal domain is resolved in only one model (175, 177). Residues Met86–Thr153 of CdiA-CT_{o11}^{EC869} form a small helical bundle that packs against the C-terminal DNase domain (177). The tertiary contacts with the nuclease domain probably facilitated the resolution of this domain. For many other CdiA-CT regions, the N- and C-terminal domains are connected by flexible peptide linkers, suggesting the domains have few or no tertiary contacts and move independently of one another. Additionally, the N-terminal domains do not make direct contacts with CdiI immunity proteins (175, 177, 193). Together, these

observations suggest that the N- and C-terminal domains are autonomous units that can be recombined in virtually any combination. Although this hypothesis is supported by the functional hybrid CdiA-CTs constructed in this work, we note that the reengineered toxins are less effective than their naturally occurring counterparts. Thus, a given nuclease domain may have a preferred translocation pathway that is more efficient than others.

It is apparent that CdiA-CT nuclease domains are delivered into the target-cell cytoplasm (172, 175, 177, 194), but the molecular details of CDI toxin translocation remain obscure. Most of the IMPs identified here are metabolite transporters, but our data indicate that transporter activity is not required for toxin import. Moreover, it seems unlikely that protein toxin domains could be transported in the same manner as small molecules due to size constraints of the pores used for transporting metabolites. An interesting caveat to this model is the translocation of FtsH-dependent CdiA-CT domains. Data obtained from co-culture assays shows that FtsH proteins lacking either the protease domain or both the protease and ATPase domains (truncations at residues Ser400 or Lys129, respectively) do not support CDI, suggesting that the function of at least one of these domains is required for the role of FtsH in CdiA-CT translocation. However, it is unknown whether these truncated proteins correctly localize to the inner membrane, thereby complicating the interpretation of these results. Targeted point mutations that alter the substrate pore or disrupt protease activity (Phe228Ala and His414Tyr, respectively) also prevent inhibition of target cells, which is unlike other IMP complexes tested in this study. The simplest explanation would posit that the activity of FtsH is directly required for translocation of CdiA-CT domains, but careful consideration of FtsH activity complicates this model. Cytoplasmic and membrane-associated FtsH substrates are threaded into the substrate pore in the cytoplasm, not the

periplasm; delivered CdiA-CT fragments reside in the periplasm before the final translocation step across the inner membrane into the cytoplasm (111, 172, 276-279). Furthermore, FtsH degrades proteins in a processive manner that produces short peptides (280). The processivity of this activity would most likely not cleave CdiA-CT proteins at a single location, and would instead produce multiple small peptides. Given the minimum size of cytotoxic CT domains (167, 169, 177, 193, 202), it is unlikely that the small byproducts of FtsH degradation would be of sufficient size to carry out toxic activity.

Instead of cleaving CdiA-CT molecules during delivery, FtsH may have an indirect influence on CDI. FtsH regulates the *E. coli* heat shock response by rapidly degrading the transcription factor RpoH (with the help of DnaKJ adaptor proteins) under normal physiological conditions (109, 276). During heat stress, RpoH is no longer efficiently degraded by FtsH, and it interacts with RNA polymerase to upregulate expression of a suite of heat shock response genes. Another FtsH regulatory network could control expression of additional inner membrane proteins that are required for inhibition by CdiA-CT^{ECL}, CdiA-CT^{EC536}, CdiA-CT$_{o1}{}^{EC93}$, and CdiA-CT^{PestA}. Alternatively, FtsH may also continually degrade the binding partner of another inner membrane protein. In the absence of the protease, this ligand could accumulate and interact with a given IMP, blocking translocation of an incoming CdiA-CT. FtsH could also regulate another protease or protein responsible for processing CdiA-CTs during delivery. In these models, the absence of FtsH could leave CDI proteins in limbo in the periplasm during delivery, unable to complete translocation into the cytoplasm. We have previously demonstrated that delivery of CdiA-CTs across the inner membrane requires the proton motive force of target cells, and that a stable fragment of CdiA resides in the periplasm of de-energized cells. Upon restoration of pmf, delivery resumes,

and CdiA-CT activity can be detected (172). Perhaps future work will consider the total proteome of FtsH targets in wild-type and Δ*ftsH* cells in an effort to determine whether another protein is required for translocation of this family of CdiA-CTs across the inner membrane of target cells.

Another mechanism by which FtsH may influence CdiA-CT delivery is through an interaction with the membrane-associated periplasmic proteins HflKC. Heterodimers of these proteins decorate the periplasmic face of FtsH and regulate activity against some substrates, including SecY (270, 278, 281, 282). The HflKC interaction is mediated by the FtsH 72-residue periplasmic loop connecting the transmembrane domains (270). If delivery of CdiA-CTs is mediated by HflK or HflC, one might predict that a non-canonical periplasmic loop would affect sensitivity of target cells. However, the $FtsH^{Ec\text{-}Proteus}$ chimera was inhibited to wild-type levels. While it remains to be determined whether HflK and HflC interact with the *P. mirabilis* periplasmic loop, the sensitivity of target cells carrying this construct diminishes the probability that CDI delivery is mediated by a sequence-specific feature or interaction involving the periplasmic loop. It would be interesting to perform the same experiment with a construct containing a drastically-different periplasmic loop region, such as that from *Bacillus subtilis*[1].

Substrate processing by FtsH can be initiated in a variety of ways. Direct interaction between substrate and FtsH can be occur via N- and C-terminal recognition motifs, and more complex processing networks (such as the DnaKJ-mediated degradation of RpoH) require internal substrate sequences (109, 110, 276, 283). This latter data is consistent with other

[1] We note that an $FtsH^{Ec\text{-}Bacillus}$ construct was made but does not rescue the growth defect observed with *ftsH* knockouts, and that this complicates the interpretation of any inhibition experiments performed with these strains. Interestingly, *ftsH* is not essential in *Bacillus subtilis*.

protease/substrate interactions, including the degradation of RepA by ClpAP and of MuA by ClpXP (284). Hoskins and colleagues found that unfolding and degradation of an N-terminal GFP-RepA fusion protein by ClpAP was dependent on the N-terminal 15 residues of RepA, even when that motif was located in the middle of the fusion protein sequence. A similar, albeit less efficient, phenomenon was observed with the ClpXP protease and the C-terminal recognition motif of MuA in a MuA-GFP chimera (284). Therefore, it is plausible that an internal motif in CdiA-CT is processed, liberating this domain from a larger CdiA fragment and allowing for translocation of only the cytotoxic CdiA-CT. Although preliminary sequence analysis has not revealed any strong or canonical FtsH recognition sequences, it remains to be determined whether CdiA-CTs contain cryptic motifs or processing sites. LpxC, which is contains a C-terminal FtsH recognition sequence (**LA**FKAPS**AVLA**, where bolded residues are required) (276). Other recognition motifs are characterized by the presence of small hydrophobic residues that are required for recognition by FtsH (108, 111, 276, 278). FtsH-dependent CdiA-CTs share a conserved N-terminal domain after the VENN tetrapeptide, and this region is not conserved with other CdiA-CTs that utilize another IMP for translocation. Therefore, if an FtsH recognition domain exists, it is plausible that it will be localized to this region. Shortly after VENN, a conserved sequence consisting mostly of hydrophobic residues (S/A**L**V/IARG**AVAA**, where bold residues are identical between all tested CdiA-CTs that require FtsH) is present in FtsH-dependent CdiA-CTs. An attractive model in the CDI field is that the VENN tetrapeptide motif is involved in processing and release of CdiA-CT into the cytoplasm during delivery. Preliminary evidence suggests that mutating these asparagines residues prevents inhibition (Julia Shimizu Webb and Grant Gucinski, unpublished data), suggesting that they may play a catalytic role in the processing

of CdiA-CT. Cleavage at this site would place the LXARGAVAA sequence near the N-terminus of the resulting peptide and may position it in a manner that would be amenable to FtsH-mediated degradation or translocation into the cytoplasm. However, this is a highly speculative model, and future studies will elucidate this translocation pathway by identifying delivered fragments in both the periplasm and cytoplasm to determine how processing events, including any mediated by FtsH, contribute to delivery of these toxins.

Our alternative hypothesis is that CDI toxins exploit IMPs as receptors to bring nuclease domains into close proximity with the membrane, thereby allowing the toxin to enter and penetrate the lipid bilayer. Further, because the target-cell proton motive force is required for CDI (172), we postulate that this electrochemical gradient provides the driving force to transport toxins into the cytosol. This mechanism is similar to that proposed for colicin E3 and E9 nuclease toxins, which spontaneously enter lipid micelles and mediate their own transport across membranes (80, 82). However, colicins do not appear to require IMP receptors, and nearly all CDI^R mutations provide no protection against colicins (285). The one exception is *ftsH*, which was originally identified as the *tolZ* mutation and confers resistance to nuclease toxins of group A and B colicins (105, 107). FtsH is a membrane-associated AAA+ superfamily member with ATP-dependent metalloprotease activity. Two models have been proposed for the role of FtsH in colicin import. De Zamaroczy and coworkers have shown that FtsH is required for the release of colicin nucleases into the cell, and they hypothesize that the protease directly cleaves the domain (91, 92). Kleanthous and coworkers have proposed that the ATP-dependent unfoldase activity of FtsH is used to pull the nuclease domain into the cell (85). AAA+ proteases are processive enzymes that actively unfold and cleave proteins into small peptides, so, in these models, the colicin nuclease

domain must resist complete degradation during transport. Intriguingly, bacteriophages are also known to exploit IMPs to transfer their genomes into host cells. Phage λ requires the ManY component of the mannose phosphotransferase system to infect *E. coli* cells (286), and it was recently reported that PtsG is required for infection by *E. coli* phage HK97 (287). Thus, CDI and phages may use similar strategies to transport macromolecules into bacterial targets.

Other toxin-delivery systems, including *Neisseria* MafB proteins (211), type VI secretion-associated Rhs proteins (176, 200, 224), and predicted type VII secretion toxins from *Bacillus* and *Mycobacteria* (155), carry C-terminal nuclease domains that are related to those in CdiA proteins. Like CDI, the genetic organization of these other toxin-delivery systems is modular, allowing toxin interchange at the C terminus of conserved delivery proteins (126). These observations imply that toxin/immunity coding sequences are subject to frequent horizontal gene transfer between systems. Therefore, widely distributed toxin domains must be active against multiple clades of bacteria. Perhaps this explains why so many of these toxins are nucleases, which should be effective against any bacterium provided the domain can be delivered into the cytoplasm. It seems likely that each competition system uses a different mechanism to deliver toxins into target bacteria. For example, type VI secretion is thought to mechanically penetrate the target cell envelope, which could explain why analogous translocation domains are not found adjacent to the C-terminal toxin domains of Rhs effectors. The physical basis for CDI toxin translocation is unknown, but the mechanism appears to be quite versatile, allowing a nuclease domain to be transported through multiple independent pathways. Further, CDI exploits several membrane protein families, suggesting that, in principle, any IMP could be hijacked as a translocation receptor.

Given this plasticity, we speculate that the mechanism could be harnessed to transport other cargos into Gram-negative bacteria and perhaps form the basis of novel antibacterial therapies.

D. Materials and Methods

1. General methods

Bacterial strains are listed in Table S1. *E. coli* EPI100 cells carrying plasmid-borne *cdi* gene clusters were used as inhibitors, and *E. coli* MC4100 and MG1655 derivatives were used as target cells. *E. coli* MC4100 was subjected to *mariner*-mediated mutagenesis by using plasmid pSC189(288). Gene disruptions were from the Keio collection(289) and were transferred into *E. coli* MC4100 by using phage P1-mediated general transduction. Plasmids and oligonucleotides are listed in Tables S2 and S3, respectively. The details of all plasmid constructions are provided in SI Materials and Methods. Competition co-cultures were performed at a 1:1 inhibitor to target cell ratio in shaking lysogeny broth medium at 37 °C as described in SI Materials and Methods. Competitions with Δ*ftsH* target cells were performed at 30 °C, and chimeric EC93-Bp1026b inhibitors were used in 10-fold excess over target bacteria. Viable target cells were enumerated as cfu counts per milliliter and expressed as the average ± SEM for three independent experiments. RNA was isolated by guanidinium isothiocyanate-phenol extraction(290). Northern blots were performed with 10 μg of total RNA using a probe for *E. coli* $tRNA_1^{Ile}$. *In vivo* DNase activity was assessed by fluorescence microscopy of DAPI-stained bacteria as described in SI Materials and Methods.

2. Plasmid construction

Plasmid-borne chimeric CDI systems were constructed by allelic exchange of the counter selectable *pheS** marker from plasmid pCH10163 as described previously (177). The

various *cdiA-CT*/*cdiI* sequences were amplified by PCR by using the following primer pairs: *Escherichia coli* NC101 (ECNC101_09164/09169), CH3176/CH3177; *E. coli* 3006 (EC3006_4140/4139), CH3172/CH3173; *E. coli* MHI813 (ECSTECMHI813_1064/1065), CH3174/CH175; *P. luminescens* TTO1 (plu0548/plu0547), CH3519/CH3520; *D. dadantii* 3937 (Dda3937_04704/02929), CH3513/CH3514; *Yersinia pestis* Pestoides A (YPS_3004/YPS_3003), CH3530/CH3531; and *Burkholderia pseudomallei* 1026b (BP1026B_II2207/*cdiI* is unannotated), CH2501/CH2504. Each *cdiA-CT*/*cdiI* fragment was fused to upstream and downstream homology regions amplified from the $cdiA^{EC93}$ gene. The $cdiA^{EC93}$ upstream homology fragment was amplified by using primers DL1527/DL2470, and the downstream fragment was amplified with primers DL1663/DL2368. The three products (*cdiA-CT*/*cdiI*, upstream $cdiA^{EC93}$, and downstream $cdiA^{EC93}$) were then fused to each other through overlapping-end PCR (OE-PCR) by using primers DL1527/DL2368. The final DNA product (100 ng) was electroporated together with plasmid pCH10163 (300 ng) into *E. coli* strain DY378 cells as described previously(177). Clones with recombinant plasmids were selected on yeast extract glucose-agar supplemented with 33 μg/mL chloramphenicol and 10 mM d/l-p-chlorophenylalanine. The CdiA-CT/$CdiI_{o1}^{EC93}$ chimera plasmid was a gift from Stephanie Aoki and David Low (University of California, Santa Barbara).

The EC3006/EC536 hybrid *cdiA-CT*/*cdiI* sequence was generated by OE-PCR. A fragment encoding the N-terminal domain of CdiA-CT^{EC3006} was amplified from plasmid pCH11483 by using primers DL1527/CH3683, and a fragment encoding the C-terminal tRNase domain of CdiA-CT^{EC536} and its immunity protein was amplified from plasmid pCH10673 by using primers CH3682/DL2368. The two PCR products were combined into one fragment through OE-PCR by using primers DL1527/DL2368, and the resulting product

was recombined into plasmid pCH10163 as described earlier. The EC3006/EC869o11 hybrid construct was generated in the same manner. A fragment encoding the N-terminal domain of CdiA-CT^{EC3006} was amplified from plasmid pCH11483 by using primers DL1527/CH3724, and a fragment encoding the C-terminal DNase domain of CdiA-CT$_{o11}{}^{EC869}$ and its immunity protein was amplified from plasmid pCH9305 by using primers CH3723/DL2368.

The *cdiI* immunity genes were amplified by PCR by using the following primer pairs: *E. coli* NC101, CH3238/CH3239; *E. coli* 3006, CH3244/CH3245; *E. coli* MHI813, CH3240/CH3241; *P. luminescens* TTO1, CH3676/CH3677; *D. dadantii* 3937, CH3674/CH3675; and *Y. pestis* Pestoides A, CH3572/CH3571. All PCR products were digested with KpnI/XhoI and ligated to plasmid pTrc99KX (10). Genes encoding CDI^{R} membrane proteins were amplified with the following primer pairs: *yciB*, CH2139/CH2140; BTH_II0599, CH2525/CH2526; *ftsH*, CH2636/CH2637; *metI*, CH3477/CH3478; *ptsG*, CH3612/CH3613; *gltK*, CH3629/3630; *rbsC*, CH3631/CH3632; and *gltJ*, CH3633/CH3634. The *yciB*, BTH_II0599, *metI*, *gltK*, *gltJ*, and *rbsC* PCR products were digested with KpnI/XhoI and ligated to plasmid pTrc99KX. The *ftsH* and *ptsG* products were digested with EcoRI/HindIII and EcoRI/PstI (respectively) and ligated to plasmid pTrc99A digested with the appropriate restriction endonucleases. The Cys421Ser mutation was introduced into *ptsG* by using megaprimer PCR. The 3′ region of *ptsG* was amplified with primers CH3481/CH3613, and the resulting product was used as a megaprimer in a second reaction with primer CH3612. The *ptsG*(E387Oc) ochre mutation that deletes the C-terminal IIB domain was made by PCR by using primers CH3612/CH3722. The CdiA-CT/CdiI^{EC3006}-DAS controllable proteolysis construct was made by amplifying the *cdiA-CT*/*cdiI*^{EC3006} gene pair with primers CH3269/CH3425 and ligating the product into NcoI/SpeI-digested plasmid

pCH9460.

Additional *ftsH* constructs were made using the pTrc99a::*ftsH* construct created in this study. Truncations were made using primer pairs CH2636/CH2638 (K129) or CH2636/CH2662 (S400) to amplify the appropriate section of DNA. Point mutations were created using megaprimer PCR in which the first fragments were amplified using primer pairs CH2636/CH2660 (F228A) or CH2663/CH2637 (H414Y) and extended to full-length using the first PCR and primer CH2637 or CH2636 in a second reaction. All truncation and point mutation PCR products were cloned into pTrc99a using EcoRI and HindIII enzymes. The *E. coli/Proteus mirabilis* FtsH chimera was constructed by amplifying the 5' end of *ftsH* from *Proteus mirabilis* genomic DNA using primers CH2685/2686. This region was then cloned into the existing pTrc99a::*ftsH(coli)* plasmid using EcoRI and an internal KpnI restriction site.

YFP-labeled *E. coli* cells were generated by integrating the *yfp* coding sequence at the *gal* locus. First, a genomic integration construct was made by amplifying the kanamycin-resistance cassette from plasmid pKAN(175) with primers CH106/CH107, followed by blunt-end ligation to SmaI-digested plasmid pBluescript. A clone was identified that had the kanamycin-resistance cassette in the opposite orientation as pKAN, and this plasmid was termed pNAK. A fragment of *galM* was then amplified by using primers CH3789/CH3790, and the product was ligated to SacI/BamHI-digested plasmid pNAK to produce plasmid pCH2500. A *yfp-galT* fragment was amplified from *E. coli* DA28100 (gift from Sanna Koskiniemi, Uppsala University, Uppsala, Sweden) by using primers CH3787/CH3788, and the product was digested with KpnI/EcoRI and then ligated into pCH2500 to yield plasmid pCH2503. The large KpnI/SacI fragment from pCH2503 was recombined into *E. coli* EPI100

and X90 cells that harbor plasmid pSIM6 as described previously(291). Target bacteria were labeled with mRaspberry by using plasmid pEL3C17 (pJ23110-mRFP-cat).

3. Transposon library construction and selection for CDI^R mutants

The *mariner* transposon was introduced into *E. coli* CH10229 cells through conjugation with *E. coli* MFDpir donor cells carrying plasmid pSC189. Donor and recipient cells were grown to mid-log phase in lysogeny broth (LB) medium supplemented with 150 µg/mL ampicillin and 30 µM diaminopimelic acid (donors) or 33 µg/mL chloramphenicol (recipients). Donors (~6.0×10^8 cfu) and recipients (~3×10^8 cfu) were mixed and collected by centrifugation for 2 min at 6,000 × g in a microcentrifuge. The supernatant was removed by aspiration and the cell pellet resuspended in 100 µL of 1× M9 salts. Cell mixtures were spotted onto 0.45-µm nitrocellulose membranes, and the filters were then incubated on LB agar (without inversion) for 4 h at 37 °C. The cells were then harvested from the filters by using 2 mL of 1× M9 salts. Transposon insertion mutants were selected by plating 10-fold serial dilution on LB-agar supplemented with 50 µg/mL of kanamycin.

More than 20,000 colonies from each transposon library were collected from the agar plates in 1× M9 salts and inoculated into 50 mL of LB medium in a 250-mL baffled flask. CDI$^+$ inhibitor strains were grown in a parallel 50 mL LB medium culture. Both cultures were grown at 37 °C until mid-log phase, then mixed at approximately a 1:1 ratio and cultured for 3 h with shaking at 37 °C. Viable target cells from the transposon mutant library were enumerated as cfu counts per milliliter on LB agar supplemented with 50 µg/mL of kanamycin. The survivors of the first round of CDI competition were harvested from the plates with 1× M9 salts and used to inoculate 50 mL LB medium culture for a second round of CDI selection. After the third round of selection, the target cell population was usually

completely resistant to the CDI inhibitor cells. Individual clones were then isolated and the CDI^R phenotype confirmed in competition co-cultures. The transposon mutations were then transferred into CDI-sensitive cells by bacteriophage P1-mediated transduction, and the resulting transductants were tested for the CDI^R phenotype.

Transposon insertions that were linked to CDI^R were identified by rescue cloning. Chromosomal DNA was prepared from each CDI^R mutant by using phenol/chloroform extraction and ethanol precipitation. Genomic DNA (1 µg) was digested with AgeI and XmaI restriction endonucleases for 2 h at 37 °C and then the enzymes were inactivated at 65 °C for 10 min. ATP and T4 DNA ligase were added and the reaction was incubated for 2 h at room temperature. The ligated DNA was precipitated with 95% (vol/vol) ethanol, washed once with 75% (vol/vol) ethanol, and dissolved in 50 µL water. The ligated DNA was electroporated into *E. coli* DH5α *pir*$^+$ cells, and transformants were selected on LB agar supplemented with 50 µg/mL kanamycin. Plasmid DNA was isolated from selected transformants, and the transposon insertion junctions were identified by DNA sequencing by using primer CH2260.

4. Competition co-cultures

Competition co-culture assays were carried out as previously described (175, 177). Briefly, inhibitor cells (*E. coli* EPI100 carrying CDI expression constructs) and target cells (*E. coli* MC4100 or MG1655 carrying pTrc99a derivatives) were grown in LB medium supplemented with appropriate antibiotics overnight at 37 °C. The next day, cells were inoculated into fresh LB medium without antibiotics in baffled flasks. Individual cultures were grown with shaking until early log phase, and then the populations were mixed at a 1:1 ratio in fresh prewarmed LB in baffled flasks. The competitions between EC93-Bp1026b

inhibitors and targets that express BTH_II0599 were conducted at a 10:1 inhibitor-to-target cell ratio. A sample of each co-culture was taken at initial mixing to enumerate viable target cells as cfu counts per milliliter. The co-cultures were incubated with shaking for 3 h at 37 °C. Viable target cell counts are presented as the average ± SEM of three independent competition experiments.

5. Activation of CdiA-CT toxins inside E. coli *cells*

E. coli X90 cells (WT and Δ*yciB* and Δ*ptsG* mutants) were co-transformed with pTrc99a constructs that express $CdiI_{o11}^{EC869}$ or $CdiI^{EC3006}$ and pCH450 derivatives that express CdiA-CT/$CdiI_{o11}^{EC869}$-DAS or CdiA-CT/$CdiI^{EC3006}$-DAS protein pairs. Transformants were selected overnight on LB agar supplemented with 150 μg/mL Amp, 15 μg/mL Tet, and 0.4% d-glucose. The following day, transformants were inoculated into 25 mL of LB medium supplemented with Amp, Tet, and glucose. Cells were grown to mid-log phase, then diluted to an OD600 of 0.05 in fresh LB supplemented with Amp, Tet, 0.2% arabinose, and 0.15 mM isopropyl β-D-1-thiogalactopyranoside (IPTG) to induce expression from both plasmids. Cell growth was monitored by measuring the OD600 of the culture every 30 min for 5 h. The presented growth curves show the average ± SEM for three independently performed experiments. Culture samples were removed at 0, 1, 3, and 5 h for microscopy or RNA isolation.

6. RNA isolation and analysis

Cells from internal expression experiments and CDI competition co-cultures were poured into an equal volume of ice-cold methanol, and cells were collected by centrifugation in a Sorvall RC 5B centrifuge at 15,000 × g for 15 min at 4 °C. Cell pellets were frozen at −80 °C and RNA was isolated by using guanidine isothiocyanate-phenol as described previously

(40). RNA (10 µg) was resolved on denaturing 8 M urea/10% (wt/vol) polyacrylamide gels and then electrotransferred onto nylon membrane (Nytran Supercharge). $tRNA_1^{Ile}$ was detected by Northern blot hybridization by using radiolabeled oligonucleotide CH577 as a probe. Blots were visualized on a Bio-Rad PhosphorImager by using Quantity One software.

7. Microscopy

Cells (equivalent to an OD600 of 0.2) were collected by centrifugation in a microcentrifuge for 2 min at 6,000 × g. Cells were fixed in freshly prepared 4% (vol/vol) formaldehyde in 1× PBS solution for 15 min, and the reaction was quenched with 125 mM glycine (pH 7.5). Cells were washed three times with 1× PBS solution, resuspended in 100 µL 1× PBS solution, and spotted onto poly-d-lysine–treated slides. Excess liquid was removed with a Kimwipe, and slides were dried and gently rinsed with Nanopure water to remove nonadherent bacteria. Slides were sealed with Fluorogel II with DAPI (Fisher Scientific/EMS) and a glass coverslip. Images were acquired on an Olympus fluorescent microscope with a 100× oil objective by using an Optronics MacroFire digital microscope camera. Light-field images were taken with a 12-ms exposure (gain 2). DAPI-stained images were acquired with a 48-ms exposure (gain 2). Fluorescent images were recorded in grayscale by using a 502-ms exposure (gain 5). Images were false-colored, overlaid by using FIJI (292), and cropped to 200 × 200 pixels using GIMP.

E. Acknowledgments

We thank Mary Raven for microscopy assistance and Sanna Koskiniemi and Dan Andersson for bacterial strains.

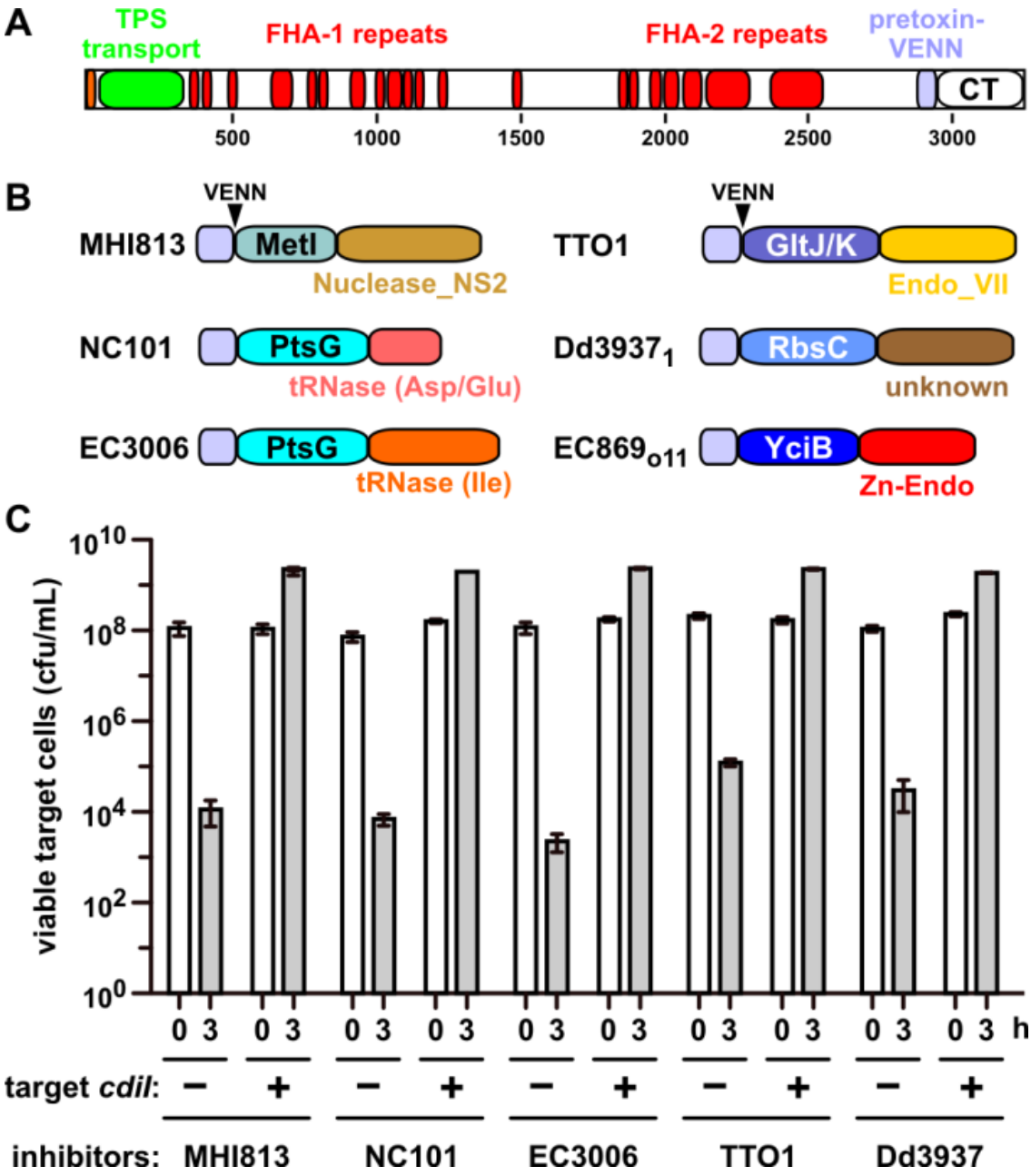

Figure 1. Activity of CdiA chimeras. (A) CdiA proteins contain an N-terminal TPS transport domain and two filamentous hemagglutinin (FHA)-peptide repeat regions. The pretoxin-VENN domain is adjacent to and demarcates the variable CdiA-CT region. (B) Predicted CdiA-CT domain structures. Toxins from *E. coli* MHI813 and *Photorhabdus luminescens* TTO1 carry predicted C-terminal Nuclease_NS2 (Pfam database ID: PF13930) and Endonuclease_VII (PF14411) domains, respectively. The C-terminal nuclease domains from *E. coli* NC101 and 3006 cleave $tRNA^{Asp}$/$tRNA^{Glu}$ and $tRNA^{Ile}$, respectively. The nuclease domain from *E. coli* EC869 is a Zn^{2+}-dependent DNase, and the activity of the *Dickeya dadantii* 3937 toxin is unknown. N-terminal domains are labeled according to their putative membrane receptors. The pretoxin-VENN domain and the conserved VENN motif are also depicted. (C) CDI competitions. *E. coli* target cells were cocultured with the indicated CDI inhibitors. Average target-cell counts (±SEM) are presented for three independent experiments. Where indicated, target cells were provided with the cognate *cdiI* immunity gene.

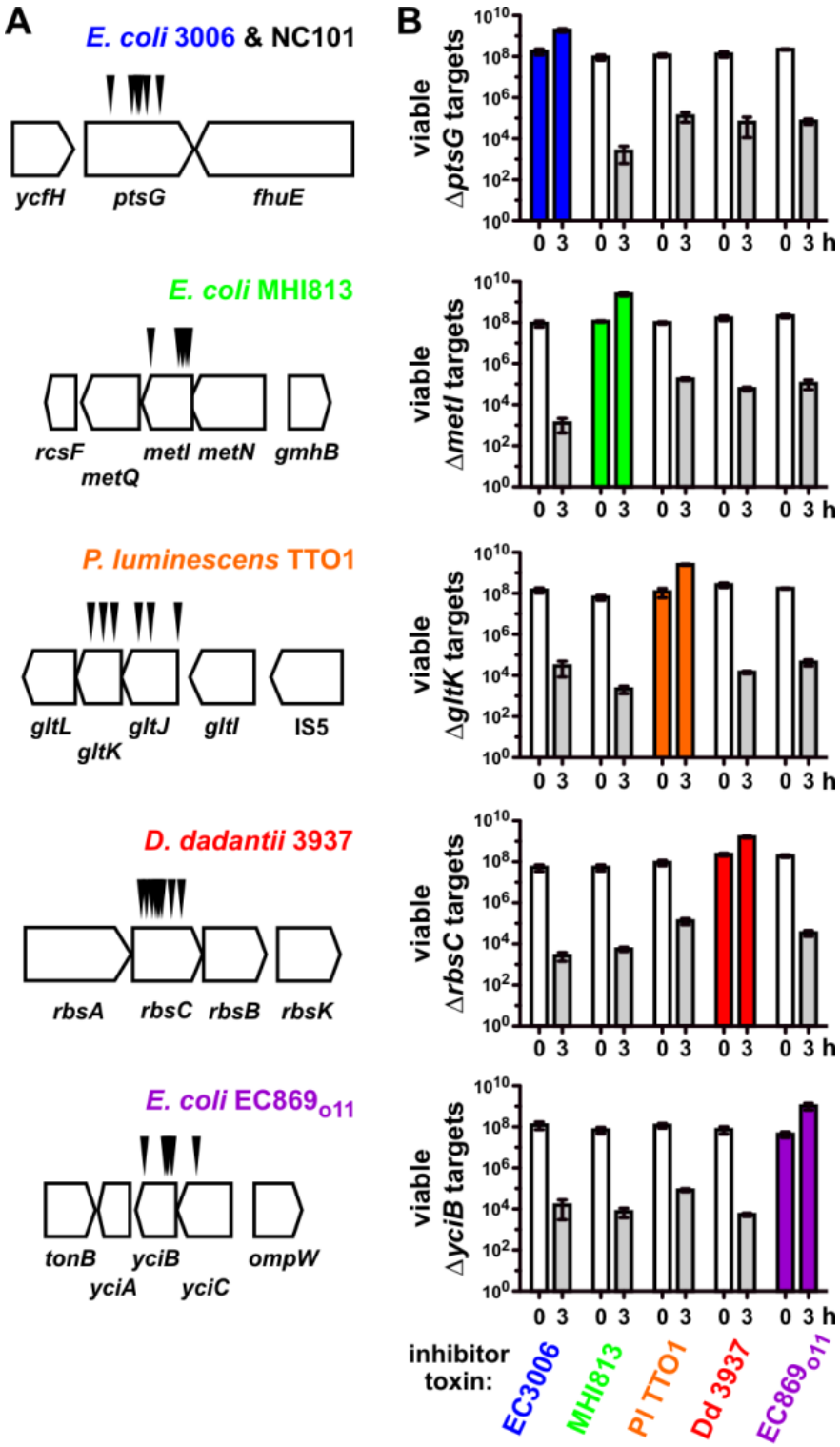

Figure 2. Specificity of CDI^{R} mutations. (A) Transposon-insertion sites are shown for each toxin. No other verified CDI^{R} mutations were identified during the selections. (B) CDI^{R} mutations are toxin-specific. The indicated target cell strains were cocultured with inhibitors that deploy CdiA-CT^{EC3006}, CdiA-CT^{MHI813}, CdiA-CT^{TTO1}, CdiA-CT$_{1}^{Dd3937}$, or CdiA-CT$_{o11}^{EC869}$ toxins. Average target-cell counts (±SEM) per mL are presented for three independent experiments.

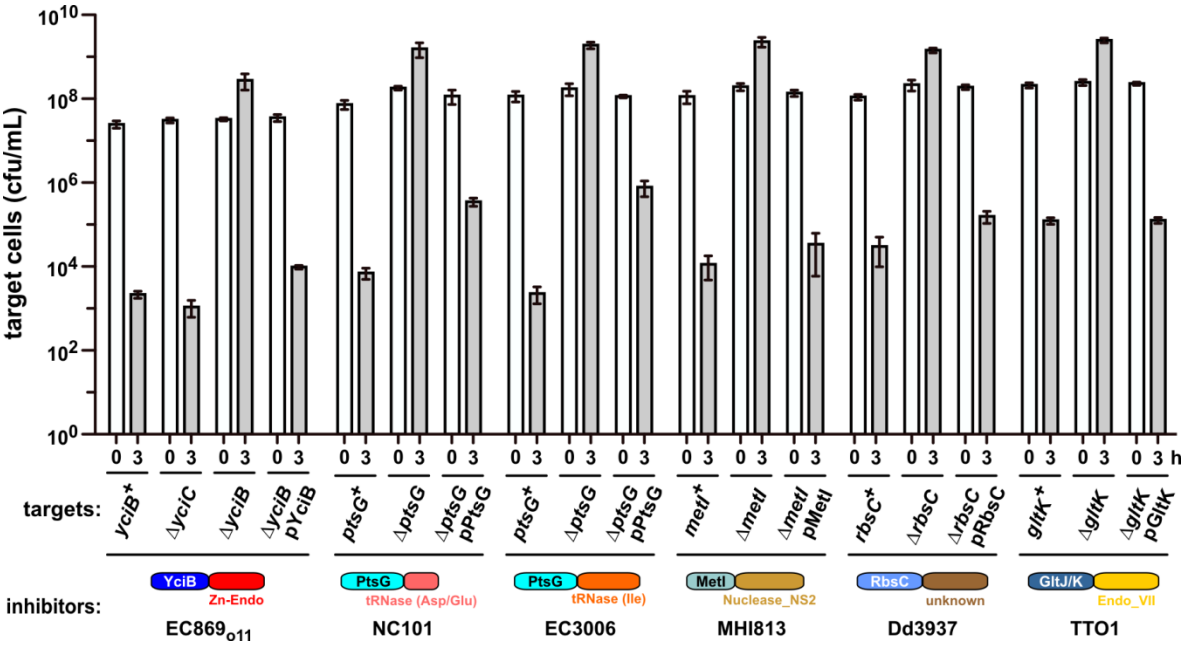

Figure 3. Complementation of CDI^R mutations. *E. coli* target cells of the indicated genotypes were cocultured for 3 h at a 1:1 ratio with inhibitor strains that deploy the indicated CdiA-CT toxins. For each CDI^R mutation, expression of the WT gene from a plasmid (e.g., pYciB) restores sensitivity to growth inhibition. Average target-cell counts (±SEM) are presented for three independent experiments.

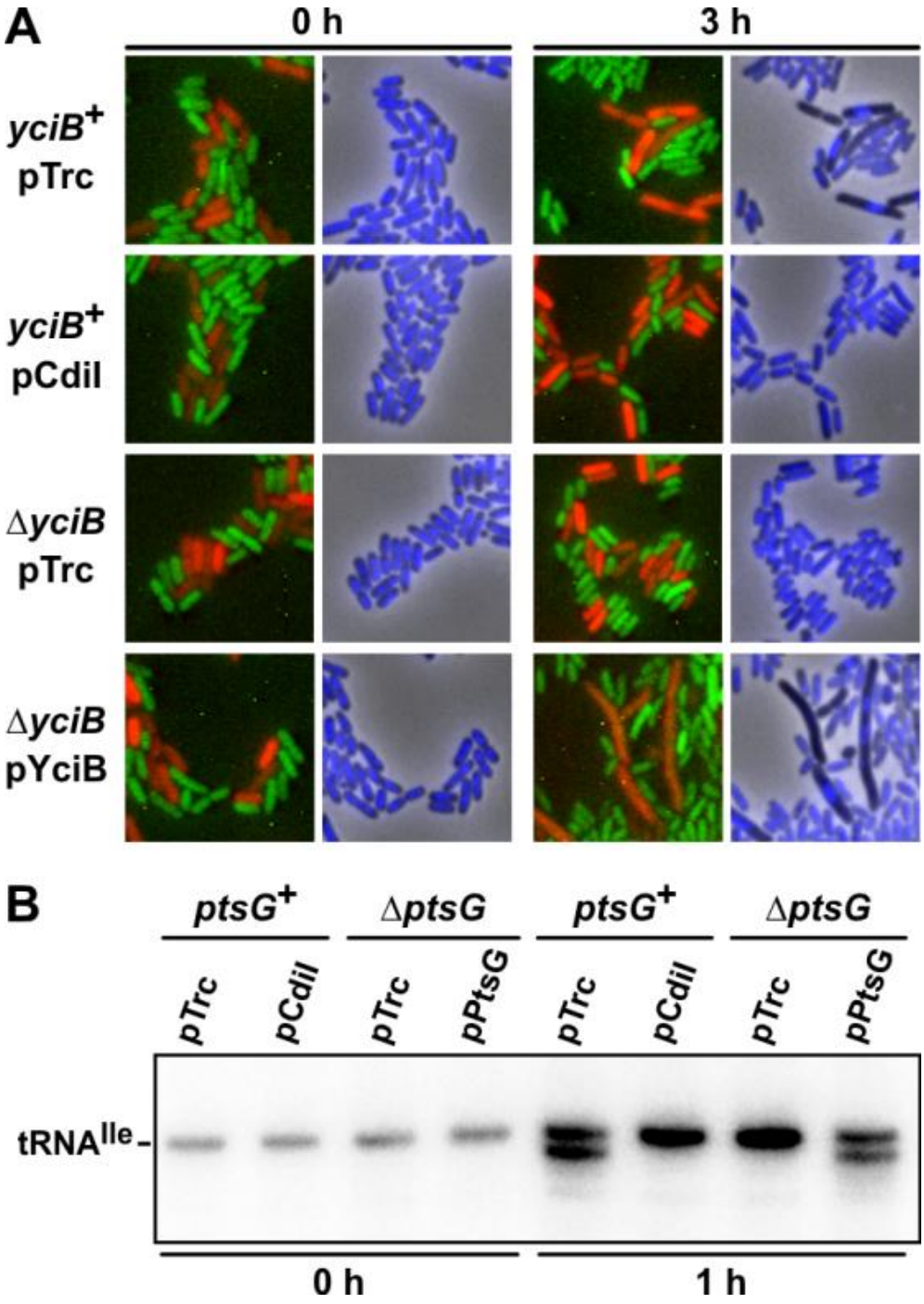

Figure 4. Toxin nuclease activities inside target bacteria. (A) Fluorescence microscopy of CDI_{o11}^{EC869} competition cocultures. Inhibitor cells (YFP-labeled) were incubated with the indicated *yciB*$^+$ or Δ*yciB* target cells (mRFP-labeled), and nucleoids were visualized with DAPI staining. (B) Northern blot analysis of CDI^{EC3006} competition cocultures. Target cells (*ptsG*$^+$ or Δ*ptsG*) were incubated with CDI^{EC3006} inhibitor cells and RNA isolated for Northern blot analysis of $tRNA_1^{Ile}$. The migration position of uncleaved $tRNA_1^{Ile}$ is indicated.

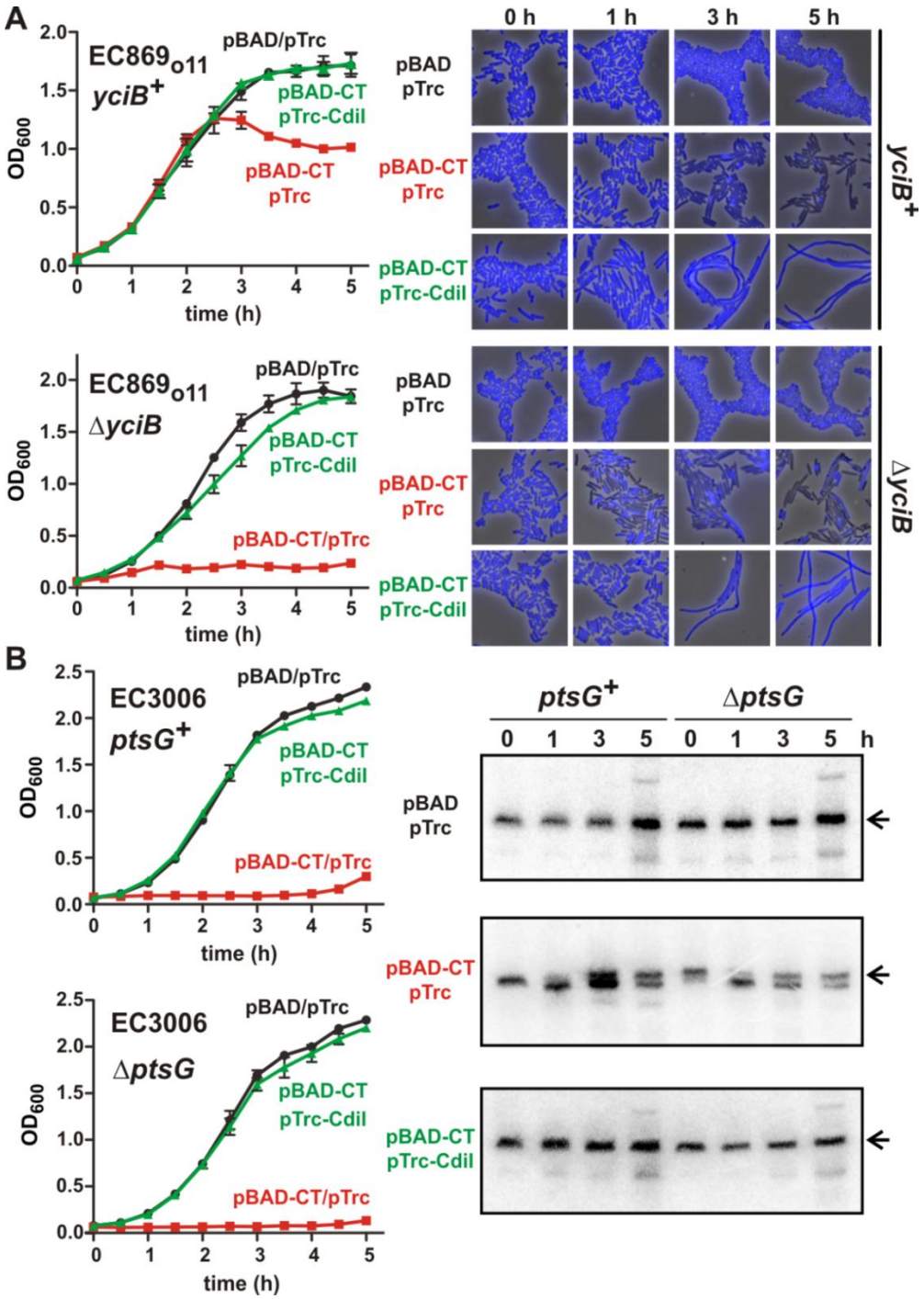

Figure 5. Toxin expression inside CDI^{R} mutants. (A) CdiA-CT$_{o11}^{EC869}$ was induced at 0 h from a pBAD vector in *yciB*$^{+}$ and Δ*yciB* cells as described previously (176). Cell growth was monitored by measuring the OD at 600 nm of the culture. CdiI$_{o11}^{EC869}$ immunity protein was coexpressed from a pTrc vector where indicated. (*Right*) DAPI-stained cells sampled at 0, 1, 3, and 5 h of culture. (B) CdiA-CT^{EC3006} was induced at 0 h from a pBAD vector in *ptsG*$^{+}$ and Δ*ptsG* cells, and growth was monitored by measuring the OD_{600} of the culture. CdiI^{EC3006} immunity protein was coexpressed from a pTrc vector where indicated. (*Right*) Northern blot analysis of RNA isolated at 0, 1, 3, and 5 h. The arrows indicate the migration position of full-length tRNA$_{1}^{Ile}$.

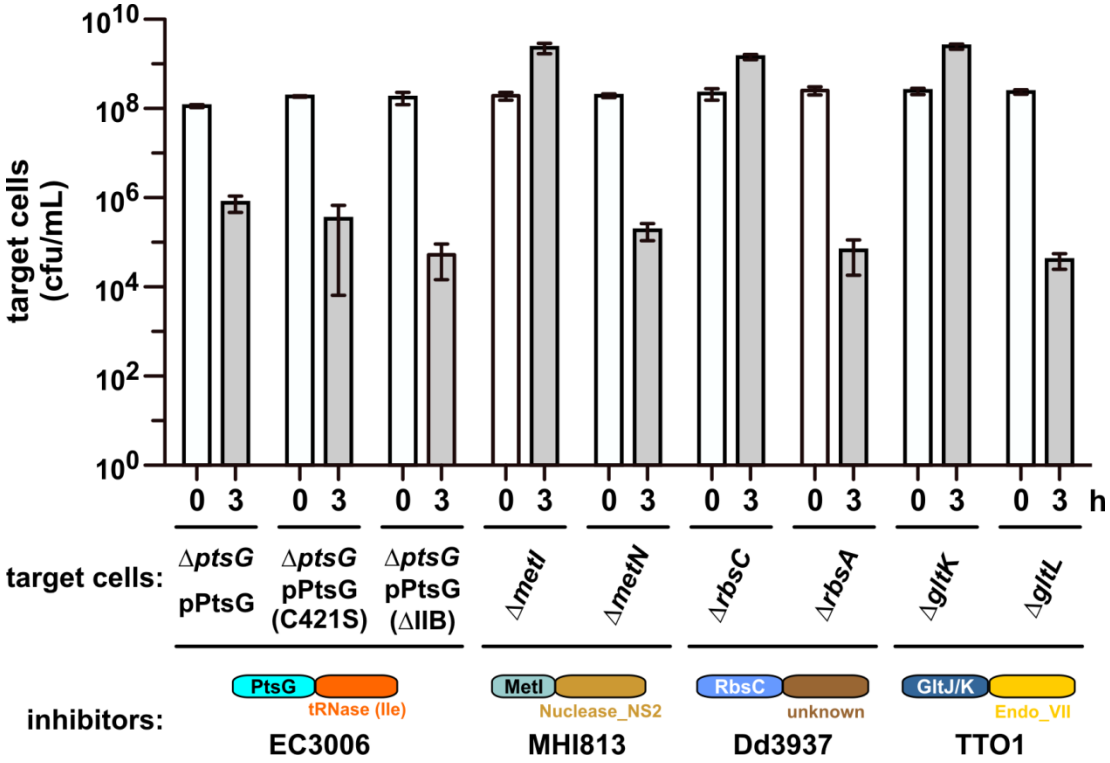

Figure 6. Metabolite transport activity is not required for CDI. *E. coli* target cells of the indicated genotypes were cocultured for 3 h at a 1:1 ratio with inhibitor strains that deploy the indicated CdiA-CT toxins. Average target-cell counts (±SEM) are presented for three independent experiments.

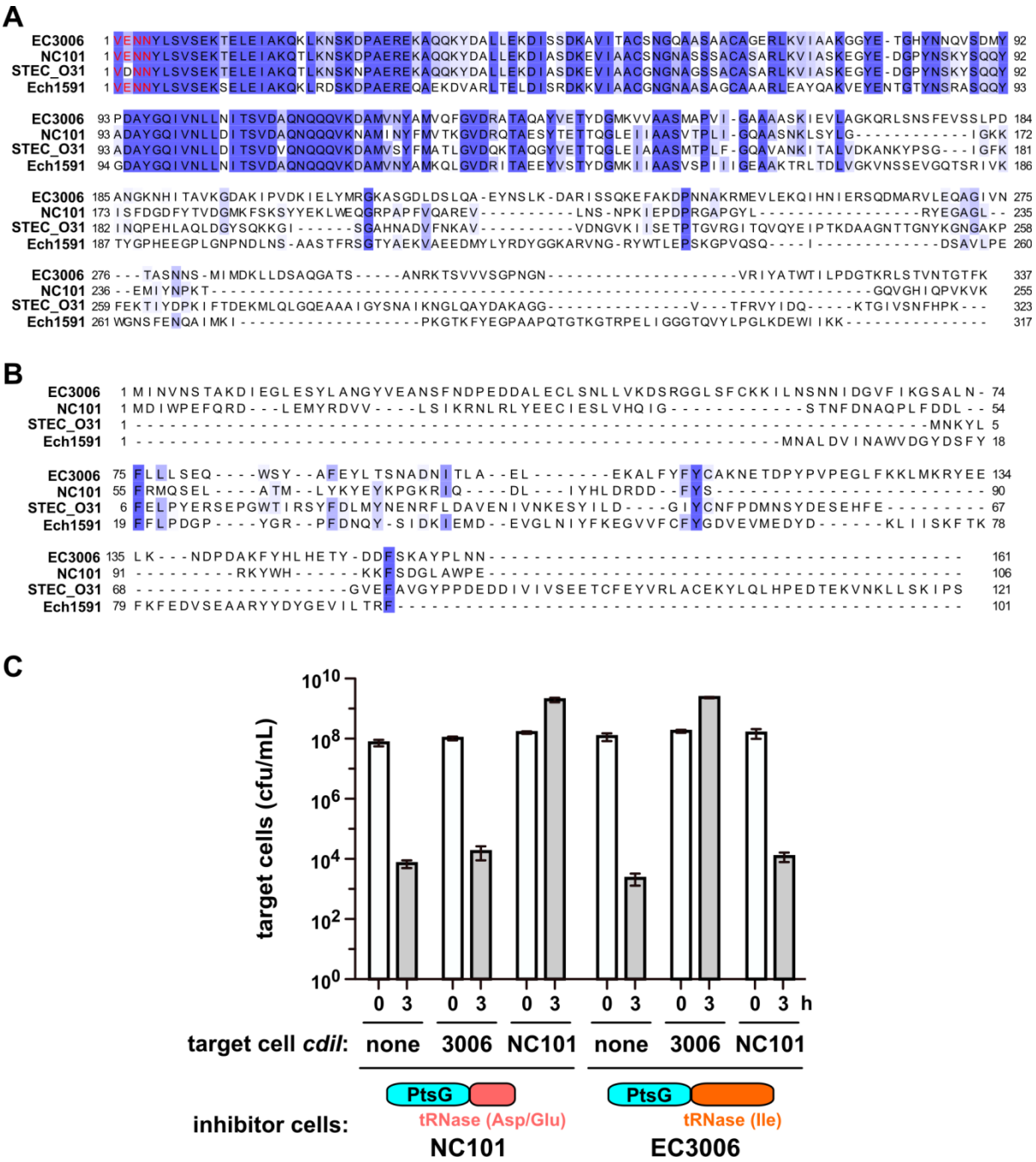

Figure 7. The N-terminal domain of the CdiA-CT region dictates the specificity of resistance. (A) Alignment of CdiA-CT sequences from *E. coli* strains 3006 (EC3006_4140), NC101 (ECNC101_09164), STEC_O31 (ECSTECO31_4009), and *Dickeya zeae* Ech1591 (Dd1591_2008). The conserved VENN peptide motif is presented in red type. Sequences were aligned by using Clustal Omega on the Uniprot server (www.uniprot.org/align/), and the results rendered at 30% sequence identity by using Jalview (www.jalview.org). (B) Alignment of CdiI immunity protein sequences from *E. coli* strains 3006 (EC3006_4139), NC101 (ECNC101_09169), and STEC_O31 (ECSTECO31_4008), and *D. zeae* Ech1591 (Dd1591_2009). (C) *E. coli* target cells expressing the indicated *cdiI* immunity genes were cocultured for 3 h at a 1:1 ratio with inhibitor strains that deploy CdiA-CT^{NC101} or CdiA-CT^{EC3006}. Average target-cell counts (±SEM) are presented for three independent experiments.

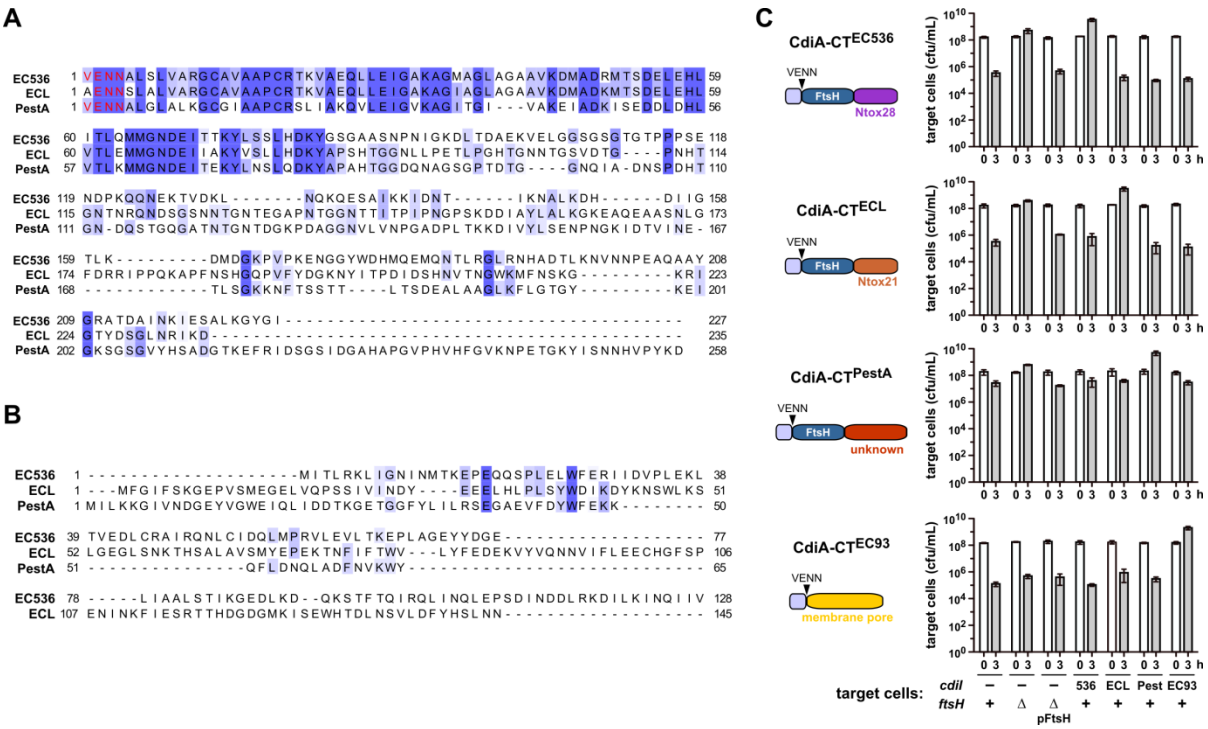

Figure 8. Analyses of FtsH-dependent CDI toxins. (A) Alignment of CdiA-CT sequences from *E. coli* EC536 (ECP_4580), ECL (ECL_04451), and *Y. pestis* Pestoides A (YPS_3004). The conserved VENN peptide motif is presented in red type. Sequences were aligned by using Clustal Omega on the Uniprot server (www.uniprot.org/align/), and the results rendered at 30% sequence identity by using Jalview (www.jalview.org). (B) Alignment of CdiI immunity protein sequences from *E. coli* EC536 (ECP_4579), ECL (unannotated), and *Y. pestis* Pestoides A (YPS_3003). (C) Inhibitor strains that deploy indicated CdiA-CT toxins were cocultured for 3 h at a 1:1 ratio with target cells of the indicated genotypes. Plasmid-borne *ftsH* (pFtsH) complements the Δ*ftsH* mutation and restores sensitivity to FtsH-dependent CDI toxins. Average target-cell counts (±SEM) are presented for three independent experiments.

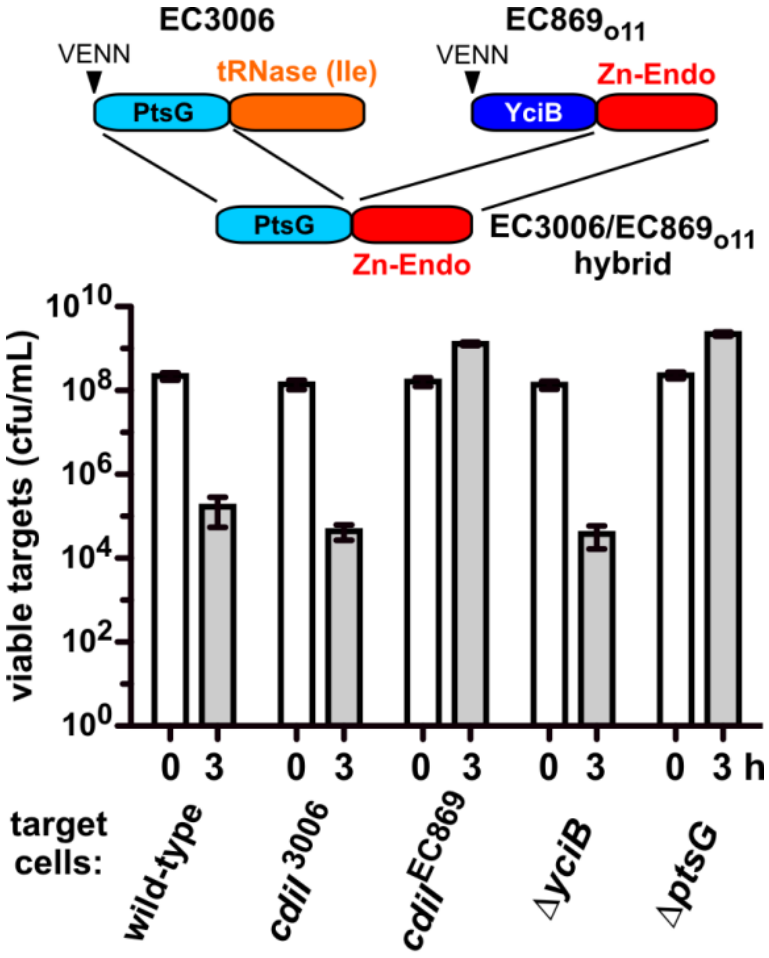

Figure 9. CdiA-CT constituent domains are modular. The N-terminal domain of CdiA-CT^{EC3006} was fused to the C-terminal DNase domain of CdiA-CT$_{o11}^{EC869}$. EC3006-EC869$_{o11}$ hybrid inhibitors were cocultured with the indicated target strains. Average target-cell counts (±SEM) are presented for three independent experiments.

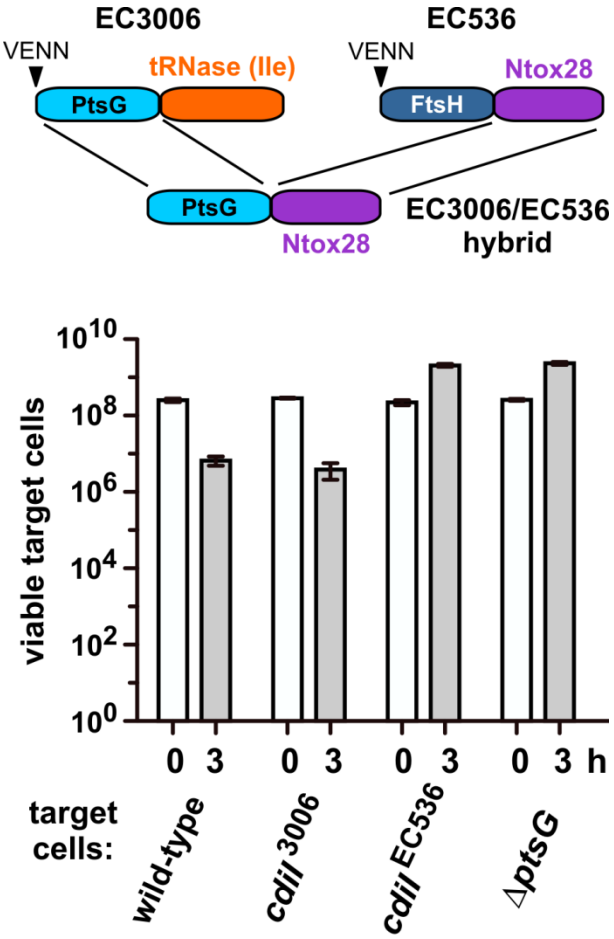

Figure 10. CdiA-CT constituent domains are modular. The N-terminal domain of CdiA-CT^{EC3006} was fused to the C-terminal tRNase domain of CdiA-CT^{EC536}. EC3006-EC536 hybrid inhibitors were cocultured with the indicated target strains. Average target-cell counts (±SEM) are presented for three independent experiments.

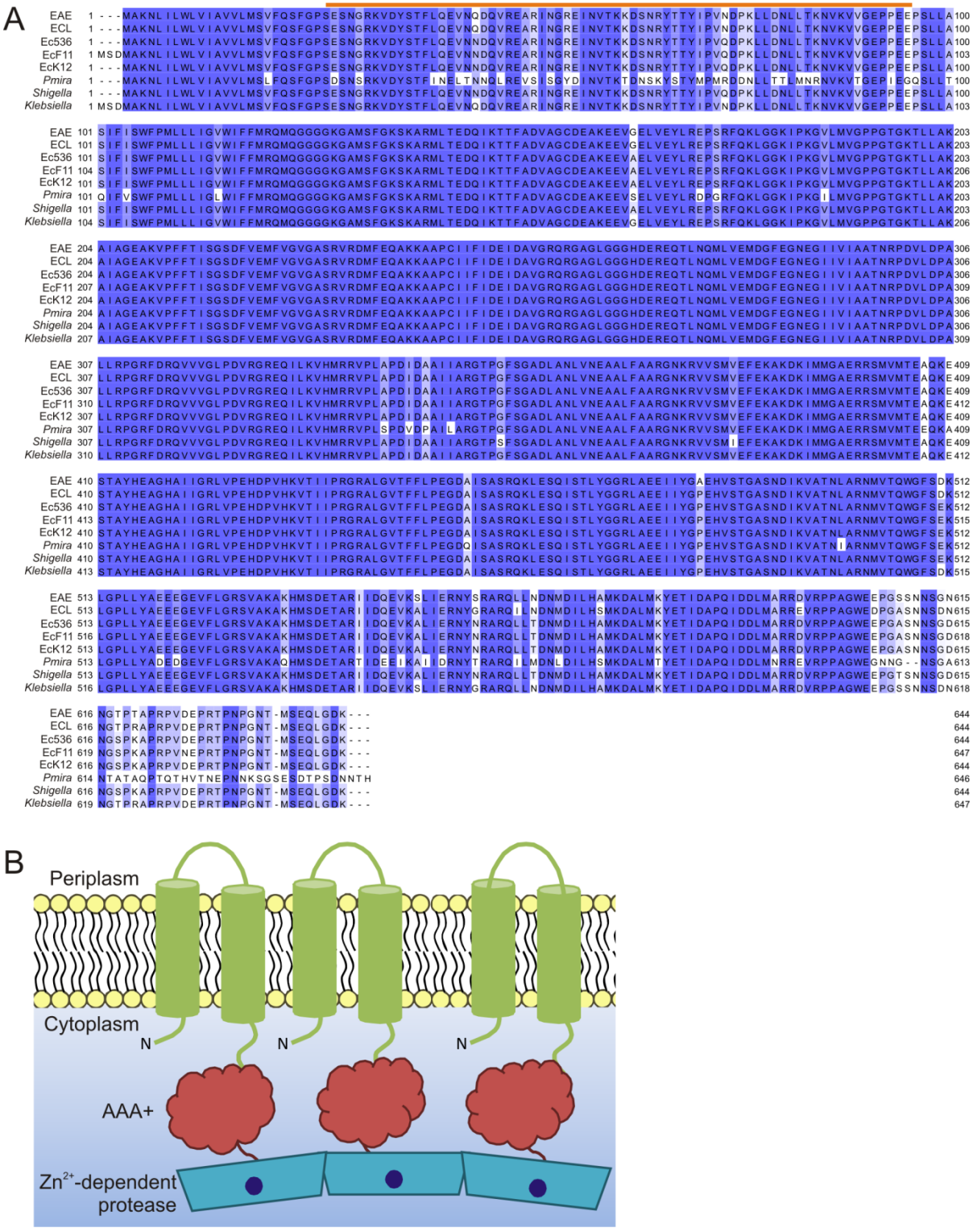

Figure 11. FtsH is a highly-conserved AAA+ protease anchored to the inner membrane. (A) FtsH sequences are conserved across Gram-negative species. Proteins from *Enterobacter aerogenes* (EAE); *Enterobacter cloacae* (ECL); *E. coli* strains 536 (Ec536), F11 (EcF11), and K12 (EcK12), *Proteus mirabilis* (*Pmira*); *Shigella flexerni* (*Shigella*); and *Klebsiella pneumoniae* (*Klebsiella*) were identified using the NCBI BLAST database and were aligned using Clustal Omega. The alignment was rendered using Jalview, and

purple highlighting indicates percent conservation. The orange line above the top sequence marks the residues that make up the periplasmic loop. (B) A cartoon schematic showing the orientation of FtsH in the cell. Two transmembrane domains spanned by a short loop anchor the protein to the inner membrane. The AAA+ ATPase domain is signified by the brick red bubble. The protease domain is represented by the turquoise trapezoid, and the zinc ion is shown as a purple circle.

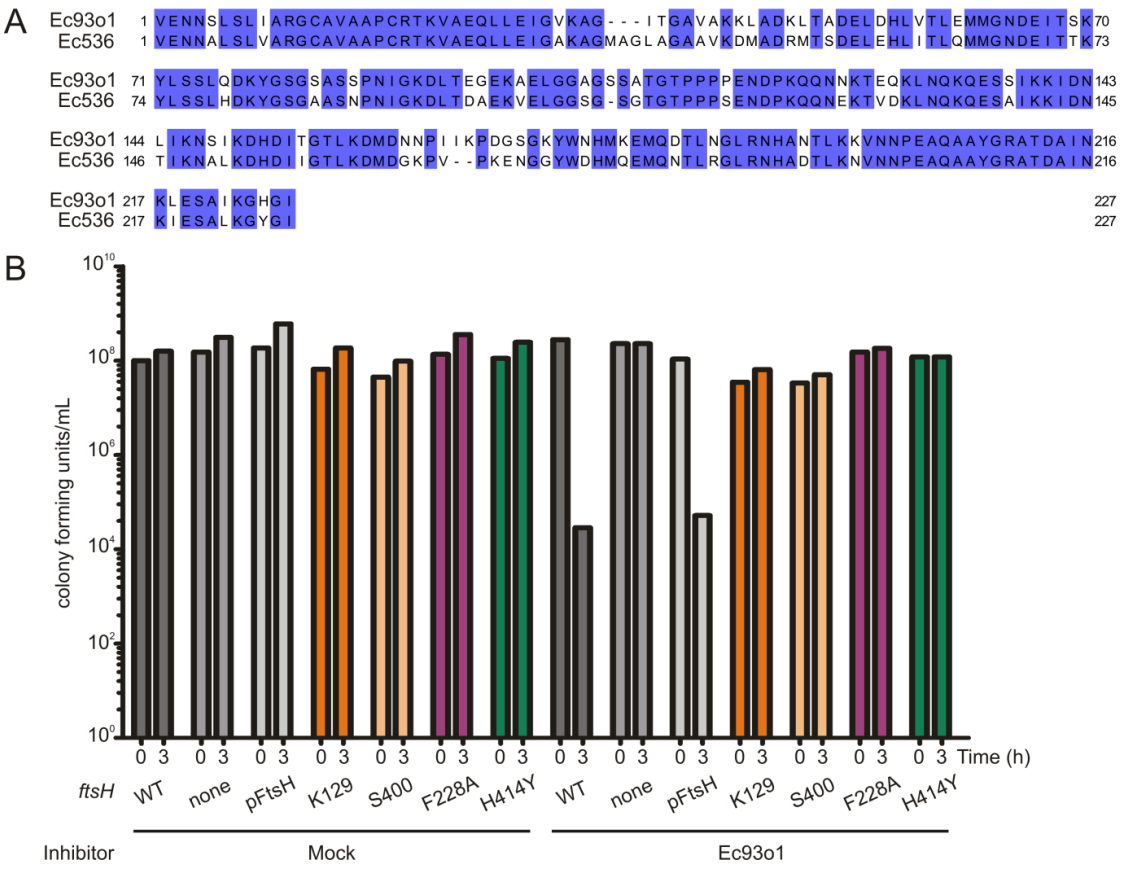

Figure 12. FtsH activity is required for CDI. (A) Alignment of the CdiA-CT sequences from Ec536 and $Ec93_{o1}$. Sequences were aligned using Clustal Omega. The image was rendered in Jalview. Purple highlighting signifies identical residues. (B) Mutations that remove or disrupt the ATPase or protease domains block CDI. Target cells carrying the indicated *ftsH* alleles were incubated with mock inhibitors or inhibitor cells delivering the CDI_{o1}^{EC93} system. Viable target bacteria were quantified at 0 and 3 h.

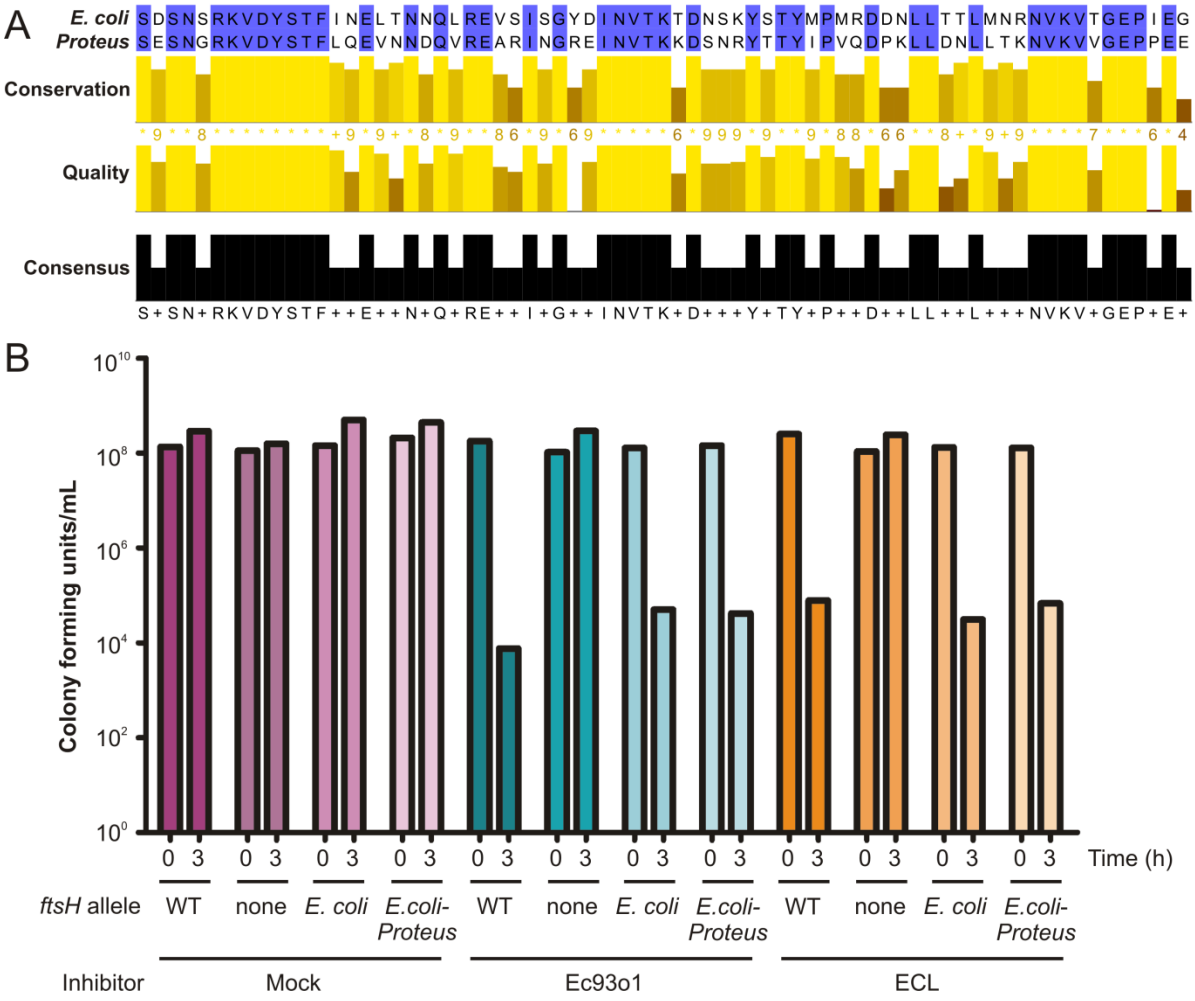

Figure 13. The FtsH periplasmic loop from *Proteus mirabilis* permits delivery of CdiA-CT toxins into *E. coli* target cells. (A) The 72-residue region constituting the periplasmic loops of FtsH from *E. coli* and *Proteus mirabilis* were aligned using Clustal Omega and rendered using Jalview. Purple highlighting signifies identical residues. (B) Inhibitor cells delivering a mock CDI system, the orphan CdiA-CT from EC93, or a CdiA-CT from *E. cloacae* were mixed with target cells expressing the indicated *ftsH* allele. Viable target cell bacteria were quantified at 0 and 3 h.

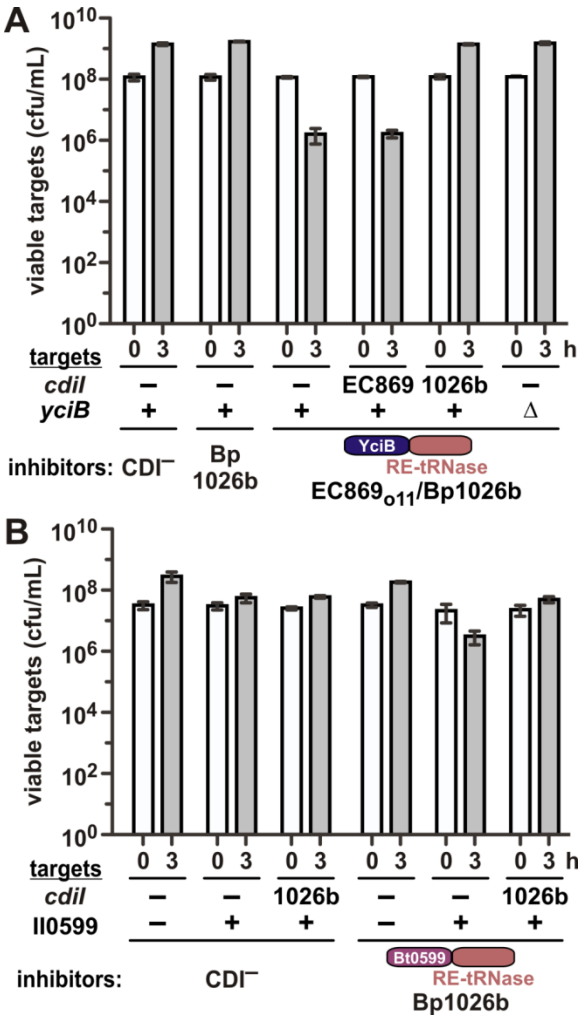

Figure 14. BTH_II0599 allows CdiA-CT$_{II}^{Bp1026b}$ delivery into *E. coli* cells. (A) Inhibitor strains (mock CDI$^-$, Bp1026b, and hybrid EC869$_{o11}$-Bp1026b) were co-cultured with target bacteria of the indicated *cdiI* and *yciB* genotypes. Viable target bacteria were quantified at 0 and 3 h. (B) Inhibitor strains (mock CDI$^-$ and Bp1026b) were cocultured with target cells that express BTH_II0599 and *cdiI*$_{II}^{Bp1026b}$ where indicated. Average target-cell counts (±SEM) are presented for three independent experiments.

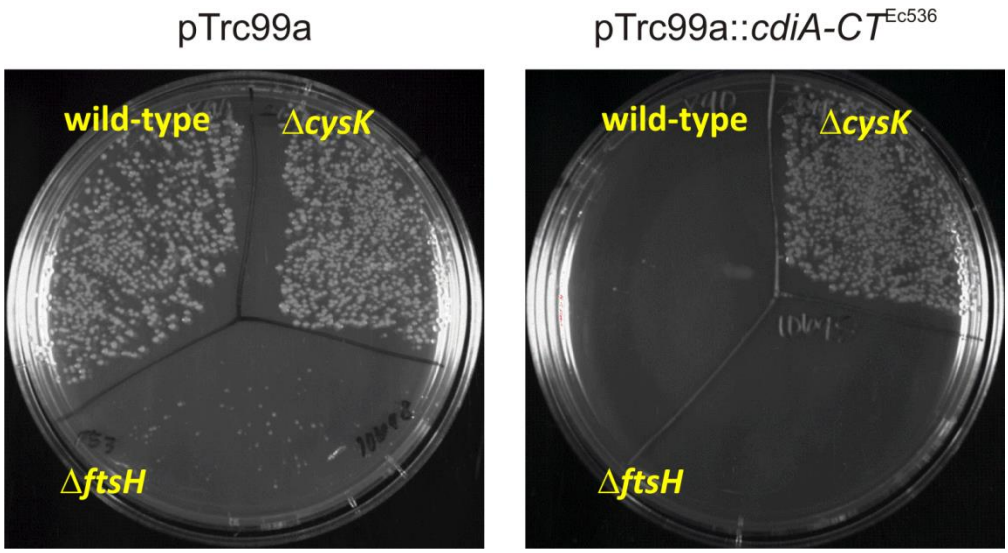

Figure 15. FtsH is not required for intracellular activation of CdiA-CT^{Ec536}. An empty plasmid vector (left panel) or a plasmid expressing CdiA-CT^{Ec536} (right panel), which requires FtsH for inhibition in co-culture, were transformed into wild-type, Δ*cysK*, or Δ*ftsH* cells. All cells grow with the empty vector, but CdiA-CT^{Ec536} inhibits growth of wild-type and Δ*ftsH* cells when intracellularly expressed. Δ*cysK* cells grow in the presence of this toxin, as CysK is a cofactor required for toxicity.

Table 1. Bacterial strains used in this study.

Strain	***Description***[a]	***Reference***
X90	F´ *lacI*^{q} *lac´ pro´/ara* Δ*(lac-pro) nal1 argE*(amb) *rif*^{r} *thi-1*, Rif^{R}	
MG1655	wild-type strain	
DA28100	*galK::sYFP2opt-cat*, Cm^{R}	Sanna Koskiniemi
EPI100	F^{-} *mcrA* Δ*(mrr-hsdRMS-mcrBC) φ80dlacZ*Δ*M15* Δ*lacXcZ*Δ*M15* Δ*lacX recA1 endA1 araD139* Δ*(ara, leu)7697 galU galK* λ^{-} *rpsL nupG*, Str^{R}	Epicentre
DY378	W3110 λ*cI857* Δ*(cro-bioA*)	(291)
MFD*pir*	MG1655 RP4-2-Tc::[ΔMu1::*aac(3)IV*-Δ*aphA*-Δ*nic*35-ΔMu2*::zeo*] *dapA::(erm-pir*) Δ*recA*, Apr^{R} Zeo^{R} Erm^{R}	(293)
CH43	MG1655 Δ*ftsH3::kan lpxC*	(294)
CH2505	X90 *galK::sYFP2opt-kan*, Rif^{R} Kan^{R}	This study
CH2550	EPI100 *galK::sYFP2opt-kan*, Kan^{R}	This study
CH7157	X90 Δ*clpX* Δ*clpA::kan*, Rif^{R} Kan^{R}	(169)
CH8119	DH5α λ*pir*$^{+}$	Biomedal
CH8251	MC4100 *rif*^{r}, Rif^{R}	This study
CH9404	CH8251 Δ*yciB::kan*, Rif^{R} Kan^{R}	This study
CH9405	X90 Δ*yciB::kan*, Rif^{R} Kan^{R}	This study
CH10013	JCM158 *rif*^{r}, Rif^{R}	(167)
CH10229	JCM158 *rif*^{r} Δ*wzb::cat*, Rif^{R} Cm^{R}	(167)
CH11843	CH8251 Δ*metI::kan*, Rif^{R} Kan^{R}	This study
CH11844	CH8251 Δ*metN::kan*, Rif^{R} Kan^{R}	This study
CH11845	CH8251 Δ*ptsG::kan*, Rif^{R} Kan^{R}	This study
CH12000	CH8251 Δ*rbsA::kan*, Rif^{R} Kan^{R}	This study
CH12002	CH8251 Δ*rbsC::kan*, Rif^{R} Kan^{R}	This study
CH12008	CH8251 Δ*gltJ::kan*, Rif^{R} Kan^{R}	This study
CH12009	CH8251 Δ*gltK::kan*, Rif^{R} Kan^{R}	This study
CH12010	CH8251 Δ*gltL::kan*, Rif^{R} Kan^{R}	This study
CH12741	X90 Δ*ptsG::kan*, Rif^{R} Kan^{R}	This study

[a]Abbreviations: Amp^{R}, ampicillin-resistant; Apr^{R}, aprimycin-resistant; Cm^{R}, chloramphenicol-resistant; Erm^{R}, erythromycin-resistant; Kan^{R}, kanamycin-resistance; Rif^{R}, rifampicin-resistant; Tet^{R}, tetracycline-resistant; Zeo^{R}, zeocin-resistant

Table 2. Plasmids used in this study.

Plasmid	***Description***[a]	***Reference***
pTrc99a	IPTG-inducible expression plasmid, Amp^{R}	GE Healthcare
pTrc99KX	Derivative of pTrc99a that contains a 5´-KpnI restriction site and 3´-SpeI and XhoI sites, Amp^{R}	(175)
pCH450	pACYC184 derivative with *E. coli araBAD* promoter for arabinose-inducible expression, Tet^{R}	(172)
pNAK	pBluescript derivative with FRT-flanked kanamycin-resistance cassette, Amp^{R} Kan^{R}	This study

pSC189	Mobilizable plasmid with R6Kγ replication origin. Carries the *mariner* transposon containing kanamycin-resistance cassette, Amp^R Kan^R	(288)
pSIM6	Heat-inducible expression of the phage l Red recombinase proteins, Amp^R	(291)
pDAL879::cat	Constitutive expression of chimeric $cdiA^{EC93}$-CT_{o1}^{EC93} and $cdiI_{o1}^{EC93}$ genes, Cm^R	Stephanie Aoki
pCH172	pEL3C17-pJ23110-*mRFP-cat*, Cm^R	Sanna Koskiniemi
pCH360	pTrc99a::*ftsH*, Amp^R	This study
pCH361	pTrc(CM)::BTH_II0599, Cm^R	This study
pCH406	pTrc99a::*ftsH* K129, IPTG-inducible expression of *ftsH* K129 truncation, Amp^R	This study
pCH407	pTrc99a::*ftsH* S400, IPTG-inducible expression of *ftsH* S400 truncation, Amp^R	This study
pCH569	pTrc99a::*ftsH(E. coli-Proteus mirabilis)*, IPTG-inducible expression of *ftsH* with *P. mirabilis* transmembrane domains and periplasmic loop, Amp^R	This study
pCH581	pTrc99a::*ftsH* F228A, IPTG-inducible expression of *ftsH* F228A point mutation, Amp^R	This study
pCH583	pTrc99a::*ftsH* H414Y, IPTG-inducible expression of *ftsH* H414Y point mutation, Amp^R	This study
pCH1417	Constitutive expression of chimeric $cdiA^{EC93}$-CT^{PestA} and $cdiI^{PestA}$ genes, Cm^R	This study
pCH2156	pTrc99KX::$cdiI^{PestA}$, IPTG-inducible expression of $cdiI^{PestA}$ immunity gene, Amp^R	This study
pCH2500	pNAK::*galM´*, Amp^R Kan^R	This study
pCH2503	pNAK::*galT´-yfp-galM´*, Amp^R Kan^R	This study
pCH7959	pCH450::*cdiA-CT/*$cdiI_{o11}^{EC869}$*-DAS*, produces $CdiI_{o11}^{EC869}$ with C-terminal ssrA(DAS) epitope for controllable proteolysis, Tet^R	(176)
pCH9305	Constitutive expression of chimeric $cdiA^{EC93}$-CT_{o11}^{EC869} and $cdiI_{o11}^{EC869}$ genes, Cm^R	(177)
pCH9315	pTrc99a::$cdiI_{o11}^{EC869}$, IPTG-inducible expression of $cdiI_{o11}^{EC869}$ immunity gene, Amp^R	(177)
pCH9433	Constitutive expression of chimeric $cdiA^{EC93}$-$CT_{II}^{Bp1026b}$ and $cdiI_{II}^{Bp1026b}$ genes, Cm^R	This study
pCH9577	pTrc99a::$cdiI_{II}^{Bp1026b}$, IPTG-inducible expression of $cdiI_{II}^{Bp1026b}$ immunity gene, Amp^R	(169)
pCH9922	pTrc99KX::*yciB*, IPTG-inducible expression of *yciB*, Amp^R	This study
pCH10163	Cosmid pCdiA-CT/*pheS** that carries a *kan-pheS** cassette in place of the *E. coli* EC93 *cdiA-CT/cdiI* coding sequence. Used for allelic exchange and counter-selection. Cm^R Kan^R	(177)
pCH10415	Constitutive expression of chimeric $cdiA^{EC93}$-NT_{o11}^{EC869}-$CT_{II}^{Bp1026b}$ and $cdiI_{II}^{Bp1026b}$ genes, Cm^R	(172)

pCH10445	Constitutive expression of chimeric *cdiA*^{EC93}-*CT*^{ECL} and *cdiI*^{ECL} genes, Cm^{R}	(175)
pCH10673	Constitutive expression of chimeric *cdiA*^{EC93}-*CT*^{EC536} and *cdiI*^{EC536} genes, Cm^{R}	(172)
pCH11434	Constitutive expression of chimeric *cdiA*^{EC93}-*CT*^{NC101} and *cdiI*^{NC101} genes, Cm^{R}	This study
pCH11446	Constitutive expression of chimeric *cdiA*^{EC93}-*CT*^{MHI813} and *cdiI*^{MHI813} genes, Cm^{R}	This study
pCH11483	Constitutive expression of chimeric *cdiA*^{EC93}-*CT*^{EC3006} and *cdiI*^{3006} genes, Cm^{R}	This study
pCH11840	pTrc99a::*ptsG*, IPTG-inducible expression of *ptsG*, Amp^{R}	This study
pCH11949	Constitutive expression of chimeric *cdiA*^{EC93}-*CT*^{TTO1} and *cdiI*^{TTO1} genes, Cm^{R}	This study
pCH11950	Constitutive expression of chimeric *cdiA*^{EC93}-*CT*$_1^{Dd3937}$ and *cdiI*$_1^{Dd3937}$ genes, Cm^{R}	This study
pCH12021	pTrc99KX::*ptsG(C421S)*, IPTG-inducible expression of *ptsG(C421S)*, Amp^{R}	This study
pCH12022	pTrc99KX::*metI*, IPTG-inducible expression of *metI*, Amp^{R}	This study
pCH12024	pTrc99KX::*rbsC*, IPTG-inducible expression of *rbsC*, Amp^{R}	This study
pCH12025	pTrc99KX::*gltK*, IPTG-inducible expression of *gltK*, Amp^{R}	This study
pCH12042	pTrc99KX::*cdiI*^{NC101}, IPTG-inducible expression of *cdiI*^{NC101} immunity gene, Amp^{R}	This study
pCH12043	pTrc99KX::*cdiI*^{MHI813}, IPTG-inducible expression of *cdiI*^{MHI813} immunity gene, Amp^{R}	This study
pCH12045	pTrc99KX::*cdiI*^{EC3006}, IPTG-inducible expression of *cdiI*^{EC3006} immunity gene, Amp^{R}	This study
pCH12077	Constitutive expression of chimeric *cdiA*^{EC93}-*NT*^{EC3006}-*CT*^{EC536} and *cdiI*^{EC536} genes, Cm^{R}	This study
pCH12082	pTrc99KX::*cdiI*$_1^{3937}$, IPTG-inducible expression of *cdiI*$_1^{3937}$ immunity gene, Amp^{R}	This study
pCH12202	pTrc99a::*ptsG(E387Oc)*, IPTG-inducible expression of PtsG lacking the C-terminal IIB domain, Amp^{R}	This study
pCH12205	pTrc99KX::*cdiI*^{TTO1}, IPTG-inducible expression of *cdiI*^{TTO1} immunity gene, Amp^{R}	This study
pCH12237	Constitutive expression of chimeric *cdiA*^{EC93}-*NT*^{EC3006}-*CT*$_{o11}^{EC869}$ and *cdiI*$_{o11}^{EC869}$ genes, Cm^{R}	This study
pCH12599	pCH450::*cdiA-CT/cdiI*^{EC3006}-*DAS*, produces CdiI^{EC3006} with C-terminal ssrA(DAS) epitope for controllable proteolysis, Tet^{R}	This study

[a]Abbreviations: Amp^{R}, ampicillin-resistant; Cm^{R}, chloramphenicol-resistant; Kan^{R}, kanamycin-resistance; Rif^{R}, rifampicin-resistant; Tet^{R}, tetracycline-resistant

Table 3. Oligonucleotides used in this study.

Oligonucleotide	*Sequence*[a]	*Reference*
DL1527	5´ - GAA CAT CCT GGC ATG AGC G	(177)
DL1663	5´ - CCC AAA GGT TAG ACA CCA GAC C	(177)
DL2368	5´ - GTT GGT AGT GGT GGT GCT G	(177)
DL2470	5´ - ATT ATT CTC AAC CGA GTT CCT ACC TG	(177)
CH106 (Kan-1)	5´ - TGT GTA GGC TGG AGC TGC TTC	This study
CH107 (Kan-2)	5´ - CAT ATG AAT ATC CTC CTT AGT TCC	This study
CH577 (Ile 1 probe)	5´ - ACC GAC CTC ACC CTT ATC AG	This study
CH2139 (yciB-Kpn-for)	5´ - AAT GGT ACC ATG AAG CAG TTT CTT GAT TTT TTA C	This study
CH2140 (yciB-Xho-rev)	5´ - GCA CTC GAG TTA GGA TTT ATC TTC CTG CGG	This study
CH2260 (mariner rev seq)	5´ - CAA GCT TGT CAT CGT CAT CC	This study
CH2501 (EC93-1026b)	5´ - CAG GTA GGA ACT CGG TTG AGA ATA ATG CAC TGG GCA ACG ACC CCC AAA AAA CG	This study
CH2504 (EC93-1026b)	5´ - GGT CTG GTG TCT AAC CTT TGG GTT ACC TCC GGT ATT CGT TAT CTT GC	This study
CH2525 (BTH0599-Kpn-for)	5´ - AAT GGT ACC ATG CAA CTG ATC GAA GTC TCC	This study
CH2526 (BTH0599-Xho-rev)	5´ - ATA CTC GAG TCA TCG ATC GGA GGT GTT CGG	This study
CH2636 (ftsH-Eco-for)	5´ - GTT TTG AAT TCA GTT GTA ATA AGA GG	This study
CH2637 (ftsH-Hind-rev)	5´ - AAA AAG CTT CAT GAT GTT ATC CCT GG	This study
CH2638 (ftsH(K129)-Hind-rev)	5' - ACA AAG CTT ATT TGC CAC CGC CGC C - 3'	This study
CH2660 (ftsH-F228A)	5' - GCA CCC ACA CCG ACG GCC ATT TCT ACG - 3'	This study
CH2662 (ftsH-S400-Hind-rev)	5' - TTA AGC TTA GGA GCG ACG TTC C - 3'	This study
CH2663 (ftsH-H414Y)	5' - CGA CGG CTT ACT ACG AAG CGG GTC ATG - 3'	This study
CH2685 (Pmir-ftsH-Eco-for)	5' - AAG GAA TTC GTT AAC ACA GTT GTA ATA TG - 3'	This study
CH2686 (Pmir-ftsH-Kpn-rev)	5' - ACC GGT ACC CGG AGG ACC AAC CAT TAG G - 3'	This study
CH3172 (3006)	5´ - CAG GTA GGA ACT CGG TTG AGA ATA ATT ATC TTA GCG TGT CTG AAA AGA CAG AGC	This study
CH3173 (3006)	5´ - GGT CTG GTG TCT AAC CTT TGG GTT AAT TAT TCA GAG GAT AAG CTT TTG AAA AAT	This study

	CAT CG	
CH3174 (MHI813)	5´ - CAG GTA GGA ACT CGG TTG AGA ATA ATT TTT TGA CCG CAG ATC AGA TCG ATA GC	This study
CH3175 (MHI813)	5´ - GGT CTG GTG TCT AAC CTT TGG GTT ATA GTT CAT CAT CAT ATT GAA AGT TTA TGC TAA	This study
CH3176 (NC101)	5´ - CAG GTA GGA ACT CGG TTG AGA ATA ATT ACC TGA GCG TGT CTG AAA AGA CAG	This study
CH3177 (NC101)	5´ - GGT CTG GTG TCT AAC CTT TGG GTT ATT CAG GCC ATG CCA ATC CAT C	This study
CH3238 (NC101-cdiI-for)	5´ - CTG GTA CCA TGG ATA TTT GGC CTG	This study
CH3239 (NC101-cdiI-rev)	5´ - GAC TCG AGT TAT TCA GGC CAT GCC AAT C	This study
CH3240 (MHI-cdiI-for)	5´ - CTG GTA CCA TGA ACG AAT TAG ATG	This study
CH3241 (MHI-cdiI-rev)	5´ - GAC TCG AGT TAT AGT TCA TCA TCA TAT TG	This study
CH3244 (3006-cdiI-for)	5´ - CTG GTA CCA TGA TAA ATG TGA ATA G	This study
CH3245 (3006-cdiI-rev)	5´ - GAC TCG AGT TAA TTA TTC AGA GGA TAA GC	This study
CH3269 (PSI-univ-Nco-for)	5´ - TTT AAG AAG GAG TCT CTC CCA TGG - 3'	This study
CH3422 (NC101-cdiI-Spe-rev)	5´ - GAA CTA GTT TCA GGC CAT GCC AAT C	This study
CH3425 (3006-cdiI-Spe-rev)	5´ - GAA CTA GTA TTA TTC AGA GGA TAA GCT TTT G	This study
CH3477 (metI-for)	5´ - CTG GTA CCA TGT CTG AGC CGA TGA TGT G	This study
CH3478 (metI-rev)	5´ - GAC TCG AGT TAC TTG CGA GTG ACA GCC	This study
CH3481 (ptsG-C421S-for)	5´ - CAT TAC TAA CCT CGA CGC AAG TAT TAC CCG TCT GC	This study
CH3513 (Dd3937-1)	5´ - CAG GTA GGA ACT CGG TTG AGA ATA ATT TCC TGA ACA AAG GAA GAC CG	This study
CH3514 (Dd3937-1)	5´ - GGT CTG GTG TCT AAC CTT TGG GTT AAC TCC ACT TCC ATT TTA TGA TCA AAT	This study
CH3519 (PlumTTO1)	5´ - CAG GTA GGA ACT CGG TTG AGA ATA ATG CGC TGG CCT CGC GAA ATC	This study
CH3520 (PlumTTO1)	5´ - GGT CTG GTG TCT AAC CTT TGG GTT AAT TAC CTT CTA TCC ATA CTT GC	This study
CH3530 (Pestoides A)	5´ - CAG GTA GGA ACT CGG TTG AGA ATA ATG CGC TGG GTC TGG CTC TGA AG	This study
CH3531 (Pestoides A)	5´ - GGT CTG GTG TCT AAC CTT TGG TTA ATA CCA TTT TAC ATT AAA ATC AGC	This study

CH3570 (pUC rev Xho)	5′ - AAA CTC GAG GCC TCT GCA GTC G	This study
CH3571 (pUC for Xho)	5′ - AAA CTC GAG TCG CGA ATG CAT C	This study
CH3572 (Pest cdiI for)	5′ - GGA GGT ACC ATG ATC TTG AAA AAA G	This study
CH3612 (ptsG-Eco-for)	5′ - GTT CCG AAT TCA AGA ATG CAT TTG CTA ACC TG	This study
CH3613 (ptsG-Pst-rev)	5′ - GAC TGC AGT TAG TGG TTA CGG ATG TAC TC	This study
CH3629 (gltK-for)	5′ - CTG GTA CCA TGT ACG AGT TTG ACT GGA G	This study
CH3630 (gltK-rev)	5′ - GAC TCG AGT TAT GCT GTC CTT CTT TTC AAG	This study
CH3631 (rbsC-for)	5′ - CTG GTA CCA TGA CAA CCC AGA CTG TCT C	This study
CH3632 (rbsC-rev)	5′ - GAC TCG AGT TAC TGC TTT TTG TTG TCT ACC	This study
CH3633 (gltJ-for)	5′ - CTG GTA CCA TGT CTA TAG ACT GGA ACT GG	This study
CH3634 (gltJ-rev)	5′ - GAC TCG AGT TAT TTG CCC CCC ATG TTG	This study
CH3674 (3937-cdiI2-Kpn-for)	5′ - GAA GGT ACC ATG AAA TGT AAT GAT TTT	This study
CH3675 (3937-cdiI2-Xho-rev)	5′ - TTT CTC GAG CTA ACT CCA CTT CCA TT	This study
CH3676 (TTO1-cdiI-Kpn-for)	5′ - TTT GGT ACC ATG AAT ACT AAA CTT AAT G	This study
CH3677 (TTO1-cdiI-Xho-rev)	5′ - TTT CTC GAG CTA ATT ACC TTC TAT CC	This study
CH3682 (536-K127-for)	5′ - AAA ACT GTA GAT AAG CTT AAT CAG AAG	This study
CH3683 (3006-L167-OE-rev)	5′ - CTT CTG ATT AAG CTT ATC TAC AGT TTT CAG AAC TTC TAT CTT ACT GGC C	This study
CH3722 (ptsG-R386-Xho-rev)	5′ - GAC TCG AGT TAA CGA CCC GGC GTT TTC	This study
CH3723 (o11CT-T151-for)	5′ - ACA GCG ACA GCG ACG	This study
CH3724 (3006NT-L167-o11CT-T151-rev)	5′ - CGT CGC TGT CGC TGT CAG AAC TTC TAT CTT ACT GGC C	This study
CH3787 (galT-Kpn-for)	5′ - CAC GGT ACC ATT TGG GCA AAT AGC TTC C	This study
CH3788 (yfp-Eco-rev)	5′ - CT GAA TTC GCG GCC GCT TCT AGA	This study
CH3789 (galM-Bam-for)	5′ - CGC GGA TCC CGG AAG AGC TGG	This study

CH3790 (galM-Sac-rev)	5´ - TCT GAG CTC AGG GCA AAC AGC ACC	This study

[a]Restriction endonuclease sites are underlined.

III. YciB is required for metal tolerance in Escherichia coli

This work is part of a manuscript in preparation and has not yet been published.

A. Introduction

A number of *E. coli* proteins are required for the binding, delivery, and activity of CdiA-CTs during CDI. These proteins have other known physiological functions (157, 173, 192, 193), and there are no examples of *E. coli* genes outside of the *cdi* locus that produce proteins specifically required for CDI and no other cellular role. Parsing apart the physiological role of metabolic proteins required for CDI and their contribution to toxin delivery is of great interest, as unraveling these complexities will allow us to better understand the evolution and function of CDI families. We have previously identified inner membrane proteins required for the translocation of nuclease CdiA-CTs, including some (such as MetI and PtsG) that are part of multiunit membrane complexes that function as metabolite and small molecule transporters (173). The physiological function of these proteins and protein complexes is not required for CDI. PtsG mutants unable to transport or phosphorylate glucose still permit the delivery of specific CdiA-CT molecules, and other parts of the MetI protein complex can be deleted from target cells without disrupting CDI (173).

During our search for inner membrane proteins required for the delivery of CdiA-CTs, we identified *yciB* as a gene necessary for the translocation of CdiA-CT_{o11}^{EC869} from *E. coli* into target cells (173). YciB is encoded by a small open reading frame and is predicted to localize to the inner membrane in *E. coli* (295, 296). As with other "*y*" genes in *E. coli*, the exact function of the *yciB* gene product is unknown (297, 298). Therefore, we were interested in characterizing YciB to better understand not only its role in normal *E. coli* physiology, but also the function of this protein in CdiA-CT transport during contact-

dependent inhibition. Here we present results implicating YciB as a component required for metal tolerance in *E. coli*.

B. Results

1. yciB *encodes a non-essential putative inner membrane protein in E. coli that is highly conserved in gammaproteobacteria*

The *yciB* gene is located on the minus strand of the *E. coli* chromosome near the φ80 phage *att* site (295, 299). It is flanked by the *opp* operon, which encodes an oligopeptide permease (300), and the *trp* operon, which regulates tryptophan biosynthesis (301) (Figure 1A). *yciB* is 540 nucleotides in length and is predicted to encode a 179-residue inner membrane protein (296). Experimental analysis of *ispA*, the *yciB* homolog in *Shigella flexneri*, revealed that *ispA* mutants have a division defect during intracellular infection of epithelial cells (302, 303). While no detailed mechanistic function has been ascribed to YciB in *E. coli*, recent reports suggest that YciB interacts with ZipA, RodZ, and MurG, which are involved in peptidoglycan synthesis and cell division (304, 305).

YciB is predicted to form a 5-pass transmembrane protein with a periplasmic N-terminal tail and a cytoplasmic C-terminus (306, 307) (Figure 1B). The *E. coli* YciB and *Shigella* IspA proteins are virtually identical (99.4% conservation, or 178/179 residues identical) (302, 303), so we asked whether this conservation extended throughout gammaproteobacteria. We identified closely-related homologs using the protein BLAST database (308) and created a sequence logo from the top 100 matches (including *Shigella*, *Citrobacter*, *Salmonella*, *Enterobacter*, *Klebsiella*, *Yokenella*, *Kluyvera*, *Raoultella*, *Trabulsiella*, *Leclercia*, and *Escherichia* species) using WebLogo (309) to easily identify completely conserved residues (Figure 1C). This protein is highly conserved across all examined species. The sequence

variations that do exist occur at the residues predicted to be localized inside transmembrane domains (Figure 1C, black lines), in the cytoplasmic loop between transmembrane passes 3 and 4, and in the cytoplasmic tail. The N-terminal sequence (up to transmembrane domain 1) is almost completely conserved across all 100 input sequences.

We next investigated the role of YciB in *E. coli* physiology under standard laboratory conditions. We performed growth curves with wild-type and Δ*yciB E. coli* MC4100 cells (Figure 2A) and found that they have almost identical growth rates. Microscopy images were captured at various timepoints during growth representing early log phase (1 hr), mid-log phase (3 hr), and stationary phase (5 hr) and were used to examine the morphology of wild-type and Δ*yciB* strains. The cells are phenotypically similar over different growth phases (Figure 2B), although we note that the Δ*yciB* cells appear less opaque in stationary phase (Figure 2B, 5 hr). Using the same microscopy images represented in Figure 2B, the length of wild-type and Δ*yciB* cells were measured at each timepoint (*N* between 160 and 192 cells for all samples). There is a statistically-significant difference between the length of wild-type cells and Δ*yciB* cells after 1 and 3 hours of growth (Figure 1C), but we note that this size difference is extremely small (Table 1) and does not match the cell-length differences observed by Badaluddin and Kitakawa (304).

2. YciB is required for tolerance to select metals under aerobic conditions

In 2012, Nichols and coworkers in the Gross lab at UC San Francisco published a comprehensive phenotypic screen of the entire Keio collection of single-gene knockouts in *E. coli* (289, 310). Their dataset, which can be accessed at http://ecoliwiki.net/tools/chemgen/, indicated that *yciB* knockouts were highly susceptible to a variety of compounds, including metals (copper and nickel), detergents (SDS and deoxycholate), chelators (EGTA and

EDTA), and antibiotics (including gentamicin, tobramycin, puromycin, bleomycin, and amikacin). To verify these results, we tested the growth of wild-type and Δ*yciB* cells on LB-agar plates supplemented with metals, EGTA, and deoxycholate (Figure 3A). Δ*yciB* cells have a severe growth defect when grown on media containing 4 mM $CuCl_2$, but we did not observe a growth defect when grown on media containing 1 mM $NiSO_4$. Interestingly, we found that Δ*yciB* cells grew better than wild-type on LB-agar supplemented with 2% deoxycholate. All growth differences were complemented to wild-type levels by providing cells a plasmid-borne copy of *yciB*.

Because the most severe growth phenotype was observed in the presence of copper, we tracked the growth rate of cells in LB media supplemented with 4 mM $CuCl_2$ to determine how growth is affected over time in these conditions. Wild-type cells continue to grow when treated with copper, albeit at a much slower rate than untreated cells (Figure 3B, compare maroon and dark purple lines). However, *yciB* knockout cells were completely unable to grow over the course of 6 hours when treated with copper (Figure 3B, light purple line). To test whether the growth deficiency observed in the presence of copper could be phenocopied in additional metal-rich envionments not tested by Nichols *et al.*, we grew wild-type, Δ*yciB*, and Δ*yciB* cells complemented with plasmid-borne *yciB* in LB media supplemented with varying concentrations of silver ($AgNO_3$) and zinc ($ZnCl_2$) in 96-well plates and measured the OD_{600} to track cell growth. Δ*yciB* cells became susceptible to both metals at a concentration 10-fold lower than the level at which growth of wild-type cells was fully inhibited (10 µM vs 100 µM $AgNO_3$ and 1 mM vs 10 mM $ZnCl_2$) (Figure 3C, D).

Two chromosomally-encoded systems are utilized by *E. coli* for handling high concentrations of copper inside the cell. Under aerobic conditions, CueR regulates the

expression of the ATPase efflux pump CopA and the periplasmic multicopper oxidase CueO (311-314). Under anaerobic conditions, the two-component signal transduction system CusRS regulates the expression of the CusABC multidrug efflux system and CusF, a periplasmic copper/silver-binding protein (312, 315, 316). To compare the toxicity of *yciB* knockouts in high copper environments with the well-characterized Cue and Cus systems, we constructed single-gene knockouts of all *cue* and *cus* genes (*copA, cueEO,* and *cusABCFRS*) by transducing these alleles from the Keio collection (289) into a fresh background. We grew these strains on LB-agar plates supplemented with 2 mM $CuCl_2$ and compared their growth to wild-type or Δ*yciB* cells (Figure 4). The most severe growth defect on copper plates occurred in the Δ*copA* strain, and the *cueO* deletion mutant also had a noticeable colony phenotype compared to wild-type cells (Figure 4, top panels). Δ*yciB* cells exhibited a growth phenotype similar to that observed with the Δ*cueO* strain. Providing plasmid-borne *yciB* complemented the growth phenotype and restored colony growth and morphology to wild-type levels. Colony morphology of the *cus* system knockouts did not change in response to copper (Figure 4, bottom panels), which is in agreement with previous studies showing that this system is important for anaerobic, not aerobic, copper tolerance (312, 315, 316).

We next wanted to determine which domains or regions in YciB are important for conferring tolerance to copper stress. As YciB is predicted to localize to the inner membrane, it is possible that this protein interacts with partners on either the periplasmic or cytoplasmic face. To test this, we constructed in-frame insertions in which the periplasmic and cytoplasmic loops connecting the transmembrane domains were individually disrupted by a 9-residue HA epitope (sequence YPYDVPDYA). The residues replaced by the HA tag

are indicated by the black brackets in Figure 5A. We then transformed these plasmids into Δ*yciB* cells and tested their ability to grown on LB-agar plates supplemented with 2 mM $CuCl_2$. All HA insertions complemented growth (Figure 5B).

We next constructed a set of point mutations in the N-terminal periplasmic domain and in loop 3, which resides in the cytoplasm. The N-terminus of YciB is highly conserved, so we reasoned that some of the most conserved residues here may contribute to function. We also made constructs containing individual polymorphisms in loop 3 that have been found in sequenced *E. coli* isolates from the ECOR database (317) (Pro99Gln, Thr110Met, Leu111Val, Pro114Ser, and Ser117Leu). We provided plasmid-borne copies of these mutated *yciB* alleles to Δ*yciB* cells and grew them on copper LB-agar plates to observe growth defects. All HA tag insertions fully complemented the growth phenotype (Figure 5B), and Δ*yciB* cells carrying all individual point mutation constructs grew as well as wild-type (Figure 5C).

3. yciB *alleles from different species are functionally equivalent*

Because none of the loop insertions or individual point mutations we constructed affected the function of YciB, we asked whether alleles from different species were functionally equivalent in *E. coli*. Although the sequence of YciB is generally conserved (Figure 1C), the genetic neighborhood surrounding this gene can vary due to its proximity to the φ80 *att* site (Figure 1A). Something about prophages, other islands present. Additionally, other species might inhabit other environments that influence the need for and expression of *yciB*, the polymorphisms in these alleles could affect function. We cloned *yciB* from the gammaproteobacteria species *Enterobacter cloacae* (ECL), *Enterobacter aerogenes* (EAE), and *Yersinia pseudotuberculosis* YPIII (YPIII), all of which are closely related to *E. coli*

(Figure 6A). We also cloned *yciB* from *Burkholderia thailandensis*, which is a betaproteobacteria and therefore more distantly-related to *E. coli* than the other organisms (Figure 6B). When provided on a plasmid to Δ*yciB* cells, these alleles all complement the copper sensitivity observed with the empty vector control (Figure 6C).

Though the normal physiological role of YciB appears to be providing resistance to metal toxicity, we are also interested in this protein because of its role in the delivery of CdiA-CT_{o11}^{EC869} during CDI, a process mediated by the N-terminal domain of this toxin (173). Because this toxin must translocate across the inner membrane of target cells, it may require direct contact with YciB on either the periplasmic or cytoplasmic face. We therefore utilized the point mutations and HA tag insertions in periplasmic and cytoplasmic domains of YciB to determine whether these regions were required for interaction with CdiA-CT_{o11}^{EC869}. Δ*yciB* cells are resistant to inhibition by CdiA-CT_{o11}^{EC869}, and this phenotype is easily quantifiable using co-culture assays to enumerate viable target cells of a given genotype. Therefore, we individually transformed all point mutations, HA tag insertion, and heterologous allele plasmids into a Δ*yciB* background and competed these against CDI_{o11}^{EC869}. As shown in Figure 7, all mutations complemented the CDI-resistant phenotype of Δ*yciB* cells, indicating that none of these regions are essential for CDI. We also tested the heterologous alleles from *E. cloacae, E. aerogenes, Yersinia pseudotuberculosis* YPIII, and *B. thailandensis* and found that they all complemented CDI resistance. Therefore, in the context of these experiments, providing a functional *yciB* gene to *E. coli* target cells is enough to confer sensitivity to CdiA-CT_{o11}^{EC869}.

C. Discussion

As with other trace metals, the physiological level of copper must be tightly regulated in

bacteria. While trace amounts of copper must be present for use in enzymes such as copper- and zinc-containing superoxide dismutase (318), excess can be toxic (313, 319). Copper can participate in the Fenton reaction, which produces free hydroxyl radicals and contributes to membrane oxidation in cells, although the *in vivo* relevance of this reaction in the presence of copper is under debate. Because of the affinity between thiol groups and copper ions, another mechanism by which excess copper can exert toxicity is by the displacement of iron from iron-sulfur clusters in dehydratases (320, 321). This delicate balance is further complicated by host-pathogen interactions; during infection, eukaryotic hosts increase serum levels of copper as well as the concentration of copper at localized areas such as wounds or burns (322, 323). The mammalian copper transporter ATP7A also transfers copper to phagolysosomes containing internalized bacteria (322, 324-326).

Two chromosomally-encoded systems are used to detoxify excess copper in *E. coli*. The Cue system is regulated by CueR, a MerR-type metal-activated transcription factor that binds cytoplasmic copper and activates the expression of *copA* and *cueO* (311-314, 327). CopA is a P-type ATPase efflux pump that is active against Cu^{+} and other heavy metals (206, 311, 319, 327). CueO is a periplasmic multicopper oxidase that converts toxic Cu^{+} to the less toxic Cu^{2+} (311). As this process requires oxygen, the Cue system is the predominant copper response system under aerobic growth conditions. The Cus system is a two-component signal transduction copper response system mediated by CueRS, which activate the expression of the *cusCFBA* operon during copper and silver stress (311, 312, 316). CusABC form a tripartite complex analogous to multidrug efflux pumps (315, 316), and CusF is a small periplasmic metal-binding protein that binds Cu^{+} and Ag^{+} (315). While there is some functional redundancy between the Cue and Cus systems, Cue generally regulates the

response to copper under aerobic conditions while the Cus system functions anaerobically (312, 313, 315, 316, 328, 329). In addition to the two chromosomal copper detoxification systems, some natural isolates of *E. coli* also carry plasmid-borne copper resistance system composed of the Pco proteins (319, 329, 330). This is analogous to the aerobic Cue system, as PcoA is partially redundant with the periplasmic oxidase activity of CueO (330).

Here, we show that YciB contributes to metal tolerance in *E. coli*. Strains lacking *yciB* phenocopied a *cueO* deletion when grown on 2 mM $CuCl_2$ (Figure 4). Because there is overlap between silver and copper detoxification systems in *E. coli* (331-333), we tested whether *yciB* mutants also show an increased sensitivity to silver. Interestingly, we observed a statistically-significant growth defect in a Δ*yciB* strain compared to wild-type when grown in the presence of not only silver, but also zinc (Figure 3C and D). However, we note that *yciB* expression did not change in response to copper or zinc stress in previous transcriptional studies (334, 335). We did not observe a colony morphology defect when grown on media supplemented with nickel (Figure 3A), suggesting that YciB is not required for tolerance to this metal under the conditions we tested. The large-scale phenotypic screen carried out by Nichols *et al.* identified high nickel as a condition in which *yciB* mutants have a growth defect, but their experiments were performed using minimal media instead of rich LB media (310). Perhaps the differences in nutrient and metal concentrations between these two media account for these contrasting results.

The first hints at YciB function came from studies on the homolog IspA in *Shigella flexneri*, in which it was observed that *ispA* mutants exhibit cell division defects during intracellular infection (302, 303). We did not observe any noticeable cell division effects or filamentation phenotypes during growth of Δ*yciB* strains in standard laboratory conditions

using rich media (Figure 2). However, an article from Badaluddin and Kitakawa reports that *yciB* deletion strains are approximately half the length of wild-type *E. coli* cells (304). Their experiments were performed using the BW25113 background, which was used for construction of the Keio collection of single-gene knockouts (289). The genotypes of this strain and the strains used in this study (MC4100 and X90) vary significantly and may give rise to the conflicting results regarding cell length. Furthermore, the reported length of their wild-type strain (3.0 ± 0.7 μm) is greater than our wild-type X90 strain (1.593 ± 0.02545 μm). We also did not observe the same growth rate defect in Δ*yciB* cells that was reported by this study, and note that the growth defect reported by Badaluddin and Kitakawa (304) is not immediately comparable to the results presented in their other study on YciB function in *E. coli* (305).

The host environments in which *Shigella* IspA mutants were observed to have morphological defects differ greatly from the laboratory conditions in which these experiments were performed, and the contribution of copper to host immune responses is well-documented (322, 324-326, 336). Perhaps in an environment mimicking intracellular or other host conditions, deletion of *yciB* would, in fact, lead to cell division defects in *E. coli* as with *Shigella*. It would also be interesting to repeat the cell measurement experiments in conditions with sub-inhibitory concentrations of copper or other metals to determine whether *yciB* mutants have a cell division defect under these conditions.

Although we constructed a number of point mutations and insertions in YciB, we were unable to find mutants that affected metal tolerance activity or function in the context of CDI (Figure 7). These activities may be mediated by the cytoplasmic C-terminal tail, which we

did not mutate.[2] Copper typically associates with the thiol side chain of cysteine residues, but histidine and methionine can also coordinate this metal. CusF, the periplasmic component of the CusABCF system, coordinates both copper and silver via a unique His-Met-Met coordination site (331-333). YciB lacks the canonical Cys-X-X-Cys copper binding motif utilized by ATPases and copper chaperones (206). Though the C-terminal tail contains residues that could be involved in metal coordination, this sequence varies among species and therefore may not contribute to a conserved function (Figure 1). It is interesting to note that the C-terminal residues of YciB (HMPQEDKS) are found at the C-terminus of a P-type ATPase involved in copper transport in *Coprothermobacter proteolyticus* (HMPQEEK), but this motif has no specific ascribed function in this organism. YciB may also interact with other proteins by dimerizing or oligomerizing via transmembrane domains. Perhaps YciB interacts with components of previously-described metal detoxification systems in an unknown way. Alternatively, YciB and any interacting partners could constitute another metal tolerance system with broad substrate specificity.

The immediate genetic neighborhood surrounding *yciB* is highly conserved throughout species (Figure 8). Using the Prokaryotic Sequence homology Analysis Tool (PSAT, available at http://www.nwrce.org/psat/index.html) (337), we examined the genes in a 25-kilobase region surrounding *yciB* from 93 closely-related organisms to compare gene conservation. A *yciB* homolog was present in all genomes (Figure 8, center orange rectangle labeled with red text). *yciC* and *yciA*, the genes immediately upstream and downstream of *yciB*, were present in almost all genomes examined (Figure 8, pink and yellow rectangles flanking *yciB*). Interestingly, insertions of other genes separate these in organisms like

[2] We note that attempts to construct a C-terminal GFP fusion protein were difficult and suggest that interfering with this region may lead to toxicity in *E. coli*.

Yersinia, *Klebsiella*, and *Photorhabdus*, but all three genes are located in the same region of the genome. We note that the organisms in which either *yciA* or *yciC* are not present, the large intergenic regions in this area may not have been properly annotated. The location of *tonB* and *ompW* genes are conserved throughout nearly all of these organisms (88/93 for *tonB* and 90/93 for *ompW*). An interesting set of exceptions are the *Klebsiella* genomes examined here; many of them lack an annotated *tonB* gene in this area. The presence of other uncharacterized *yci* genes in this region (including *yciEFG*) is not widely-conserved throughout Gram-negative bacteria.

Although the location of *yciB* and the adjacent genes is well-conserved, the genomic region surrounding them is remarkably fluid (Figure 8, observe insertions upstream and downstream of the central *yciABC* region). The φ80 *att* site is located immediately upstream of *yciB*, and many sequenced isolates contain prophages or other insertions (like the type 3 secretion system in *E. coli* strain O111:H11128) that separate the *opp* locus from *tonB*, *yciABC*, and *ompW*.[3] Other isolates contain prophages or genomic islands downstream of *ompW* (such as the prophage CP933O/genomic island OI-57 in many enteropathogenic and Shiga toxin-producing *E. coli* isolates (338, 339)) although there is no annotated integration site here. Perhaps the conservation of genes in this area is indicative of co-expression or interaction patterns involved in the function of YciB.

In addition to metal tolerance, YciB may play a role in the maintenance of membrane integrity. Nichols *et al.* (cite) reported that *yciB* mutants showed growth deficiencies in a number of conditions, including high EGTA, high EDTA, and 4% SDS, which would promote destabilization or disruption of membranes. The presence of EGTA and EDTA

[3] *E. coli* DH10B contains a φ80 derivative, but this is a result of direct laboratory genetic manipulation to facilitate α-complementation, not natural variation in this region.

results in chelation of the magnesium and calcium ions that contribute to the integrity of the outer membrane of Gram-negative cells by bridging LPS chains, and SDS is a anionic detergent that solubilizes membrane proteins and lipids. Our own preliminary results confirm these data and show that *yciB* deletion strains have a growth defect in the presence of EGTA, EDTA, and SDS, but not the membrane-disrupting antibiotic polymixin B (data not shown). We also do not detect any defects in the levels of outer membrane proteins such as LamB and OmpA (data not shown). Additional experiments will be required to fully understand the role of YciB in *E. coli* physiology and whether this involves any other interacting partners in the cytoplasm, periplasm, or membrane. A more in-depth understanding of the motifs and domains required for YciB activity can also help elucidate the role of this protein in CdiA-CT translocation during CDI. Based on other inner membrane proteins required for delivery of CdiA-CT domains, we predict that the yet-unknown metal tolerance activity of YciB will be distinct from its contribution to CDI.

D. Materials and methods

1. Plasmid construction

All *E. coli yciB* mutations were constructed using pCH9922 as a template. The HA tag insertions were constructed via megaprimer PCR as follows. The HA tag sequence was fused to the coding region of *yciB* using primers CH2139/CH2616 (loop 1), CH2139/CH2617 (loop 2), CH2618/CH2140 (loop 3), or CH2619/CH2140 (loop 4). The resulting PCR product was purified and used in a second PCR reaction with either primer CH2140 (loops 1 and 2) or CH2139 (loops 3 and 4) and pCH9922 as template. The N-terminal P9A and V12P mutations were amplified using primers CH2804/CH2140 and CH2805/CH2140, respectively. The point mutations in loop 3 were constructed using

megaprimer PCR as follows. First, *yciB* was amplified with the appropriate codon substitutions using forward primers CH2634 (P99Q), CH2635 (T110M), CH2636 (L111V), CH2637 (P114S), and CH2638 (S117L) with reverse primer CH2140. The resulting PCR products were purified and used in a second reaction with template pCH9922 and primer CH2139. All final PCR products were purified, digested with KpnI and XhoI restriction enzymes, and ligated to a pTrc99KX vector treated with the same enzymes. Mutations and insertions were confirmed by DNA sequencing (University of California, Berkeley).

Heterologous alleles were amplified from genomic DNA or bacterial colonies using primers CH2460/CH2461 (*Yersinia pseudotuberculosis* YPIII YPK_2053), CH2139/CH2462 (*Enterobacter aerogenes* EAE21485), CH2139/CH2463 (*Enterobacter cloacae* ECL01649), or CH2683/CH2684 (*Burkholderia thailandensis*). *B. thailandensis* and *Yersnia pseudotuberculosis* YPIII genomic DNA was graciously provided by David Low and Natasha Edman.

2. In silico *analysis*

Genetic analysis of the *yciB* gene location was primarily done with the PEColi and EcoCyc databases (295, 296). The Prokaryotic Sequence homology Analysis Tool (PSAT) was used for the large genetic neighborhood analysis (337). The *E. coli* MG1655 *yciB* gene was used as an input, and output alignments were constrained only by the available genome sequences in the PSAT database. Predictions of the YciB membrane orientation were performed using the TMHMM server to predict transmembrane helices (306). The top predictions were put through additional transmembrane prediction software to confirm their validity. Transmembrane maps were created by using the domains predicted by TMHMM as input parameters for Topo2 (307). Sequence logos were created by using the NCBI protein

BLAST database to identify highly-conserved non-*E. coli* YciB sequences (308). These were aligned using Clustal Omega, and the FASTA output was loaded onto the WebLogo server (available at http://weblogo.berkeley.edu/logo.cgi, University of California, Berkeley).

3. Growth conditions

Media ingredients and chemicals were purchased from Sigma-Aldrich unless otherwise indicated. Cells were routinely grown in lysogeny broth (LB) with antibiotics as indicated. For growth curve analysis of growth rate, wild-type *E. coli* MC4100 as well as a *yciB* knockout strain were grown overnight in LB media with antibiotics (200 µg/mL rifampicin or 50 µg/mL kanamycin) and were diluted into fresh LB media without antibiotics the next day. These cells were grown to mid-log phase at 37 °C with shaking, at which point they were diluted to an OD_{600} of 0.05 in fresh pre-warmed LB media without antibiotics. OD_{600} values were measured every 30 m to track growth. 4 mM $CuCl_2$ was added after 30 minutes where indicated. Data is presented as the average of two independent experiments.

To observe colony morphology under different stress conditions, strains were grown overnight in LB media supplemented with antibiotics. The next day, cells were diluted into 2 mL LB media without antibiotics and grown at 37 °C with shaking until they reached mid-log phase. Each culture was adjusted to the same cell number per volume based on OD600 values, and 10-fold serial dilutions were performed in 1xM9 salts. 1 µL of each dilution was spotted onto LB-agar plates (plain or supplemented with chemicals, as indicated). Plates were incubated upright at 37 °C to allow the cultures to soak in, after which point they were turned upside down and incubated for 12-18 hours at 37 °C.

Growth assays in varying concentrations of $ZnCl_2$ and $AgNO_3$ were performed in flat-bottom 96 well plates (Nunc). Overnight cultures of the indicated strains were grown in LB

supplemented with antibiotics and were diluted into fresh LB media without antibiotics the next day. Cultures were grown to mid-log phase, at which point 1 µL of culture was seeded into the appropriate wells. OD_{600} values of each strain were measured to ensure equal cell per volume loading. 96 well plates were incubated at 37 °C with shaking on a Lab-Line 4625 Titer plate shaker at speed 5 for the indicated time, at which point the OD_{600} values were read using a 96-well plate reader. Data is represented as the mean of three independent replicates ±SEM.

4. Competition co-culture

Co-culture competitions with CDI inhibitor cells were carried out as previously described (177). Briefly, *E. coli* EPI100 inhibitor cells carrying pCH9305 and CH8251 target cells (wild-type or Δ*yciB::kan*) carrying a pTrc99a vector or the indicated *yciB* derivatives were grown overnight at 37 °C in LB media with antibiotics (150 µg/mL ampicillin). The next day, cells were diluted into separate 25 mL flasks in fresh LB without antibiotics and were grown until mid-log phase. Inhibitors and targets were mixed together at a 10:1 inhibitor:target ratio in fresh pre-warmed LB and were co-cultured for the indicated amount of time at 37 °C with shaking. At 0 and 3 hours, an aliquot of each was removed, diluted in 1xM9 salts, and plated onto LB-agar supplemented with 200 µg/mL rifampicin and 150 µg/mL ampicillin to select for viable target cells. Data presented is the average of three independent experiments ±SEM (where error bars are shown).

5. Microscopy and cell length analysis

Cells used for microscopy were wild-type or Δ*yciB E. coli* X90 derivatives. These cultures were grown overnight in LB supplemented with antibiotics and were diluted into fresh LB at 37 °C with shaking the next day. In mid-log phase, cells were diluted to an

OD_{600} of 0.05 in fresh pre-warmed media. At the indicated timepoints, samples were removed and spotted onto agarose pads for visualization. Agarose pads were made by mixing 1xM9 salts with 1% molecular biology grade agarose (Fisher Scientific) and pouring the solution between two plain microscopy slides. After solidifying, agarose pads were cut into strips and placed onto a glass microscopy slide. 5 µL of cell culture was pipetted onto the center of the agarose strip and covered by a glass coverslip. Slides were incubated face-up for 10 minutes at room temperature to allow the cells to adhere to the agarose and were imaged with an Olympus fluorescent microscope using a 100x oil objective and an Optronics MacroFire digital microscope camera. For length analysis, images were imported into FIJI (292), and cell lengths were measured using the line tool and ROI manager as previously described (202). Fields of view were cropped to 200x200 pixels using the GIMP software suite, and representative images are shown.

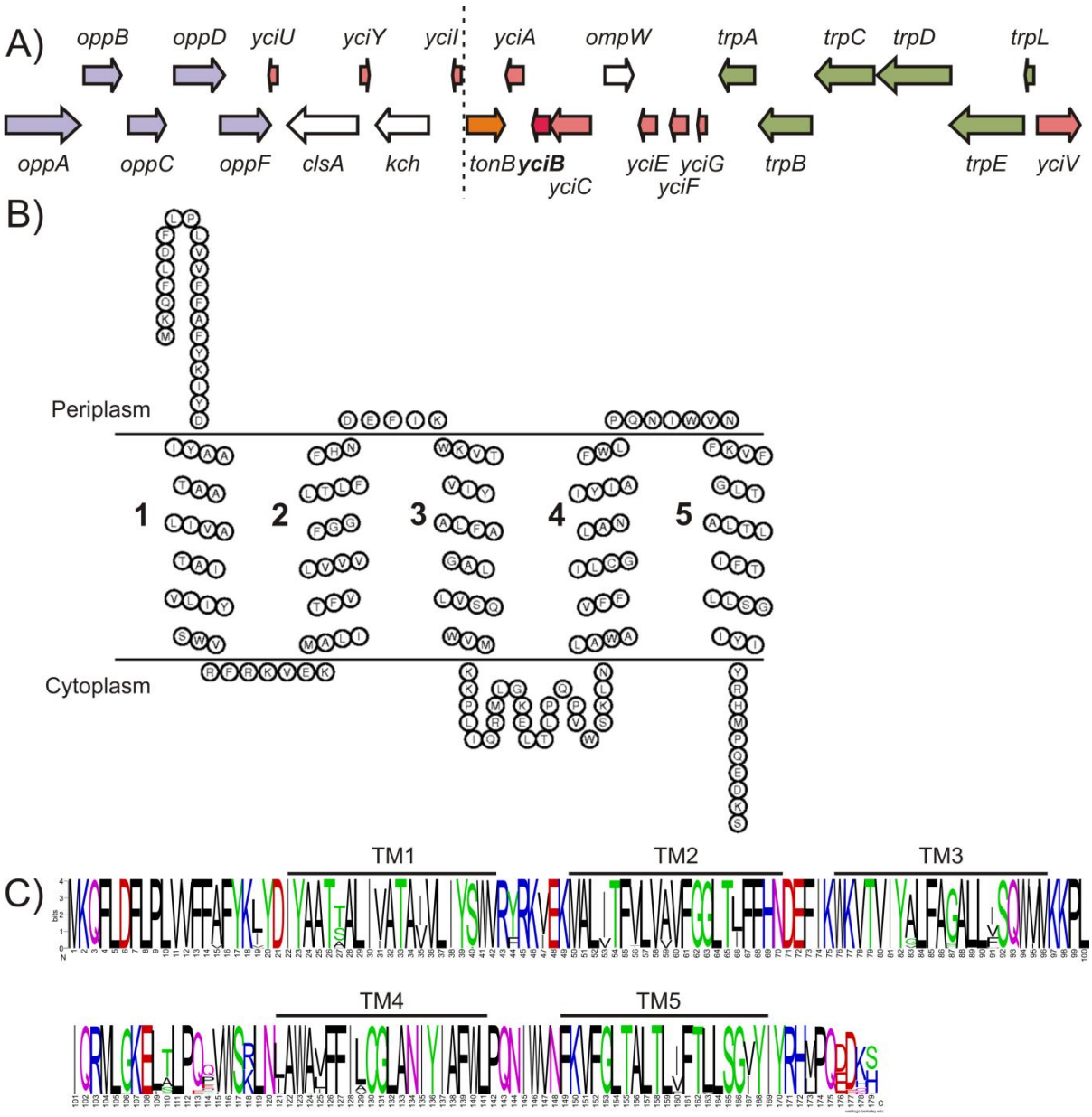

Figure 1. *yciB* encodes a putative inner membrane protein in *E. coli* that is highly conserved throughout gammaproteobacteria. (A) Genetic location of *yciB*. Genes in the *opp* operon are shaded light purple. Genes in the *trp* operon are shaded green. Other *yci* genes are colored salmon. *yciB* is shown in the center and is colored red. The φ80*att* site between *yciI* and *tonB* is indicated by the dashed line. (B) Transmembrane prediction of YciB as predicted by TMHMM and rendered by Topo2. (C) YciB proteins are highly conserved. A sequence logo was generated from the top 100 BLAST results (with *E. coli* sequences excluded). Letters spanning the entire y-axis are invariant among input sequences. Residues included in transmembrane domains are indicated, and the numbers correspond to the labels in (B).

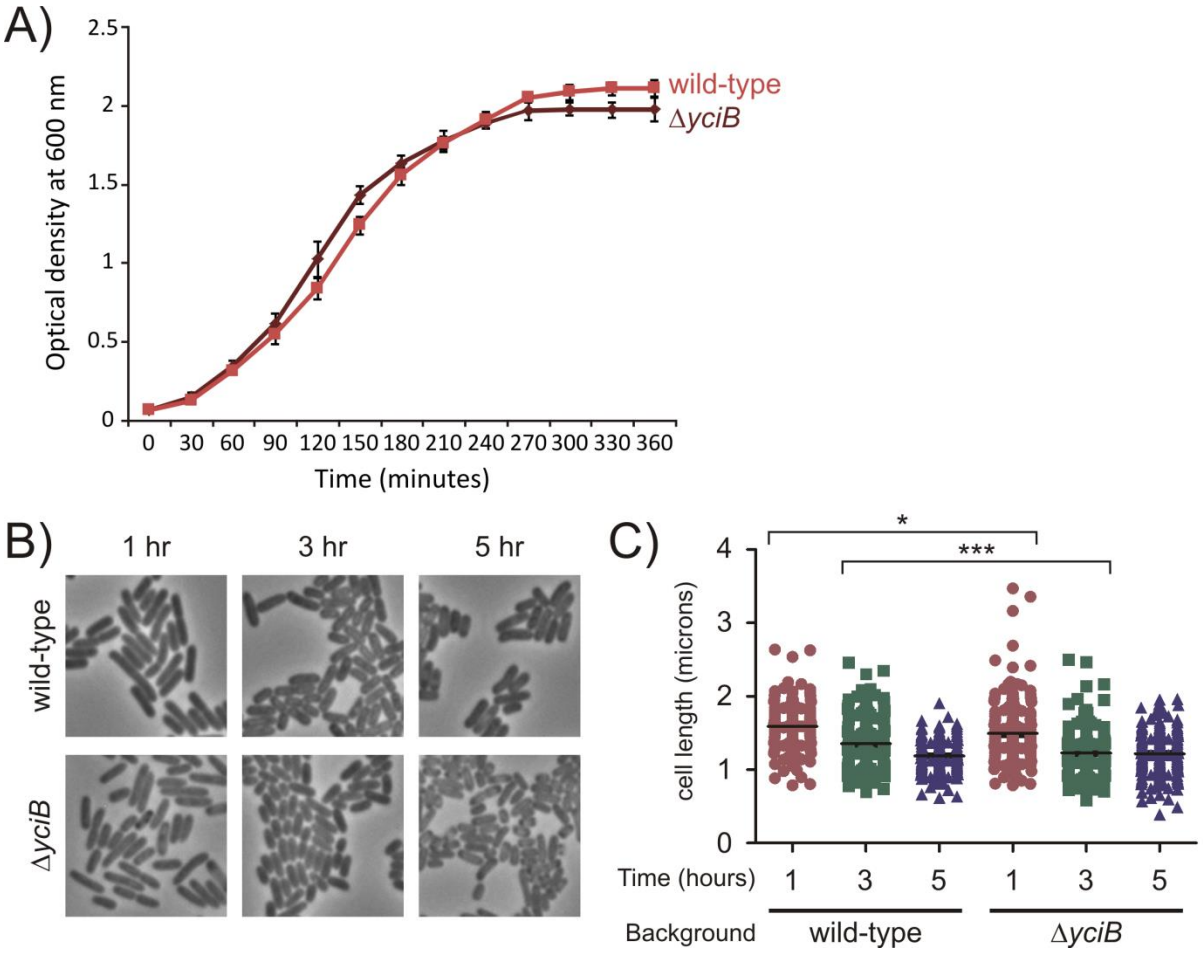

Figure 2. ***yciB* is a nonessential gene under laboratory conditions.** (A) Wild-type and yciB cells have similar growth rates when grown with aeration in LB media. Values reported are the mean of three independent replicates. Wild-type and yciB cells have (B) similar morphologies and (C) similar cell lengths over a 5 hour growth period (1 hour = early log phase, 3 hours = mid-log phase, 5 hours = stationary phase). Representative microscopy fields are shown in (B). In (C), each point represents a single measured cell. Unpaired two-tailed *t*-tests were used to determine significant length differences. *, $P = 0.0175$; ***, $P = 0.0002$.

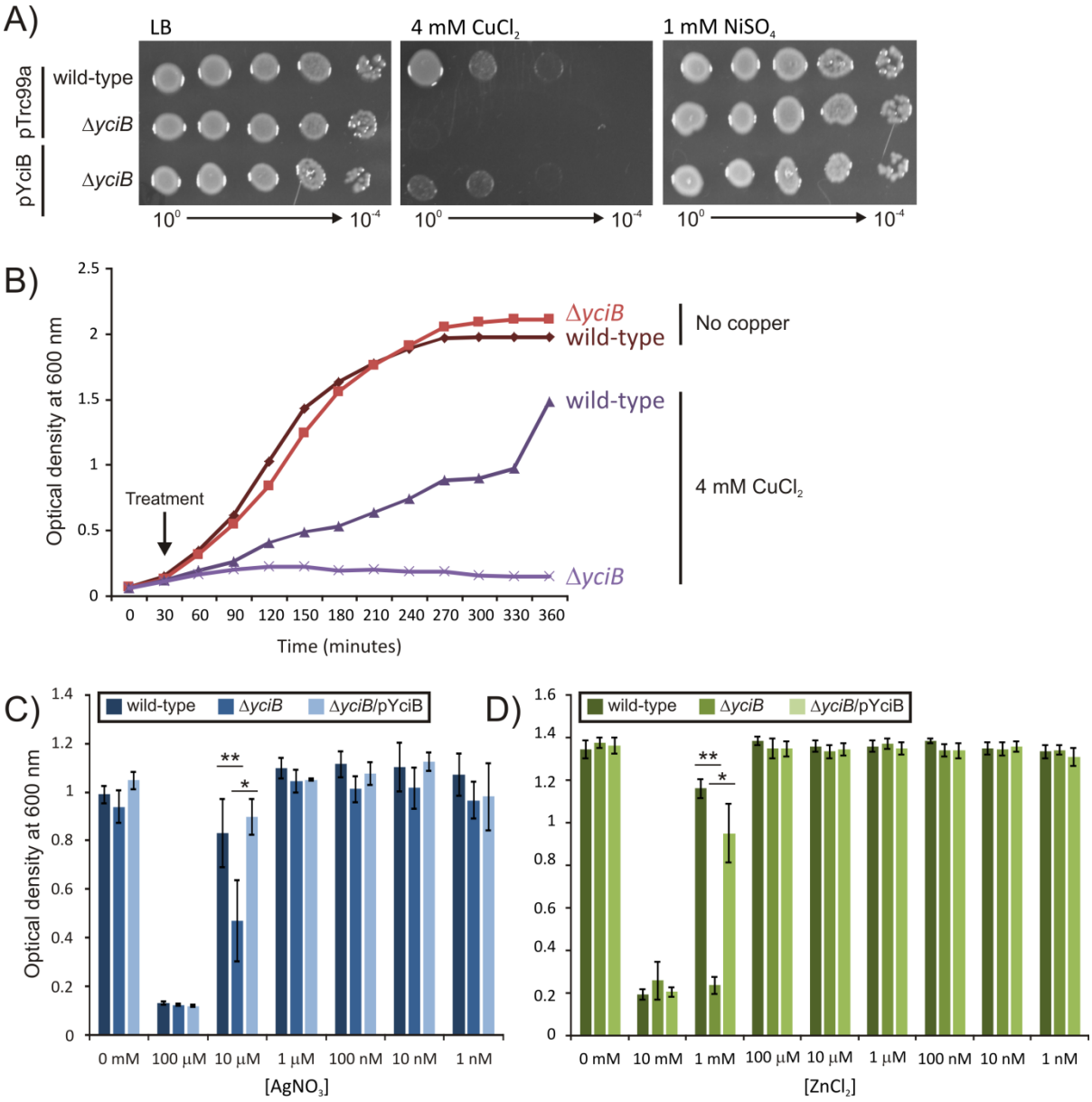

Figure 3. *yciB* is required for metal tolerance in *E. coli*. (A) Wild-type, Δ*yciB*, and Δ*yciB* pYciB derivatives of *E. coli* MC4100 were grown to mid-log phase and spotted onto LB-agar plates supplemented with a variety of compounds to assess growth. Δ*yciB* cells exhibit a severe growth defect compared to a wild-type control when grown with 4 mM $CuCl_2$ and have a growth advantage when grown with 2% deoxycholate. (B) Δ*yciB* cells (light purple line) have a severe growth defect compared to wild-type cells (dark purple line) when treated with 4 mM $CuCl_2$. Δ*yciB* cells also exhibit a growth defect when grown with (C) $AgNO_3$ and (D) $ZnCl_2$.

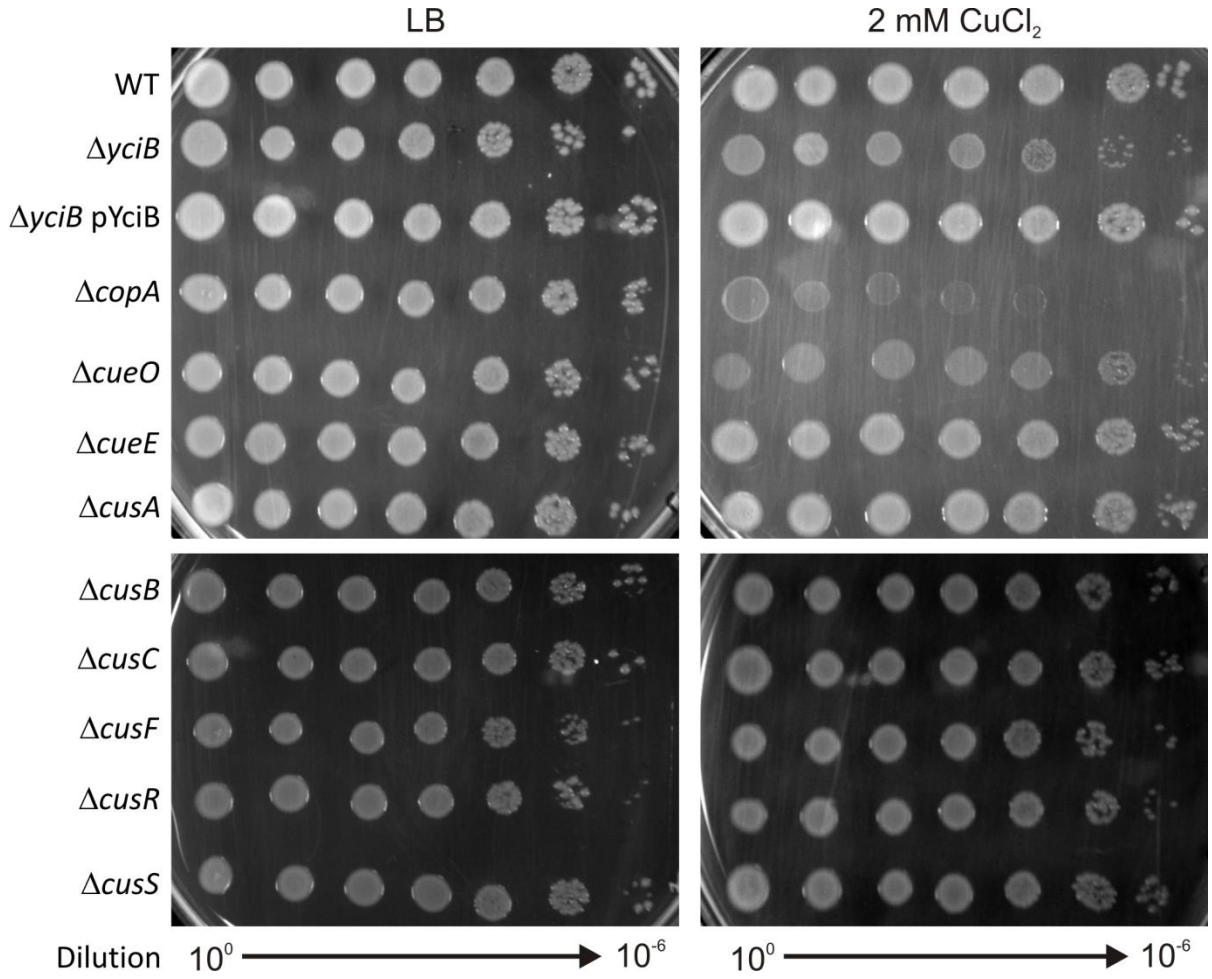

Figure 4. Deleting *yciB* phenocopies the loss of the aerobic copper response regulator CueO. All cells were grown to mid-log phase, diluted, and spotted onto LB-agar or LB-agar/$CuCl_2$ plates as indicated. Plates were imaged after overnight growth at 30 ^{o}C.

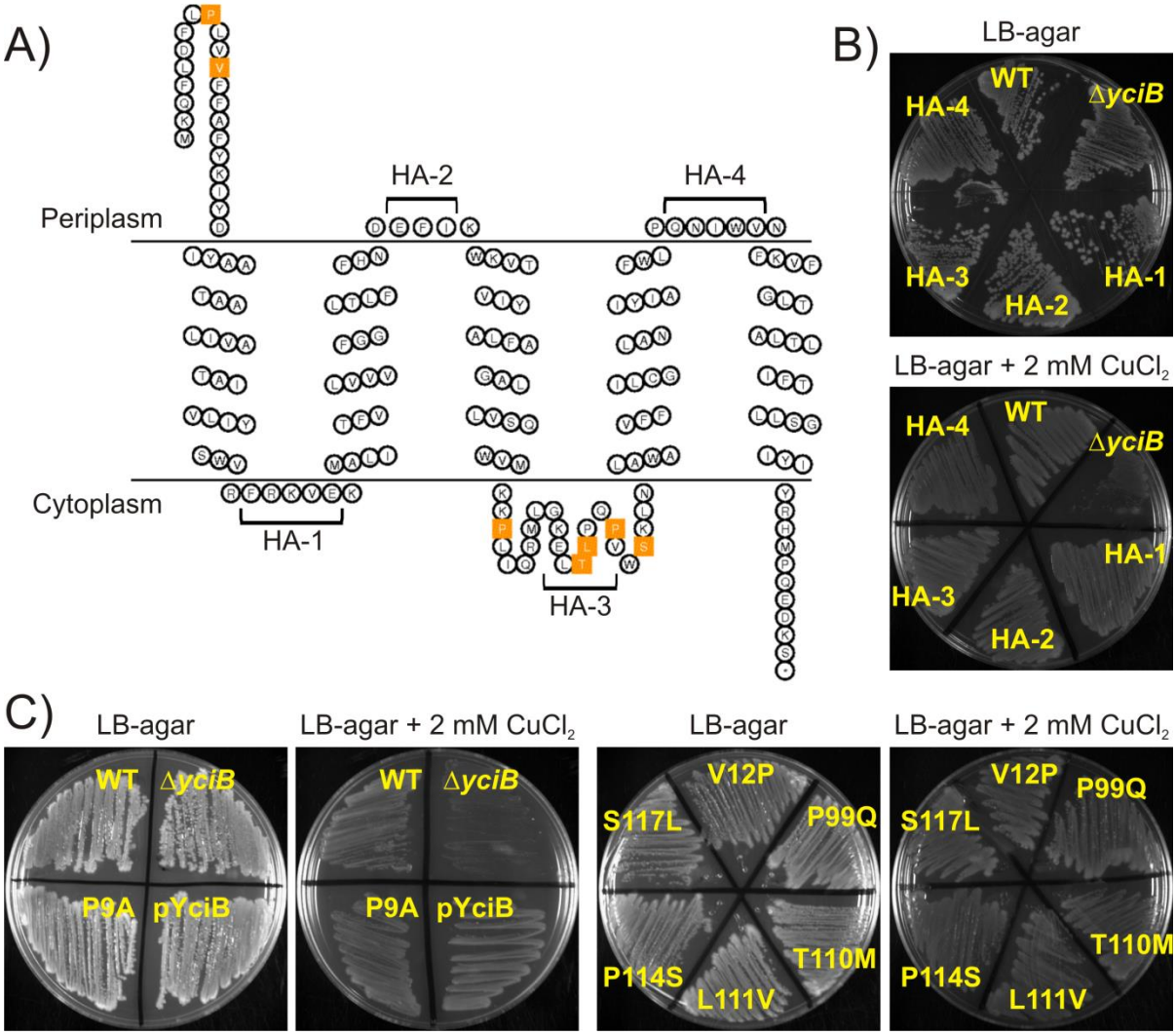

Figure 5. Individual loop domains in the periplasm and cytoplasm are not required for function of YciB. (A) The locations of all single point mutations constructed in this study were mapped onto the predicted transmembrane orientation of YciB. Mutated residues are shown in orange squares. The four loops in which HA epitope insertions were constructed are labeled and numbered accordingly. (B) Plasmids expressing *yciB* with single HA epitope insertions were transformed into *yciB* deletion strain and grown on LB-agar and LB-agar supplemented with 2 mM $CuCl_2$ to qualitatively analyze growth deficiencies. (C) pYciB constructs with the individual point mutations highlighted in (A) were transformed into Δ*yciB* cells and grown on LB-agar or LB-agar supplemented with 2 mM $CuCl_2$.

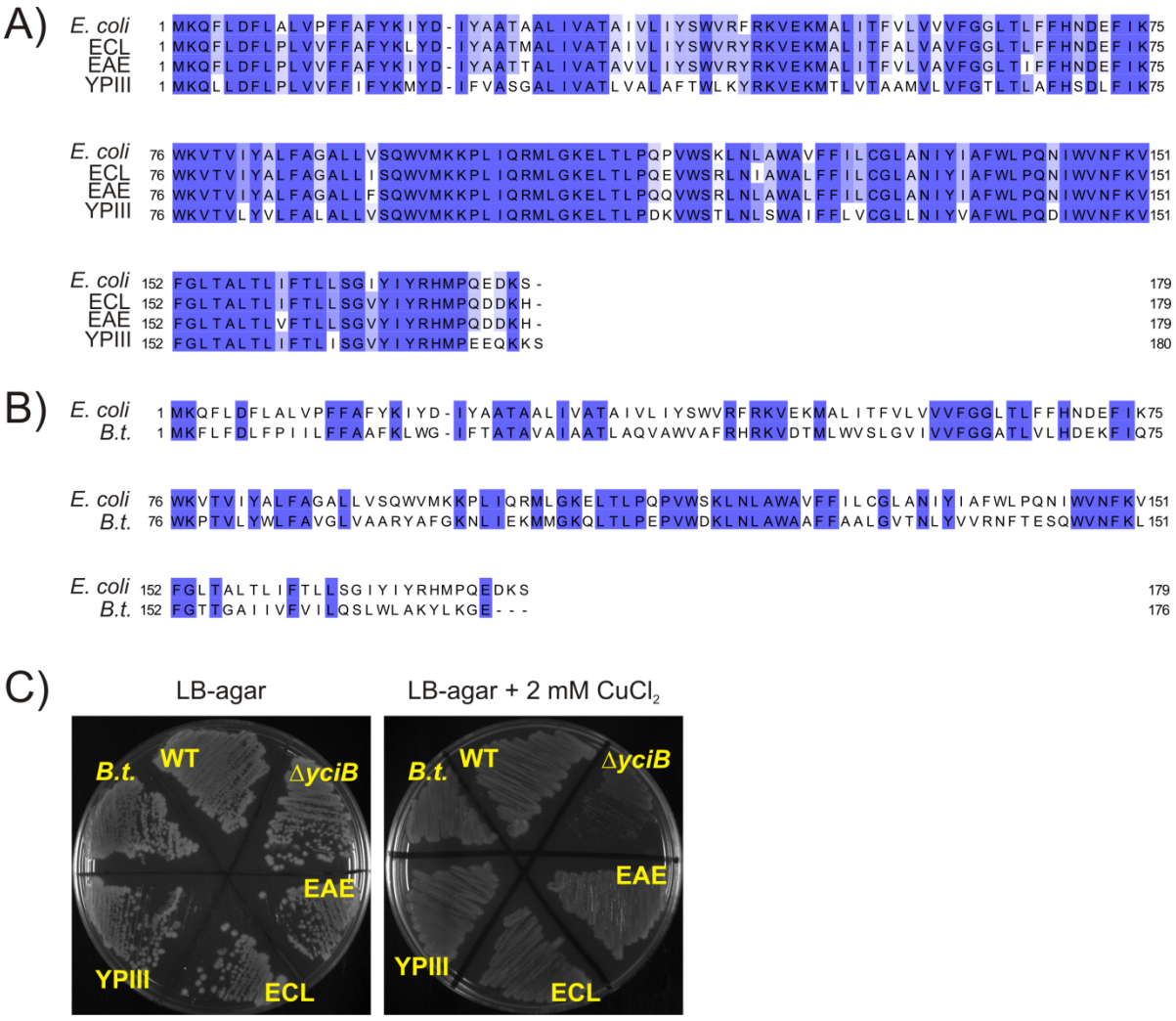

Figure 6. Heterologous *yciB* alleles are functionally equivalent . (A) YciB proteins from *E. coli* MG1655, *Yersinia pseudotuberculosis* YPIII, *Enterobacter cloacae* (ECL), and *Enterobacter aerogenes* (EAE) were aligned using the Clustal Omega server (http://www.ebi.ac.uk/Tools/msa/clustalo/). The image was rendered using Jalview (available at http://www.jalview.org/). Purple shading indicates residue conservation. (B) YciB sequences from *E. coli* and *Burkholderia thailandensis* (*B.t.*) were aligned to show the lack of conservation between these proteins. (C) Plasmids carrying the *yciB* alleles from the indicated species were transformed into *E. coli* Δ*yciB* cells and grown on LB-agar and LB-agar supplemented with 2 mM $CuCl_2$.

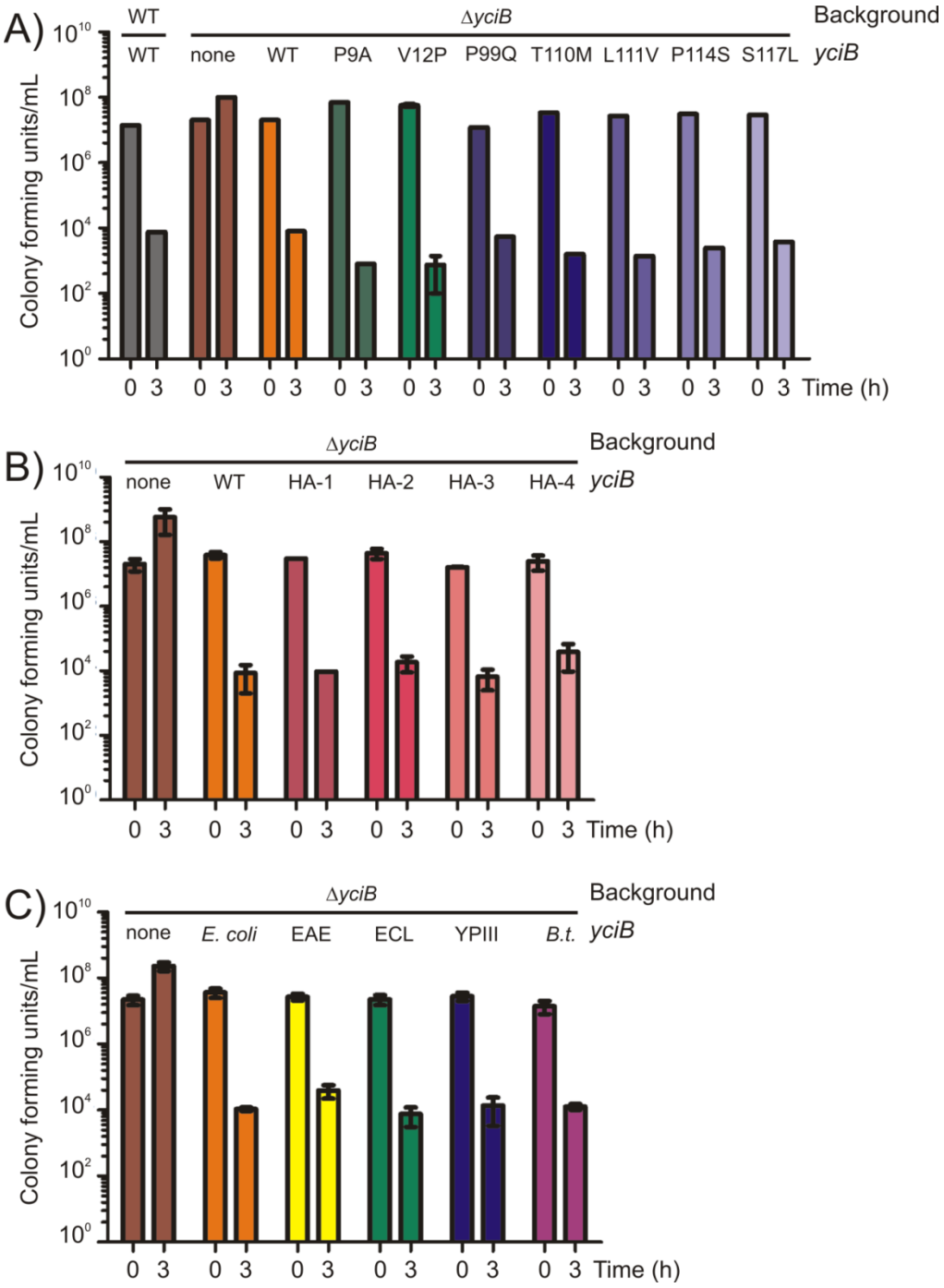

Figure 7. Mutations in *yciB* complement CDI resistance. (A) Point mutations were constructed at well-conserved residues in the N-terminal periplasmic tail (green bars) or in loop 3 as identified in the ECOR database (purple bars). These were transformed into Δ*yciB* cells and co-cultured with inhibitor cells at a 1:10 target:inhibitor ratio. Viable target cell numbers were measured at 0 and 3 h timepoints. (B) Individual HA tag constructs and (C) heterologous *yciB* alleles were transformed into Δ*yciB* cells and mixed with inhibitor cells under the same conditions as in (A). Viable target cells were scored at 0 and 3 h. Data presented is the mean of 3 independent experiments ±SEM.

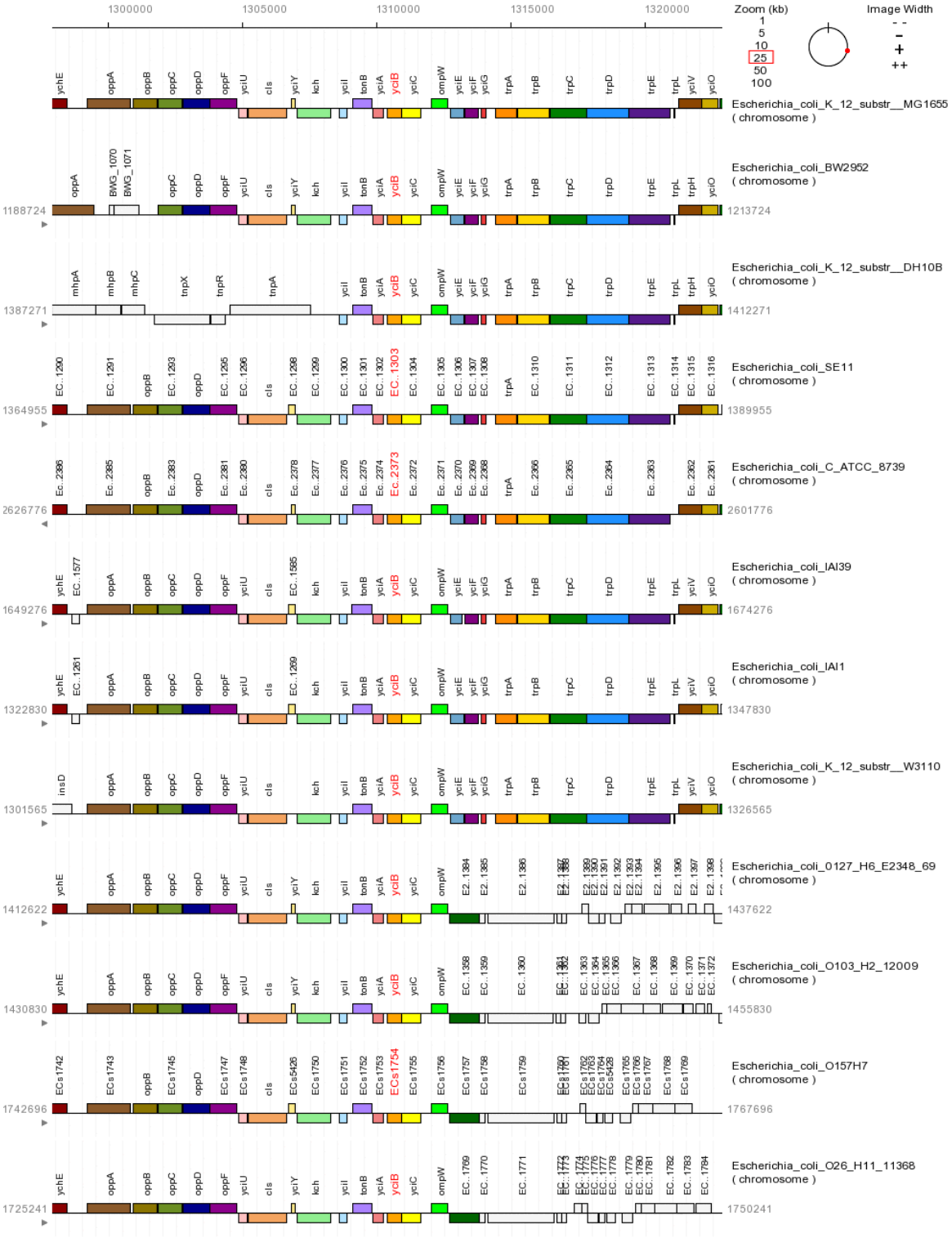
1300000
1305000
1310000
1315000
1320000
Zoom (kb)
1
5
10
25
50
100
Image Width
- -
-
+
++
Escherichia_coli_K_12_substr__MG1655
(chromosome)
Escherichia_coli_BW2952
(chromosome)
1188724
1213724
Escherichia_coli_K_12_substr__DH10B
(chromosome)
1387271
1412271
Escherichia_coli_SE11
(chromosome)
1364955
1389955
Escherichia_coli_C_ATCC_8739
(chromosome)
2626776
2601776
Escherichia_coli_IAI39
(chromosome)
1649276
1674276
Escherichia_coli_IAI1
(chromosome)
1322830
1347830
Escherichia_coli_K_12_substr__W3110
(chromosome)
1301565
1326565
Escherichia_coli_0127_H6_E2348_69
(chromosome)
1412622
1437622
Escherichia_coli_O103_H2_12009
(chromosome)
1430830
1455830
Escherichia_coli_O157H7
(chromosome)
1742696
1767696
Escherichia_coli_O26_H11_11368
(chromosome)
1725241
1750241

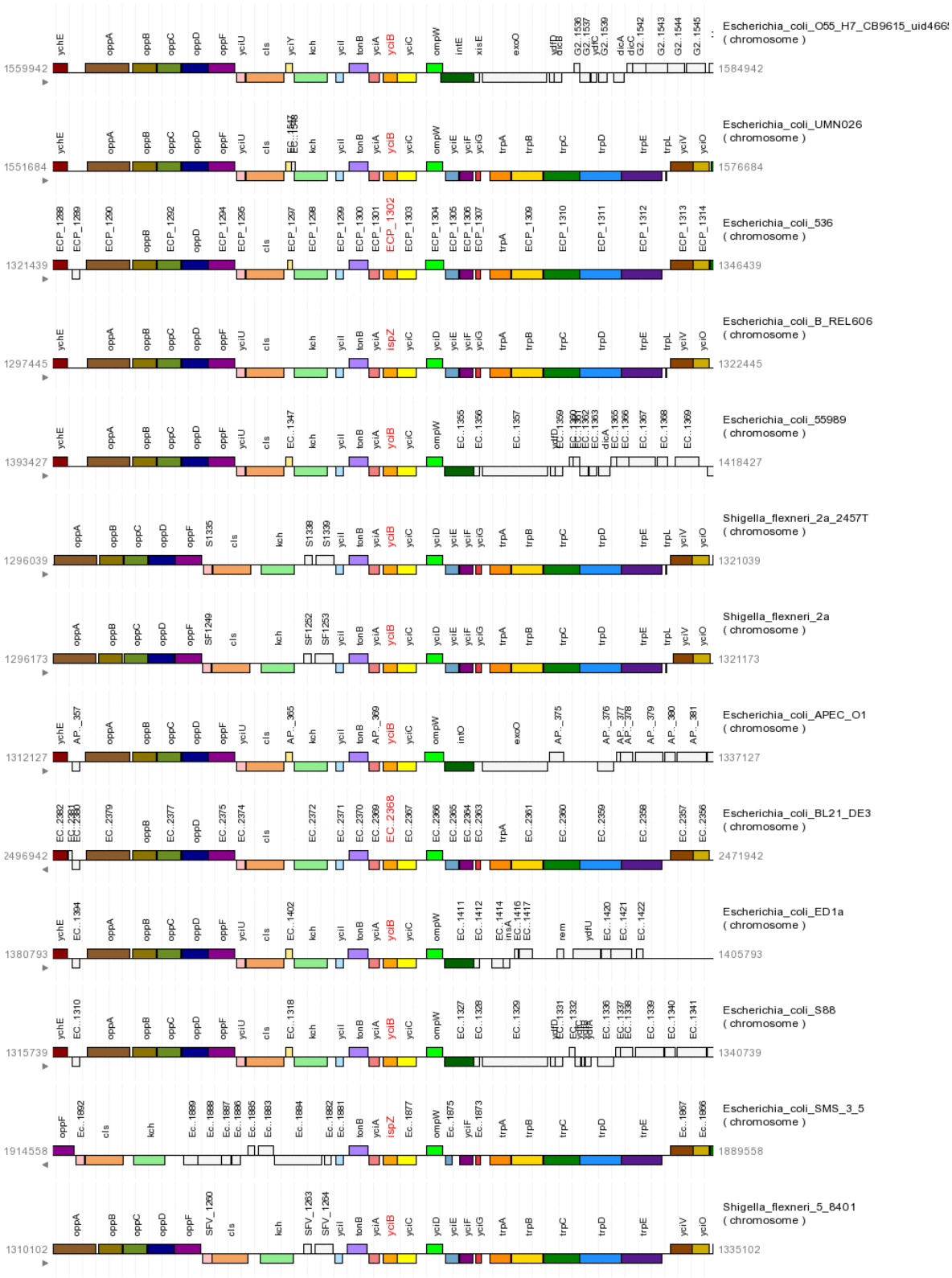
Escherichia_coli_O55_H7_CB9615_uid46695 (chromosome)
1559942
1584942
Escherichia_coli_UMN026 (chromosome)
1551684
1576684
Escherichia_coli_536 (chromosome)
1321439
1346439
Escherichia_coli_B_REL606 (chromosome)
1297445
1322445
Escherichia_coli_55989 (chromosome)
1393427
1418427
Shigella_flexneri_2a_2457T (chromosome)
1296039
1321039
Shigella_flexneri_2a (chromosome)
1296173
1321173
Escherichia_coli_APEC_O1 (chromosome)
1312127
1337127
Escherichia_coli_BL21_DE3 (chromosome)
2496942
2471942
Escherichia_coli_ED1a (chromosome)
1380793
1405793
Escherichia_coli_S88 (chromosome)
1315739
1340739
Escherichia_coli_SMS_3_5 (chromosome)
1914558
1889558
Shigella_flexneri_5_8401 (chromosome)
1310102
1335102

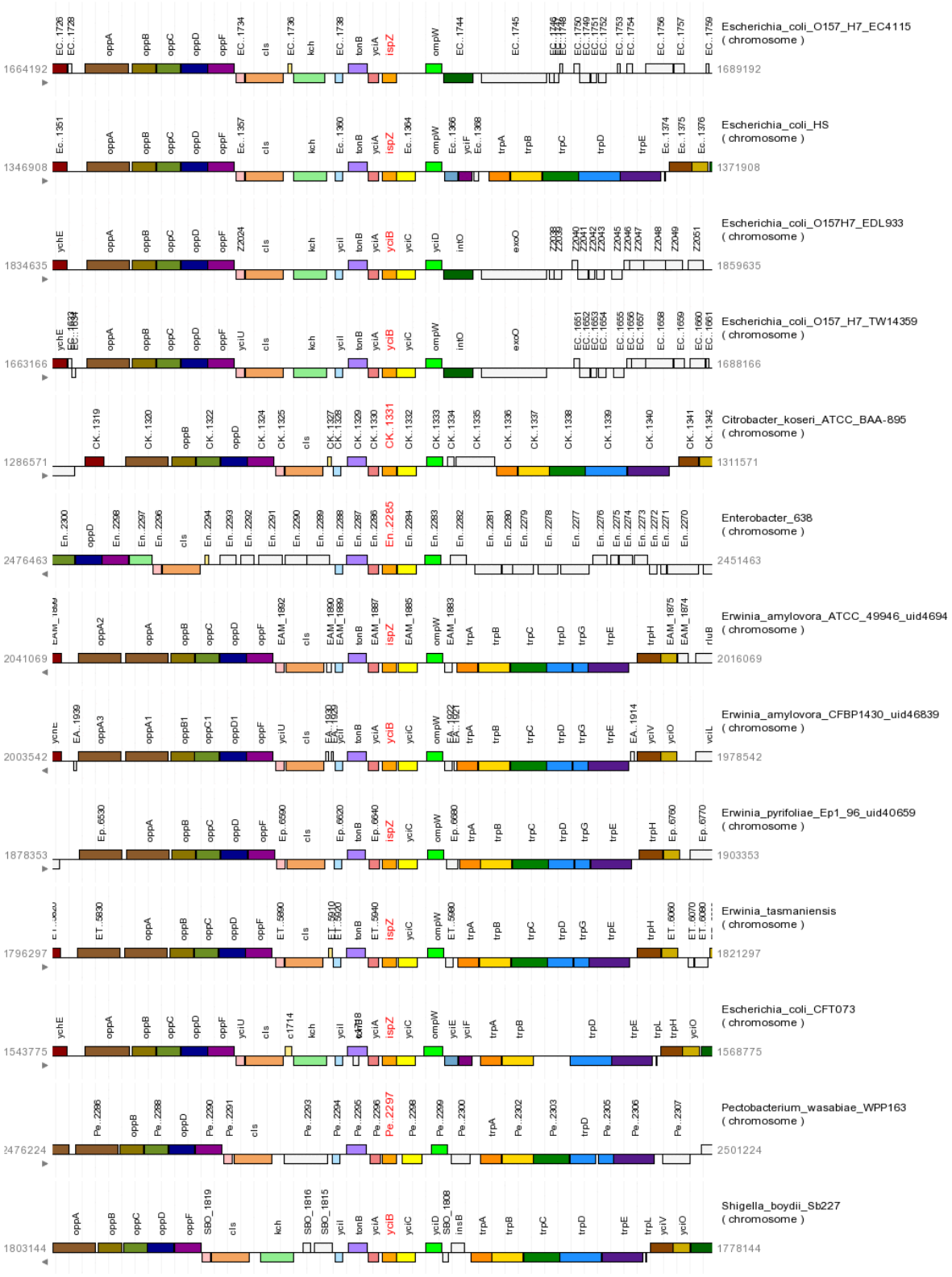
Escherichia_coli_O157_H7_EC4115
(chromosome)
1664192
1689192
Escherichia_coli_HS
(chromosome)
1346908
1371908
Escherichia_coli_O157H7_EDL933
(chromosome)
1834635
1859635
Escherichia_coli_O157_H7_TW14359
(chromosome)
1663166
1688166
Citrobacter_koseri_ATCC_BAA-895
(chromosome)
1286571
1311571
Enterobacter_638
(chromosome)
2476463
2451463
Erwinia_amylovora_ATCC_49946_uid4694
(chromosome)
2041069
2016069
Erwinia_amylovora_CFBP1430_uid46839
(chromosome)
2003542
1978542
Erwinia_pyrifoliae_Ep1_96_uid40659
(chromosome)
1878353
1903353
Erwinia_tasmaniensis
(chromosome)
1796297
1821297
Escherichia_coli_CFT073
(chromosome)
1543775
1568775
Pectobacterium_wasabiae_WPP163
(chromosome)
2476224
2501224
Shigella_boydii_Sb227
(chromosome)
1803144
1778144

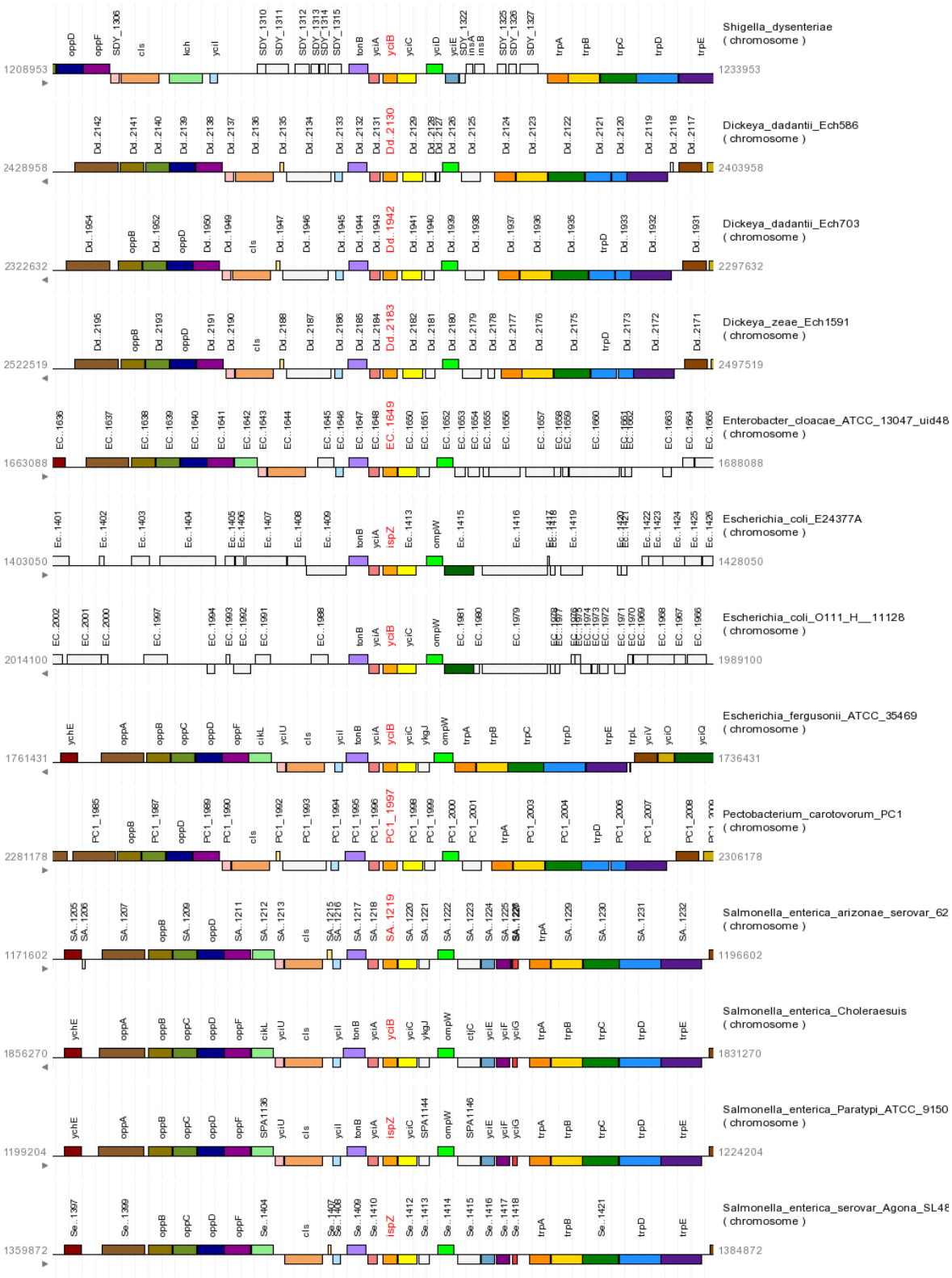
Shigella_dysenteriae
(chromosome)
1208953
1233953
Dickeya_dadantii_Ech586
(chromosome)
2428958
2403958
Dickeya_dadantii_Ech703
(chromosome)
2322632
2297632
Dickeya_zeae_Ech1591
(chromosome)
2522519
2497519
Enterobacter_cloacae_ATCC_13047_uid48
(chromosome)
1663088
1688088
Escherichia_coli_E24377A
(chromosome)
1403050
1428050
Escherichia_coli_O111_H__11128
(chromosome)
2014100
1989100
Escherichia_fergusonii_ATCC_35469
(chromosome)
1761431
1736431
Pectobacterium_carotovorum_PC1
(chromosome)
2281178
2306178
Salmonella_enterica_arizonae_serovar_62
(chromosome)
1171602
1196602
Salmonella_enterica_Choleraesuis
(chromosome)
1856270
1831270
Salmonella_enterica_Paratypi_ATCC_9150
(chromosome)
1199204
1224204
Salmonella_enterica_serovar_Agona_SL48
(chromosome)
1359872
1384872

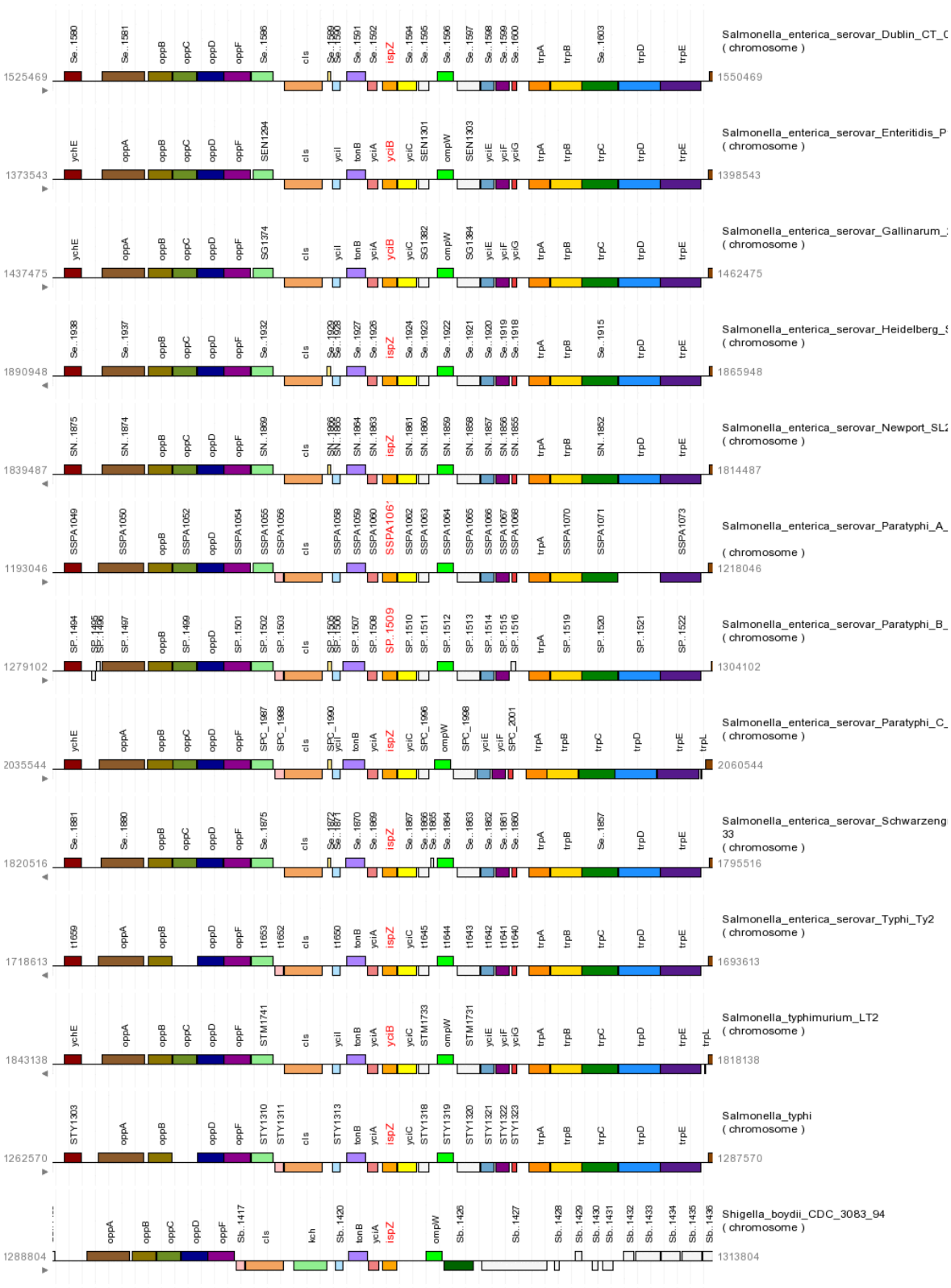
Salmonella_enterica_serovar_Dublin_CT_(
(chromosome)
1525469
1550469
Salmonella_enterica_serovar_Enteritidis_P
(chromosome)
1373543
1398543
Salmonella_enterica_serovar_Gallinarum_
(chromosome)
1437475
1462475
Salmonella_enterica_serovar_Heidelberg_S
(chromosome)
1890948
1865948
Salmonella_enterica_serovar_Newport_SL2
(chromosome)
1839487
1814487
Salmonella_enterica_serovar_Paratyphi_A_
(chromosome)
1193046
1218046
Salmonella_enterica_serovar_Paratyphi_B_
(chromosome)
1279102
1304102
Salmonella_enterica_serovar_Paratyphi_C_
(chromosome)
2035544
2060544
Salmonella_enterica_serovar_Schwarzeng
33
(chromosome)
1820516
1795516
Salmonella_enterica_serovar_Typhi_Ty2
(chromosome)
1718613
1693613
Salmonella_typhimurium_LT2
(chromosome)
1843138
1818138
Salmonella_typhi
(chromosome)
1262570
1287570
Shigella_boydii_CDC_3083_94
(chromosome)
1288804
1313804

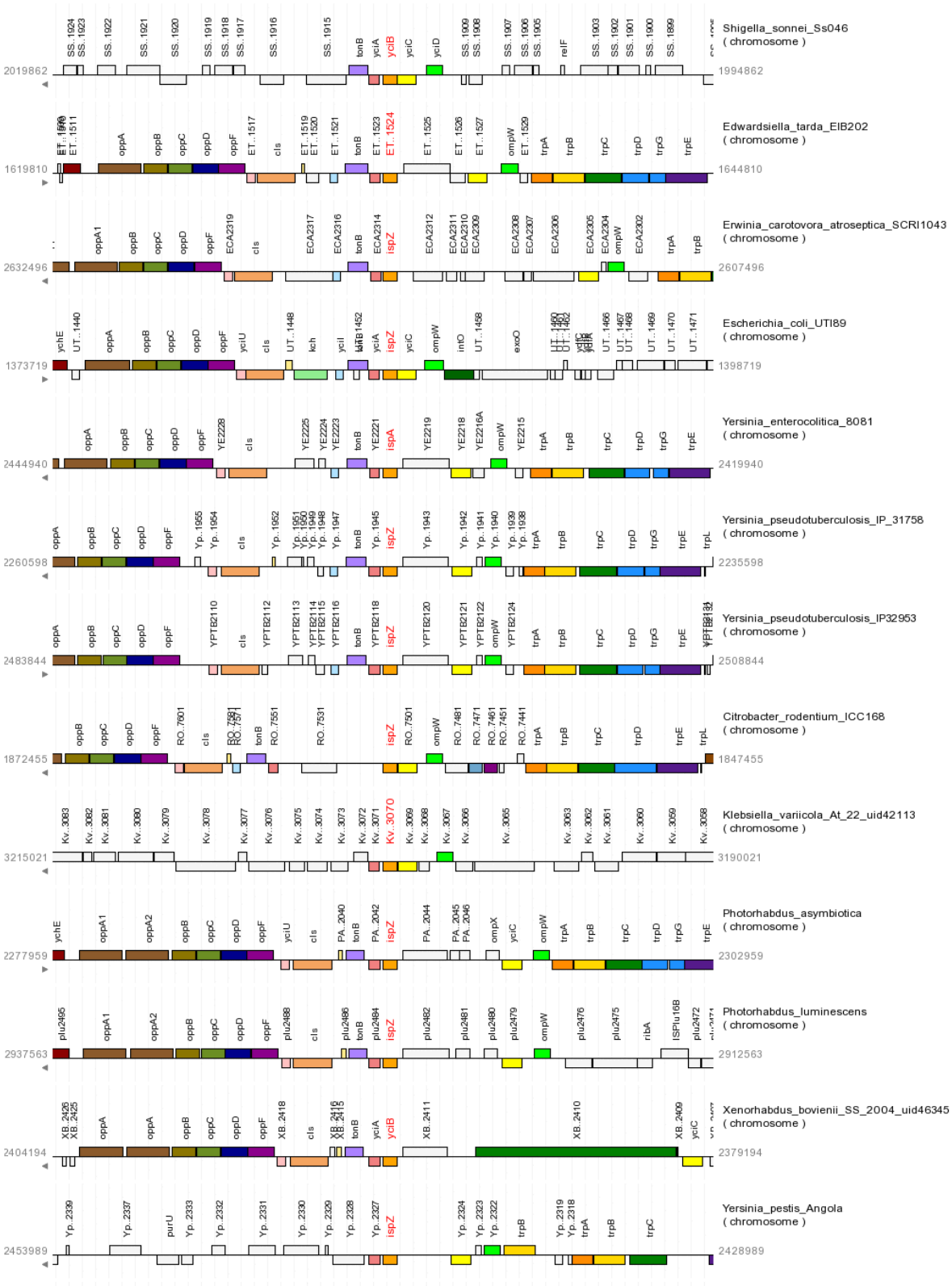
Shigella_sonnei_Ss046
(chromosome)
2019862
1994862
Edwardsiella_tarda_EIB202
(chromosome)
1619810
1644810
Erwinia_carotovora_atroseptica_SCRI1043
(chromosome)
2632496
2607496
Escherichia_coli_UTI89
(chromosome)
1373719
1398719
Yersinia_enterocolitica_8081
(chromosome)
2444940
2419940
Yersinia_pseudotuberculosis_IP_31758
(chromosome)
2260598
2235598
Yersinia_pseudotuberculosis_IP32953
(chromosome)
2483844
2508844
Citrobacter_rodentium_ICC168
(chromosome)
1872455
1847455
Klebsiella_variicola_At_22_uid42113
(chromosome)
3215021
3190021
Photorhabdus_asymbiotica
(chromosome)
2277959
2302959
Photorhabdus_luminescens
(chromosome)
2937563
2912563
Xenorhabdus_bovienii_SS_2004_uid46345
(chromosome)
2404194
2379194
Yersinia_pestis_Angola
(chromosome)
2453989
2428989

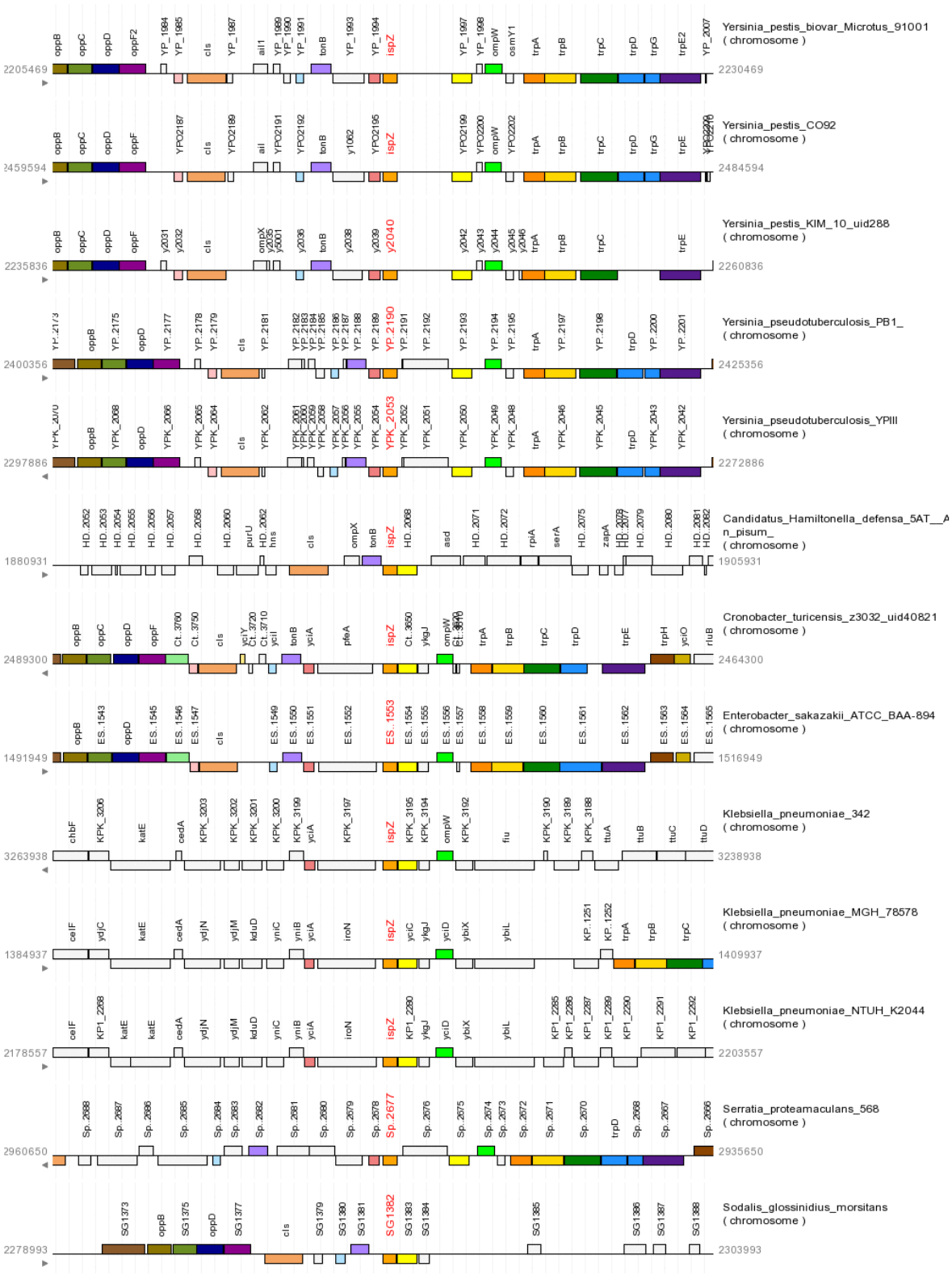
Yersinia_pestis_biovar_Microtus_91001
(chromosome)
2205469
2230469
Yersinia_pestis_CO92
(chromosome)
2459594
2484594
Yersinia_pestis_KIM_10_uid288
(chromosome)
2235836
2260836
Yersinia_pseudotuberculosis_PB1_
(chromosome)
2400356
2425356
Yersinia_pseudotuberculosis_YPIII
(chromosome)
2297886
2272886
Candidatus_Hamiltonella_defensa_5AT__A
n_pisum_
(chromosome)
1880931
1905931
Cronobacter_turicensis_z3032_uid40821
(chromosome)
2489300
2464300
Enterobacter_sakazakii_ATCC_BAA-894
(chromosome)
1491949
1516949
Klebsiella_pneumoniae_342
(chromosome)
3263938
3238938
Klebsiella_pneumoniae_MGH_78578
(chromosome)
1384937
1409937
Klebsiella_pneumoniae_NTUH_K2044
(chromosome)
2178557
2203557
Serratia_proteamaculans_568
(chromosome)
2960650
2935650
Sodalis_glossinidius_morsitans
(chromosome)
2278993
2303993

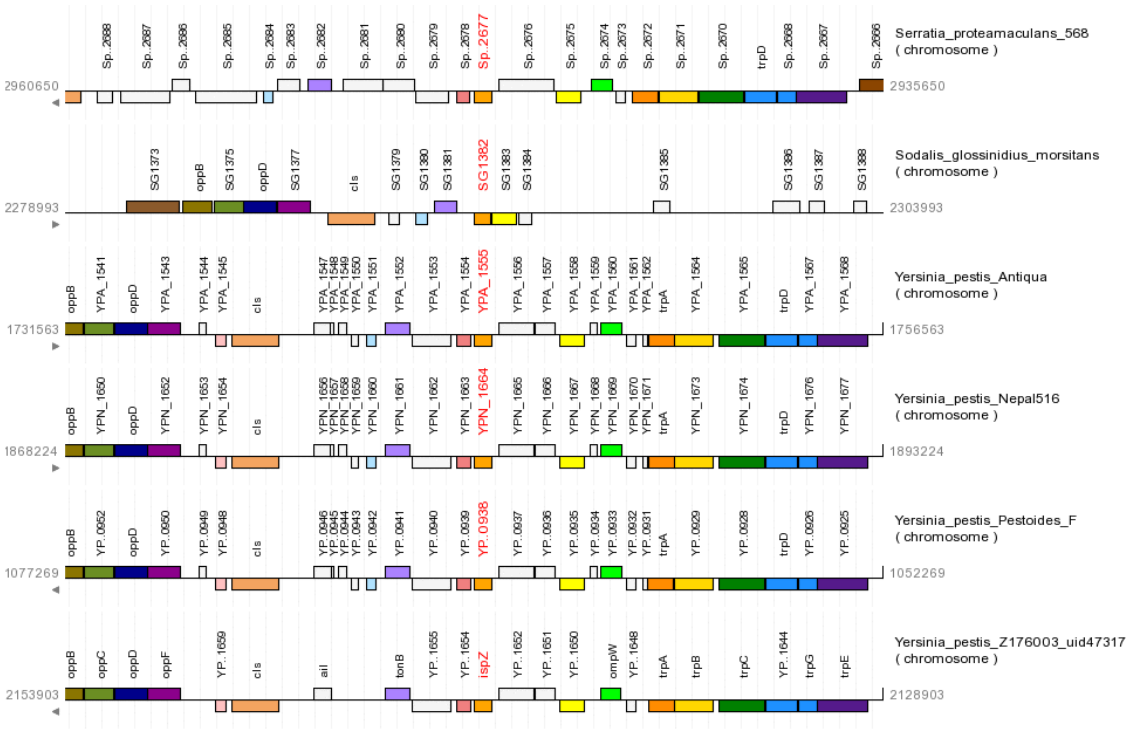

Figure 8. Genetic neighborhood analysis of *yciB*. Conserved genomic regions near *yciB* from 93 organisms were aligned using the PSAT website (available at http://www.nwrce.org/psat/index.html). *yciB* or the relevant homolog gene is depicted as the orange rectangle with red text in the center of each frame. Conserved genes across species are annotated with the same color scheme as the *E. coli* MG1655 reference genome (top).

Table 1. Measurements of wild-type and Δ*yciB* cells.

	Wild-type		Δ*yciB*	
Timepoint	***N* (cells)**	**Measurement (μm)**	***N* (cells)**	**Measurement (μm)**
1 hr	160	1.593 ± 0.02545	178	1.494 ± 0.03187
3 hr	167	1.355 ± 0.02613	192	1.229 ± 0.02145
5 hr	177	1.190 ± 0.01698	183	1.219 ± 0.02330

Table 2. YciB variations present in the *E. coli* Reference (ECOR) Collection (317).

ECOR Strain	YciB variant	Serotype	Host
28	T110M	O104:HNM	Group B1 strain from a healthy human child
28	S117L	O104:HNM	Group B1 strain from a healthy human child
31	P99Q	O79:H43	Group E strain from a healthy leopard in captivity
52	P114S	O25:H1	Group B2 strain from a healthy orangutan
60	L111V	O4:HN	Group B2 strain from a human host with a UTI and acute cystitis

Table 3. Bacterial strains and plasmids used in this study.

Strain	***Description*[a]**	***Reference***
X90	F′ *lacI*^{q} *lac′ pro′/ara* Δ*(lac-pro) nal1 argE*(amb) *rif*^{r} *thi-1*, Rif^{R}	
EPI100	F^{-} *mcrA* Δ*(mrr-hsdRMS-mcrBC) φ80dlacZ*Δ*M15* Δ*lacXcZ*Δ*M15* Δ*lacX recA1 endA1 araD139* Δ*(ara, leu)7697 galU galK* λ^{-} *rpsL nupG pir*$^{+}$*(DHFR)*, Str^{R} Tp^{R}	Epicentre
CH1426	X90 Δ*copA::kan*, Rif^{R} Kan^{R}	This study
CH1427	X90 Δ*cueO::kan*, Rif^{R} Kan^{R}	This study
CH1428	X90 Δ*cueR::kan*, Rif^{R} Kan^{R}	This study
CH1429	X90 Δ*cusA::kan*, Rif^{R} Kan^{R}	This study
CH1430	X90 Δ*cusB::kan*, Rif^{R} Kan^{R}	This study
CH1431	X90 Δ*cusC::kan*, Rif^{R} Kan^{R}	This study
CH1432	X90 Δ*cusF::kan*, Rif^{R} Kan^{R}	This study
CH1433	X90 Δ*cusR::kan*, Rif^{R} Kan^{R}	This study
CH1434	X90 Δ*cusS::kan*, Rif^{R} Kan^{R}	This study
CH7838	*Enterobacter aerogenes* ATCC 13048	American Type

		Culture Collection
CH7839	*Enterobacter cloacae* ATCC 13047	American Type Culture Collection
CH8251	MC4100 rif^{r}, Rif^{R}	(173)
CH9404	CH8251 Δ*yciB::kan*, Rif^{R} Kan^{R}	(173)
CH9405	X90 Δ*yciB::kan*, Rif^{R} Kan^{R}	(173)
Plasmid	***Description*[a]**	***Reference***
pTrc99a	IPTG-inducible expression plasmid, Amp^{R}	GE Healthcare
pTrc99KX	Derivative of pTrc99a that contains a 5´-KpnI restriction site and 3´-SpeI and XhoI sites, Amp^{R}	(175)
pCH351	pTrc99KX::*yciB*-HA1, IPTG-inducible expression of *yciB* in which the first loop has been replaced by an HA tag, Amp^{R}	This study
pCH353	pTrc99KX::*yciB*-HA2, IPTG-inducible expression of *yciB* in which the second loop has been replaced by an HA tag, Amp^{R}	This study
pCH355	pTrc99KX::*yciB*-HA3, IPTG-inducible expression of *yciB* in which the third loop has been modified to include an HA tag, Amp^{R}	This study
pCH357	pTrc99KX::*yciB*-HA4, IPTG-inducible expression of *yciB* in which the fourth loop has been replaced by an HA tag, Amp^{R}	This study
pCH839	pTrc99KX::*yciB* (*B. thailandensis*), IPTG-inducible expression of the *yciB* allele from *Burkholderia thailandensis* E264, Amp^{R}	This study
pCH1084	pTrc99KX::*yciB* P9A, IPTG-inducible expression of *yciB* with a Pro9Ala point mutation, Amp^{R}	This study
pCH1086	pTrc99KX::*yciB* V12P, IPTG-inducible expression of *yciB* with a Val12Pro point mutation, Amp^{R}	This study
pCH2145	pTrc99KX::*yciB* P99Q, IPTG-inducible expression of *yciB* with a Pro99Gln point mutation, Amp^{R}	This study
pCH2147	pTrc99KX::*yciB* T110M, IPTG-inducible expression of *yciB* with a Tyr110Met point mutation, Amp^{R}	This study
pCH2149	pTrc99KX::*yciB* L111V, IPTG-inducible expression of *yciB* with a Leu111Val point mutation, Amp^{R}	This study
pCH2151	pTrc99KX::*yciB* P114S, IPTG-inducible expression of *yciB* with a Pro114Ser point mutation, Amp^{R}	This study
pCH2153	pTrc99KX::*yciB* S117L, IPTG-inducible expression of *yciB* with a Ser117Leu point mutation, Amp^{R}	This study
pCH9922	pTrc99KX::*yciB*, IPTG-inducible expression of *yciB*, Amp^{R}	(173)
pCH9305	Constitutive expression of chimeric *cdiA*^{EC93}-*CT*$_{o11}$^{EC869} and *cdiI*$_{o11}$^{EC869} genes, Amp^{R}	(177)
pCH10416	pTrc99KX::*yciB* (*E. cloacae*), IPTG-inducible expression of the *yciB* allele from *Enterobacter cloacae* ATCC 13047, Amp^{R}	This study
pCH10417	pTrc99KX::*yciB* (*E. aerogenes*), IPTG-inducible expression of the *yciB* allele from *Enterobacter aerogenes*ATCC 13048,	This study

	Amp^R	
pCH10418	pTrc99KX::*yciB* (YPIII), IPTG-inducible expression of the *yciB* allele from *Yersinia pseudotuberculosis* YPIII, Amp^R	This study

[a]Abbreviations: Amp^R, ampicillin-resistant; Apr^R, aprimycin-resistant; Cm^R, chloramphenicol-resistant; Erm^R, erythromycin-resistant; Kan^R, kanamycin-resistance; Rif^R, rifampicin-resistant; Tet^R, tetracycline-resistant; Zeo^R, zeocin-resistant.

Table 4. Oligonucleotides used in this study.

Oligonucleotide	***Sequence[a]***	***Reference***
CH2139 (yciB-Kpn-for)	5' – AAT GGT ACC ATG AAG CAG TTT CTT GAT TTT TTA C – 3'	(173)
CH2140 (yciB-Xho-rev)	5' – GCA CTC GAG TTA GGA TTT ATC TTC CTG CGG – 3'	(173)
CH2634 (yciB-P99Q)	5' – GAA AAA GCA GCT AAT TCA GCG G – 3'	This study
CH2635 (yciB-T110M)	5' – AGA ACT CAT GCT GCC GCA ACC GG – 3'	This study
CH2636 (yciB-L111V)	5' – AGA ACT CAC GGT GCC GCA ACC GG – 3'	This study
CH2637 (yciB-P114S)	5' – CTC ACG CTG CCG CAA TCG GTA TGG – 3'	This study
CH2638 (yciB-S117L)	5' – TAT GGT TGA AGC TGA ATC TGG – 3'	This study
CH2460 (YPK2053-Kpn-for)	5' – AAT GGT ACC ATG AAG CAA CTT TTA G – 3'	This study
CH2461 (YPK2053-Xho-rev)	5' – GCA CTC GAG TTA AGA CTT CTT CTG C – 3'	This study
CH2462 (EAE21485-Xho-rev)	5' – GCA CTC GAG TTA GTG CTT ATC GTC C – 3'	This study
CH2463 (ECL01649-Xho-rev)	5' – GCA CTC GAG TCA GTG TTT ATC ATC C – 3'	This study
CH2616 (yciB-HA-1)	5' – GCC ATC TTA GCG TAA TCT GGA ACA TCG TAT GGG TAG CGA ACC C – 3'	This study
CH2617 (yciB-HA-2)	5' – CTT CCA TTT AGC GTA ATC TGG AAC ATC GTA TGG GTA ATC ATT GTG G – 3'	This study
CH2618 (yciB-HA-3)	5' – GAT GCT GTA CCC ATA CGA TGT TCC AGA TTA CGC TGT ATG GTC G – 3'	This study
CH2619 (yciB-HA-4)	5' – GGC TGC CGT ACC CAT ACG ATG TTC CAG ATT ACG CTA ACT TTA AAG TC – 3'	This study
CH2683 (Bth-yciB-Kpn-for)	5' – GCG GGT ACC ATG AAA TTC	This study

	CTG TTC GAT C – 3'	
CH2684 (Bth-yciB-Xho-rev)	5' – CGC TCG AGG TTA TTC TCC CTT CAG GTA TTT CG – 3'	This study
CH2804 (yciB-P9A-Kpn)	5' – TTT GGT ACC ATG AAG CAG TTT CTT GAT TTT TTA GCG CTG GTT GTC – 3'	This study
CH2805 (yciB-V12P-Kpn)	5' – TTT GGT ACC ATG AAG CAG TTT CTT GAT TTT TTA CCG CTG GTT CCC TTT TTC GCG – 3'	This study

[a]Restriction enzyme recognition sites are underlined.

IV. Insertion element transposition provides transient resistance against contact-dependent inhibition toxins from *E. coli*

This work is part of a manuscript in preparation and has not yet been published.

A. Introduction

Contact-dependent inhibition (CDI) systems that deploy nuclease toxins must ensure that these domains reach the cytoplasmic compartment of target cells, where their DNA and RNA substrates reside. We recently demonstrated that nuclease CdiA-CTs require the presence of specific inner membrane proteins to accomplish this (Chapter II and (173)). These proteins were primarily identified using transposon mutagenesis screens and the selective pressure of CDI toxin delivery to isolate resistant mutants from a large starting population. The inner membrane proteins identified are required for the transport of a variety of sugars, amino acids, and small metabolites into the cell. Interestingly, we have shown that for some of these proteins, such as the methionine transporter MetI and the glucose transporter PtsG, their metabolic function is not required for their role in CDI.

Delivery of CdiA-CT_{o11}^{EC869}, a DNase toxin from *E. coli* EC869, requires the uncharacterized putative inner membrane protein YciB (173). As we showed in Chapter III, *yciB* is required for tolerance to metals, including copper and zinc. Though it is a non-essential gene under standard laboratory growth conditions, a *yciB* deletion strain is unable to grow under copper stress and phenocopies the loss of the well-characterized aerobic copper response regulator CueO (see Chapter III and (312). During CDI, YciB is required for the delivery of toxins with the same N-terminal domain as CdiA-CT_{o11}^{EC869}. We previously showed that a chimera toxin containing the N-terminal domain from CdiA-CT_{o11}^{EC869} fused to the C-terminal tRNase domain from CdiA-$CT_{II}^{Bp1026b}$ inhibits cells in a YciB-dependent

manner (Chapter II and (173)).

While characterizing isolates resistant to CdiA-CT_{o11}^{EC869}, we isolated a subset of mutants with transposon insertions disrupting the coding sequence of *yciB* (Chapter II and (173)). Subsequent experiments confirmed that YciB is required for the delivery of this toxin to the cytoplasm of target cells. Here, we describe another set of mutants isolated in these experiments that do not contain transposon insertions in *yciB*. The transposons in this second class of isolates are not genetically linked to resistance, and the CDI-resistant phenotype is mediated by secondary mutations in *yciB*. A majority of these mutations are attributed to insertion sequence elements that appear to have transposed into the *yciB* open reading frame in response to stress induced by the delivery of CdiA-CT_{o11}^{EC869}. We propose that genomic rearrangements such as these transposition events could be a transient resistance mechanism that allows cells to escape immediate inhibition by a neighboring CDI^+ cell while ultimately retaining the ability to revert to the wild-type allele to regain physiological function in the absence of selective pressure from CDI.

B. Results

1. A subset of CDI^R isolates have unlinked transposon insertions and secondary mutations in yciB

We previously showed that the inner membrane protein YciB is required for the delivery of CdiA-CT_{o11}^{EC869} (Chapter II and (173)). Mutants with transposon insertions in *yciB* were isolated from co-culture enrichment experiments in which a transposon pool was iteratively mixed with cells expressing CDI_{o11}^{EC869} (173). As discussed in Chapter II, a number of CDI^R strains had transposon hops in *yciB* or the upstream gene *yciC*, although single-gene knockout experiments suggested that insertions in *yciC* were likely polar mutations affecting

expression of *yciB*. These insertions were all genetically linked to CDI resistance, and resistance to this toxin could be conferred to a CDI-sensitive strain of *E. coli* K-12 by transducing the antibiotic resistance marker associated with the transposon into a fresh cell background (Chapter II). During the course of these experiments, we also isolated a number of clones with transposon insertions that were unlinked to the CDI resistance phenotype. When grown in co-culture assays with CDI_{o11}^{EC869} cells, these strains were all resistant as measured by viable colony counts at 0 and 3 h post-mixing (Figure 1A). However, these transposon insertions did not confer resistance to a CDI^S background when transferred into a fresh cell background via P1 phage transduction (Figure 1B). We sequenced the transposon/genomic DNA junction in these isolates to identify the location of these insertions in an effort to determine whether the unlinked mutations were related to one another (Table 1). The genes in which transposon insertions were found in these strains belonged to a number of cellular pathways (295, 296), including those involved in cell division (340) and sugar metabolism (341, 342), but no common operons or biochemical themes that seemed like plausible CdiA-CT translocation pathways could be identified from this genetic data.

Isolating CDI^R clones from a transposon pool entails iterative co-culture of transposon-mutagenized target cells and inhibitor cells expressing a CDI system of interest. CDI_{o11}^{EC869} is potent and can decrease the number of viable target cells in a given culture more than 10,000-fold over the course of a few hours (177). As such, these enrichment experiments put significant selective pressure onto a population of target cells. Additionally, target cells undergo a round of transposon mutagenesis to generate the input library, representing another source of potential cellular stress. We reasoned that some target cells may accumulate secondary mutations outside of the transposon during the three rounds of co-culture. Given

the requirement of YciB for the delivery of CdiA-CT_{o11}^{EC869}, cells that gained secondary mutations in this gene could be selected for over the course of the enrichment procedure. We therefore decided to examine *yciB* alleles from CDI^R mutants with unlinked transposon insertions in an effort to identify secondary mutations that could confer resistance to CDI_{o11}^{EC869}. As described in Chapter III, YciB is a putative inner membrane protein with two periplasmic and two cytoplasmic loops that connect 5 transmembrane domains. Because CdiA-CT_{o11}^{EC869} must be translocated through the periplasm across the inner membrane to reach the cytoplasmic DNA substrate, we hypothesized that we might find mutations in the periplasmic loop regions that prevented or altered an interaction with CdiA-CT_{o11}^{EC869} during delivery to the cytoplasm.

To test this hypothesis, we transformed a plasmid construct expressing *yciB* into the mutants listed in Table 1 and repeated the co-culture assays with CDI_{o11}^{EC869}, reasoning that if secondary mutations were present in *yciB*, then a expression of wild-type allele may restore the pathway needed for import of this toxin and thus render these cells CDI-sensitive. In all mutants tested, the plasmid-borne copy of *yciB* complemented the CDI^R phenotype of these isolates, and cells were as sensitive as a wild-type, unmutagenized control strain of *E. coli* (Figure 2A). We then amplified the *yciB* open reading frame as well as several hundred base pairs upstream and downstream of the start and stop codons and analyzed these pieces of DNA via gel electrophoresis to determine whether these genes were still intact. Surprisingly, 4 of 5 mutant alleles we amplified were larger than the wild-type control (Figure 2B). The *yciB* gene from one mutant, A3, ran at approximately the same distance as wild-type. We sequenced these mutant alleles to find the source of the size differences and found that in the 4 mutants with larger alleles, the *yciB* open reading frames were disrupted by insertion

sequence (IS) elements (Table 2). Mutant A3, which had a wild-type *yciB* allele as assessed by PCR, contained a nonsense mutation created by an A to T transversion at nucleotide position 223, which created a premature stop codon and a protein product 74 residues in length (Table 2).

IS elements are small, mobile pieces of DNA that catalyze their own transposition throughout the genomes of bacteria. They commonly flank larger genomic islands and are involved in complex genome rearrangements, even in laboratory strains of *E. coli* (343). Approximately 30 distinct families of IS elements have been identified in prokaryotic organisms to date, with many families containing multiple sub-groups (ISFinder, see https://www-is.biotoul.fr/index.php and (344-346)). We analyzed the IS elements disrupting *yciB* in these mutants and found examples of IS1 and IS10 transposition; these are from two distinct families of IS elements. Each mutant contained an independent transposon hop as evidenced by unique insertion sites and the nucleotide location of the 9-base pair inverted repeat sequences that flank IS elements in the genome (347) (Table 2).

2. Spontaneous resistance to CDI_{o11}^{EC869} can be achieved by IS element transposition

The IS elements detected in mutants A1, A4, A5, and B1 represent rare transposition events. IS elements undergo spontaneous transposition at rates of $10^{-3} – 10^{-8}$ events per element per generation (347, 348). The cells in which they were identified were first subjected to transposon mutagenesis before enrichment against CDI_{o11}^{EC869}. Therefore, it is possible that secondary mutations in *yciB* accumulated during the initial mutagenesis and are an artifact of the experimental procedure. We wished to test whether co-culturing CDI_{o11}^{EC869} with unmutagenized cells would result in the same pattern of IS element-mediated CDI resistance, which could suggest that the specific activity of CDI_{o11}^{EC869} was

inducing IS element transposition in target cells. To do this, we performed iterative co-culture assays with an unmutagenized input pool of target cells. This approach was designed to isolate spontaneous mutations leading to resistance to CDI_{o11}^{EC869}. Both *E. coli* MC4100 and EPI100 target cells were used to test cell responses to delivery of this toxin in multiple cell backgrounds. Complete population resistance to CDI_{o11}^{EC869} was achieved after three rounds of co-culture. We then amplified *yciB* alleles (including regions upstream and downstream) from isolated clones from each enrichment pool and analyzed them with gel electrophoresis and DNA sequencing (Figure 3). Both target populations produced spontaneous mutants in which *yciB* was larger than the wild-type gene (Figure 3). Sequencing confirmed that the change in allele size was attributed to the presence of IS elements, specifically IS1, IS5, and IS10 (Table 3). Interestingly, a number of smaller *yciB* alleles were also observed, and sequencing revealed that these are due to deletions between small direct repeat sequences in the *yciB* coding region (Figure 3 and Table 3). These deletion mutants create new open reading frames that would translate through to the native *yciB* stop codon, and they are predicted to contain transmembrane domains (data not shown).

3. IS element transposition does not occur in response to delivery of a tRNase toxin

CdiA-CT_{o11}^{EC869} is a potent nuclease that cleaves DNA both *in vitro* and *in vivo* (177, 202). DNA damage response pathways in Gram-negative bacteria are well-characterized, and the canonical SOS response requires cleavage of the LexA repressor protein by the ssDNA-binding protease RecA (41). This releases transcriptional repression of the suite of SOS-response genes, which include those required for nucleotide excision repair (41). The late stages of SOS response stop cell division to ensure that DNA damage is fixed before the cell divides (41). Because CdiA-CT_{o11}^{EC869} is a DNase, we wished to determine whether the

transposition of IS elements observed in transposon-mutagenized and spontaneous CdiA-CT_{o11}^{EC869}-resistant mutants was triggered by the activity of this toxin. To test this, we took advantage of the fact that many CdiA-CTs are bipartite and modular (173, 176). We previously demonstrated that the C-terminal catalytic DNase domain of CdiA-CT_{o11}^{EC869} could be replaced with the corresponding region from CdiA-$CT_{II}^{Bp1026b}$, a tRNase from *Burkholderia pseudomallei* (169, 173). This results in a functional chimera that inhibits target cells in a YciB-dependent manner yet requires $CdiI_{II}^{Bp1026b}$ to protect against inhibition (173). We reasoned that by delivering a different toxic effector through the same pathway as CdiA-CT_{o11}^{EC869}, we could determine whether spontaneous mutations in *yciB* accumulate, and whether the pattern of mutations matches those obtained from co-culture with CDI_{o11}^{EC869}. Using the same procedure outlined previously, we isolated spontaneous mutants that were resistant to CdiA-$CT^{NT}(_{o11}^{EC869})$-$^{CT}(_{II}^{Bp1026b})$ and amplified the *yciB* alleles from these strains to examine via gel electrophoresis. All PCR products from mutants enriched against $CDI^{NT}(_{o11}^{EC869})$-$^{CT}(_{II}^{Bp1026b})$ appeared to be the same size as wild-type *yciB* (Figure 4). We then sequenced these PCR products to determine whether they also contained mutations and found that all CDI^{R} strains had mutated *yciB* alleles, but that these were nonsense or frameshift mutations leading to a prematurely-truncated protein product (Table 4). We did not observe the same pattern of alleles disrupted by IS element transposition in response to $CDI^{NT}(_{o11}^{EC869})$-$^{CT}(_{II}^{Bp1026b})$ as with CDI_{o11}^{EC869}. This suggests that the high percentage of IS elements mutations observed in CDI_{o11}^{EC869}-resistant cells may be attributed to delivery of a specific DNase toxin, not just the general process of CDI.

4. IS element transposition in response to CdiA-CT_{o11}^{EC869} does not require recA

Because induction of the SOS response relies on the activation of RecA and subsequent

cleavage of the transcriptional repressor LexA, we hypothesized that DNA damage from delivery of CdiA-CT_{o11}^{EC869} could induce SOS response, leading to an upregulation of IS element transposition. The SOS response and DNA damage have also been linked to transposition of some families of IS elements and other transposable elements (349, 350). Although the EPI100 background that was used for the enrichments shown in Figure 3 has a defective *recA1* allele that can bind single-stranded DNA but lacks ATPase activity and cannot stimulate SOS response, we created a clean *recA* knockout in MC4100 and EPI100 backgrounds and repeated the enrichment process. As shown in Figure 5, alleles both larger and smaller than wild-type *yciB* were observed in Δ*recA* CDI^R spontaneous mutants. These mutations are attributed to both IS element transposition as well as small internal deletions. Therefore, induction of SOS response via the canonical RecA cleavage of LexA is not required for the IS transposition that takes place in response to CdiA-CT_{o11}^{EC869}.

5. IS elements in yciB *are unstable over time*

IS element transposition under wild-type conditions happens extremely infrequently (347, 348). This is advantageous for cells, because random transposition events have some probability of disrupting essential processes, ultimately leading to decreased cell fitness or cell death. Because IS element transposition into *yciB* was observed in response to conditions of increased stress, we wondered whether it would be advantageous for cells to retain these IS elements in this new genomic location in the absence of selective pressure from CDI_{o11}^{EC869}. To determine this, we isolated single colonies of *yciB*-IS mutants and grew them as monocultures in rich media under standard laboratory conditions, allowing the cultures to go through all stages of the bacterial growth cycle and enter stationary phase. An aliquot of each culture was transferred to a new tube with fresh media every 7 generations.

Every 49 generations, we removed an aliquot of the population and competed it in a co-culture experiment with CDI_{o11}^{EC869} to assay the population level of resistance to this toxin over time. We chose a variety of mutants to represent multiple IS element families. A wild-type, unmutagenized strain with wild-type *yciB* was included as a control. As shown in Figure 6A, wild-type cells do not spontaneously become CDI-resistant with repeated passaging (up to 300 generations). With extended passaging, the mutant cultures became less resistant to CDI_{o11}^{EC869} as measured by viable cell counts (Figure 6B to D). Mutants A1 and A4 were inhibited as much as wild-type cells after 298 generations.

This trend may be explained in part by data presented in Chapter III, which describes a physiological role for YciB. Clearly *yciB* is required for metal tolerance and possibly membrane integrity in *E. coli*, but careful growth curve measurements show that these mutants have a growth pattern that is nearly identical to wild-type cells. However, the timescale of this growth curve experiment does not capture what happens in extended cultures that are allowed to persist in stationary phase. Therefore, it is possible that *yciB* mutants are less fit over long-term periods of growth during which cells must cycle in and out of logarithmic and stationary phase. To determine whether *yciB* mutants have a general defect in long-term evolution experiments, we performed passaging series with a mixture of wild-type and Δ*yciB* cells and measured the viability of each by selective antibiotic markers. After several generations, wild-type bacteria are higher at present numbers than the Δ*yciB* strain (Figure 7). This data suggests that deletion of *yciB* contributes to a defect in exiting stationary phase. Because passaging experiments allow cells to grow to stationary phase before passage into fresh media, this growth defect could be the driving force behind IS element loss over time.

6. Spontaneous IS element transposition into genes required for CdiA-CT delivery is observed after co-culture with other CDI systems

We did not observe substantial IS element-mediated CDI resistance in response to delivery of the tRNase domain from CdiA-$CT_{II}^{Bp1026b}$. We therefore wondered whether *yciB* is a special target for IS element transposition, or whether this effect could be observed with other CDI toxins that have DNase activity. We chose a CdiA-CT from *E. coli* MHI813, which degrades chromosomal DNA in target cells as measured by DAPI staining and epifluorescence microscopy (Figure 8). This toxin requires the inner membrane protein MetI for delivery, which is normally used for transport of methionine into *E. coli* (173). We isolated spontaneous mutants using iterative co-culture assays and examined the *metI* alleles for the presence of IS elements. 9 of the 14 *metI* alleles tested contained IS elements in the coding region (Table 5), consistent with the theory that DNA damage leads to increased IS element transposition. These insertion elements were largely IS1, although an IS5 transposition event was also detected. These IS1 insertions were unique events and were not duplicates of other mutants (Table 5). The other 5 mutants that were sequenced contained 1 nucleotide frameshifts leading to a premature stop codon. Again, these mutations were scattered throughout the coding sequence and were not localized to a single region.

We performed the same experiment using CDI^{Ec536}, which delivers a general tRNase that requires the non-essential permissive factor CysK for activity (193). *cysK* was amplified from resistant clones, but surprisingly, 8 of 10 sequenced alleles contained an IS element in the coding sequence (Table 6). All 8 IS elements were IS10, although multiple alleles could be detected based on sequence identity. Furthermore, all IS10 insertions were located at the same position in *cysK* (nucleotide 187), even across 5 independent pools of mutants. Upon

close examination of *cysK*, we discovered that the location at which IS10 had integrated in these mutants is nearly identical to a known Tn10 hotspot and an IS10 hotspot in *hisD* (351). Therefore, it is possible that an IS10 element in this location in *cysK* was present in the parent population, and that it was selected for due to its resistance to CDI^{EC536}. The pattern of IS elements distribution (or lack of distribution) does not match the spread of IS elements throughout the coding sequences of *yciB* and *metI* that are detected in response to DNA damage.

C. Discussion

In this study, we have demonstrated that transposition of insertion elements into a gene required for delivery of CdiA-CT_{o11}^{EC869} can be detected after co-culture. This is presumably a result of increased global IS element transposition, but the selection bias of our experiments results in detection in only *yciB*. We have made several efforts to detect a general increase in IS element transposition above a basal level after competition of cells with CDI_{o11}^{EC869}, but have been unable to detect individual transposition events. This may be the result of several phenomena. Our experimental attempts utilized reporter systems that would indicate the presence of absence of an IS element by growth on an antibiotic or by development of a blue color in blue/white screening. However, these tests rely on the presence or absence of protein products. IS element transposition into a gene would disrupt future transcription and translation of these gene products, but would not disrupt translation from pre-existing mRNA and would not deplete the current levels of protein. Therefore, it may take time to dilute out these proteins through cell division, complicating the interpretation of these results.

An additional compounding factor may be the number of stress "events" a cell needs to undergo before upregulating IS element transposition. Perhaps the accumulation of stress

events and DNA damage over the iterative cycles of enrichment culminates in the transposition of IS elements, but a single damage event is not enough to stimulate this. This goes against the dogma of colicin inhibition, which posits that a "single hit" or delivery of a single toxin is enough to result in cell death. The ability of CDI target cells to respond and accumulate IS element transposition events in favorable locations argues that more than one "event" must occur to ultimately kill the cell. This makes sense in the context of cell division. If a single CDI toxin is delivered to a target cell in a bacterial environment, and that cell is able to undergo division before cell death occurs, then one daughter cell would not contain toxin and would presumably be able to survive. This may be indicative of the true role of CDI systems in bacterial physiology, which may be to induce signaling cascades or alter gene expression through microevents instead of inducing true cell death.

If DNase toxins can induce IS element transposition, is there an analogous course of action in response to other toxins? The obvious system to test in the presence of RNase toxins is stringent response, although preliminary evidence suggests that the stringent response is not activated by delivery of RNase toxins (Zach Ruhe, unpublished data). However, another translation stress pathway may be activated by the slow degradation of tRNA or ribosomal RNA substrates. While a tRNase toxin tested here did lead to IS element accumulation in the gene encoding its cofactor, we do not believe that this occurs through the same process as the DNA damage-mediated transposition observed with CdiA-CT_{o11}^{EC869} and CdiA-CT^{MHI813}. First, the distribution patterns of the IS elements in *yciB* and *metI* show random spread throughout the coding region of these genes. Additionally, multiple IS elements, including IS1, IS5, an IS10 were observed in these genes. In *cysK*, only IS10 elements were present, and they were all located at the same nucleotide position, even in

mutants derived from different starting pools of cells. This suggests that this region is a hotspot for IS element transposition, and that this particular IS insertion may exist at some low frequency in a parental population of cells. Enriching for resistant mutants would result in detection of this allele as well as true spontaneous mutants. Finally, we note that previous transposon mutagenesis experiments using a related toxin produced more than 100 mutants with transposon hops in CysK, indicating that toxicity-mediated IS element transposition into *cysK* does not greatly contribute to resistance using a mutagenized pool of target cells. This is in stark contrast to the results observed from transposon mutagenesis using the CDI_{o11}^{EC869} system, where IS element-mediated resistance was observed at an equal or greater frequency than resistance caused by insertion of the transposon element into *yciB*.

Perhaps the most interesting observation made here is that IS element transposition into *yciB* is not a permanent event that remains fixed in the absence of selective pressure from CDI_{o11}^{EC869}. Monocultures of IS mutants that were serially passaged eventually lost population resistance to this toxin, and PCR screens confirm that these alleles have reverted to wild-type *yciB*. This supports the hypothesis that YciB has a "normal" role in *E. coli* physiology, and that some growth defect is attributed to *yciB* mutants. This is supported by the general growth defect observed in *yciB* cells after co-culture with wild-type mutants strains. Additionally, *yciB* is highly conserved across gammaproteobacteria, and we have found no examples of sequenced strains in which this allele is defective or shows evidence of degrading. This is suggestive of an important physiological role for this gene product. Perhaps the flexibility in IS element transposition in response to DNA damage is representative of how cells respond to CDI systems in a natural environment. One could imagine a model in which a population of cells undergoes stress when it encounters a CDI

system deploying CdiA-CT_{o11}^{EC869}. Accumulation of DNA damage results in random IS element transposition throughout the genome, but only cells in which IS elements have transposed into *yciB* would be resistant to further insult from this toxin. These cells could then propagate in the presence of this selective pressure. When a shift in environment causes relief of this pressure in the absence of this CDI system, *yciB* mutants would be at a disadvantage over cells in the environment with a wild-type copy of this allele. This would then contribute to the overall loss of IS elements from *ycB* and reversion of this allele to wild-type. The cells would then regain the physiological function associated with *yciB*. In this way, IS element transposition may act as a genetic switch that results in transient resistance to CDI systems but allows cells to regain wild-type function in the absence of this selective pressure. This may be a method by which cells adapt to ever-changing conditions in dynamic microbial communities without affecting permanent changes that would become fixed in a population (Figure 9).

A final note of interest is that CdiA-CT_{o11}^{EC869} intoxication results in a dramatic phenotype in target cells. Inhibited cells become extremely long and filamentous, indicated that some response is taking place. Filamentation of bacterial cells can occur during the SOS response after DNA damage but has also been attributed to a variety of other pathways and factors. Perhaps for CDI_{o11}^{EC869}, this morphological change associated with upregulation of IS element transposition. Future work is needed to elucidate the damage response pathways associated with inhibition by this toxin and to determine whether this response is conserved across DNase toxins in CDI systems and in other bacterial inhibition systems. We have preliminary evidence that at least two responses take place after attack by DNase toxins. A CdiA-CT from *Dickeya dadantii* is also a DNase, but cells inhibited by this system do not

become elongated or filamentous like cells inhibited by CdiA-CT_{o11}^{EC869} (194). The inner membrane transporter for this toxin is unknown, but it would be interesting to repeat the spontaneous mutant enrichment procedure once a target gene has been identified to determine whether DNA damage from this toxin also induces IS element transposition.

D. Materials and methods

1. Transposon library construction and selection for mutants

The *mariner* transposon was introduced into *E. coli* CH10229 cells through conjugation with *E. coli* MFDpir donor cells carrying plasmid pSC189. Donor and recipient cells were grown to mid-log phase in lysogeny broth (LB) medium supplemented with 150 µg/mL ampicillin and 30 µM diaminopimelic acid (donors) or 33 µg/mL chloramphenicol (recipients). Donors (~6.0×10^8 cfu) and recipients (~3×10^8 cfu) were mixed and collected by centrifugation for 2 min at 6,000 × g in a microcentrifuge. The supernatant was removed by aspiration and the cell pellet resuspended in 100 µL of 1× M9 salts. Cell mixtures were spotted onto 0.45-µm nitrocellulose membranes, and the filters were then incubated on LB agar (without inversion) for 4 h at 37 °C. The cells were then harvested from the filters by using 2 mL of 1× M9 salts. Transposon insertion mutants were selected by plating 10-fold serial dilution on LB-agar supplemented with 50 µg/mL of kanamycin.

More than 20,000 colonies from each transposon library were collected from the agar plates in 1× M9 salts and inoculated into 50 mL of LB medium in a 250-mL baffled flask. CDI^+ inhibitor strains were grown in a parallel 50 mL LB medium culture. Both cultures were grown at 37 °C until mid-log phase, then mixed at approximately a 1:1 ratio and cultured for 3 h with shaking at 37 °C. Viable target cells from the transposon mutant library were enumerated as cfu counts per milliliter on LB agar supplemented with 50 µg/mL of

kanamycin. The survivors of the first round of CDI competition were harvested from the plates with 1× M9 salts and used to inoculate 50 mL LB medium culture for a second round of CDI selection. After the third round of selection, the target cell population was usually completely resistant to the CDI inhibitor cells. Individual clones were then isolated and the CDI^R phenotype confirmed in competition co-cultures. The transposon mutations were then transferred into CDI-sensitive cells by bacteriophage P1-mediated transduction, and the resulting transductants were tested for the CDI^R phenotype.

Transposon insertions linked to the CDI^R phenotype were identified by rescue cloning. Chromosomal DNA was prepared from each mutant by using phenol/chloroform extraction and ethanol precipitation. Genomic DNA (1 µg) was digested with AgeI and XmaI restriction endonucleases for 2 h at 37 °C, and the enzymes were inactivated at 65 °C for 10 min. ATP and T4 DNA ligase were added and the reaction was incubated for 2 h at room temperature. The ligated DNA was precipitated with 95% (vol/vol) ethanol, washed once with 75% (vol/vol) ethanol, and dissolved in 50 µL water. The ligated DNA was electroporated into *E. coli* DH5α pir^+ cells, and transformants were selected on LB agar supplemented with 50 µg/mL kanamycin. Plasmid DNA was isolated from selected transformants, and the transposon insertion junctions were identified by DNA sequencing by using primer CH2260.

2. Competition co-culture

Competition co-culture assays were carried out as previously described (175, 177). Briefly, inhibitor cells (*E. coli* EPI100 carrying CDI expression constructs) and target cells (*E. coli* MC4100 or MG1655 carrying pTrc99a derivatives) were grown in LB medium supplemented with appropriate antibiotics overnight at 37 °C. The next day, cells were inoculated into fresh LB medium without antibiotics in baffled flasks. Individual cultures

were grown with shaking until early log phase, and then the populations were mixed at a 1:1 ratio in fresh prewarmed LB in baffled flasks. The competitions between EC93-Bp1026b inhibitors and targets that express BTH_II0599 were conducted at a 10:1 inhibitor-to-target cell ratio. A sample of each co-culture was taken at initial mixing to enumerate viable target cells as cfu counts per milliliter. The co-cultures were incubated with shaking for 3 h at 37 °C. Viable target cell counts are presented as the average ± SEM of three independent competition experiments.

3. Microscopy

Cells (equivalent to an OD600 of 0.2) were collected by centrifugation in a microcentrifuge for 2 min at 6,000 × g. Cells were fixed in freshly prepared 4% (vol/vol) formaldehyde in 1× PBS solution for 15 min, and the reaction was quenched with 125 mM glycine (pH 7.5). Cells were washed three times with 1× PBS solution, resuspended in 100 μL 1× PBS solution, and spotted onto poly-d-lysine–treated slides. Excess liquid was removed with a Kimwipe, and slides were dried and gently rinsed with Nanopure water to remove nonadherent bacteria. Slides were sealed with Fluorogel II with DAPI (Fisher Scientific/EMS) and a glass coverslip. Images were acquired on an Olympus fluorescent microscope with a 100× oil objective by using an Optronics MacroFire digital microscope camera. Light-field images were taken with a 12-ms exposure (gain 2). DAPI-stained images were acquired with a 48-ms exposure (gain 2). Fluorescent images were recorded in grayscale by using a 502-ms exposure (gain 5). Images were false-colored, overlaid by using FIJI (61), and cropped to 200 × 200 pixels using GIMP.

E. Acknowledgments

We thank Sanna Koskiniemi for helpful discussions.

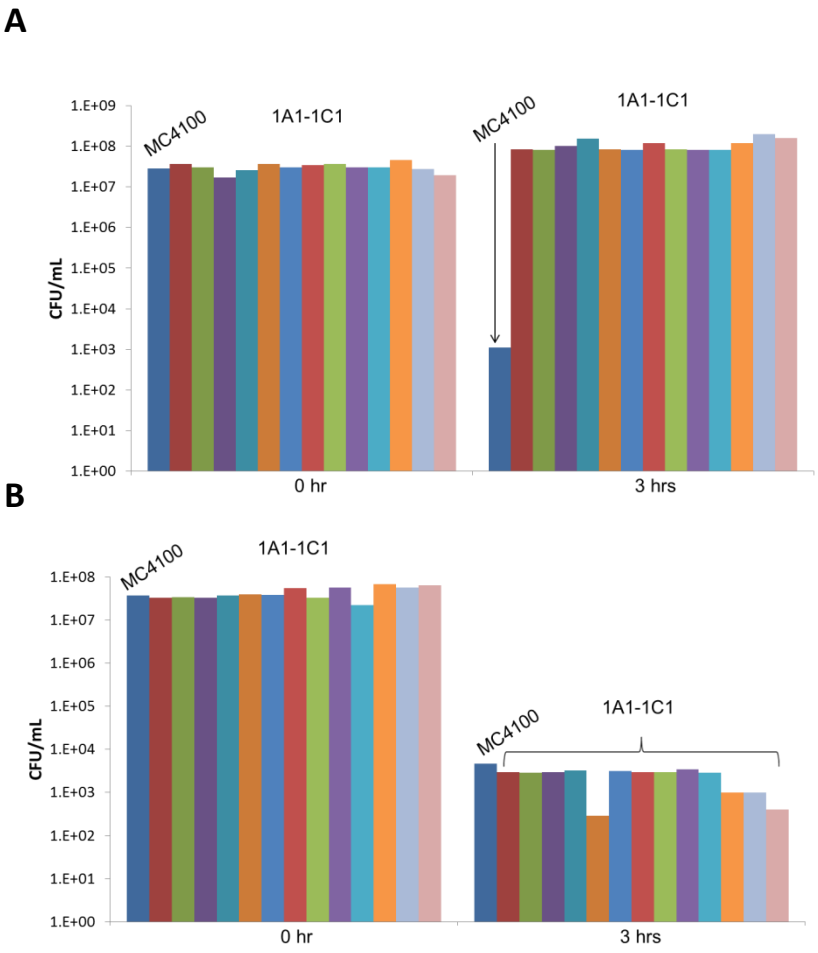

Figure 1. A subset of transposon mutants are CDI^{R} and have secondary mutations in *yciB*. (A) Initial mutants isolated from transposon mutagenesis are resistant to inhibition by CdiA-CT$_{o11}^{EC869}$. (B) The transposon insertions from (A) were moved into a fresh background and tested for linked resistance.

A

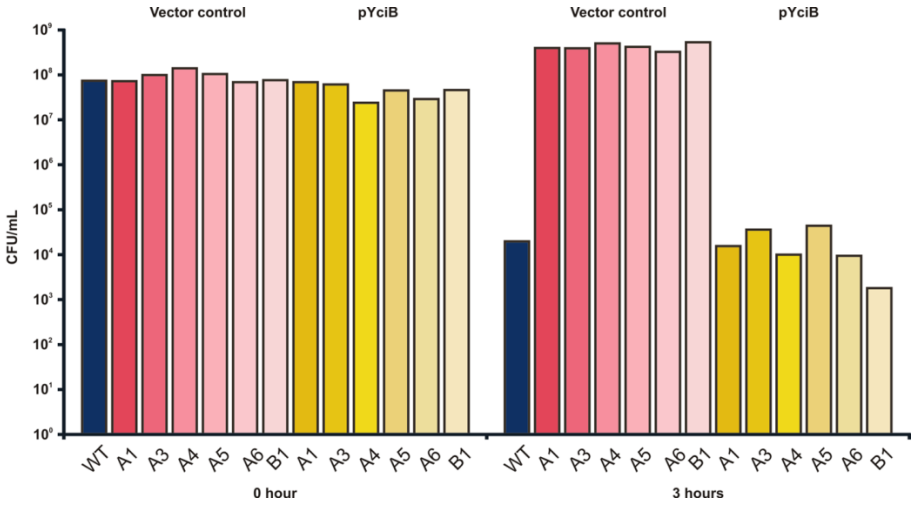

B

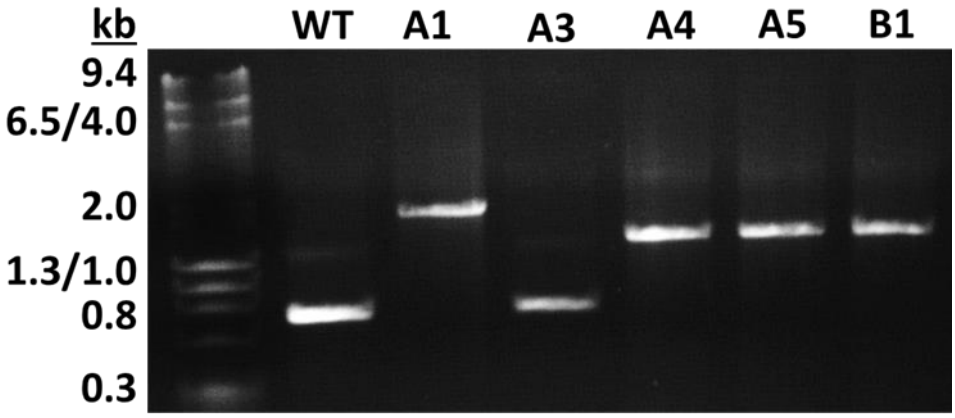

Figure 2. Unlinked transposon isolates have secondary mutations in *yciB*. (A) Plasmids expressing wild-type *yciB* were transformed into the original mutants and tested for sensitivity. (B) *yciB* alleles were amplified from several different mutants and analyzed via gel electrophoresis. 4 of 5 strains tested had alleles that ran larger than the wild-type gene on an agarose gel.

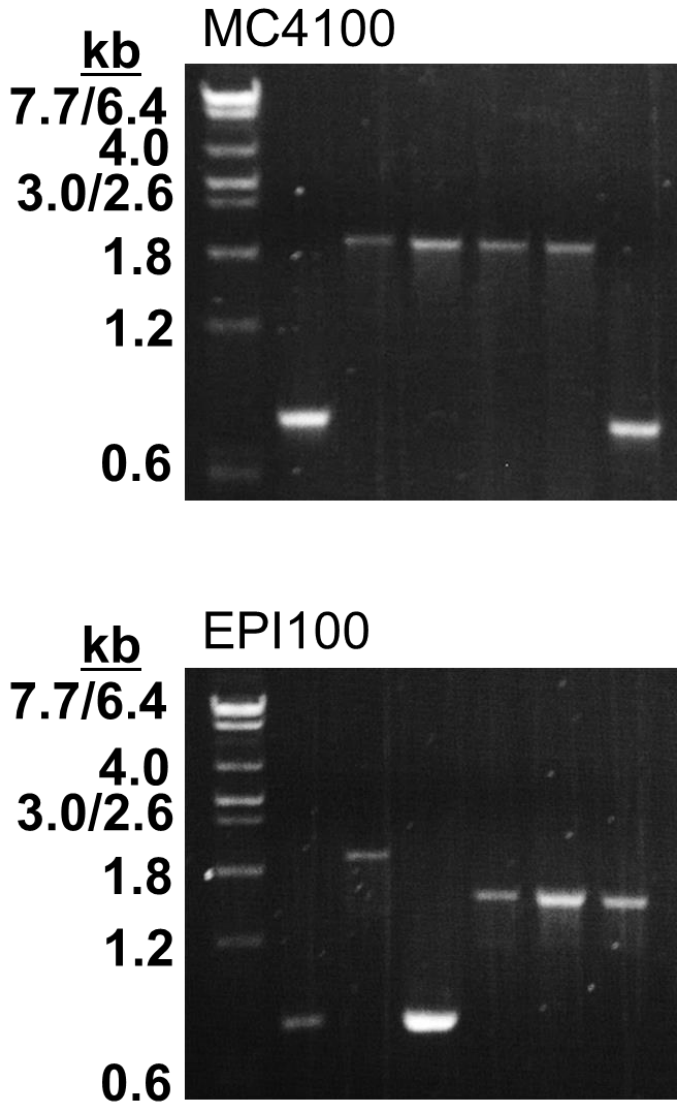

Figure 3. Isolation of unmutagenized, spontaneous CDI^{R} mutants reveals disruptions in *yciB*. The indicated *E. coli* strains were competed in co-culture assays against cells expressing CDI_{o11}^{EC869}. Resistant clones were isolated, and *yciB* was amplified and analyzed via gel electrophoresis.

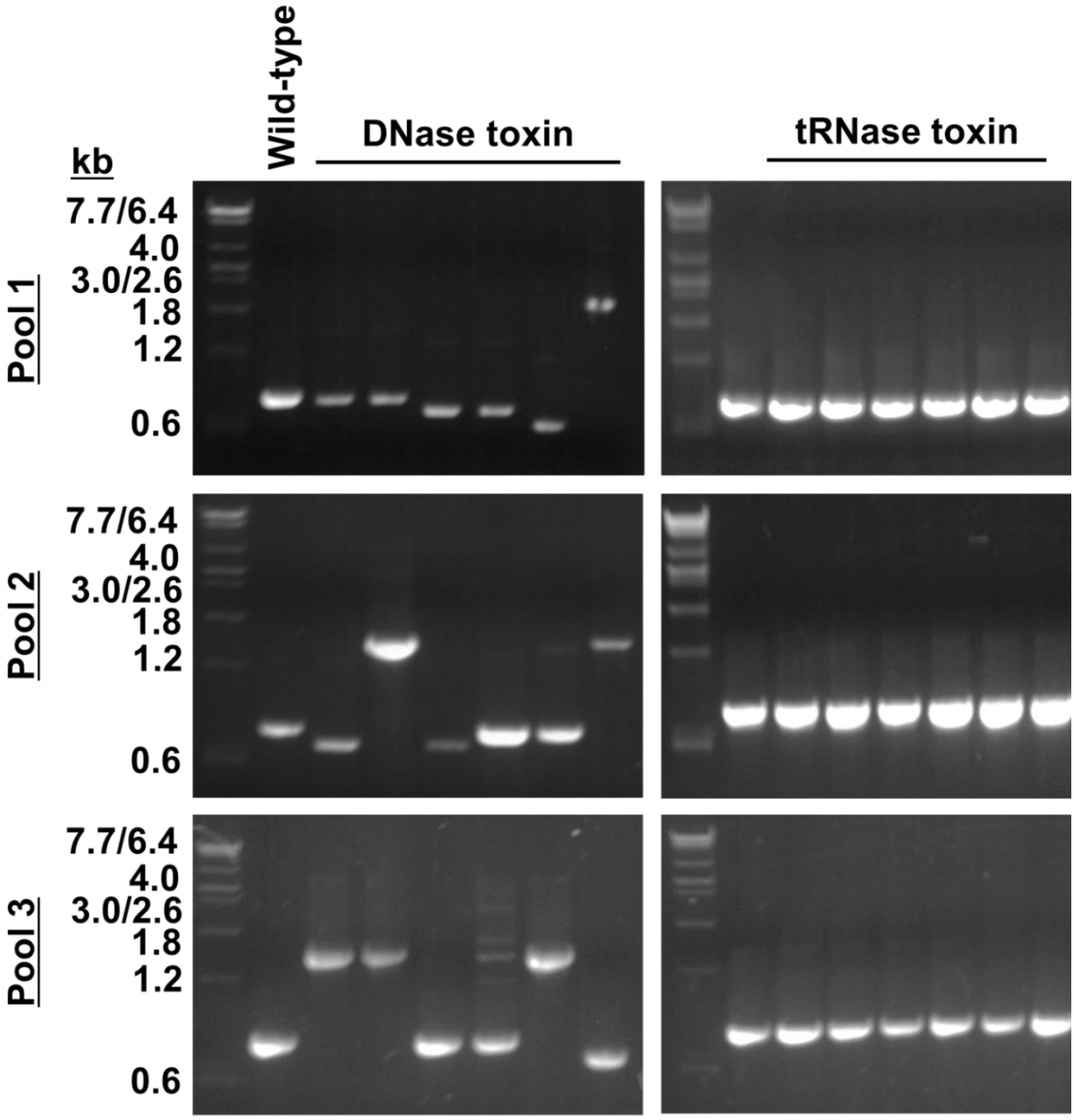

Figure 4. Insertion elements do not accumulate in *yciB* in response to delivery of a tRNase CdiA-CT. Unmutagenized *E. coli* target cells were co-cultured with CDI_{o11}^{EC869} or CDI^{EC93}-NT_{o11}^{EC869}-$CT_{II}^{Bp1026b}$. After enrichment, *yciB* alleles from isolated clones were amplified and analyzed via gel electrophoresis and ethidium bromide staining. A wild-type *yciB* PCR is run in the first lane for size comparison.

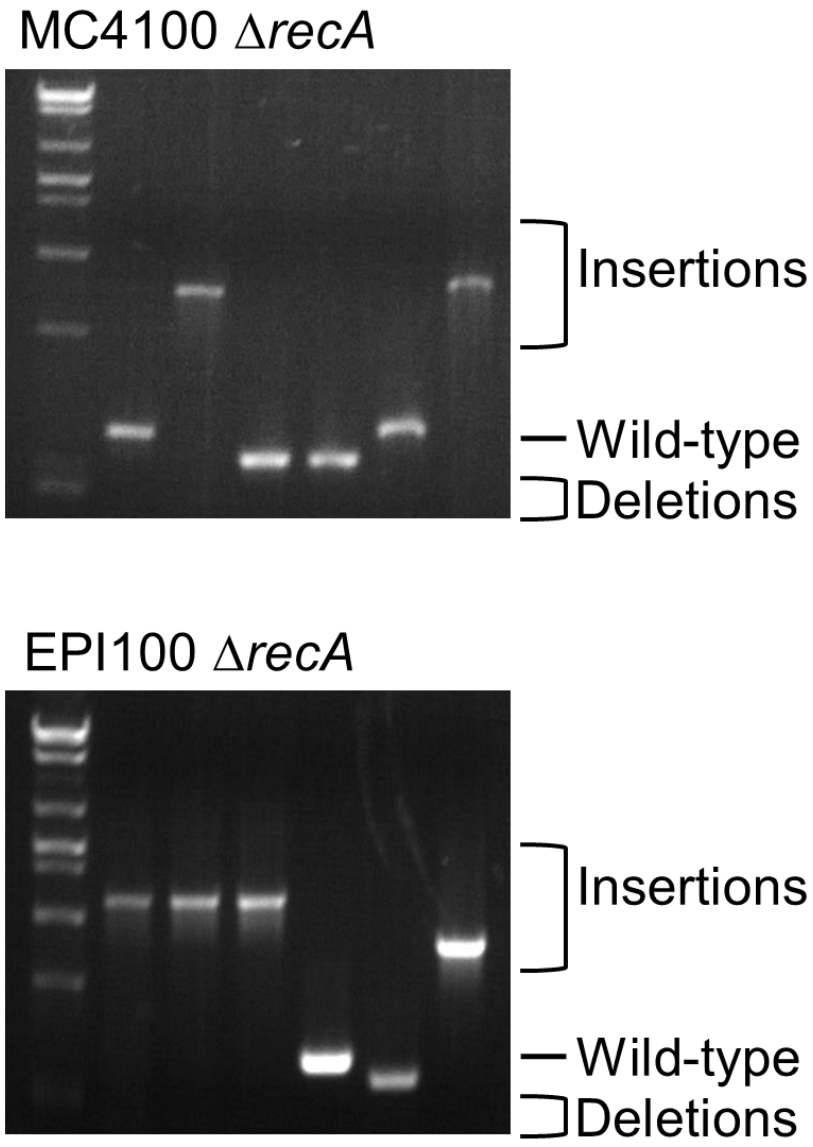

Figure 5. Transposition of insertion elements does not depend on RecA. Unmutagenized *E. coli* target cells lacking *recA* were co-cultured with CDI_{o11}^{EC869}. After enrichment, *yciB* alleles from isolated clones were amplified and analyzed via gel electrophoresis and ethidium bromide staining.

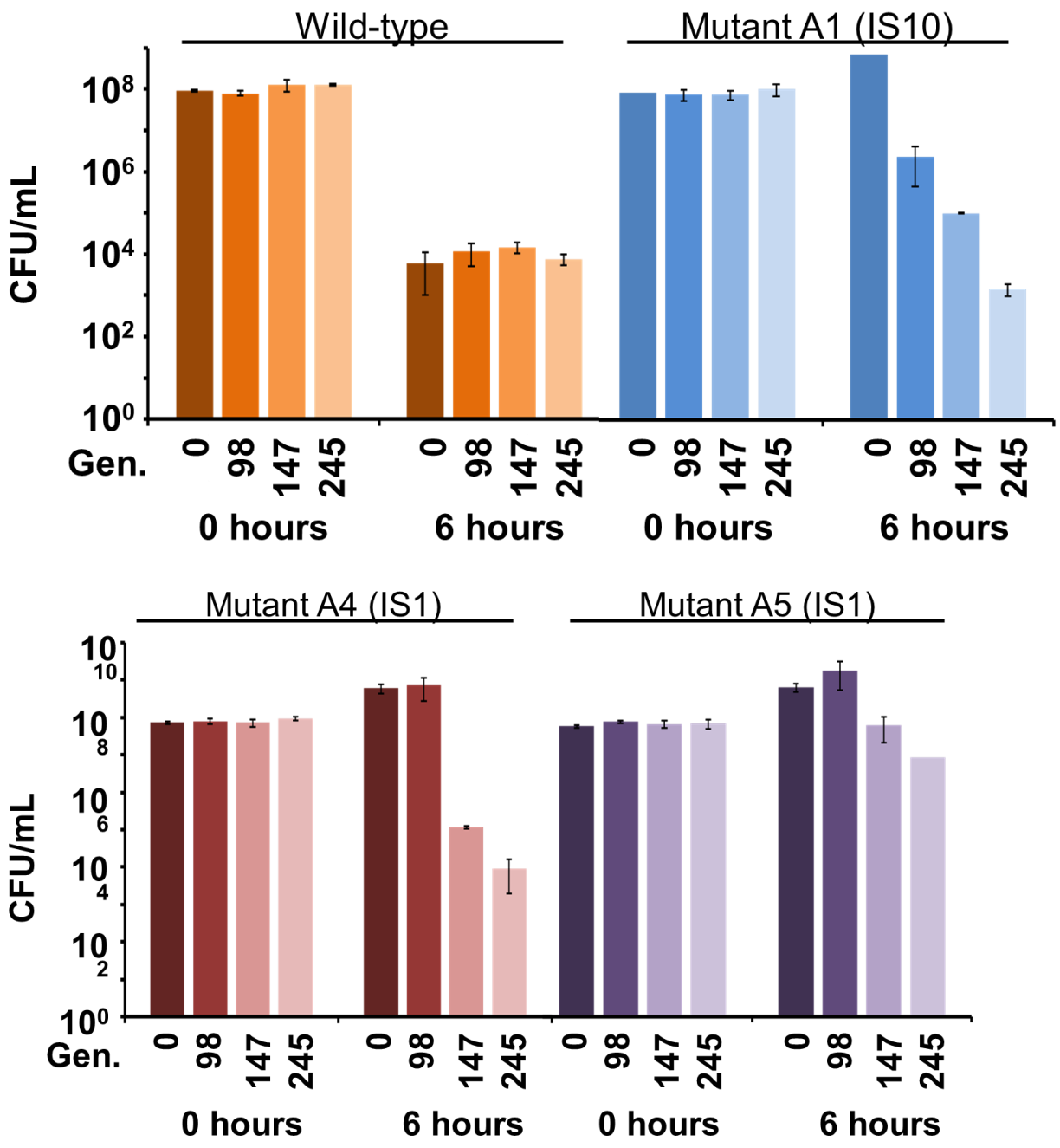

Figure 6. Insertion element transposition is reversible in the absence of selective pressure from CDI_{o11}^{EC869}. Mutants from the original transposon mutagenesis screen that contained IS element insertions in *yciB* were grown in monocultures in the absence of CDI_{o11}^{EC869}. Every 7 generations, the culture was diluted into fresh LB media and grown again. Every 49 generations, an aliquot of the culture was removed and mixed with cells expressing CDI_{o11}^{EC869} to estimate the overall CDI resistance of the population. A wild-type, unmutagenized strain was passaged alongside the mutants as a control for spontaneous mutations in *yciB* that would result in CDI resistance.

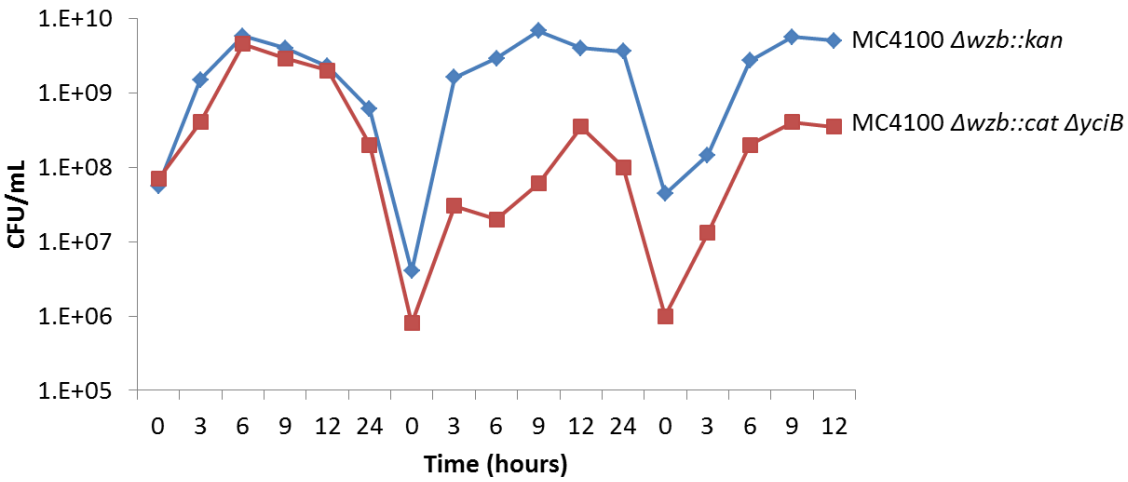

Figure 7. *yciB* deletion strains have a fitness defect over time in co-culture with wild-type cells. Wild-type cells and cells lacking *yciB* were grown to mid-log phase and mixed together at a 1:1 ratio. The culture was grown for 10 generations, at which point the cells were diluted into fresh LB media. The culture was propagated for another 10 generations and diluted; this process was repeated once more. At each indicated timepoint, a sample was removed and diluted in M9 salts before plating onto LB-agar plates. Data presented is viable cells per mL culture.

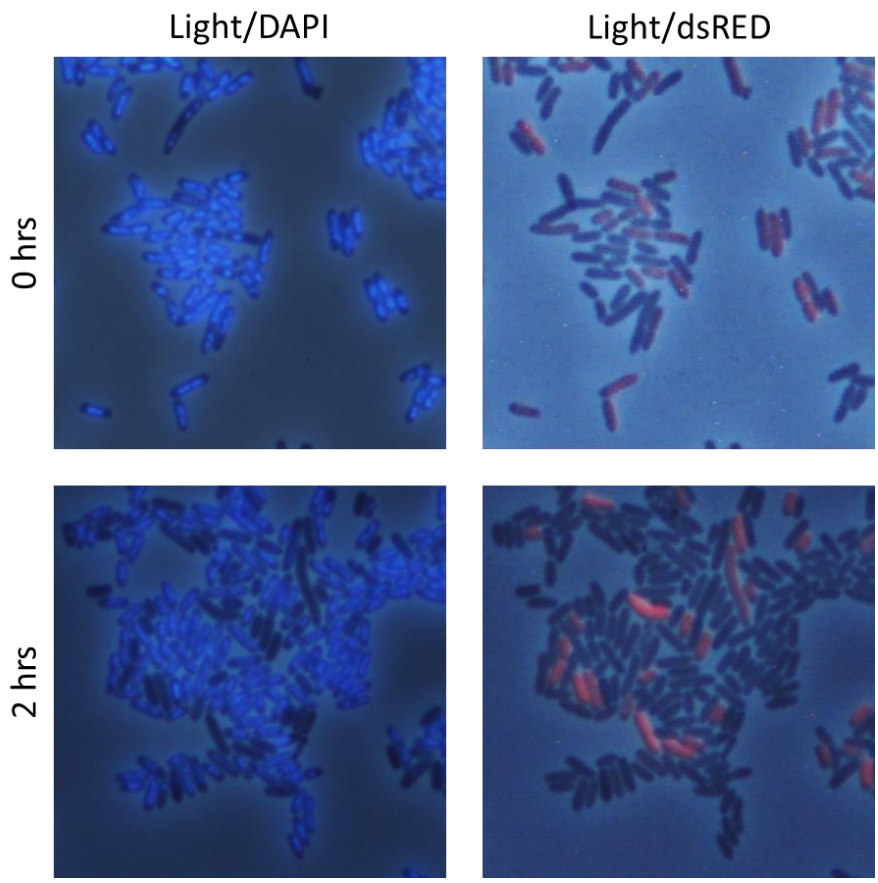

Figure 8. CdiA-CT^{MHI813} is a DNase. Unlabeled inhibitor cells were mixed with dsRED-labeled target cells at a 1:1 ratio. At 0 and 2 h timepoints, cells were removed and spotted onto an agarose pad for imaging. Red cells stain with DAPI at 0 h but lose DAPI staining at 2 h, indicating loss of chromosomal DNA.

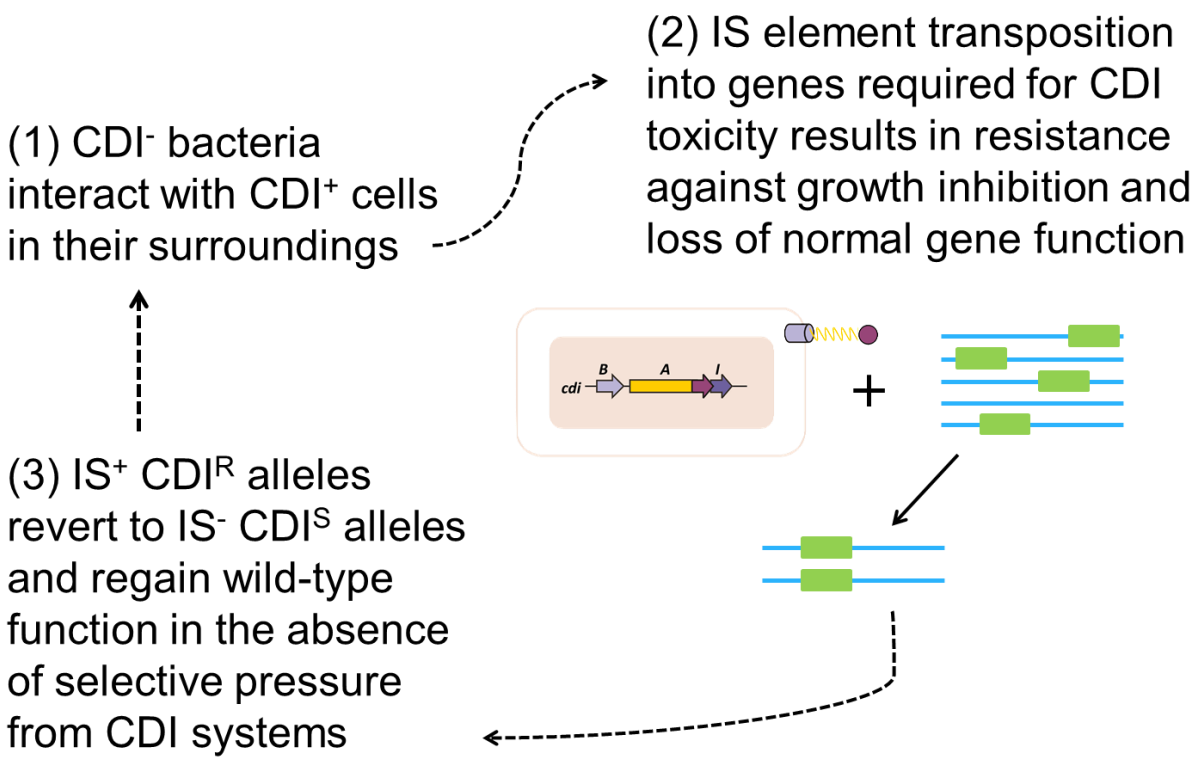

Figure 9. Model for transient CDI resistance mediated by insertion element transposition.

Table 1. Location of transposon insertions outside of *yciB*.

Gene	Predicted protein product
uhpC	Regulatory membrane protein
gnd	6-phosphogluconate dehydrogenase
yiiE/yiiF	Uncharacterized protein
yjcD	Predicted permease
amiB	N-acetylmuramoyl-l-alanine amidase II
ybaY	outer membrane lipoprotein
yigI/pldA	4HBT family of thioesterases
16S rRNA	

Table 2. Location and identity of insertion sequence elements in *yciB* from transposon-mutagenized isolates.

Identifier	Mutation	Duplication	Nucleotide position
A1	IS10	AGCTGAATC	360
A3	Stop codon	N/A	223
A4	IS1	AATGGAAGG	232
A5	IS1	ATGGAAGGT	233
B1	IS1	GACCGCCCT	470

Table 3. Location and identity of *yciB* mutations detected in spontaneously-resistant clones.

Identifier	*Mutation*	*Location*
J1	Stop codon	K90 → stop
J2	Deletion	30 AA deletion after L111
J3	Deletion	62 AA deletion after P112
J4	IS5	Insertion after nt 397
J5	Deletion	Sibling with J2
J6	Deletion	Sibling with J2
J7	Stop codon	L116 → stop
J8	IS1	Insertion after nt 84

Table 4. Nonsense and frameshift mutations are present in *yciB* alleles from spontaneous mutants generated against a tRNase toxin delivered through YciB.

Identifier	Mutation (nucleotide position)	Outcome	
J1	G369A	Premature stop codon, 123-residue product	Siblings present in same pool

E1-1	Insertion after position 291	IS1 insertion	
E2-1	Insertion of C after position 437	Frameshift and premature stop codon, 150-residue product	Siblings present in same pool
E2-3	Deletion of G256	Frameshift and premature stop codon, 90-residue product	Siblings present in same pool
NT1-2	G123A	Nonsense mutation, 41-residue product	Siblings present in same pool
NT3-5	Deletion of T29	Frameshift and premature stop codon, 29-residue product	
NT4-1	T538G	TAA → Glu, extends open reading frame approximately 15 residues	Siblings present in same pool
NT4-3	A539C	TAA → Ser, extends open reading frame approximately 15 residues	Siblings present in same pool
NT1	G123A	Nonsense mutation, 41-residue product	Independent of mutant NT1-2
NT3	G510C	Nonsense mutation, 170-residue product	
NT5	Insertion after position 246	IS10 insertion	

Table 5. Mutations present in *metI* after enrichment of spontaneous mutants resistant to CDI^{MHI813}.

Pool	Mutant	Mutation	Details
1	MHI3	1 nt insertion	T inserted after nt T405, frameshift leads to stop
	MHI4	1 nt insertion	G inserted after G539, frameshift leads to stop
	MHI5	IS5	NT 146, forward orientation
2	13	IS1	NT 19, reverse orientation

3	21	1 nt deletion	nt 384C, leads to frameshift/premature stop codon
	23	IS1	NT167, forward orientation
4	13	IS1	NT 592, reverse orientation
	16	1 nt deletion	T deleted after NT 477
5	21	1 nt insertion	C inserted after NT 634
6	N=2	1S1	PCR confirmed
7	N=2	1S1	PCR confirmed

Table 6. Mutations present in *cysK* alleles from spontaneous mutants resistant to CDI^{EC536}.

Pool	Mutant	Mutation	Details
1	13	IS10	NT 187, forward orientation
	14 (sib 15)	1 nt deletion	Frameshift leads to premature stop codon (also has 15 nt in-frame deletion downstream)
	16	IS10	NT 187, reverse orientation
2	21	IS10	NT 187, forward orientation
	23 (sib 24)	1 nt deletion	Frameshift leads to premature stop codon (also has 15 nt in-frame deletion downstream)
3	31	IS10	NT 187, forward orientation
	32	IS10	NT 187, reverse orientation
4	54-528	IS10	NT 187, reverse orientation, different IS10 allele based on SNPs
5	51 (sib 54, 55)	IS10	NT 187, reverse orientation
	52 (sib 53)	IS10	NT 187, forward

			orientation, different IS10 allele based on SNPs

Table 7. Strains used in this study.

EPI100	F⁻ *mcrA* Δ*(mrr-hsdRMS-mcrBC) φ80dlacZ*Δ*M15* Δ*lacXcZ*Δ*M15* Δ*lacX recA1 endA1 araD139* Δ*(ara, leu)7697 galU galK λ⁻ rpsL nupG*, Str^R	Epicentre
CH8251	MC4100 *rif*⁻, Rif^R	(177)
pCH9305	Constitutive expression of chimeric $cdiA^{EC93}$-$CT_{o11}{}^{EC869}$ and $cdiI_{o11}{}^{EC869}$ genes, Cm^R	(177)
pCH10415	Constitutive expression of chimeric $cdiA^{EC93}$-$NT_{o11}{}^{EC869}$-$CT_{II}{}^{Bp1026b}$ and $cdiI_{II}{}^{Bp1026b}$ genes, Cm^R	(172)

V. Diversification of β-augmentation interactions between CDI toxin/immunity proteins

This research was conducted in collaboration with Robert Morse and Celia Goulding at the University of California, Irvine. A majority of this work was published in October 2015 in the Journal of Molecular Biology (doi: 10.1016/j.jmb.2015.09.020), and much of the text appears as published. The Goulding laboratory performed all crystallography and binding affinity studies.

A. Introduction

Bacteria possess many strategies to compete and cooperate with other microorganisms in the environment. Contact-dependent growth inhibition (CDI) is one competitive mechanism used by some Gram-negative species to inhibit the growth of neighboring bacteria (156, 167). CDI^+ cells express CdiB/CdiA two-partner secretion systems, which deliver protein toxins into target bacteria through a receptor-mediated process. CdiB is an Omp85 outer-membrane protein that exports and assembles toxic CdiA effectors onto the surface of CDI^+ cells. CdiA proteins range from 180 – 630 kDa depending on bacterial species and form β-helical filaments that are predicted to extend several hundred Å from the inhibitor-cell surface. CdiA binds to specific receptors on susceptible bacteria and subsequently delivers a toxin domain derived from its C-terminus (CdiA-CT) into the target cell (157, 159, 194). CDI^+ bacteria deploy a variety of CdiA-CT toxins with distinct activities. The $CdiA\text{-}CT^{EC93}$ from *Escherichia coli* EC93 dissipates ion gradients by forming membrane pores (158), but most other characterized CDI toxins have specific nuclease activities. CDI toxins from *E. coli* EC869 and *Dickeya dadantii* 3937 are potent DNases capable of degrading target-cell chromosomes (177, 194), and $CdiA\text{-}CT^{ECL}$ from *Enterobacter cloacae* ATCC 13047 cleaves

16S rRNA to block protein synthesis (175). CDI^+ bacteria protect themselves from auto-inhibition by producing small CdiI immunity proteins that bind to the CdiA-CT and block its toxin activity. Because CDI toxins are diverse, CdiA-CT/CdiI protein interactions are necessarily specific between cognate pairs. Therefore, CdiI immunity proteins neutralize their cognate CdiA-CT, but provide no protection against the toxins deployed by other bacteria (176, 177). This diverse network of toxin/immunity pairs suggests that CDI plays an important role in inter-cellular competition and self/non-self recognition.

We recently surveyed the Uniprot database and identified at least 120 distinct CdiA-CT toxin families. Only 26 of these toxins have Pfam designations (200) and the remaining domains are uncharacterized. We initiated structural studies of these protein pairs to discover new toxin activities and toxin/immunity binding interactions. The first CDI toxin/immunity protein complex structures to be determined were from *Burkholderia pseudomallei* 1026b and enterohemorrhagic *E. coli* strain EC869 (177). The CdiA-CT toxin sequences from these bacteria are not related, yet the three-dimensional structures of the domains superimpose with an RMSD of 3.9 Å. Structural homology searches revealed significant similarity to type IIS restriction endonucleases, suggesting that both toxins are DNases. Indeed, the C-terminal domain of CdiA-CT_{o11}^{EC869} has potent Zn^{2+}-dependent DNase activity *in vitro* and *in vivo* (177). However, CdiA-$CT_{II}^{Bp1026b}$ has no detectable activity on DNA, and instead this toxin preferentially cleaves near the 3´-end of $tRNA^{Ala}$ molecules (169). Thus, the same toxin fold is used to target different nucleic acid substrates. Though CdiA-CT_{o11}^{EC869} and CdiA-$CT_{II}^{Bp1026b}$ are similar in structure, other CDI toxins do not share the type IIS restriction endonuclease fold. The crystal structure of CdiA-CT^{ECL} from *E. cloacae* ATCC 13047 reveals similarity to the C-terminal nuclease domain of colicin E3 (79, 176, 207), and

sequence homology and activity studies strongly suggest that CdiA-CT^{K96243} from *B. pseudomallei* K96243 is related to the C-terminal nuclease domain of colicin E5 (167, 169). Moreover, Aravind and colleagues have predicted that CDI systems deploy two classes of RNA deaminase (Pfam: PF14424 and PF14437), as well as homologues of the EndoU poly(U)-specific endonuclease that processes eukaryotic snoRNAs (Pfam: PF14436)(200, 352, 353). Thus, CDI represents a versatile platform to deliver structurally diverse toxins into Gram-negative bacteria.

Although toxin/immunity pairs within a given family are homologous, there is often considerable sequence diversity between members, suggesting that families continue to diverge and evolve. When viewed in the context of available crystal structures, it is apparent that residues at the interface of the toxin/immunity protein complexes are diversifying most rapidly. This phenomenon is exemplified by toxin/immunity proteins that are homologous to the orphan-11 (o11) CdiA-CT/CdiI pair from E. coli EC869 (176, 177). CdiA-CT$_{o11}^{EC869}$ interacts with CdiI$_{o11}^{EC869}$ through β-augmentation, in which the toxin domain extends a β-hairpin to complete a six-stranded anti-parallel β-sheet within the immunity protein (Figure 1A)(177). The sequences encoding the β-hairpin (corresponding to β4 and β5) are the most variable between members of the CdiA-CT$_{o11}^{EC869}$ nuclease family (Figure 1B). Moreover, CdiI$_{o11}^{EC869}$ residues that interact with the toxin are not conserved between related immunity proteins (Figure 1C), suggesting that each immunity protein is specific for its cognate toxin. Here, we use structure-function analyses to examine the β-augmentation interactions of two homologous CdiA-CT/CdiI complexes to study the diversification of CDI toxin/immunity protein interfaces. We find that the CdiA-CT/CdiI^{YPIII} complex from *Yersinia pseudotuberculosis* YPIII also features a β-augmentation interaction; however, the precise

intermolecular contacts differ substantially between the complexes. In accord with these differences, each CdiI immunity protein only protects against its cognate toxin, demonstrating that each pair is a distinct cognate toxin/immunity pair. Finally, we synthesized a macrocyclic peptide mimic of the β-hairpin from CdiA-CT_{o11}^{EC869} and solved its crystal structure in complex with the $CdiI_{o11}^{EC869}$ immunity protein. This structure forms the basis to refine the β-hairpin mimic to increase affinity with the goal of producing compounds that activate DNase toxins through sequestration of immunity proteins.

B. Results

1. Structure of the CdiA-CT/CdiI^{YPIII} complex reveals conservation of the β-augmentation interaction

Alignment of CdiA-CT_{o11}^{EC869} toxin homologues indicates that most secondary-structure elements have high sequence conservation with the exception of strands β4 and β5, which mediate the β-augmentation interaction with $CdiI_{o11}^{EC869}$ (Figure 1A and B). To determine whether β-augmentation occurs in other homologous toxin/immunity pairs, we performed structural and functional analyses of the CdiA-CT/$CdiI^{YPIII}$ complex encoded by the YPK_0575/YPK_0576 genes of Yersinia pseudotuberculosis YPIII. The C-terminal nuclease domain of CdiA-CT^{YPIII} is 70.4% identical to CdiA-CT_{o11}^{EC869} and shares all of the predicted active-site residues (Figure 1B). Similarly, the $CdiI^{YPIII}$ and $CdiI_{o11}^{EC869}$ immunity proteins share 49.1% identity, though $CdiI^{YPIII}$ contains a 10-residue insertion between α1 and α2 that is predicted to produce an elongated loop (Figure 1C). We solved the crystal structure of the CdiA-CT/$CdiI^{YPIII}$ complex to 2.1 Å resolution by molecular replacement using the structure of the CdiA-CT/ $CdiI_{o11}^{EC869}$ complex (PDB code: 4G6U) as a search model (Figure 2A). As with other CdiA-CTs (175, 177), the N-terminal region (residues

Val1 – Gly173) was not resolved in the structure. The final model included CdiA-CT^{YPIII} residues 174 – 298 and 148 water molecules resulting in an Rwork/Rfree (%) of 20.5/25.6 (Table 1). The CdiA-CT/CdiI$_{o11}^{EC869}$ and CdiA-CT/CdiI^{YPIII} complexes have very similar structures. The toxin domains superimpose with RMSD of 0.84 Å over 101 of 123 α-carbons, and the immunity proteins superimpose with RMSD of 1.01 Å over 133 of 173 α-carbons (Figure 2B). The CdiA-CT/CdiI^{YPIII} complex also contains a β-augmentation interaction in which the toxin extends its β4/β5-hairpin into binding pocket within the immunity protein (Figure 2A and B). However, in contrast to CdiA-CT$_{o11}^{EC869}$, which contains an ordered Zn^{2+} ion in the active site (177), no zinc was detected by metal K-edge absorption analysis of multiple CdiA-CT/CdiI^{YPIII} crystals. Furthermore, the electron density spheres within the active site vicinity of CdiA-CT^{YPIII} were not within zinc coordinating distances with the catalytic residues and would not form a zinc tetra- or hexa-coordination sphere, and thus were modeled as water molecules (Figure 3).

CdiA-CT^{YPIII} and CdiI^{YPIII} bind one another through a network of 14 direct H-bonds and ion-pairs (Table 2) combined with several hydrophobic interactions. Only two CdiA-CT^{YPIII} β-hairpin side-chains (Glu242 and Lys243) interact directly with CdiI^{YPIII}, compared to the six direct side-chain interactions in the CdiA-CT/CdiI$_{o11}^{EC869}$ complex (Table 2 and Figure 4). The CdiA-CT/CdiI^{YPIII} β-hairpin pocket also contains a network of bridging water molecules and several more hydrophobic interactions than the CdiA-CT/CdiI$_{o11}^{EC869}$ complex (Figure 4). Additionally, extensive interactions outside of the β-augmentation region contribute to CdiA-CT/CdiI^{YPIII} complex stability. Loop L1 of CdiA-CT^{YPIII} forms several hydrophobic contacts with the elongated loop of CdiI^{YPIII}. Residue Lys195 within L1 forms a salt-bridge with CdiI^{YPIII} residue Glu137 within β6. The loop connecting strands β2 and β3

also has several H-bond interactions, and Asp201 forms a prominent salt-bridge with Arg69 in the elongated loop of $CdiI^{YPIII}$ (Table 2 and Figure 2B). In contrast, the CdiA-CT/$CdiI_{o11}^{EC869}$ complex has a less extensive interaction network outside of the β-augmentation region. Loop L1 of CdiA-CT_{o11}^{EC869} has fewer hydrophobic contacts and one ionic interaction between Asp183 and Arg71 of $CdiI_{o11}^{EC869}$ (Table 2). Together, these structures reveal overall conservation between the toxin/immunity protein pairs, but reveal important differences in the network of bonds that stabilize each complex (Figure 5).

2. CdiA-CTs in the EC869 superfamily have DNase activities in vitro

The conservation of nuclease active-site residues strongly suggests that CdiA-CT^{YPIII} has DNase activity similar to that described for CdiA-CT_{o11}^{EC869} (177). We isolated the CdiA-CT^{YPIII} domain from its immunity protein and tested for DNase activity *in vitro* using supercoiled plasmid as a substrate. CdiA-CT^{YPIII} degraded the linear DNA template in the presence of both Mg^{2+} and Zn^{2+}. This differs from the characterized activity of the CdiA-CT_{o11}^{EC869} toxin, which has detectable DNase activity with Mg^{2+} and completely degrades plasmid DNA in the presence of Zn^{2+} ions (177). CdiA-CT^{Nlact} also degrades linear DNA in the presence of both Mg^{2+} and Zn^{2+} (Figure 6B). We next tested the $CdiI^{YPIII}$, $CdiI_{o11}^{EC869}$, and other homolgoy immunity proteins for the ability to neutralize DNase activity *in vitro*. Each immunity protein was able to block the activity of its cognate toxin (Figure 6C and D), and CdiA-CT^{YPIII} was protected by all tested CdiI proteins. However, we note that this cross-protection may be an artifact of the protein concentrations used in this experiment, based on the calculated binding affinities between non-cognate CdiA-CT and CdiI domains (discussed below).

Metal co-factors that support the activity of CdiA-CT_{o11}^{EC869} *in vitro* are restricted to

Mg^{2+} and Zn^{2+} (177). Given the strong structural conservation between this toxin and related homologs, we wondered whether these other toxins retained the tight metal utilization profile, or whether they were more promiscuous in their use of co-factors. We isolated CdiA-CT^{Nlact} and incubated it with linearized DNA in the presence of $CoCl_2$, $CuCl_2$, and $MnCl_2$, none of which support the DNase activity of CdiA-CT_{o11}^{EC869} *in vitro*. Surprisingly, we detected DNase activity in the presence of both Co^{2+} and Mn^{2+} (Figure 7). None of the concentrations of Cu^{2+} tested supported activity. However, this activity could not be blocked by the addition of the cognate CdiI at the highest metal concentrations tested.

3. Binding affinities of non-cognate CdiA-CT/CdiI pairs

We next measured the dissociation constants (K_d) for cognate and non-cognate complexes using biolayer interferometry. CdiA-CT^{YPIII} and $CdiI^{YPIII}$ form a high-affinity complex with K_d = 16 ± 1 nM, which is similar to the value (18 ± 7 nM) previously reported for the CdiA-CT/$CdiI_{o11}^{EC869}$ complex(177). In contrast, $CdiI^{YPIII}$ has ~ 1,000-fold lower affinity for non-cognate CdiA-CT_{o11}^{EC869} with a K_d of 13 ± 2 μM. This highly reduced affinity between CdiA-CT_{o11}^{EC869} and $CdiI^{YPIII}$ compared to cognate protein pairs is perhaps due, in part, to the shape and electrostatic incompatibility of the CdiA-CT_{o11}^{EC869} β-hairpin with the binding pocket of $CdiI^{YPIII}$ immunity protein (Figure 8). Similarly, CdiA-CT_{o11}^{EC869} does not strongly interact with $CdiI^{Pasy}$, $CdiI^{Ykris}$, or $CdiI^{Nlact}$ as observed by bait-prey binding assays (Figure 13).

4. Immunity proteins only provide protection against their cognate toxins during cell-mediated CDI

The CdiA-CT^{YPIII} toxin is encoded within a defective *cdi* locus that has been inactivated by complex gene rearrangements and deletions. To ascertain whether the toxin is functional

in cell-mediated CDI, we fused the CdiA-CT^{YPIII} nuclease domain to the C-terminus of $CdiA^{EC93}$ and tested the resulting chimera for inhibition activity against *E. coli* target cells. Inhibitor cells that express the $CdiA^{EC93}$-CT^{YPIII} chimera reduced viable target-cell counts more than 500-fold after four hours of co-culture, but target cells that express the cognate $CdiI^{YPIII}$ immunity protein were completely protected from inhibition (Figure 9A). In contrast, target cells that express $CdiI_{o11}{}^{EC869}$ immunity protein were inhibited to the same extent as cells that lack any immunity gene (Figure 9A). Similarly, the $CdiI^{YPIII}$ immunity protein was unable to protect target cells from inhibitor cells that deploy the CdiA-$CT_{o11}{}^{EC869}$ toxin (Figure 9A). We also examined competition co-cultures by fluorescence microscopy to detect DNase activity in target bacteria. We labeled inhibitor cells with YFP and target cells with mKate2 to differentiate the two populations and also stained the cells with DAPI to visualize nucleoids. Immediately after cell mixing, both inhibitor and target cell populations had similar morphologies and nucleoid staining was uniform (Figure 9B). After four hours of co-culture, target cells that lack the appropriate immunity protein became filamentous and lost DAPI staining (Figure 9B), indicating significant damage to the chromosome. In contrast, target cells that express cognate CdiI immunity proteins retained normal morphology and DAPI staining (Figure 9B). Together, these data demonstrate that these two toxin/immunity systems have diverged into distinct non-overlapping immunity groups.

5. *Intracellular expression of CdiA-CTs in the EC869 superfamily phenocopies inhibition by CdiA-$CT_{o11}{}^{EC869}$*

A hallmark of target cells inhibited by CdiA-$CT_{o11}{}^{EC869}$ is the formation of long, filamentous cells with severely-damaged chromosomal DNA (Figures 9 and 10). Although the mechanism of filamentation is unknown, this phenotype is not observed during inhibition

by all DNases, suggesting that this target cell response is mounted with some specificity to the activity of the CdiA-CT_{o11}^{EC869} toxin. Given the structural similarity between CdiA-CT_{o11}^{EC869} and CdiA-CT^{YPIII} as well as the strong sequence conservation between these two toxins and CdiA-CT^{Nlact}, we wondered whether other toxins in the EC869 superfamily induced morphological changes in target cells similar to those observed after inhibition by CdiA-CT_{o11}^{EC869}.

First, we tested whether intracellular expression of CdiA-CT^{YPIII} and CdiA-CT^{Nlact} is toxic using a two-plasmid transformation assay. *E. coli* X90 cells were co-transformed with pCH450 constructs carrying *cdiA-CT* genes and pTrc99A derivatives carrying the corresponding *cdiI*. Induction of CdiA-CT^{YPIII} inside cells results in growth inhibition, as evidence by the lack of viable colonies on these plates (Figure 11A). Expression of the cognate $CdiI^{YPIII}$ rescues this growth defect. $CdiI^{Nlact}$ and $CdiI^{Pasy}$ do not fully protect against growth inhibition. Similarly, CdiA-CT^{Nlact} is toxic when intracellularly expressed, and $CdiI^{YPIII}$ and $CdiI^{Pasy}$ do not protect against growth inhibition (Figure 11B). $CdiI_{o11}^{EC869}$ was not included in this assay, as overexpression of this immunity protein in the absence of any CdiA-CT domain is toxic to cells (data not shown). Because the active site of these toxins is highly conserved, we mutated the residues corresponding to the aspartic acid at position 198 that has been shown to be essential for activity of CdiA-CT_{o11}^{EC869}. Mutating the corresponding aspartic acid residues in CdiA-CT^{YPIII} and CdiA-CT^{Nlact} resulted in attenuation of inhibitory activity when expressed intracellularly (Figure 11C and D), indicating that the structural conservation at the active site is important for the activity of these toxins.

To determine whether intracellular expression of these homolog toxins results in the same filamentous phenotype associated with inhibition by CdiA-CT_{o11}^{EC869}, we transformed cells

with the pCH450::*cdiA-CT*^{YPIII} plasmid and the indicated pTrc99A *cdiI* constructs and grew the cells in liquid culture, removing an aliquot for microscopy at the indicated timepoints. With induction, cells filament and lose DAPI staining (Figure 12, left panels, 5 h). This activity is blocked by co-expression of CdiI^{YPIII}. CdiI^{Nlact}, CdiI^{Pasy}, and CdiI^{Ykris} were unable to fully block the filamentation and DNase activity conferred by CdiA-CT^{YPIII} (Figure 12, middle 4 panels). The Asp198Ala mutation that prevented *in vitro* DNA degradation also did not support intracellular activity (Figure 12, right panels). Therefore, the filamentation observed with inhibition by CDI$_{o11}^{EC869}$ is a phenotypic response that is induced by other related toxins.

6. β-augmentation is required for toxin/immunity protein complex formation

The β-augmentation interactions observed in the two toxin/immunity protein complexes suggest that the proteins bind using a lock-and-key mechanism. Therefore, we sought to crystallize and solve the structures of isolated toxins and immunity proteins to determine if the proteins undergo any conformational changes upon complex formation. Neither of the isolated toxin domains formed crystals, but we were able to crystallize and solve the 1.8 Å structure of an isolated immunity protein (CdiI^{Ykris}) encoded by the Ykris_10740 locus of *Yersinia kristensenii* ATCC 33638 (Table 1). CdiI^{Ykris} shares 68.9% and 51.5% sequence identity with CdiI$_{o11}^{EC869}$ and CdiI^{YPIII} (respectively) (Figure 1C), and its structure superimposes onto CdiI$_{o11}^{EC869}$ and CdiI^{YPIII} with RMSD of 0.626 and 0.984 Å over all α-carbons (respectively) (Figure 14). In addition, structural homology searches identified yet another immunity protein homolog (CdiI^{NMB}) encoded by the NMB0488 locus in *Neisseria meningitidis* MC58 (PDB: 2GKP). CdiI^{NMB} superimposes onto each of the other immunity proteins with RMSD values < 0.7 Å over all α-carbons (Figure 14). Collectively, these

structures indicate that $CdiI_{o11}^{EC869}$ homologues retain the same β-hairpin binding pocket architecture in the absence of bound toxin. This finding suggests that β-hairpins are modular, raising the possibility that interaction specificity could be altered by exchanging β4/β5 (β-hairpin) sequences between toxins.

To test whether β-augmentation is required for stable complex formation, we replaced the CdiA-CT_{o11}^{EC869} β-hairpin (residues Lys242 – Thr252) with a Gly-Ser-Gly peptide linker to generate CdiA-CT_{o11}^{EC869}/Δβ4β5 (Figure 15A). Wild-type CdiA-CT_{o11}^{EC869} binds to its cognate immunity protein with nanomolar affinity and co-purifies with His6-tagged $CdiI_{o11}^{EC869}$ during Ni^{2+}-affinity chromatography (Figure 15B). In contrast, CdiA-CT_{o11}^{EC869}/Δβ4β5 did not co-purify with His6-tagged $CdiI_{o11}^{EC869}$ (Figure 15B), suggesting the mutant domain has lower affinity for the immunity protein. We purified CdiA-CT_{o11}^{EC869}/Δβ4β5 to homogeneity by anion-exchange chromatography and measured its affinity for $CdiI_{o11}^{EC869}$-His6 using biolayer interferometry. However, no binding interaction was detected, indicating that the dissociation constant is > 300 μM. To test whether deletion of the β-hairpin disrupts toxin structure, we examined the CdiA-CT_{o11}^{EC869}/Δβ4β5 domain using circular dichroism (CD) spectroscopy. This analysis revealed that CdiA-CT_{o11}^{EC869}/Δβ4β5 has essentially the same secondary structure content as the wild-type domain (Figure 15C). Taken together, these results demonstrate that the CdiA-CT_{o11}^{EC869} β-hairpin is critical for complex formation. Moreover, despite the very low affinity of CdiI to CdiA-CT_{o11}^{EC869}/Δβ4β5, a high level of expression of CdiA-CT_{o11}^{EC869}/Δβ4β5 was observed (Figure 15B) together with healthy cell growth, suggesting that the β-hairpin is also required for toxic DNase activity. This was confirmed by testing *in vitro* DNase activity in the presence of supercoiled plasmid DNA and Zn2 +, which showed that the CdiA-

CT_{o11}^{EC869}/Δβ4β5 domain had no observable DNase activity (data not shown).

We next asked whether CdiI binding specificity can be altered by grafting heterologous β-hairpins onto the CdiA-CT_{o11}^{EC869} toxin. Using a catalytically inactive version of CdiA-CT_{o11}^{EC869} that contains an Asp198Ala mutation in the active site, we replaced residues Lys242 – Glu250 with the corresponding sequences from homologous toxins from *Y. kristensenii* ATCC 33638 (CdiA-CT^{Ykris} encoded by ykris0001_10730) and *Neisseria lactamica* ATCC 23970 (CdiA-CT^{Nlact} encoded by NEILACOT_05635) (Figure 16A). We co-expressed CdiA-$CT_{o11}^{EC869/Nlact}$ and CdiA-$CT_{o11}^{EC869/Ykris}$ together with His6-tagged $CdiI_{o11}^{EC869}$ and purified the tagged immunity protein by Ni^{2+}-affinity chromatography. Chimeric CdiA-$CT_{o11}^{EC869/Nlact}$ toxin co-purified with His6-tagged $CdiI_{o11}^{EC869}$, but CdiA-$CT_{o11}^{EC869/Ykris}$ eluted in the void volume of the column (Figure 16B). These results suggest that CdiA-$CT_{o11}^{EC869/Nlact}$ binds with relatively high affinity to $CdiI_{o11}^{EC869}$, whereas the CdiA-$CT_{o11}^{EC869/Ykris}$ toxin does not. We first confirmed that each chimeric toxin was folded properly using CD spectroscopy (Figure 16C), then measured binding affinities for $CdiI_{o11}^{EC869}$ using biolayer interferometry. CdiA-$CT_{o11}^{EC869/Nlact}$ and CdiA-$CT_{o11}^{EC869/Ykris}$ bound to $CdiI_{o11}^{EC869}$ with dissociation constants of 180 ± 100 nM and 46 ± 36 μM, respectively (Table 3), consistent with the co-purification data. The difference in affinities of *the N. lactamica* and *Y. kristensenii* chimeric toxins for the $CdiI_{o11}^{EC869}$ immunity protein is in part due to the differences in electrostatic and shape complementarity (Figure 17). The *N. lactamica* and EC869 β-hairpins share similar electrostatics and shape (Figure 17A and B), allowing CdiA-$CT_{o11}^{EC869/Nlact}$ to retain nanomolar affinity for $CdiI_{o11}^{EC869}$ (Table 3). In contrast, the *Y. kristensenii* β-hairpin has a different shape and altered electrostatics compared with CdiA-CT_{o11}^{EC869}, which results in low micromolar affinity of chimeric CdiA-

$CT_{o11}^{EC869/Ykris}$ toxin for $CdiI_{o11}^{EC869}$ (Figures 14 and 17). We then tested whether the grafted β-hairpins confer higher affinity for $CdiI^{Nlact}$ and $CdiI^{Ykris}$ immunity proteins. The CdiA-$CT_{o11}^{EC869/Ykris}$ chimera bound to $CdiI^{Ykris}$ with about the same affinity as $CdiI_{o11}^{EC869}$, but somewhat surprisingly this domain bound to $CdiI^{Nlact}$ with ~10-fold higher affinity (Table 3). The CdiA-$CT_{o11}^{EC869/Nlact}$ domain bound to $CdiI^{Nlact}$ with essentially the same affinity as for $CdiI_{o11}^{EC869}$ and interacted with $CdiI^{Ykris}$ with approximately 10-fold lower affinity (Table 3).

7. Structure of the MAC/$CdiI_{o11}^{EC869}$ complex

In principle, molecules that disrupt CdiA-CT/CdiI complexes should liberate the toxin domain and induce CDI^{+} bacteria to undergo auto-inhibition. Nowick and coworkers have previously developed macrocyclic peptides containing δ-linked ornithine turn units that adopt a β-hairpin conformation and should be suitable to disrupting the CdiA-CT/CdiI complex(354, 355). To test the feasibility of this strategy, we designed a macrocyclic peptide (MAC) that mimics the β-hairpin of CdiA-CT_{o11}^{EC869}. The MAC peptide contains residues corresponding to Lys242 – Ser253 of CdiA-CT_{o11}^{EC869}, which were connected through a δ-linked ornithine residue (Figure 18). Biolayer interferometry experiments failed to detect a binding interaction between MAC and $CdiI_{o11}^{EC869}$; and the MAC peptide was unable to promote DNase activity when added in ~103-fold molar excess to the CdiA-CT/$CdiI_{o11}^{EC869}$ complex *in vitro* (data not shown). Despite its low affinity for $CdiI_{o11}^{EC869}$, we were able to crystallize the MAC peptide in complex with the immunity protein and solve the structure to 2.0 Å resolution by molecular replacement (Figure 19A). As anticipated, the MAC peptide forms a two-stranded β-sheet, though there are only four cross-strand H-bonds compared to the five in the CdiA-CT/$CdiI_{o11}^{EC869}$ complex. The ornithine turn creates a bulge that prevents formation of the fifth H-bond (Figure 19B). The MAC/$CdiI_{o11}^{EC869}$

structure superimposes well with $CdiI_{o11}^{EC869}$ (RMSD of 0.437 Å over all α-carbons), though helix α3* is displaced 3.0 Å to create a slightly altered β-hairpin binding pocket (Figure 19B). Five MAC peptide side-chains form H-bonds or ion-pair interactions with the immunity protein, in contrast to the six direct interactions observed in the CdiA-CT/$CdiI_{o11}^{EC869}$ complex. In the CdiA-CT/$CdiI_{o11}^{EC869}$ complex, β-hairpin residue Ser247 interacts with the immunity protein. However, the corresponding Ser7 residue within the MAC peptide does not interact with $CdiI_{o11}^{EC869}$ (Figure 19C). Additionally, the side-chain conformation of MAC residue Arg10 is altered compared to that of Arg249 in the CdiA-CT/$CdiI_{o11}^{EC869}$ structure, resulting in a H-bond interaction with the hydroxyl of Ser80 rather than the backbone carbonyl of Phe75 in the toxin/immunity structure. The MAC/$CdiI_{o11}^{EC869}$ structure establishes that structure-based designed macrocyclic peptides can bind in the $CdiI_{o11}^{EC869}$ β-hairpin binding pocket (Figure 19D), forming contacts that mimic those found in the CdiA-CT/CdiI complexes.

C. Discussion

CDI toxin/immunity protein pairs are diverse and comprise more than 100 distinct families. Even within a given family, there is considerable sequence variability suggesting that toxin/immunity protein families continue to evolve. This phenomenon is well-illustrated by homologues of the CdiA-CT/$CdiI_{o11}^{EC869}$ toxin/immunity protein pair. Alignment of 26 closely related toxin domains from this family reveals that nearly all of the secondary-structure elements are highly conserved (Figure 5A). The obvious exception is the β4/β5-hairpin, which mediates the β-augmentation interaction and is the least-conserved element in the family. Loop L1 of the toxin domain is responsible for all other contacts with the immunity protein; in contrast to the β-hairpin, this region is well-conserved with five

invariant residues (Arg189, Leu190, Pro19, Phe194 and Asp198). Although loop L1 is highly conserved, it interacts with immunity proteins using distinct contacts in the CdiA-CT/CdiI$_{o11}^{EC869}$ and CdiA-CT/CdiI^{YPIII} complexes. Loop L1 of CdiA-CT$_{o11}^{EC869}$ engages almost exclusively in hydrophobic and van der Waals interactions, whereas the C-terminal portion of the CdiA-CT^{YPIII} loop is dominated by direct H-bond and ion-pair interactions involving residues Asp201, Ala203 and Thr204. The differences are striking because these three residues are also present in CdiA-CT$_{o11}^{EC869}$, yet do not form the same interactions. Similar phenomena are observed for the immunity proteins. CdiI strand β3* anneals with the toxin's variable β5 strand during β-augmentation; accordingly, β3* varies between immunity proteins in the family (Figure 5B). CdiI strands β7*, β8*, β9*, and the intervening loops are highly conserved, yet this region interacts with cognate toxins using distinct molecular contacts. In several instances, highly conserved residues engage in direct H-bonds in one complex, but fail to make any intermolecular contact in another closely related complex. Therefore, even conserved sequence elements can be exploited to discriminate against near-cognate partners. The idiosyncratic nature of these interactions most likely explains why immunity-binding specificity cannot be switched through a simple exchange of β4/β5-hairpins between homologous toxins.

The divergence of toxin/immunity protein interactions was first recognized and characterized in a subset of E-class colicins. Colicins are diffusible protein toxins released by some strains of *E. coli* to kill other competing bacteria (23). Though colicins and CdiA proteins are not related, there are several features common to both competition systems. One striking parallel is the variability of C-terminal toxin domains. The eight characterized E-class colicins share nearly identical N-terminal domains, but their C-terminal nuclease

domains are distinct with either DNase (E2, E7, E8 and E9), ribosomal RNase (E3, E4 and E6), or tRNase (E5) activities (23). Like CdiA proteins, colicins are always encoded in tandem with a specific immunity protein that binds the nuclease domain and blocks its activity. Colicins E2, E7, E8 and E9 carry homologous DNase domains, yet their respective immunity proteins do not protect against near-cognate toxins (63, 356). Structure-function analyses show that E-class immunity proteins bind to a contiguous stretch of ~30 residues that are highly variable between the different nuclease domains (71, 72, 357). Similarly, the interaction surfaces on the immunity proteins are also variable, but contain a conserved core interaction comprised of Tyr54 and Tyr55 (ImmE9 annotation) (71, 78). This invariant core provides significant binding energy, and near-cognate colicin toxin/immunity protein interactions often have dissociation constants of 10^{-8} M (358), which are similar in affinity to the cognate CdiA-CT/CdiI complexes studied here. An analogous core interaction centered at the tip of the β-hairpin is found in the CdiA-CT/$CdiI_{o11}^{EC869}$ toxin/immunity family. Leu246 of the toxin engages in a hydrophobic interaction with an aliphatic residue in the immunity protein (Ala131 in $CdiI_{o11}^{EC869}$ and Val141 in $CdiI^{YPIII}$). Similarly, toxin residue Ser247 interacts with a Tyr residue (Tyr84 in $CdiI_{o11}^{EC869}$ and Tyr94 in $CdiI^{YPIII}$) that is invariant in the immunity protein family (Figure 5B). However, these core interactions do not provide significant binding affinity for near-cognate toxin/immunity pairs. A final important parallel between the colicin E-class and CdiA-CT_{o11}^{EC869} DNases is that the immunity proteins both bind to exosites, leaving the nuclease active site exposed in the toxin/immunity complex (23, 177). The spatial segregation of substrate and immunity binding sites presumably provides the flexibility to evolve unique protein-protein interactions while retaining catalytic activity. The fact that two unrelated DNase toxin/immunity pairs

appear to be diverging rapidly suggests that this is a general and perhaps universal feature of toxin/immunity systems.

Protein-protein interactions presumably evolve through mutational drift followed by reciprocal changes in the binding partner to maintain overall affinity while the underlying molecular contacts change. Riley and colleagues have proposed a diversification-selection model to explain the observed diversity in E-class colicin/immunity protein pairs. According to their model, some mutations expand immunity function and allow the newly evolved immunity protein to not only protect against its cognate toxin, but also against the colicins released by other strains (39, 212). Such mutations would appear to be rare, but have been identified and characterized experimentally (359, 360). One striking example that supports this model is the Asp33Leu mutation in ImmE2 immunity protein, which increases affinity for non-cognate colicin E9 more than a 3,000-fold (360). The advantage conferred by the new immunity gene would provide the selective pressure to retain the allele and allow it to become fixed in the population. This in turn allows for subsequent mutations in the linked colicin gene. Further mutations in the colicin are predicted to produce "super-killer" toxins, to which the ancestral bacteria are not immune (212). Thus, the evolved colicin/immunity pair kills ancestral cells, thereby allowing fixation of the new pair in the population. Multiple iterations of this process are predicted to eventually produce a family of divergent toxin/immunity pairs. Of course, mutations that disrupt the toxin/immunity protein complex should be lethal to the cell, so the pressure to retain high-affinity interactions is presumably a significant barrier to diversification. However, colicin/immunity protein complexes have some of the highest known binding affinities, with cognate pairs characterized by femtomolar dissociation constants (357, 358, 360, 361). Therefore, even if a mutation results in a 1000-

fold decrease in affinity, the complex will still have a sub-nanomolar dissociation constant, which is sufficient to provide complete protection against toxicity (358, 361). Thus, the extraordinarily high affinity of cognate colicin/immunity protein complexes provides a buffer against the potentially lethal effects of mutations that disrupt the toxin/immunity protein interface. In contrast, the CDI toxin/immunity proteins studied here have much lower binding affinities with dissociation constants of about 20 nM for cognate pairs. Therefore, CDI toxin/immunity systems must exploit other biophysical mechanisms to avoid self-intoxication during evolution. One possible mechanism involves the over-expression of immunity proteins relative to the toxins. The majority (21 of 25) of CdiA-CT_{o11}^{EC869} homologues presented in Figure 5A are encoded by truncated *cdiA* gene fragments that lack the N-terminal coding sequences required for secretion. These pseudogene pairs are termed "orphan" modules, because they resemble *cdiA-CT*/*cdiI* coding sequences that have been displaced from full-length *cdiA* genes (176). Orphan *cdiA-CT* reading frames usually lack translation initiation signals, whereas the linked orphan *cdiI* genes have canonical ribosome-binding sites upstream of the initiating Met codon. These observations suggest that the toxins are expressed at very low levels, but the immunity proteins are highly expressed. Under these conditions, the selective pressure to retain immunity function would be relieved and allow the immunity gene to undergo drift without lethal consequences. This hypothetical scenario is supported by the observation that non-cognate/mutated immunity proteins can fully protect cells when over-expressed (358, 362). Therefore, we propose that the organization of *cdiA-CT*/*cdiI* gene pairs into orphan modules serves to accelerate toxin/immunity evolution by attenuating toxin expression. We note that this could be a general strategy to generate diversity in inter-bacterial competition systems because similar

clusters of orphan gene pairs are associated with *rhs* genes in type VI secretion systems(176, 230) and the *mafB* genes of *Neisseria* species (211).

CDI systems are widespread throughout proteobacteria and are most commonly found in pathogenic species, such as *Yersinia pestis*, *Neisseria meningitides*, and *Burkholderia pseudomallei* (167, 213). Because CDI^+ bacteria exchange CdiA-CT toxins with one another, it may be possible to induce bacterial suicide with small molecules that specifically disrupt CDI toxin/immunity protein binding interactions. The β-hairpin binding pocket within $CdiI_{o11}^{EC869}$ and homologous immunity proteins is an attractive target to test this antimicrobial strategy. Small cyclic peptides that fold into β-hairpins have been used to study protein-protein and protein-DNA interactions and in some instances have been used to specifically disrupt protein complexes (363, 364). As illustrated by the MAC/$CdiI_{o11}^{EC869}$ structure, cyclic β-hairpin mimics can be designed to bind CdiI immunity proteins. Our design could be improved to enhance binding affinity and possibly be utilized as a protein-protein complex inhibitor by increasing the number of residues or designing additional contacts. Although the current MAC contains pentapeptide strands, we have previously reported cyclic β-hairpin mimics containing heptapeptide and nonapeptide β-strands (365, 366). Homologous MACs containing larger β-hairpin mimics and designed to achieve more contacts may allow rational design of a higher affinity macrocyclic peptide that specifically may disrupt toxin/immunity complexes within bacterial pathogens, setting the stage for the development of a new class of antibacterials.

D. Materials and methods

1. Bacterial strains and plasmid constructs

All bacterial strains and plasmids used in this study are presented in Table S2. All

primers used in this study are presented in Table S3. Yellow fluorescent protein (YFP)-labeled *E. coli* EPI100 cells were generated by integrating the *yfp* coding sequence at the *gal* locus. First, a genomic integration construct was made by amplifying the kanamycin-resistance cassette from plasmid pKAN(367) with primers Kan-1/Kan-2, followed by blunt-end ligation to SmaI-digested plasmid pBluescript. One plasmid clone was identified with the kanamycin-resistance cassette in the opposite orientation as pKAN, and this plasmid was termed pNAK. A fragment of *galM* was then amplified using primers CH3789/CH3790, and the product was ligated to SacI/BamHI-digested plasmid pNAK to produce pCH2500. A *yfp-galT* fragment was amplified from *E. coli* DA28100 (a gift from Sanna Koskiniemi, Uppsala University) using primers CH3787/CH3788, digested with KpnI/EcoRI, then ligated into pCH2500 to yield plasmid pCH2503. The large KpnI/SacI fragment from pCH2503 was recombined into *E. coli* EPI100 cells that harbor plasmid pSIM6 as previously described(291, 368). mKate2-labeled target bacteria were generated by integrating the coding sequence of mKate2 at the phage HK022 *attP* site using plasmids pDE1013 and pAH69 as described previously(369).

The coding sequence for CdiA-CT/CdiI^{YPIII} was amplified from *Y. pseudotuberculosis* YPIII genomic DNA with primers YPK0575-Kpn-for/YPK0576-Xho-rev. The resulting product was digested with KpnI/XhoI and ligated to pET21S to generate plasmid pCH10413. The CdiA-CT$_{o11}^{EC869}$/Δβ4β5 expression construct was generated by replacing the β4/β5-hairpin coding sequence with a Gly-Ser linker. The 5´-end of the construct was amplified with primers β-deletion-for1/β-deletion-rev1 and the 3´-end with primers β-deletion-for2/β-deletion-rev2. The two PCR fragments were ligated at the BamHI site, and the joined fragments re-amplified with β-deletion-for1/β-deletion-rev2. The resulting product was

ligated to pET21d using NcoI and XhoI restriction sites to generate pCH10369. Catalytically-inactive CdiA-CT_{o11}^{EC869} domains carrying the Asp198Ala mutation and heterologous β-hairpin sequences were generated by PCR. Plasmid pCH10164 was amplified with primers EC869-CT-Nco/EC869-Nlact(beta)-rev and EC869-Nlact(beta)-for/EC869-cdiI-Spe, and the two products combined by overlap extension PCR (OE-PCR)(370) using primers EC869-CT-Nco/EC869-cdiI-Spe. The final product was digested with NcoI/SpeI and ligated to pET21S to generate plasmid pCH10365. The same procedure was used to introduce the *Y. kristensenii* β-hairpin by PCR with primers EC869-CT-Nco/EC869-Ykris(beta)-rev and EC869-Ykris(beta)-for/EC869-cdiI-Spe. The two products were combined by OE-PCR and ligated to pET21S to generate plasmid pCH10175. The coding sequences for $CdiI^{Ykris}$ (ykris0001_10740) and $CdiI^{Nlact}$ (NEILACOT_05636) were chemically synthesized (Genscript, Inc.) with flanking restriction sites and ligated to plasmid pUC57. The ykris0001_10740 sequence was sub-cloned into pTrc99KX to generate plasmid pCH10103, which was then used as a template for PCR with primers pTrc-seq2/Ykris-cdiI-Spe-rev. The resulting product was digested with KpnI/SpeI and ligated to pET21K to generate plasmid pCH10170. The NEILACOT_05636 sequence was subcloned into pCH450 to generate plasmid pCH10101, which was then used as a template for PCR with primers pCH450-for/Nlact-cdiI-Spe-rev. The resulting product was digested with NcoI/SpeI and ligated to pET21S to generate plasmid pCH10172.

The chimeric CDI system that deploys CdiA-CT^{YPIII} toxin was generated by replacing the CdiA-CT_{o11}^{EC869} DNase domain with the corresponding region of CdiA-CT^{YPIII}. Regions upstream and downstream of the *cdiA-CT/cdiI*$_{o11}^{EC869}$ sequence were amplified from plasmid pCH9305 using primers DL1527/EC869o11-G173-rev (upstream) and EC93-YPIII-down-

for/DL2368 (downstream). The *cdiA-CT/cdiI*^{YPIII} sequence was amplified from *Y. pseudotuberculosis* YPIII genomic DNA using primers EC869o11-G173-for/EC93-YPIII-chim-rev. The three PCR products were combined by OE-PCR using primers DL1527/DL2368. The final product was electroporated together with plasmid pCH10163 into *E. coli* strain DY378 as described(175, 177). Recombinants were selected on yeast extract/glucose-agar supplemented with 33 μg/mL chloramphenicol and 10 μM D/L-o-chlorophenylalanine. All plasmid constructs were verified by DNA sequence analysis.

2. Protein purification

All proteins were over-produced from pET21-derived plasmid using either *E. coli* CH2016 or *E. coli* BL21-Gold(DE3). Cells were grown aerobically at 37 °C in LB medium containing 150 μg/mL ampicillin. CdiA-CT/CdiI^{YPIII} expression was induced by the addition of 1 mM isopropyl-β-D-thiogalactoside at an OD_{600} ~0.8 and grown for a further 3-4 h before harvesting. Cells were collected by centrifugation at 5,500 × g for 25 min and then washed with resuspension buffer [20 mM sodium phosphate (pH 7.0), 150 mM NaCl]. Cells were resuspended and disrupted by sonication on ice in resuspension buffer containing 10 mg/mL lysozyme and1 mM phenylmethylsulfonyl fluoride. Cell debris was removed by centrifugation at 18,000 × g for 30 min followed by filtration through a 1.0 μm filter. Clarified lysates were loaded onto a Ni^{2+}-charged HiTrap column (5 mL; GE Healthcare) or Ni^{2+}-nitrilotriacetic acid (Ni^{2+}-NTA) agarose resin (MCLAB) and washed with resuspension buffer supplemented with 10 mM imidazole. Proteins were eluted with a linear gradient of imidazole (10 – 500 mM) in resuspension buffer. Fractions were collected, combined, and concentrated to a volume of ~500 μL using a 10-kDa centrifugal concentrator (Centricon; Millipore). Proteins were further purified by gel filtration on a Superdex 200 column for the

CdiA-CT/CdiI^{YPIII} complex or Superdex 75 for individual immunity proteins (GE Healthcare). Gel filtration columns were equilibrated with 20 mM sodium phosphate (pH 7.0), 150 mM NaCl using an AKTA FPLC. Purification of CdiI^{Ykris} and CdiI$_{o11}$^{EC869} followed the same protocol, except all buffers contained 20 mM Tris-HCl (pH 7.4) instead of sodium phosphate. CdiA-CT/CdiI^{YPIII}, CdiI^{Ykris}, and CdiI$_{o11}$^{EC869} were concentrated to 10, 12.5 and 7.5 mg/mL (respectively) for crystallization trials.

The individual His6-tagged CdiI proteins were over-produced from plasmid pET21d constructs and purified as described above for CdiI$_{o11}$^{EC869}. CdiA-CT proteins were isolated from co-expressed His6-tagged CdiI proteins by two methods, depending on whether the two proteins co-eluted following Ni^{2+}-affinity chromatography. CdiA-CT/CdiI-His6 complexes were denatured overnight in 6 M urea and then subjected to Ni^{2+}-affinity chromatography in buffers containing 6 M urea. Denatured CdiA-CT toxins were collected from the void volume, refolded by dialysis into 20 mM Tris-HCl (pH 8.0), 10 mM NaCl, then concentrated on a HiTrap Q anion-exchange column and eluted with a salt gradient, yielding 95% pure CdiA-CT protein. Purified toxins were then exchanged into 20 mM Tris-HCl (pH 7.4), 150 mM NaCl by gel filtration on a S75 column.

3. Crystallization and structure determination

Protein crystals were grown by hanging-drop vapor diffusion, with drops containing a 1:1 ratio (vol/vol) of protein solution to reservoir liquor. Crystals were mounted and collected under cryo-conditions with the addition of 40% glycerol as cryoprotectant to the reservoir solution. Datasets were collected at 70K at a wavelength of 1.0 Å and images were indexed, integrated and reduced using either iMOSFLM (CdiA-CT/CdiI^{YPIII} complex)(371) or the HKL2000 suite (CdiI^{Ykris} and MAC/CdiI$_{o11}$^{EC869})(372). Initial phases were determined by

molecular replacement by autoMR in PHENIX using the CdiA-CT/CdiI$_{o11}^{EC869}$ structure (PDB: 4G6U) as a search model. Initial model building was performed by Autobuild in PHENIX. The final models were built through iterative manual building in Coot and refined with phenix.refine. Data collection and refinement statistics are presented in Table 1. All molecular graphics were prepared with PyMOL(373).

CdiA-CT/CdiI^{YPIII} crystals were grown from a 10 mg/mL solution and a reservoir containing 50 mM HEPES (pH 7.0), 20% PEG 3350, 1% tryptone. The complex crystallized in space group C2 with unit cell dimensions 65.51 Å × 65.51 Å × 71.49 Å and one complex per asymmetric unit. The model contains residues Met174 – Lys297 (numbered from Val1 of the VENN motif) of CdiA-CT^{YPIII} and residues Asp3 – Lys176 of CdiI^{YPIII}. CdiA-CT^{YPIII} residues Lys182, Lys220, Lys240 and Lys297 were modeled as Ala due to lack of observable side-chain density. Similarly, CdiI^{YPIII} residues Asp3, Lys108, Lys118, Lys148 and Lys176 were modeled as Ala residues. The final CdiA-CT/CdiI^{YPIII} model includes 148 water molecules resulting in an Rwork/Rfree (%) of 20.5/25.6 (Table 1). CdiI^{Ykris} immunity protein crystals were grown from a 12.5 mg/mL solution over a reservoir containing 0.2 M ammonium fluoride, 20% PEG 3350. The crystal space group was P31 with unit cell dimensions 54.448 Å × 54.448 Å × 54.472 Å and one molecule per asymmetric unit. The final model contains CdiI^{Ykris} residues Met1 – Gly165 and 130 water molecules resulting in an Rwork/Rfree (%) of 18.1/22.1. CdiI^{Ykris} residues Lys4, Glu67, Lys96, Lys126 and Lys136 were modeled as Ala due to lack of observable side-chain density. In addition, the CdiI^{Ykris}-His6 expression construct contained an Ala84Thr mutation.

The macrocyclic peptide (MAC) that mimics the CdiA-CT$_{o11}^{EC869}$ β-hairpin (Figures 18 and 19) was prepared according to previously described procedures(354, 374, 375). MAC

peptide (2 mg) was added to 200 μL of 7.5 mg/mL $CdiI_{o11}^{EC869}$ to yield a solution at a ~ 10:1 peptide:protein ratio. MAC/$CdiI_{o11}^{EC869}$ co-crystals were grown over two days in 0.2 M sodium acetate (pH 5.6), 0.1 M bis-tris propane, pH 6.9, and 20% (wt/vol) PEG 3350, using the protein/peptide mixture described. Initial crystals were of poor quality and resulted in highly mosaic diffraction data. Crystal quality was improved by microseeding(376). Briefly, crystals were harvested into 80 μL of crystallization solution and a seed stock was generated using a seed bead (Hampton). Following optimization, suitable diffraction quality crystals were generated using a hanging drop containing 1 μL of seed stock and 1 μL of the protein/peptide mixture following a three-fold dilution. The MAC/$CdiI_{o11}^{EC869}$ complex crystallized in space group P21 with unit cell dimensions 34.776 Å × 128.166 Å × 44.953 Å (Table 1). Each asymmetric unit contained two MAC/$CdiI_{o11}^{EC869}$ complexes. The final model contains two molecules of $CdiI_{o11}^{EC869}$ residues Ala2 – Gly167, two macrocyclic peptides and 132 water molecules, resulting in Rwork/Rfree (%) of 18.4/23.1. Residues Lys5, Gln43, Glu78, Lys85, Glu93 of one $CdiI_{o11}^{EC869}$ molecule (chain D only), Asp117 and Glu139 of both $CdiI_{o11}^{EC869}$ molecules were modeled as Ala due to lack of observable side-chain density.

4. Protein analyses

The secondary structure of purified toxins (0.1 mg/mL in 20 mM Tris-HCl, pH 7.4) was analyzed by CD spectroscopy on a Jasco J-720 spectropolarimeter using a 0.1 cm path-length. Spectra were collected at 20 nm/min with a 2 nm bandwidth and 4 s response time. Three consecutive scans were collected and averaged for each analysis. CdiA-CT/CdiI binding affinities were determined by biolayer interferometry as described previously [7]. Binding reactions were performed at 25 °C in 20 mM Tris-HCl (pH 7.4), 150 mM NaCl.

CdiI-His6 immunity proteins were immobilized onto Ni^{2+}-NTA biosensors and exposed to cognate or heterologous CdiA-CT toxins at 0.5 – 300 μM. A reference was subtracted from all binding curves before curve fitting. Curve fitting and data processing were performed using BLitz Pro software (ForteBio Inc.).

5. In vitro *analysis of nuclease activities*

The activity of purified CdiA-CT_{o11}^{EC869} and CdiA-CT^{YPIII} were assayed *in vitro* using supercoiled plasmid pUC18 as a substrate. CdiA-CT (at 1 μM final concentration) was incubated with 250 ng of plasmid DNA in 20 mM Tris-HCl (pH 7.5), 100 mM NaCl, 0.1 mg/mL bovine serum albumin supplemented with 2 mM $MgCl_2$ or $ZnCl_2$ for 1 h at 37 °C. Where indicated, purified CdiI-His6 proteins were included at 2 μM final concentration and allowed to bind CdiA-CT for 30 min at room temperature prior to adding substrate DNA. Reactions were quenched with 10 mM EDTA followed by the addition of 300 μL of denaturing solution (4 M guanidine-HCl, 33% 2-propanol). The reactions were purified over silica membrane spin columns (Epoch Life Sciences). Columns were then washed with 70% ethanol, 10 mM Tris-HCl (pH 8.0) followed by elution with 10 mM Tris-HCl (pH 8.0). Purified DNA from reactions was run on 1% agarose gels containing ethidium bromide and visualized using Bio-Rad Gel Doc 2000.

6. Competition co-cultures and fluorescence microscopy

Inhibitor cells (*E. coli* EPI100 carrying plasmids pCH9305, pCH2409 or pDAL878) and target cells (CH8251 carrying plasmids pTrc99a, pCH9315 or pCH848) were grown individually in LB media with 33 μg/μL Cm for inhibitors and 150 μg/μL Amp for targets. The overnight cultures were diluted into fresh LB medium without antibiotics and grown in baffled flasks at 37 °C. At mid-log phase, the inhibitor and target strains were mixed

together at a 1:1 ratio in baffled flasks and a sample was withdrawn to score viable target cells as colony forming units (cfu) per mL on LB-agar supplemented with 200 μg/mL rifampicin (Rif). After four hours of co-culture, another sample was taken and viable target cells enumerated on Rif-supplemented LB agar. Viable target cell counts are the mean cfu/mL ± the standard error of the mean for three independent experiments. Competitions with fluorescent inhibitor and target bacteria were conducted as described above, except YFP-labeled inhibitor CH2550 cells and mKate2-labeled targets cells were used. Cells were diluted into fresh LB medium and grown to late log phase at 30 °C in the dark to maximize fluorescence. Inhibitor and target cells were mixed at a 1:1 ratio in baffled flasks and incubated at 37 °C with shaking in the dark for the duration of the experiment. Samples (equivalent to OD600 = 0.2) were removed at the indicated times and cells were collected by centrifugation. Cells were briefly resuspended in freshly prepared 4% formaldehyde in 1 × phosphate buffered saline (PBS), and the fixation reaction quenched with 125 mM glycine. Fixed cells were washed with 1 × PBS and spotted onto a poly-D-lysine coated slide (Gold Seal Fluorescent Antibody Rite-On Slides from Fisher prepared by coating with a 1% poly-D-lysine solution prior to addition of cells). Unbound cells were removed gently with Nanopure water, and the slides treated with Fluorogel II with DAPI mounting medium (Fisher Scientific/EMS) and a coverslip was overlaid prior to imaging. Images were acquired on an Olympus fluorescent microscope with a 100 × oil objective using an Optronics MacroFire digital microscope camera. Lightfield images were captured with a 12 ms exposure (gain 2) and DAPI images were acquired in grayscale with a 48 ms exposure (gain 2). Fluorescent images were captured in grayscale using a 502 ms exposure/gain 5 (for YFP) or a 1 s exposure/gain 5 (for mKate2). Images were overlaid and false-colored using

FIJI(292), and stacked images were cropped to 400 × 400 pixels using GIMP. The same microscope images used to display fluorescence were used to obtain cell length measurements. Cells were manually measured using the line tool in FIJI, and between 175 and 328 cells from three microscopy fields were measured for each co-culture competition. Each object plotted represents a single cell length measurement. *P* values were obtained using two-tailed unpaired t-tests.

E. Accession numbers

Coordinates and structure factors have been deposited in the Protein Data Bank with accession numbers 4ZQU, 4ZQV and 4ZQW.

F. Acknowledgements

This research was supported by the National Institutes of Health (GM102318 to C.S.H. and C.W.G); and the National Science Foundation (CHE-1058825 to J.S.N. and DGE-1144085 to J.L.E.W.). Structure determination was, in part, supported by the Advanced Light Source (U.S. Department of Energy under Contract No. DE-AC02-05CH11231) at Berkeley National Laboratories, and The Stanford Synchrotron Radiation Lightsource (supported in part by National Institutes of Health P41 GM103393 and U.S. Department of Energy DE-AC02-76SF00515). Funding for open access charge came from the National Institutes of Health. We would like to thank the staff at ALS and SSRL for their invaluable help in data collection. We would also like to thank Elias Gerrick and Sonya Donato for technical support. The funders had no role in study design, data collection and analysis, decision to publish, or preparation of the manuscript.

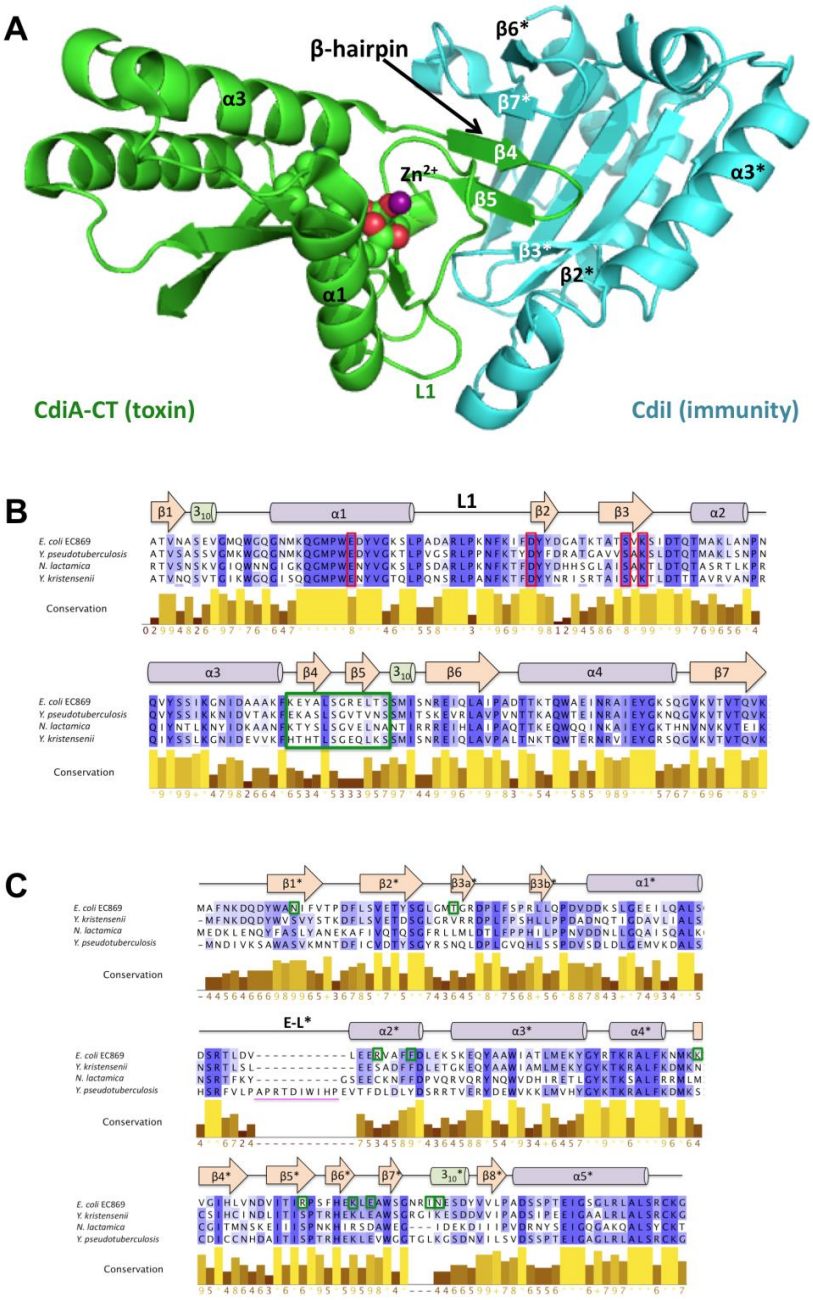

Figure 1. Structure of the CdiA-CT/CdiI$_{o11}^{EC869}$ complex and alignments of toxin and immunity homologues. (B) Cartoon representation of the CdiA-CT/CdiI$_{o11}^{EC869}$ complex structure (PDB ID: 4G6U) with the toxin and immunity colored green and cyan, respectively. Toxin active-site residues are rendered in space-filling model and the Zn^{2+} ion is represented by a purple sphere. (B) Protein sequence alignment of the CdiA-CT$_{o11}^{EC869}$ nuclease domain and its homologues. Active-site residues are outlined in red boxes, and the β4/β5-hairpin is outlined in a green box. (C) Protein sequence alignment of the CdiI$_{o11}^{EC869}$ immunity protein and its homologues. Residues that form H-bond or ion-pair interactions with CdiA-CT$_{o11}^{EC869}$ are marked with green boxes. The location of CdiI^{YPIII} elongated loop (E-L*) is indicated with a magenta bar. For (B) and (C), alignments were prepared using Jalview, with progressively darker shades of blue indicating greater residue conservation. The secondary-structure elements shown are from the CdiA-CT/CdiI$_{o11}^{EC869}$ complex structure.

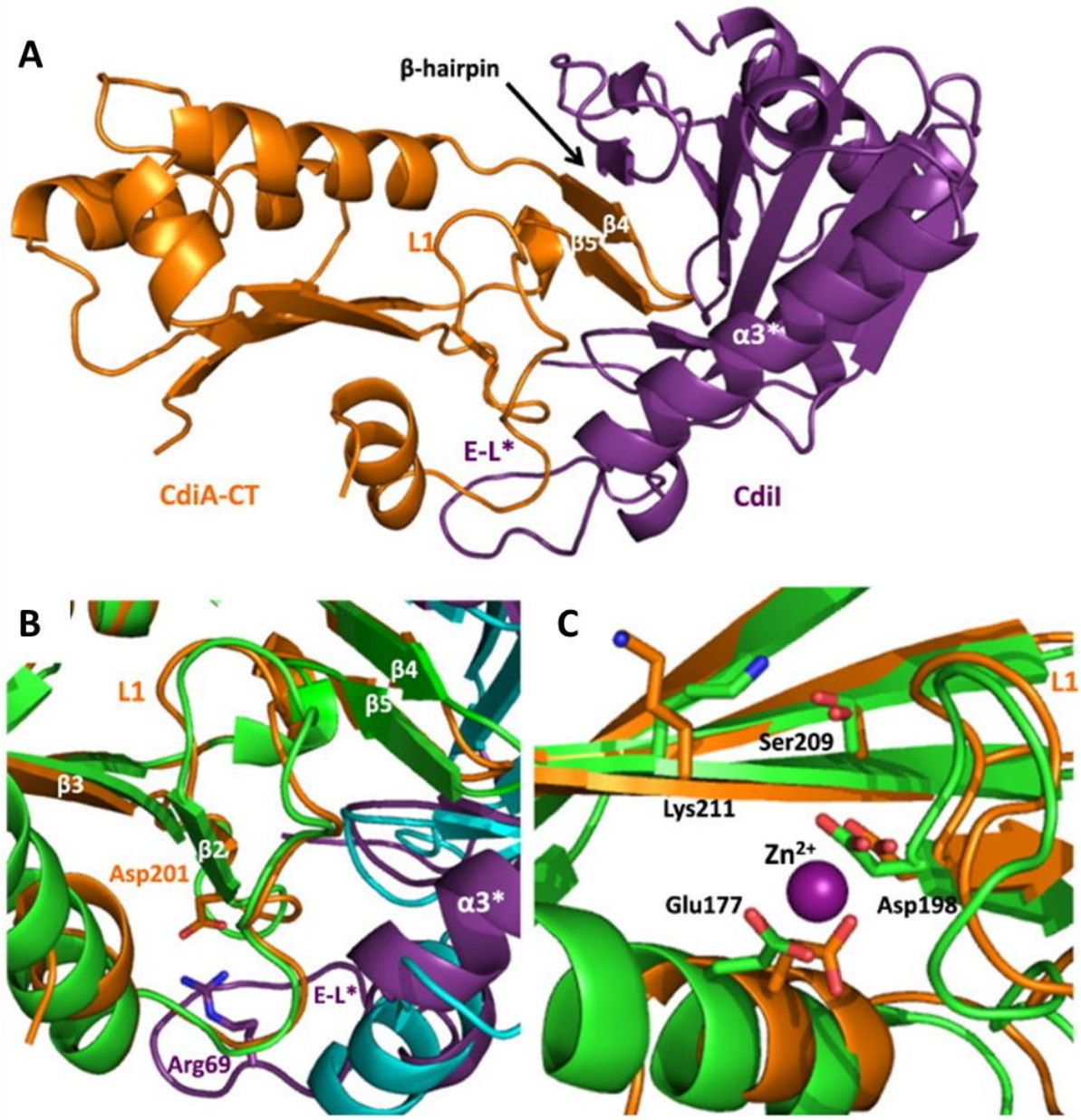

Figure 2. The structure of the CdiA-CT/CdiI^{YPIII} complex. (A) Ribbon representation of the CdiA-CT/CdiI^{YPIII} complex with toxin and immunity proteins colored orange and purple, respectively. Location of the CdiA-CT^{YPIII} β4/β5-hairpin is indicated. (B) Structural superimposition of the β-hairpin binding regions of CdiA-CT/CdiI$_{o11}^{EC869}$ and CdiA-CT/CdiI^{YPIII}. CdiA-CT$_{o11}^{EC869}$ and CdiI$_{o11}^{EC869}$ are colored green and cyan, respectively. CdiA-CT^{YPIII} residues that form a salt-bridge via loop L1 are depicted as sticks. (C) Predicted active-site residues of CdiA-CT$_{o11}^{EC869}$ (carbons in green) and CdiA-CT^{YPIII} (carbons in orange). Oxygen and nitrogen atoms are colored red and blue, respectively. Residue labels correspond to both toxins. The Zn^{2+} ion was observed in the CdiA-CT$_{o11}^{EC869}$ structure and is shown as a purple sphere. Extended loop (E-L*) of CdiI^{YPIII} is labeled in (A) and (B).

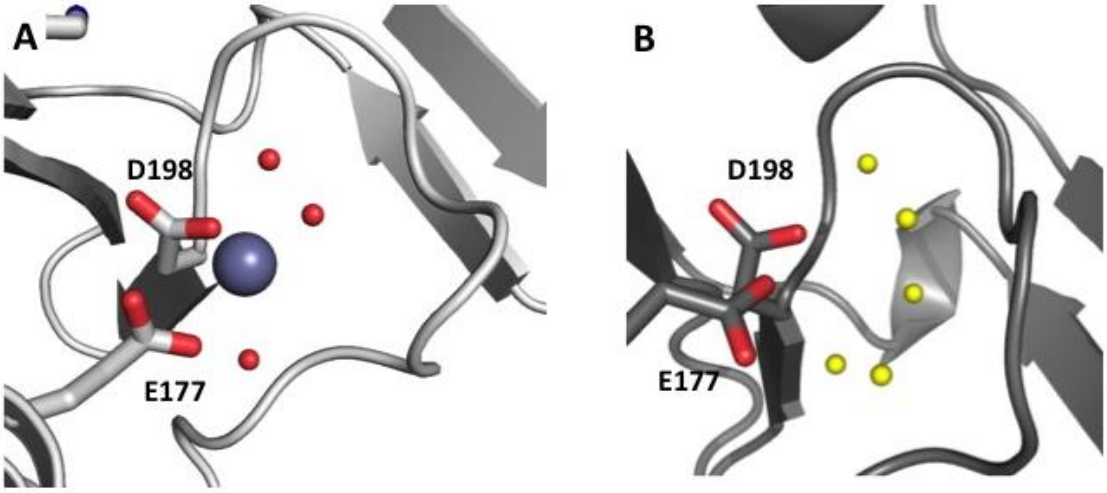

Figure 3. Comparison of CdiA-CT catalytic sites. In both panels EC869 and YPIII carbon atoms are depicted in white and grey, respectively, and oxygen and nitrogen atoms are colored red and blue, respectively. (**A**) CdiA-CT_{o11}^{EC869} active site contains a Zn^{2+} ion, depicted by at purple sphere with water molecules depicted as smaller red spheres, and interacting bons with Zn^{2+} are depicted as black dotted lines. (**B**) CdiA-CT^{YPIII} active site has no extra density that would create a zinc coordination sphere. Water molecules are depicted as yellow spheres.

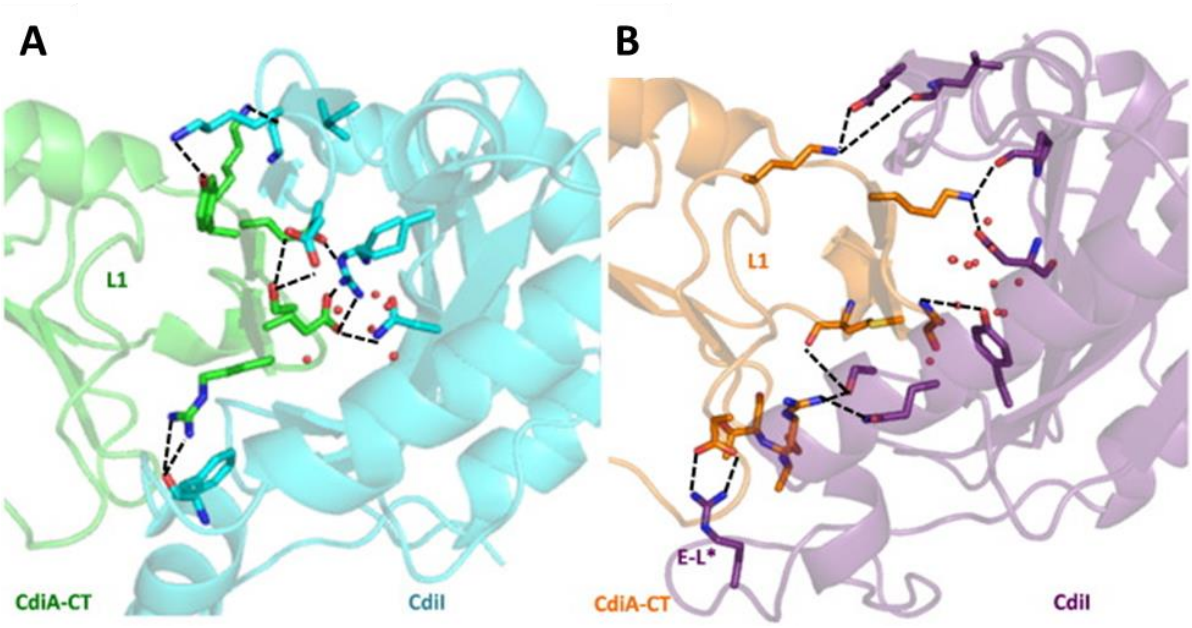

Figure 4. Comparison of the β-augmentation interactions. (A) Ribbon representation of the CdiA-CT/CdiI$_{o11}^{EC869}$ complex with toxin and immunity proteins are colored green and cyan, respectively. Residues at the complex interface involved in direct ion pair or H-bond interactions are shown in stick representation, with carbon atoms colored as stated for above: oxygen and nitrogen atoms are colored red and blue, respectively. Water molecules at the interface are represented as red spheres. (B) Ribbon representation of the CdiA-CT/CdiI^{YPIII} complex with toxin and immunity proteins colored orange and purple, respectively. Residues and water molecules represented and colored as in (A).

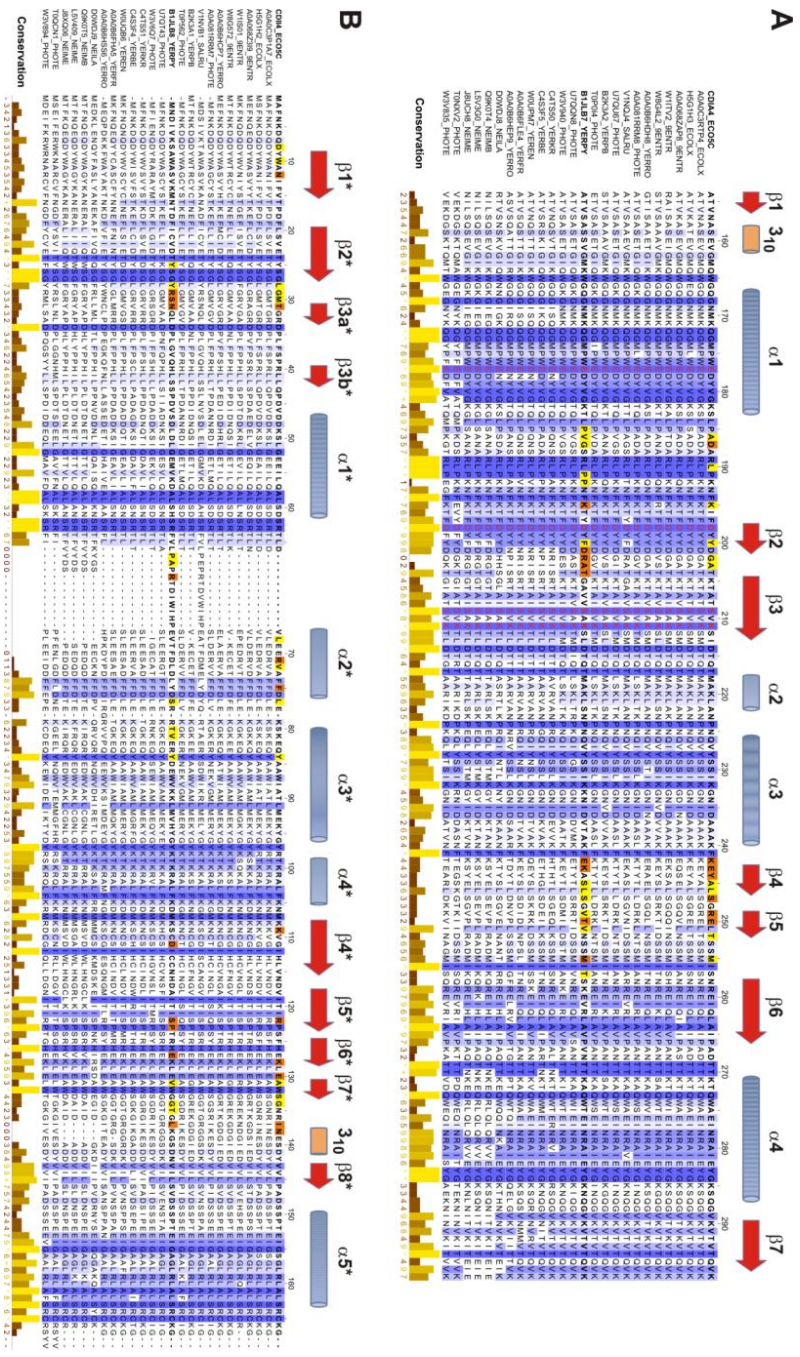

Figure 5. **Alignments of CdiA-CT/CdiI$_{o11}^{EC869}$ family members.** (**A**) Alignment of DNase toxin domain homologues. Residue are numbered according to the CdiA-CT$_{o11}^{EC869}$ sequence beginning with Val1 of the VENN peptide motif. The alignment was rendered with Jalview at 30% sequence identity with progressively darker shades of purple indicating greater residue conservation. Secondary structure elements correspond to CdiA-CT$_{o11}^{EC869}$. CdiA-CT$_{o11}^{EC869}$ and CdiA-CT^{YPIII} residues that form H-bonds/ion-pairs with cognate immunity proteins are shown in orange, and residues that form hydrophobic/van der Waals contacts are shown in blue. (**B**) Alignment of immunity protein homologues. Residue numbers and secondary structure elements correspond to CdiI$_{o11}^{EC869}$. Residues that interact with toxins are color coded according the scheme described for panel **A**.

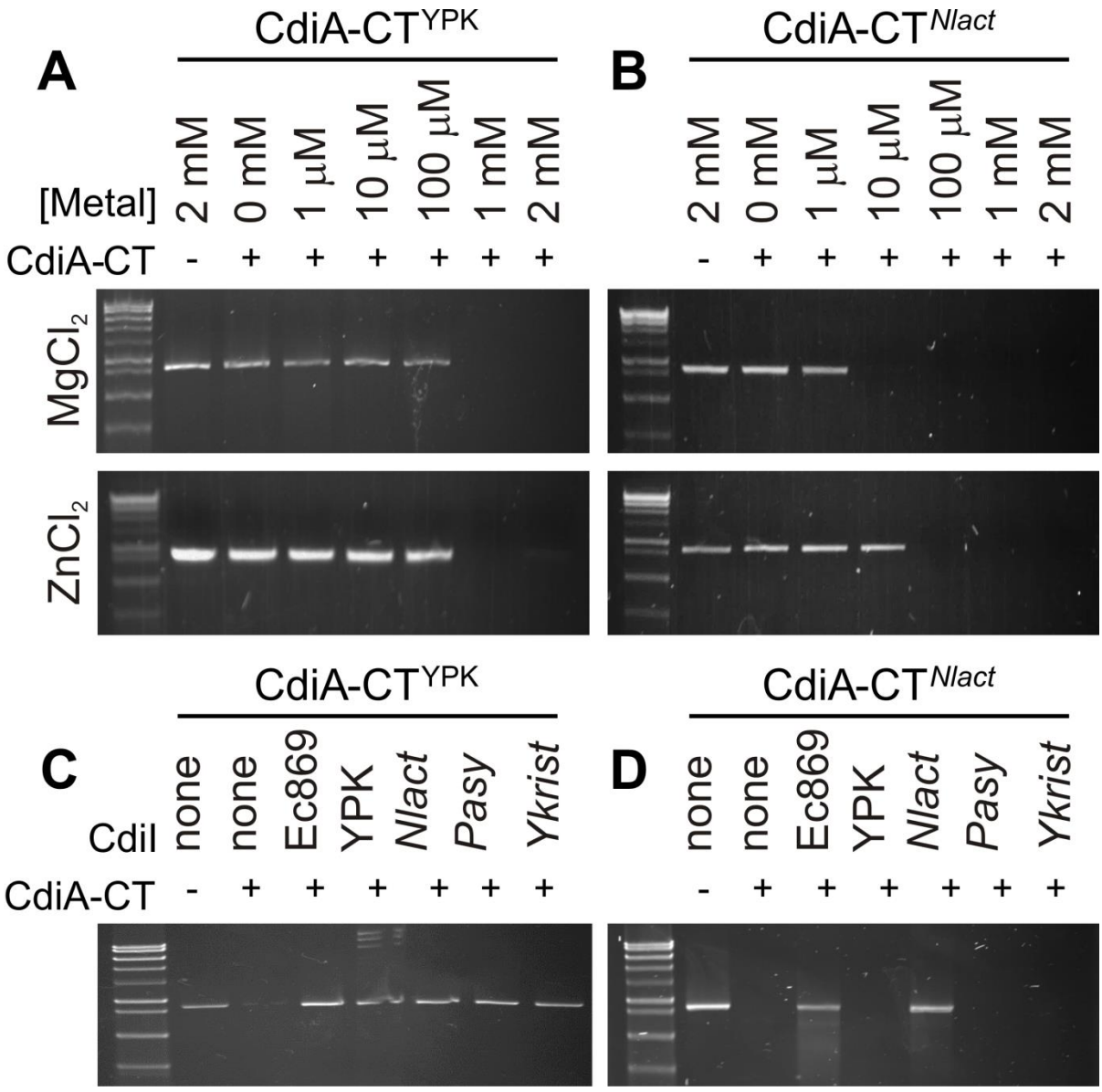

Figure 6. CdiA-CT^{YPIII} has DNase activity *in vitro*. Linearized plasmid DNA was incubated with purified (A) CdiA-CT^{YPK} or (B) CdiA-CT^{Nlact} in the presence of either Mg^{2+} or Zn^{2+} and then analyzed by agarose gel electrophoresis and ethidium bromide staining. (C) and (D) Reactions were supplemented CdiI immunity proteins where indicated. Untreated linearized plasmid substrate was included as controls for the migration of undigested DNA.

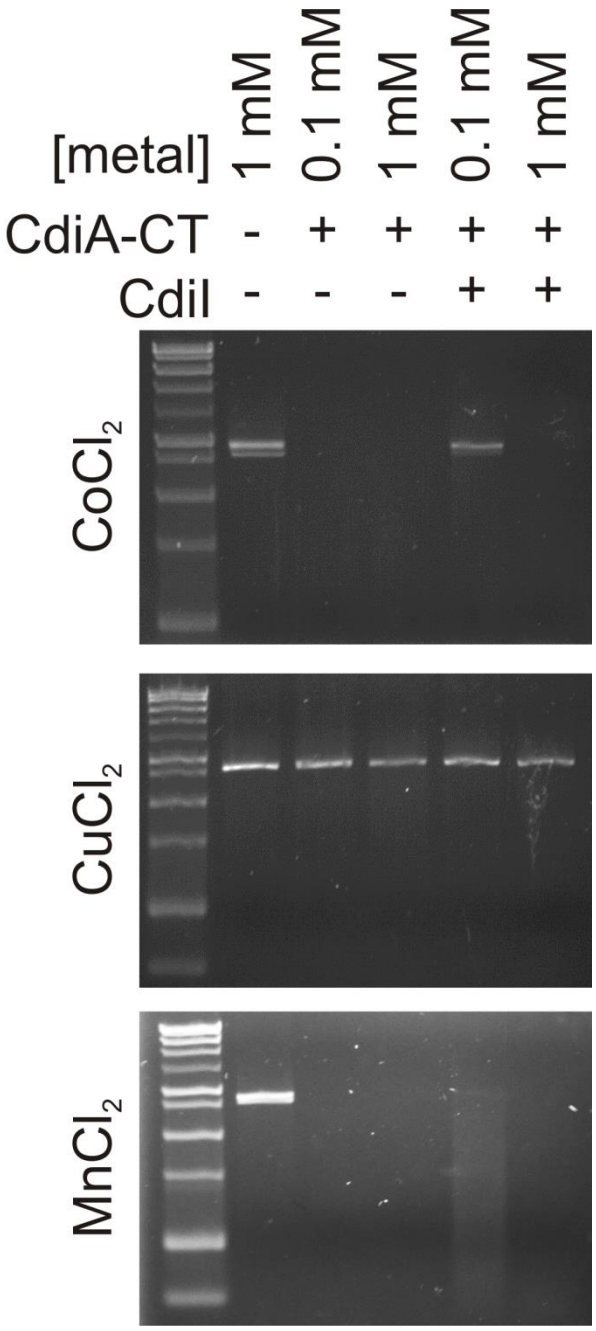

Figure 7. CdiA-CT^{Nlact} can utilize other metals as co-factors for DNase activity. Linearized plasmid DNA was incubated with purified CdiA-CT^{Nlact} in the presence of the indicated metals and then analyzed by agarose gel electrophoresis and ethidium bromide staining. Reactions were supplemented CdiI immunity proteins where indicated. Untreated linearized plasmid substrate was included as controls for the migration of undigested DNA.

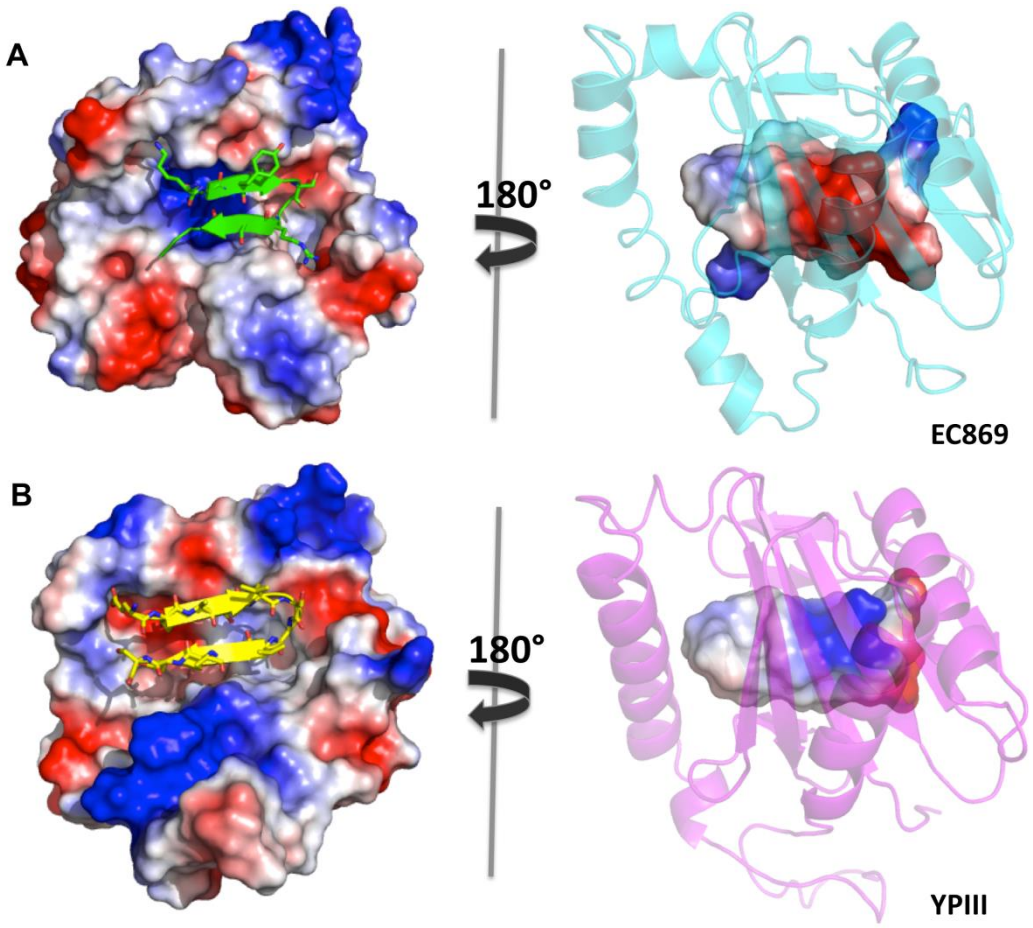

Figure 8. **Electrostatic surfaces of CdiA-CT/CdiI$_{o11}^{EC869}$ and CdiA-CT/CdiI^{YPIII} complexes.** Electrostatic surface representation of CdiI$_{o11}^{EC869}$ (**A**) and CdiI^{YPIII} (**B**). Red and blue surfaces correspond to positive and negative surface potentials (respectively) and white indicates hydrophobic surfaces. Toxin β-hairpins are show in stick representation in the left panels. Right panels are rotated 180° around the y-axis with respect to the left panels and the immunity proteins are shown in cartoon representation.

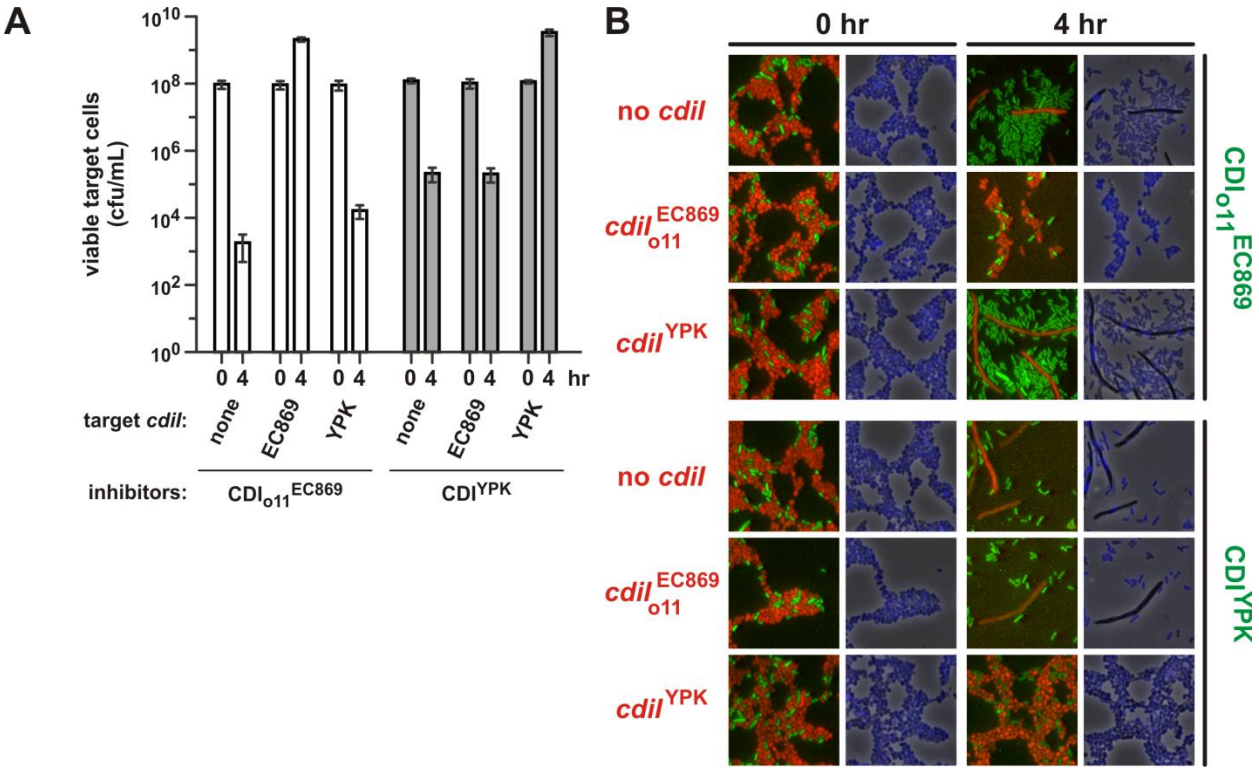

Figure 9. CdiI$_{o11}^{EC869}$ and CdiI^{YPIII} confer specific immunity to CDI. (A) Competition co-cultures. Inhibitors cells that deploy CdiA-CT$_{o11}^{EC869}$ (from pCH9305) or CdiA-CT^{YPIII} (from pCH2409) were incubated at a 1:1 ratio with target cells that express CdiI$_{o11}^{EC869}$ (from pCH9315), CdiI^{YPIII} (from pCH848) or no immunity at all (none, pTrc99a vector). Viable target cells were quantified as colony-forming units (c.f.u.) per milliliter at the beginning of the co-culture and after 4 h. Data represent the average ± standard error of the mean for three independent experiments. (B) Fluorescence microscopy of competition co-cultures. YFP-labeled inhibitor cells were co-cultured with mKate2-labeled target strains that carry the indicated immunity genes. Cells were stained with DAPI to visualize genomic DNA at 0 and 4 h of co-culture.

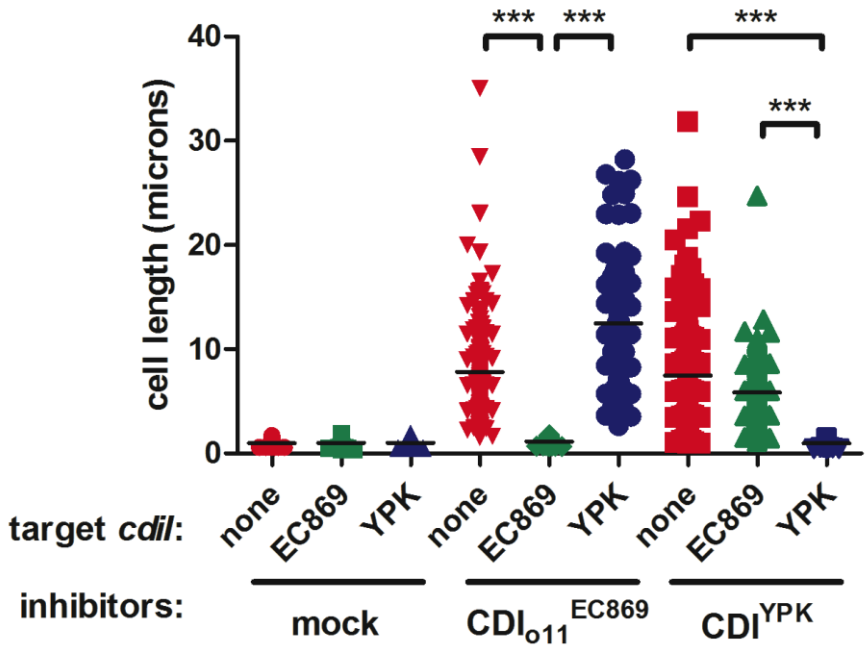

Figure 10. Target cells become filamentous after inhibition by the CDI_{o11}^{EC869} and CDI^{YKris} systems. Co-culture competitions were performed using mock inhibitors or inhibitor cells deploying the CDI_{o11}^{EC869} and CDI^{YPIII} systems and target cells carrying an empty vector (none) or a plasmid expressing $CdiI_{o11}^{EC869}$ or $CdiI^{YPIII}$. Cell length values were measured from microscopy images taken of each competition. Each object plotted represents the length of a single cell. Black bars indicate the mean of each data set. *P* values from two-tailed unpaired t-tests are reported. ***, *P*=<0.0001.

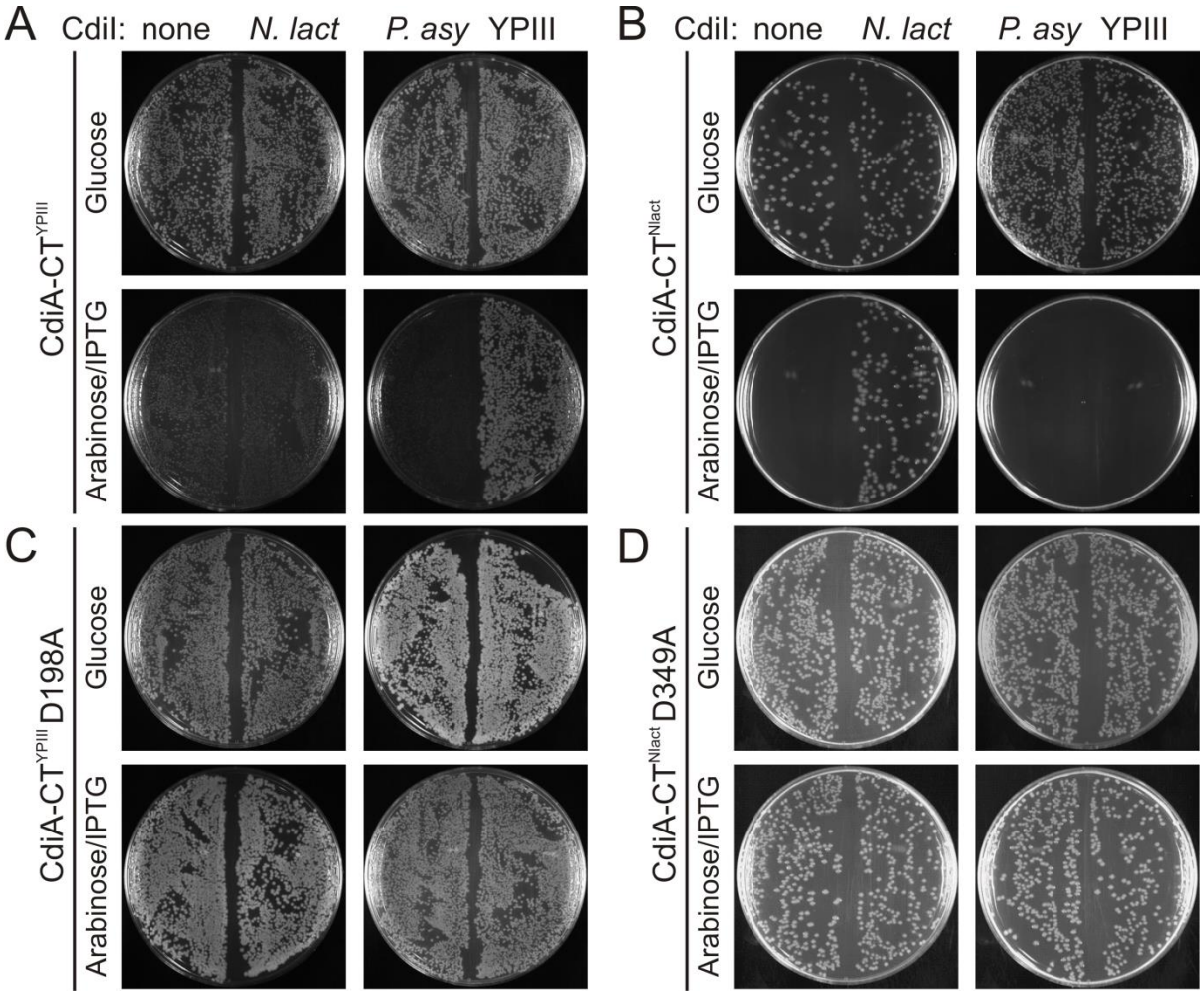

Figure 11. CdiA-CT^{YPIII} and CdiA-CT^{Nlact} are toxic when expressed intracellularly. Plasmids expressing either (A) active CdiA-CT^{YPIII}, (B) active CdiA-CT^{Nlact}, or inactive point mutations (corresponding to the CdiA-CT$_{o11}^{EC869}$ residue D198) were co-transformed into *E. coli* X90 cells with empty pTrc99a or pTrc99a derivatives carrying the indicated immunity gene. Transformants were selected on LB-tetracycline-ampicillin-agar plates supplemented with either glucose or arabinose and IPTG as indicated.

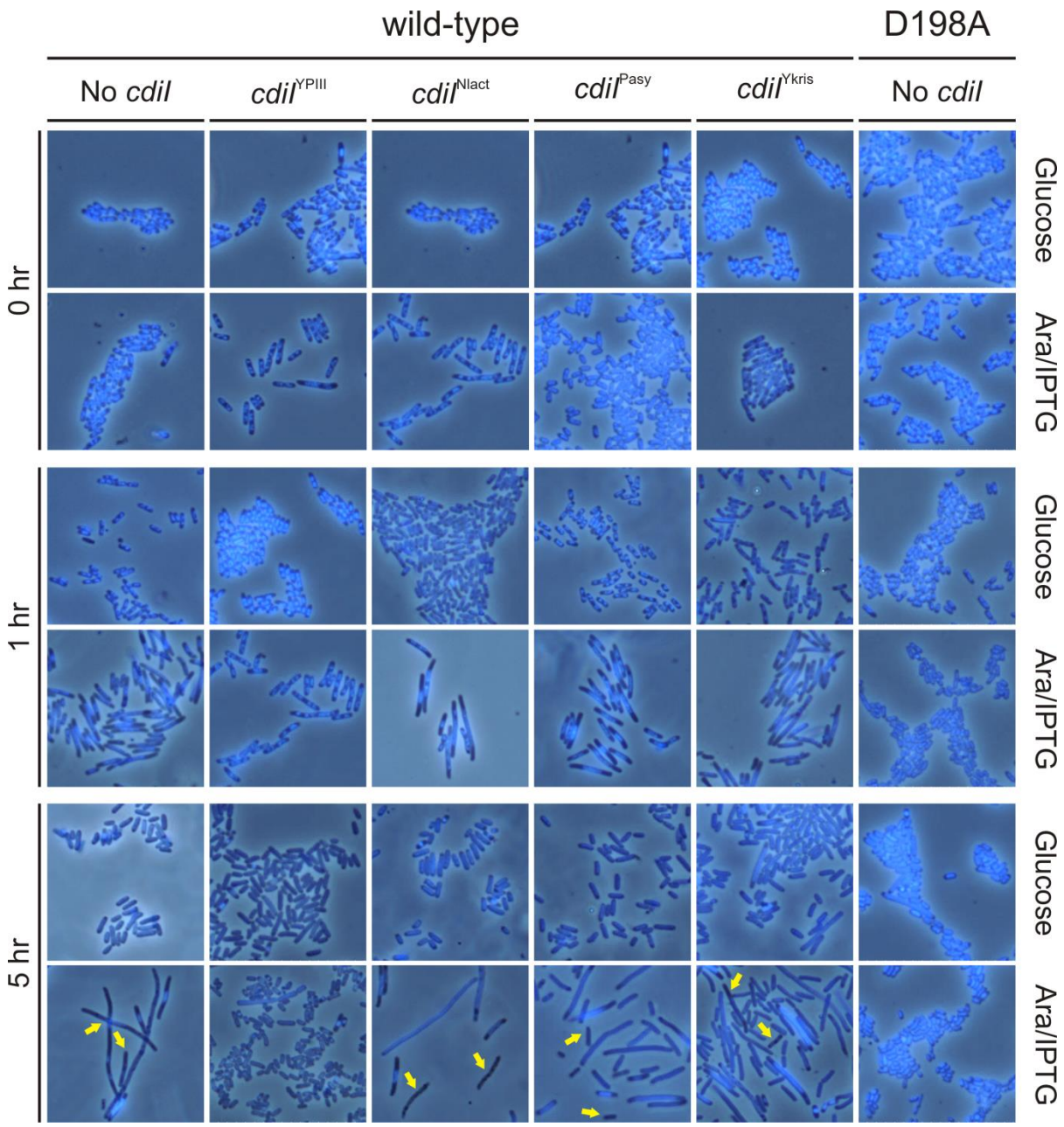

Figure 12. CdiA-CT^{YPIII} causes cell filamentation and loss of DNA staining when expressed intracellularly.

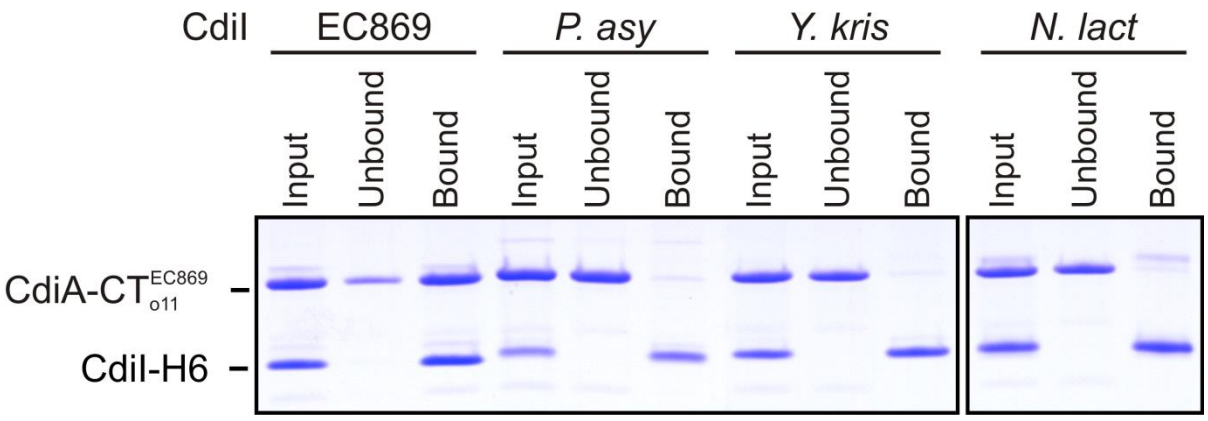

Figure 13. CdiA-CT$_{o11}^{EC869}$ does not strongly interact with non-cognate immunity proteins *in vitro*. Purified CdiA-CT$_{o11}^{EC869}$ was mixed with purified His6-CdiI proteins and subjected to pulldown using Ni-NTA beads. Input, unbound, and bound (eluted) fractions were analyzed via SDS-PAGE and Coomassie staining.

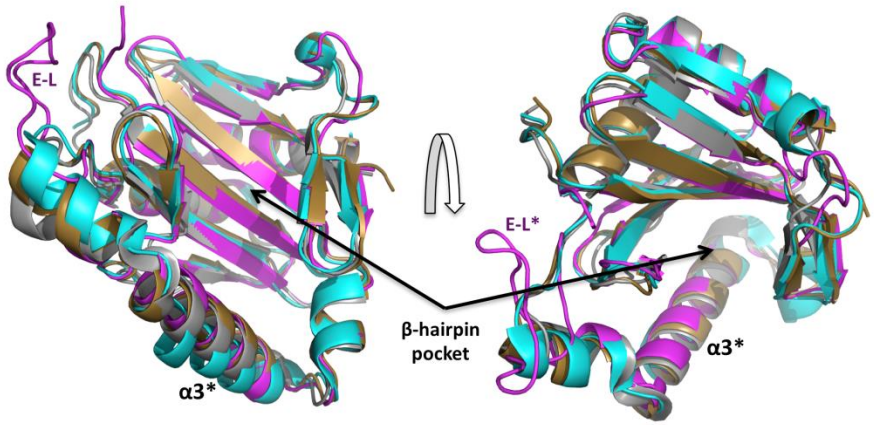

Figure 14. **Superimposition of immunity protein homologues**. The CdiI^{YPIII}, CdiI$_{o11}^{EC869}$, CdiI^{Ykris} and CdiI^{Nmen} immunity proteins are depicted in cartoon representations colored in magenta, cyan, gold and gray, respectively. The structures of CdiI^{Nmen} (PDB ID: 2GKP) and CdiI^{Ykris} were determined in the absence of bound toxin. The location of the β-hairpin binding pocket is indicated and the extended loop (E-L) connecting α1* to α2* of CdiI^{YPIII} is labeled.

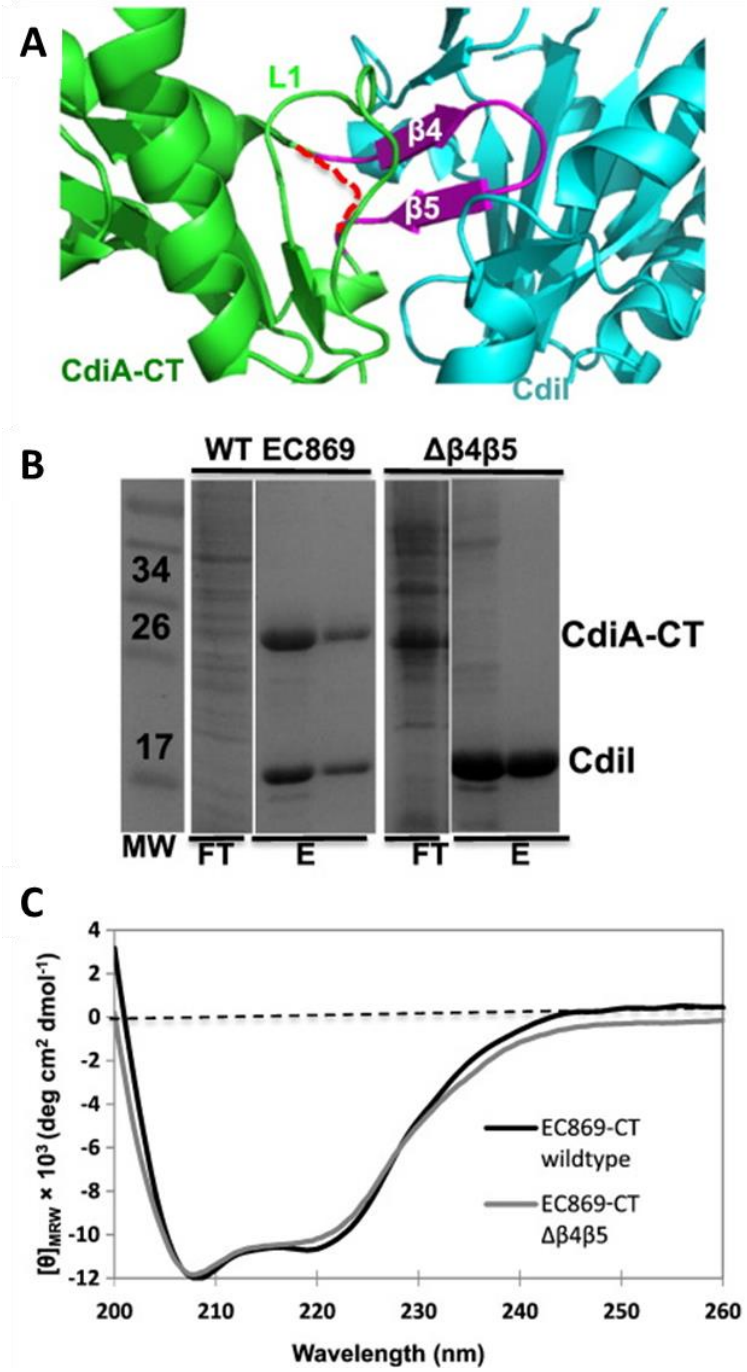

Figure 15. Deletion of the CdiA-CT$_{o11}^{EC869}$ β-hairpin disrupts complex formation. (A) Ribbon representation of the CdiA-CT/CdiI$_{o11}^{EC869}$ complex interface. CdiA-CT$_{o11}^{EC869}$, CdiI$_{o11}^{EC869}$ and the β-hairpin colored green, cyan and olive, respectively. The Gly-Ser-Gly linker in CdiA-CT$_{o11}^{EC869/Δβ4β5}$ is depicted as a red broken line. (B) His$_6$-tagged CdiI$_{o11}^{EC869}$ was co-expressed with CdiA-CT$_{o11}^{EC869}$ or CdiA-CT$_{o11}^{EC869/Δβ4β5}$, followed by purification via Ni^{2+}-affinity chromatography and then analysis by SDS/PAGE gel. Relevant molecular weight standards are labeled. The flow-through (FT), wash (W) and elution fractions (E) are indicated. (C) CD spectra of purified CdiA-CT$_{o11}^{EC869}$ and CdiA-CT$_{o11}^{EC869/Δβ4β5}$.

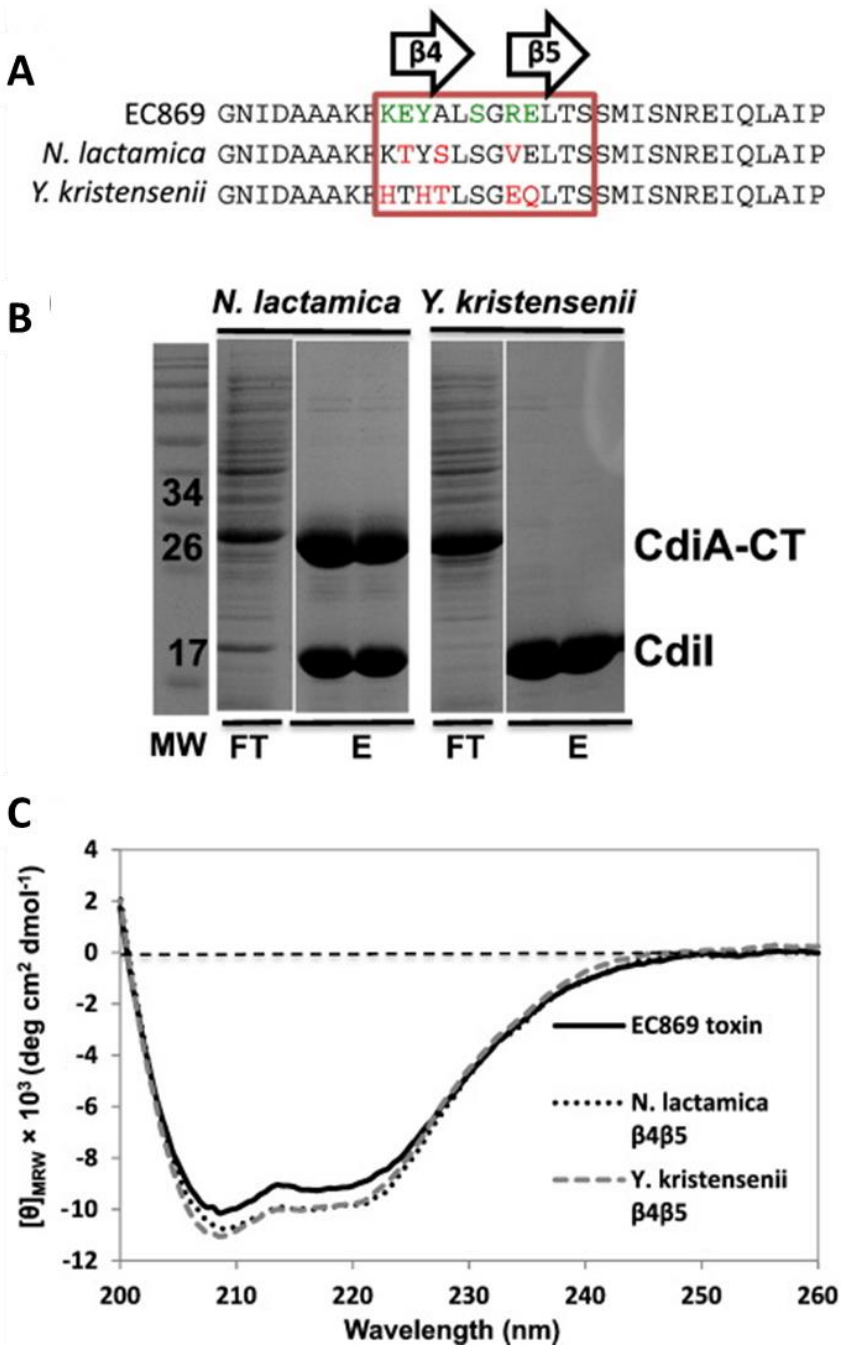

Figure 16. Toxin β-hairpin sequence contributes to complex binding affinity. (A) Protein sequence alignment of the β-hairpin region (boxed) of CdiA-CT_{o11}^{EC869}, CdiA-CT^{Nlact} and CdiA-CT^{Ykris}. CdiA-CT_{o11}^{EC869} residues that interact with $CdiI_{o11}^{EC869}$ are shown in green. Red residues indicate sequence differences with respect to CdiA-CT_{o11}^{EC869}. (B) $CdiI_{o11}^{EC869}$-His_6 was co-expressed with CdiA-CT_{o11}^{EC869} containing the β-hairpins from either *N. lactamica* or *Y. kristensenii* then purified by Ni^{2+}-affinity chromatography and analyzed by SDS-PAGE. The molecular mass standards are indicated in kilodaltons (kDa). The flow-though (FT) and wash fractions (W1 and W2) are indicated followed by elution with imidazole gradient. (C) CD spectra of purified CdiA-$CT_{o11}^{EC869/Nlact}$ and CdiA-$CT_{o11}^{EC869/Ykris}$ show similar secondary-structure content compared to wild-type CdiA-CT_{o11}^{EC869}.

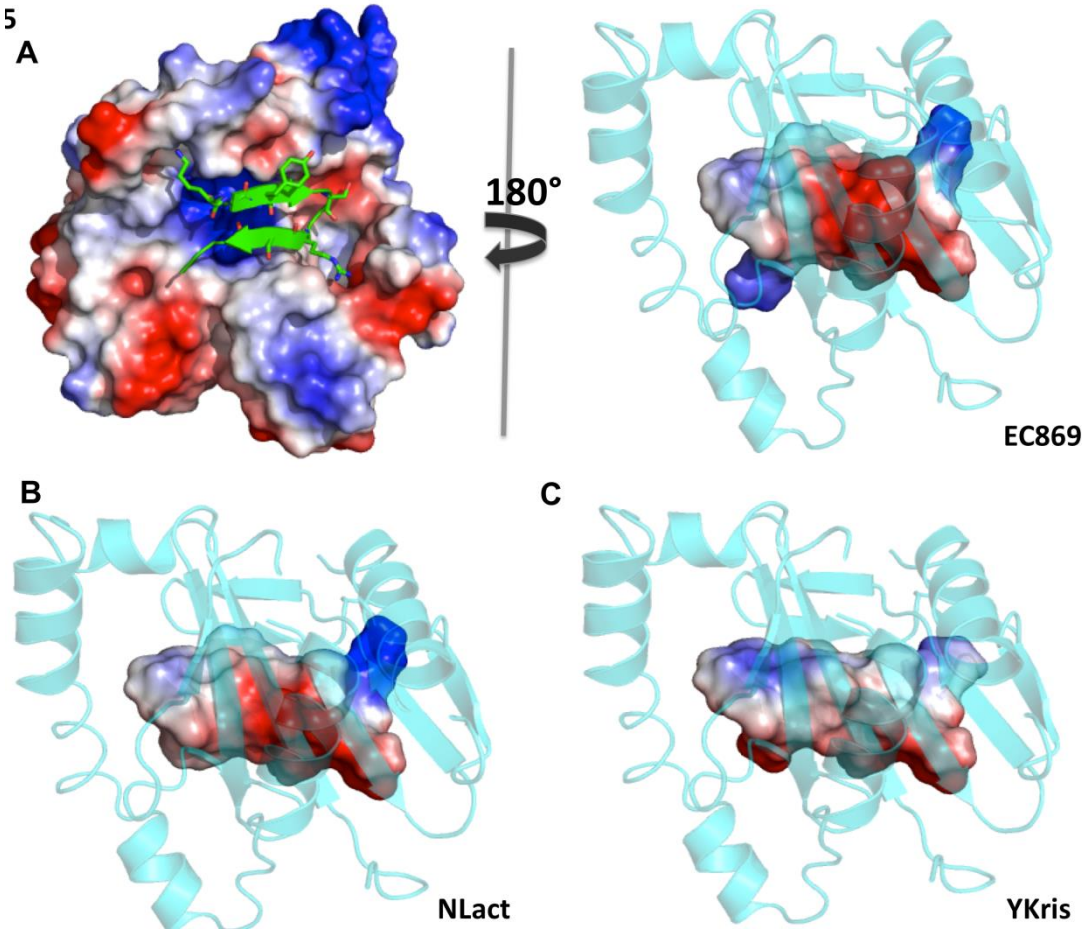

Figure 17. **Electrostatic surface potential of toxin β-hairpin chimeras.** (**A**) Electrostatic surface representation of $CdiI_{o11}^{EC869}$ with the toxin β-hairpin in cartoon and sticks colored green (left panel). The right panel is rotated 180° around the y-axis with respect to the left panel. The immunity protein is depicted as cartoon representation and the toxin β-hairpin is rendered as an electrostatic surface representation. (**B**) and (**C**) Models of $CdiA\text{-}CT^{Nlact}$ and $CdiA\text{-}CT^{Ykris}$ β-hairpins docked onto $CdiI_{o11}^{EC869}$ immunity protein. The models are viewed in the same orientation as the right image in panel **A**. The β-hairpins are rendered as electrostatic surface representations, with red and blue representing positive and negative surface potentials (respectively) and white indicating hydrophobic surfaces.

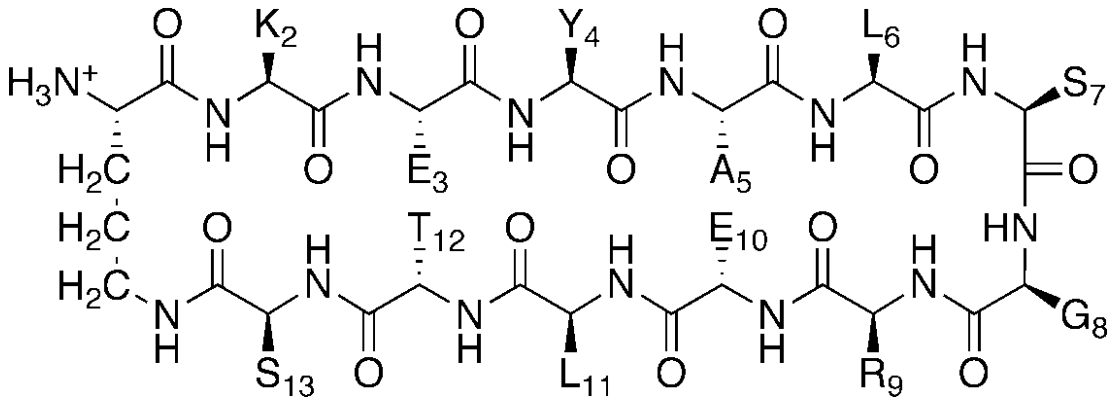

Figure 18. The macrocyclic peptide mimic of the β-hairpin from CdiA-CT_{o11}^{EC869}. The β-hairpin in this synthetic peptide mimics the β-hairpin that forms the basis of the interaction face between CdiA-$CT/CdiI_{o11}^{EC869}$. The synthetic construct corresponds to residues lysine 242 through serine 253 of CdiA-CT_{o11}^{EC869}.

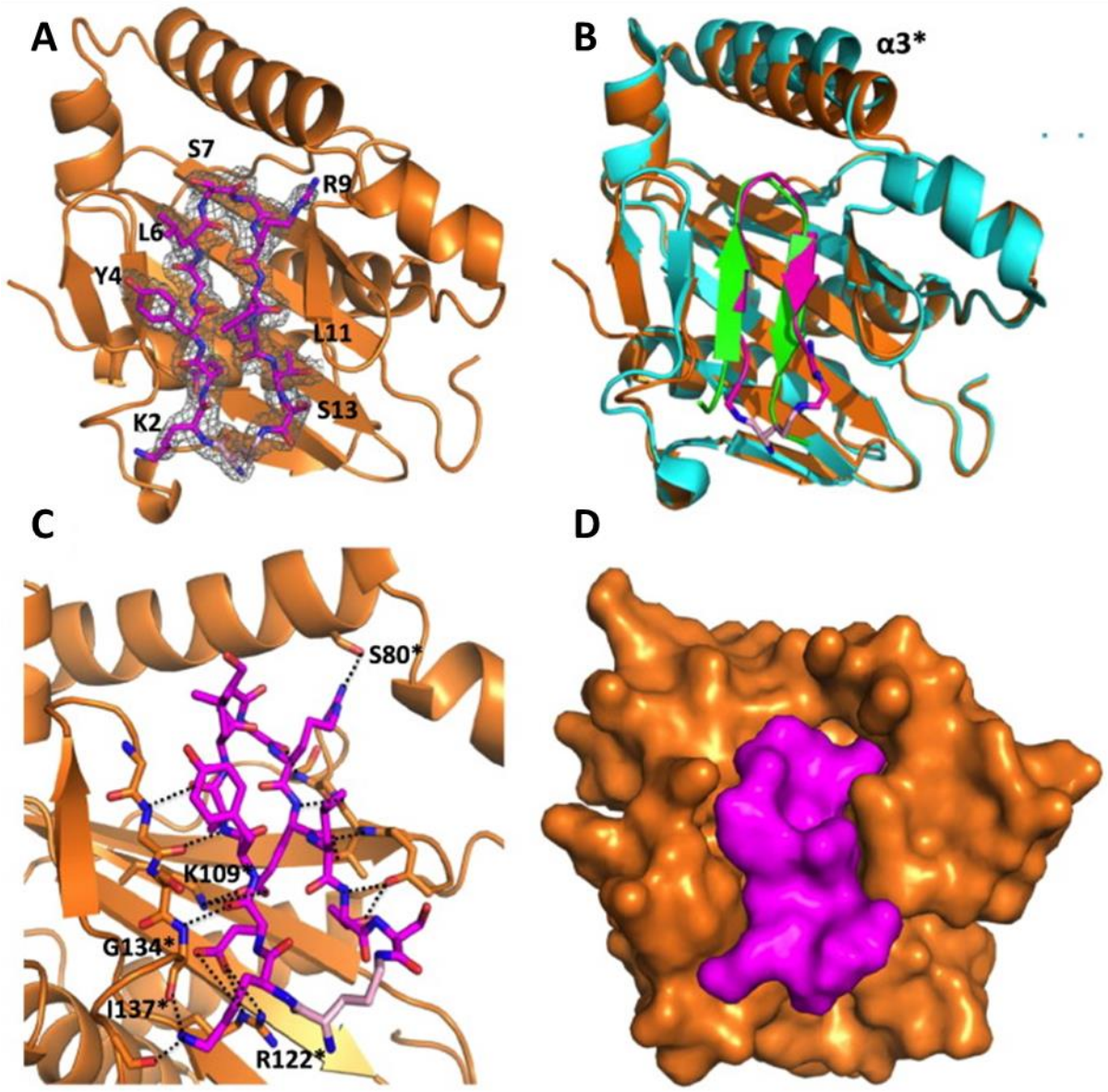

Figure 19. Structure of the MAC-CdiI$_{o11}^{EC869}$ complex. (A) Crystal structure with CdiI$_{o11}^{EC869}$ depicted as orange ribbons and MAC displayed as sticks, carbon, nitrogen, oxygen and ornithine carbons colored magenta, blue, red and pink, respectively. The MAC $2F_o - F_c$ electron density map is shown in a gray mesh and contoured at 1.0 σ. (B) Structural superimposition of MAC [colored same as (A)] and the CdiA-CT/CdiI$_{o11}^{EC869}$ complex. Only residues Lys242–Ser253 of the CdiA-CT$_{o11}^{EC869}$ β-hairpin are shown (green). CdiI$_{o11}^{EC869}$ is colored teal and helix α3* is labeled. (C) MAC interacts with CdiI$_{o11}^{EC869}$ through a network of H-bonds and ion pairs. Interacting bonds are shown as black dotted lines. CdiI$_{o11}^{EC869}$ β-strands that H-bond with MAC (β3* and β7*) are shown as sticks. (D) Surface representation of the CdiI$^{CT\text{-}MAC}$ structure, oriented as in (A) and (B), depicting the complementarity of MAC and CdiI$_{o11}^{EC869}$.

Table 1. X-ray diffraction data and atomic refinement.

	CdiA-CT/CdiI^{YPIII}	CdiI^{Ykris}	MAC/CdiI$_{o11}^{EC869}$
Space group	*C*2	$P3_1$	$P2_1$
Unit cell dimensions			
***a, b, c* (Å)**	65.5, 65.5, 71.5	54.4, 54.4, 54.4	34.8, 128.2, 45.0
β (°)	92.18		112.73
pH of crystallization condition	7.0	7.4	6.0
Protein concentration (mg/mL)	10	12.5	7.5
Dataset			
Wavelength (Å)	1.0	1.0	1.0
Resolution range	46.49–2.1	50.0–1.8	50.0–2.0
Unique reflections (total)	18,152	16,618	23,561
Completeness (%)[a]	99.4 (98.3)	99.7 (100)	96.5 (92.1)
Redundancy[a]	3.5 (3.5)	5.4 (5.5)	3.1 (3.1)
R_{merge} [a and b]	0.059 (0.460)	0.161 (0.607)	0.076 (0.485)
$I/\sigma(I)$[a]	10.0 (1.6)	9.48 (3.1)	11.1 (3.1)
NCS copies	1	1	2
Other ions	2 Cl^-	—	2 Cl^-
Model refinement			
Resolution range (Å)	46.49–2.09	23.58–1.80	34.81–2.00
No. of reflections (working/free)	18,149/1851	16,580 (1673)	23,526 (2004)
No. of protein atoms	2308	1283	2596
No. of water molecules	148	130	132
No. of CT-MAC atoms	—	—	222
Missing residues	1–173, 298 (CdiA)	None	1, 168, 169
	1–2 (CdiI)		
R_{work}/R_{free}[c] **(%)**	20.5/25.6	18.1/22.1	18.4/23.1
rmsd			
Bond lengths (Å)	0.003	0.007	0.009
Bond angles (°)	0.694	0.998	1.222
Ramachandran plot			
Most favorable region (%)	95.25	98.77	97.13
Additional allowed region (%)	4.75	1.23	2.87
Disallowed region	0	0	0
PDB code	4ZQU	4ZQV	4ZQW

R_{free} was computed identically except where all reflections belong to a test set of 10% randomly selected data.

a. Statistics for the highest-resolution shell are given in brackets.

b. $R_{merge} = \sum|I - \langle I \rangle| / \sum \langle I \rangle$.

c. $R_{work} = \sum|F_o - F_c| / \sum F_o$.

Table 2. Dissociation constants (μM) of CdiA-CT and CdiI interactions determined using biolayer interferometry.

	CdiA-CT$_{o11}^{EC869}$	**CdiA-CT$_{o11}^{EC869/Ykris}$**	**CdiA-CT$_{o11}^{EC869/Nlact}$**
CdiI$_{o11}^{EC869}$	0.018 ± 0.007	46 ± 36	0.18 ± 0.10
CdiI^{Ykris}	5.0 ± 0.4	24 ± 14	5.8 ± 3
CdiI^{Nlact}	82 ± 18	3.2 ± 2	0.17 ± 0.09

Table 3. Direct hydrogen bonds and ion pairs between CdiA-CT/CdiI toxin/immunity proteins.

	CdiA-CT toxin	**CdiI immunity**	**Distance (Å)**
EC869$_{o11}$			
Main-Side	Lys242 NZ	Ile137 O	2.73
	Arg249 NH2	Phe75 O	2.72
	Glu250 O	Thr31 OG1	3.65
	Asp187 OD2	Arg71 NE	2.82
Side-Side	Lys242 NZ	Asn138 OD1	3.90
	Tyr244 OH	Lys128 NZ	3.99
	Glu243 OE1	Arg122 NE	3.15
	Glu243 OE2	Arg122 NE	3.70
	Glu243 OE2	Lys109 NZ	3.33
	Glu243 OE2	Arg122 NH2	3.10
	Ser247 OG	Glu130 OE1	3.36
	Glu250 OE1	Arg122 NH2	3.18
	Glu250 OE2	Arg122 NH2	3.39
	Glu250 OE2	Thr31 OG1	3.82
	Glu250 OE2	Asn12 ND2	3.08
	Glu250 OE1	Lys109 NZ	3.12
YPIII			
Main-Side	Thr250 O	Asn30 ND2	3.89
	Lys243 NZ	Pro133 O	2.85
	Glu242 OE2	Leu147 N	3.72

Side-Side	Ala203 O	Arg28 NE	2.92
	Thr204 O	Arg28 NE	3.43
	Thr204 O	Arg28 NH2	3.43
	Met255 O	Arg28 NH1	2.79
	Lys243 NZ	Ser132 OG	2.55
	Lys195 NZ	Glu137 OE1	2.68
	Lys195 NZ	Glu137 OE2	3.01
	Arg202 NH1	Ser29 OG	2.99
	Lys243 NZ	Asp121 OD2	3.05
	Asp201 OD1	Arg69 NH1	2.71
	Asp201 OD2	Arg69 NH2	3.09

Table 4. Bacterial strains and plasmids.

Strain or plasmid	***Description***[a]	***Reference or source***
Strains		
BL21-Gold(DE3)	*E. coli* B F^- *ompT hsdS*(r_B^- m_B^-) *dcm*$^+$ *gal* λ(DE3) *endA*, Tet^R	Agilent
EPI100	F^- *mcrA* Δ*(mrr-hsdRMS-mcrBC) φ80dlacZ*Δ*M15* Δ*lacXcZ*Δ*M15* Δ*lacX recA1 endA1 araD139* Δ*(ara, leu)7697 galU galK* λ$^-$ *rpsL nupG*, Str^R	Epicentre
EPI100 *pir*$^+$	F^- *mcrA* Δ*(mrr-hsdRMS-mcrBC) φ80dlacZ*Δ*M15* Δ*lacXcZ*Δ*M15* Δ*lacX recA1 endA1 araD139* Δ*(ara, leu)7697 galU galK* λ$^-$ *rpsL nupG pir*$^+$*(DHFR)*, Str^R Tp^R	Epicentre
X90	F´ *lacI*^{q} *lac´ pro´/ara* Δ*(lac-pro) nal1 argE*(amb) *rif*^{r} *thi-1*, Rif^R	(377)
DY378	W3110 λ*cI857* Δ*(cro-bioA*)	(378)
DA28100	*galK*::sYFP2opt-cat	Dan Andersson
CH2016	X90 (DE3) Δ*rna* Δ*slyD::kan*, Rif^R Kan^R	(379)
CH2550	EPI1100 *galK*::sYFP2opt-kan	This study
CH2567	MC4100 *mKate::cam* Str^R Cm^R	This study
CH8251	MC4100 *rif*^{r}, Str^R Rif^R	(177)
Plasmids		
pTrc99a	IPTG-inducible expression plasmid, Amp^R	GE Healthcare
pTrc99KX	Derivative of pTrc99A that contains KpnI restriction	(380)

	site immediately downstream of the ribosome-binding site, Amp^R	
pCH450	pACYC184 derivative with *E. coli araBAD* promoter for arabinose-inducible expression, Tet^R	(381)
pSIM6	Heat-inducible expression of the phage λ Red recombinase proteins, Amp^R	(291)
pET21S	pET21d derivative with SpeI restriction site for in-frame fusion to His_6 coding sequences, Amp^R	(176)
pDE1013	pEndy1013-mKate2::cat	(369)
pNAK	pBluescript derivative with FRT-flanked kanamycin-resistance cassette, Amp^R Kan^R	This study
pDAL878	Constitutive expression of $cdiA^{EC93}$-*(ΔCT)*, in which the toxin-encoding sequence has been deleted, Cm^R	(176)
pCH10164	Constitutive expression of chimeric $cdiA^{EC93}$-$CT(D198A)_{o11}^{EC869}$ and $cdiI_{o11}^{EC869}$. The Asp198Ala mutation inactivates the DNase domain. Cm^R	(177)
pCH848	pTrc99KX::$cdiI^{YPIII}$, Amp^R	This study
pCH2409	Constitutive expression of chimeric $cdiA^{EC93}$-CT^{YPIII} and $cdiI^{YPIII}$ genes, Cm^R	This study
pCH2500	pNAK::*galM´*, Amp^R Kan^R	This study
pCH2503	pNAK::*galT´-yfp-galM´*, Amp^R Kan^R	This study
pCH9305	Constitutive expression of chimeric $cdiA^{EC93}$-CT_{o11}^{EC869} and $cdiI_{o11}^{EC869}$ genes, Cm^R	(177)
pCH9315	pTrc99A::$cdiI_{o11}^{EC869}$, Amp^R	(177)
pCH9938	pUC57::NEILACOT_05636 encoding $CdiI^{Nlact}$ from *Neisseria lactamica* ATCC 23970, Amp^R	This study
pCH9940	pUC57::Ykris_10749 encoding $CdiI^{Ykris}$ from *Yersinia pseudotuberculosis* ATCC 33638, Amp^R	This study
pCH10101	pCH450::NEILACOT_05636, Tet^R	This study
pCH10103	pTrc99KX::Ykris_10749, Amp^R	This study
pCH10163	Cosmid pCdiA-CT/*pheS** that carries a *kan-pheS** cassette in place of the *E. coli* EC93 *cdiA-CT/cdiI* coding sequence. Used for allelic exchange and counter-selection. Cm^R Kan^R	(177)
pCH10170	pET21-derivative that expresses $CdiI^{Ykris}$-His_6 from *Y. kristensenii* ATCC 33638, Amp^R	This study
pCH10172	pET21-derivative that expresses $CdiI^{Nlact}$-His_6 *N. lactamica* ATCC 23970, Amp^R	This study
pCH10175	pET21-derivative that expresses CdiA-$CT(D198A)_{o11}^{EC869}$ containing the β4/β5 hairpin from CdiA-CT^{Ykris}, Amp^R	This study
pCH10365	pET21-derivative that expresses CdiA-$CT(D198A)_{o11}^{EC869}$ containing the β4/β5 hairpin from CdiA-CT^{Nlact}, Amp^R	This study
pCH10367	pET21-derivative that expresses $CdiI^{YPIII}$-His_6 from from *Y. pseudotuberculosis* YPIII, Amp^R	This study

pCH10369	pET21-derivative that expresses CdiA-$CT_{o11}^{EC869/\Delta\beta4\beta5}$ lacking the β4/β5 hairpin, Amp^R	This study
pCH10407	pET21-derivative that expresses CdiA-CT/$CdiI_{o11}^{EC869}$-His_6 complex from *E. coli* EC869, Amp^R	(177)
pCH10413	pET21-derivative that expresses CdiA-CT/$CdiI^{YPIII}$-His_6 complex from *Y. pseudotuberculosis* YPIII, Amp^R	This study

[a]Abbreviations: Amp^R, ampicillin-resistant; Cm^R, chloramphenicol-resistant; Kan^R, kanamycin-resistance; Rif^R, rifampicin-resistant; Tet^R, tetracycline-resistant; Tp^R, trimethoprim-resistant

Table 5. Oligonucleotides used in this study.

Oligonucleotide	***Sequence***	***Reference***
Kan-1 (CH106)	5′ - TGT GTA GGC TGG AGC TGC TTC	(367)
Kan-2 (CH107)	5′ - CAT ATG AAT ATC CTC CTT AGT TCC	(367)
galM-Bam-for (CH3789)	5′ - CGC GGA TCC CGG AAG AGC TGG	This study
galM-Sac-rev (CH3790)	5′ - TCT GAG CTC AGG GCA AAC AGC ACC	This study
galT-Kpn-for (CH3787)	5′ - CAC GGT ACC ATT TGG GCA AAT AGC TTC C	This study
yfp-Eco-rev (CH3788)	5′ - CT GAA TTC GCG GCC GCT TCT AGA	This study
YPK0575-Kpn-for (CH2447)	5′ - TTT GGT ACC ATG GTA GAG AAT AAT TAT CTA AAC TCC	This study
YPK0576-Xho-rev (CH2448)	5′ - TTC CTC GAG ACC TTT ACA GCG ACT CAA TGC CAG	This study
YPK0576-Kpn-for (CH2449)	5′ - TGA GGT ACC ATG AAC GAT ATA GTA AAA AG	This study
YPK0576-Xho-rev2 (CH2790)	5′ - TTT CTC GAG TTA ACC TTT ACA GCG	This study
Nlact-cdiI-Spe-rev (CH2345)	5′ - AAA ACT AGT CTT ACA ATA ACT TAG	This study
Ykris-cdiI-Spe-rev (CH2346)	5′ - AAA ACT AGT GCC TTT ACA GCG GC	This study
Trc-seq2 (CH823)	5′ - GTT CTG GCA AAT ATT CTG AAA TGA GC	This study
ara seq (CH943)	5′ - GAT TAG CGG ATC CTA CCT GAC GCT TTT TAT CGC	This study
β-deletion-for1	5′ - GCC CAA TGG GCA CAA ACC AGT CTC TGA CCT TCG AT	This study

β-deletion-rev1	5´ - GCG GAT CCG CTT TTA AAC TTA GCC GCA GCA TCG ATG	This study
β-deletion-for2	5´ - GCG GAT CCG GCA CTT CAT CAA TGA TCT CTA ACA GGG	This study
β-deletion-rev2	5´ - GCC TCG AGA CTA GTA CCT TTG CAG CGA CTC AAG	This study
EC869-CT-Nco	5´ - ATT CCA TGG GCA CAA ACC AGT CTC TGA CCT TCG	(177)
EC869-cdiI-Spe	5´ - TCT ACT AGT ACC TTT GCA GCG ACT CAA GGC CAG	(177)
EC869-Nlact(beta)-for (CH2341)	5´ - AAA ACT TAC TCT CTT TCT GGT GTT GAG TTA ACT TCA TCA ATG ATC TC	This study
EC869-Nlact(beta)-rev (CH2342)	5´ - CTC AAC ACC AGA AAG AGA GTA AGT TTT AAA CTT AGC CGC AGC ATC G	This study
EC869-Ykris(beta)-for (CH2343)	5´ - CAT ACA CAT ACT CTT TCA GGC GAA CAG TTA ACT TCA TCA ATG ATC TC	This study
EC869-Ykris(beta)-rev (CH2344)	5´ - CTG TTC GCC TGA AAG AGT ATG TGT ATG AAA CTT AGC CGC AGC ATC G	This study
DL1527 (CDI204)	5´ - GAA CAT CCT GGC ATG AGC G	(177)
EC869o11-G173-rev (CH3640)	5´ - CCC AAC ATA ATC CTC CCA CGG CAT ACC	This study
EC869o11-G173-for (CH3641)	5´ - GGT ATG CCG TGG GAG GAT TAT GTT GGG	This study
EC93-YPIII-chim-rev (CH2689)	5´ - GGT CTG GTG TCT AAC CTT TGG GTT AAC CTT TAC AGC GAC TCA ATG C	This study
EC93-YPIII-down-for (CH2690)	5´ - GCA TTG AGT CGC TGT AAA GGT TAA CCC AAA GGT TAG ACA CCA GAC C	This study
DL2368 (CDI205)	5´ - GTT GGT AGT GGT GGT GCT G	(177)

Restriction enzyme sites are underlined.

VI. EF-Tu is a general co-factor required for inhibition by a subset of contact-dependent inhibition systems from Gram-negative bacteria

This work was done in collaboration with Argonne National Laboratory (Darien, Illinois) as well as with Allison Jones, Fernando Garza-Sánchez, Grant Gucinski, and David Low (University of California, Santa Barbara).

A. Background

CdiA-CT domains inhibit target cells by disrupting essential cellular components such as RNA and DNA or destroying the integrity of the inner membrane. Many CdiA-CTs function independently and do not require other protein cofactors for activity, the need for which can be assessed by performing *in vitro* activity assays with purified proteins and substrates. If a CdiA-CT is toxic in co-culture assays or when expressed intracellularly but not *in vitro*, then a cofactor may be required. This approach was used to identify the cofactor required by CdiA-CT^{Ec536}, which has tRNase activity inside cells but not when purified and added to total RNA *in vitro*. Further investigation revealed a role for CysK, which is a biosynthetic enzyme that catalyzes the second step in the conversion of serine to cysteine during cysteine biosynthesis (214, 215, 217). CdiA-CT^{Ec536} physically interacts with CysK, and this interaction is required for tRNase activity both *in vitro* and *in vivo*. The C-terminal 4 residues (GYGI) of CdiA-CT^{Ec536} interact with CysK in a manner that mimics the interaction between CysK and the tail of its cofactor CysE (220). This complex forms a heterotrimer with CdiI^{Ec536} and crystallizes as a dimer of heterotrimers (Robert Morse, Christina Beck, Christopher Hayes, and Celia Goulding, unpublished data).

That the CysK/CdiA-CT^{Ec536} interaction so closely mimics a biosynthetic interaction with physiological relevance outside of CDI suggests evolution of CdiA-CT^{Ec536} to "hijack" the

structure of CysK, although the exact contribution of CysK in positioning CdiA-CT^{Ec536} in an optimal position to cleave tRNA subtrates has yet to be revealed. Given the diversity of CDI toxins across Gram-negative bacteria, we wondered whether other CdiA-CT families require protein cofactors for inhibition or whether this is a unique trait of CdiA-CT^{Ec536}. Using both biochemical and genetic approaches, we have discovered a role for the translation factor EF-Tu in the activity of CdiA-CT from different families and species..

B. Results

1. Transposon mutagenesis fails to reveal cofactors required for activity of three CdiA-CTs from E. coli *EC869*

We constructed cosmids in which the CdiA-CT from EC93 was replaced with the main CdiA-CT/CdiI sequence or orphan CdiA-CT/CdiI modules (EC869$_{o5}$ and EC869$_{o10}$) from *E. coli* EC869 at the conserved VENN tetrapeptide motif. These peptides encode functional toxins, and inhibition can be blocked by expression of the cognate immunity (Figure 1A). We then performed transposon mutagenesis experiments in which a library of *mariner*-mutagenized *E. coli* targets were co-cultured with strains expressing each CDI$^+$ cosmid. Surviving cells were selected and mixed with a fresh inhibitor culture; this process was repeated iteratively to enrich for the presence of CDI-resistant target cells. At the end of three rounds of enrichment, no increase in resistance was observed in target cells co-cultured with CDI$_{o5}^{EC869}$ or CDI$_{o10}^{EC869}$ (data not shown). The target cells co-cultured with CDI^{EC869} showed an increase in resistance, although the pool did not become completely resistant. We note that the colony morphology of surviving cells was markedly different than the input population, indicating some upregulation of capsule production (data not shown).

Two colonies (CT1-3 and CT1-7) isolated from this enrichment process were isolated,

and the kanamycin resistance marker linked to the *mariner* transposon was moved into a fresh CDI^{S} background using P1 phage transduction. Transductants were co-cultured with CDI^{EC869} cells to test for genetic linkage of the CDI^{R} phenotype. When tested as individual monocultures, the transposon isolates showed a partial CDI^{R} phenotype compared to wild-type cells (Figure 1B). Each transductant showed the same level of partial resistance (Figure 1B, labels marked "x" to indicate transductant as opposed to original mutant). We identified the location of the CT1-3 and CT1-7 transposons using arbitrary PCR to amplify the transposon/genomic DNA junction. CT1-3 contained a transposon in *uhpB*, and the transposon in CT1-7 was determined to be upstream of the open reading frame for *uvrY*. UhpB is part of the UhpABC system that regulates the expression of UhpT, a sugar-phosphate transporter and can sense and transport glucose-6-phosphate into the cell (342, 382). UvrY is part of a two-component system with BarA that is involved in growth adaptation to different carbon sources (383, 384). This two-component system also regulates the non-coding RNAs CsrA and CsrB, which ultimately control a suite of activities including metabolism, biofilm formation, flagella, and virulence of some uropathogenic *E. coli* strains (385-388). We reasoned that these membrane complexes might serve as transporters for CdiA-CT^{EC869} during delivery, so we constructed single-gene knockouts of *uhpB*, *uvrY*, and associated genes from their respective operons and pathways. These strains were used as target cells in co-culture assays with CDI^{EC869}. As indicated by the cell viability counts, none of the clean deletion strains were tested showed significant resistance to CDI^{EC869} (Figure 1C). Therefore, none of these proteins are bonafide members of the CDI^{EC869} pathway, and it is likely that compounding factors from the transposon mutagenesis experiments influenced the resistance of these cells.

2. *Mutations in* tsf *confer resistance to CdiA-CT^{Ec869}*

Subsequent enrichment experiments were performed using UV-mutagenized target pools, which yielded a CDI^{Ec869}-resistant strain with a mutation in *tsf* at codon 202, changing a small, uncharged alanine residue to a bulky, negatively-charged glutamic acid (Allison Jones and David Low, unpublished data). *tsf* encodes elongation factor EF-Ts, which is a guanine-nucleotide exchange factor (GEF) involved in the translation cycle in which EF-Tu delivers aminoacyl-tRNAs (aa-tRNAs) to the ribosome (389). During translation, a ternary complex of GTP, EF-Tu, and aa-tRNA docks with the A site of the ribosome. Codon recognition leads to GTP hydrolysis, and the resulting GDP:EF-Tu complex is released. In order to complete another cycle of aa-tRNA delivery, EF-Tu must be recharged with GTP; release of GDP is facilitated by the GEF activity of EF-Ts (389-391). EF-Tu then associates with GTP and can form another ternary complex.

Bacterial EF-Ts contains four domains: an N-terminal domain, the core domain, a dimerization domain that contains a coiled-coil motif, and a C-terminal domain (390, 392, 393). The coiled-coil motif, in which the CDI-resistant Ala202Glu mutation was identified, mediates dimerization between EF-Tu:EF-Ts complexes in the crystal structure, but the physiological relevance of this tetramer is unclear (393). While the coiled-coil domain is conserved throughout bacteria and chloroplasts, it is noticeably absent from mammalian EF-Ts proteins (392). This suggests that this motif plays some essential albeit unknown role in prokaryotic translation. While the coiled-coil domain is not essential for cell viability or GEF activity of EF-Ts, activity is reduced in a coiled-coil deletion mutant (390, 392). Mutants lacking the coiled-coil motif also display a growth defect when rapidly dividing, but not at lower growth rates (392). This is most likely due to the decreased GEF activity and a

subsequent reduction of EF-Tu turnover, which results in slower than maximal growth. Cells lacking the entire coiled-coil domain are also resistant to inhibition by CDI^{Ec869} (Allison Jones and David Low, unpublished data).

Binding data using purified CdiA-CT^{Ec869} revealed that this toxin tightly interacts with EF-Tu but not EF-Ts *in vitro* (Fernando Garza-Sanchez, Allison Jones, Christopher Hayes, and David Low, unpublished data). The EF-Ts Ala202Glu and Δcoiled-coil mutants are also resistant to inhibition by CdiA-CT^{NC101} and CdiA-CT$^{96.154}$, two other toxins from *E. coli* strains (Allison Jones and David Low, unpublished data). Taken together, this suggests that a genetic or biochemical interaction with EF-Tu, EF-Ts, or translation machinery may be a general feature of some classes of CDI toxins. To further investigate this hypothesis, we used a combination of genetic and biochemical approaches to identify additional CdiA-CTs that interact with EF-Tu and EF-Ts.

3. *CdiA-CT^{Kp342} has a genetic interaction with* tsf *but does not interact with EF-Tu or EF-Ts* in vitro

Given the magnitude of distinct CdiA-CT families in *E. coli* alone (170), we wondered whether additional CdiA-CTs had a genetic requirement for *tsf*. We employed a co-culture assay to rapidly identify additional CdiA-CTs unable to inhibit *tsf* mutants (Table 1). Individual CdiA-CT/CdiI modules were fused to the CdiA core from *E. coli* EC93; these constructs retained identical receptor-binding domains. To facilitate data interpretation, we calculated the fold inhibition of *tsf* Ala202Glu and Δcoiled-coil strains relative to wild-type *E. coli* targets and color-coded each value (Figure 3A). As predicted, CdiA-CT^{NC101} and CdiA-CT^{EC869} did not inhibit *tsf* mutants. Well-characterized nuclease toxins such as CdiA-CT^{Dda3937} and a homolog of CdiA-CT^{Ec536} were used as negative controls, and both were able

to inhibit all target strains, regardless of *tsf* allele (Figure 3A). CdiA-CT^{Dda3937} is a CDI toxin from *Dickeya dadantii* 3937 that degrades DNA (194), and CdiA-CT^{Ec536} is a general tRNase that requires CysK for activity (193). From this screen, we found that CdiA-CT^{Kp342}, a toxin from *Klebsiella pneumonia* 342, was able to inhibit wild-type cells but not *tsf* mutants. The EF-Ts and Δcoiled-coil strains had approximately 100-fold higher cell viability than wild-type *E. coli* targets when co-cultured with the CDI^{Kp342} inhibitor strain. Interestingly, none of the toxins that have a genetic connection to *tsf* are closely related to each other, as determined by pairwise sequence comparisons (Figure 3B).

Because CdiA-CT^{Kp342} shares a genetic interaction with CdiA-CT^{Ec869}, we next wished to determine whether this similarity extends to the biochemical relationship between CdiA-CT^{Ec869}, EF-Tu, and EF-Ts. We first asked whether EF-Tu or EF-Ts co-purified with CdiA-CT^{Kp342} when the toxin was overexpressed inside *E. coli* cells. Using a CdiA-CT/CdiI^{Kp342}-His6 overexpression construct, we trapped CdiI^{Kp342}-His6 using Ni-NTA beads and used denaturing washes to elute CdiA-CT^{Kp342} along with any proteins that might be bound to the CdiA-CT/CdiI-His6 complex. A single band migrating at approximately 28 kDa on an SDS-PAGE gel was detected using this procedure (Figure 3A); this corresponds to the predicted size of CdiA-CT^{Kp342}. This species was the sole protein detected, and no additional proteins corresponding to EF-Tu or EF-Ts were observed.

The CdiA-CT^{Kp342} variant used in this experiment was expressed and purified in complex with a tagged form of CdiI^{Kp342} using nickel agarose beads. If EF-Tu or EF-Ts interact with this toxin, it is possible that the location of this His6 tag could interfere with co-factor binding. Alternatively, the presence of the immunity protein bound to CdiA-CT^{Kp342} could occlude a co-factor binding site, preventing detection of this interaction. Therefore, we asked

whether CdiA-CT^{Kp342} interacts with EF-Tu *in vitro* in the absence of the immunity protein. Untagged and His-tagged variants of CdiA-CT^{Kp342} were overexpressed, purified, and mixed with either untagged or His6-tagged EF-Tu or EF-Ts, then added to Ni-NTA beads. Fractions were collected and analyzed via SDS-PAGE and Coomassie staining. No interactions between CdiA-CT^{Kp342} and EF-Tu were observed under any of the conditions tested. Furthermore, His-tagged CdiA-CT^{Kp342} constructs did not pull down any proteins when added to an *E. coli* S30 lysate (Figure 3B). CdiA-CT^{Kp342} is able to bind purified CdiI^{Kp342} *in vitro*, indicating that this toxin refolds correctly undergoing denaturation during the purification process (Figure 3B).

4. EF-Ts regulates intracellular activity, not translocation of CdiA-CTs

An overarching goal of studying CDI cofactors is to understand how they influence CdiA-CT activity. Delivery of nuclease CdiA-CTs into target cells encompasses three basic steps: 1) recognition and binding of CdiA at the outer membrane, 2) translocation across the outer membrane, periplasm, and inner membrane into the cytoplasm, and 3) carrying out toxic function upon reaching the cytoplasm (157, 167, 173, 193, 194). Therefore, mutations in *tsf* could theoretically influence any of these steps. One could imagine a scenario in which mutations in *tsf* affect the translation of multiple proteins, and that these proteins are involved in different steps of the CDI pathway for given CdiA-CTs. Because CdiA-CT^{EC869} and CdiA-CT^{Kp342} both genetically interact with *tsf* but have different biochemical interactions with EF-Tu, the step in CDI affected by *tsf* mutations is not necessarily the same for all toxins.

We first considered whether *tsf* mutations could affect the first step in CDI delivery, which is binding an outer membrane receptor at the target cell surface. All CDI chimeras

constructed in this study were made by replacing the native EC93 CdiA-CT at the VENN tetrapeptide with the CdiA-CT/CdiI sequence of choice. Therefore, the receptor-binding domain of CdiA, which lies in the middle of the primary sequence, is unchanged in all constructs. CdiA truncations containing the receptor-binding domain but lacking any CdiA-CT sequence still bind to target cells (225), indicating that this event is functionally separate from toxin translocation. As such, it is unlikely that *tsf* mutations would disrupt receptor recognition given that this occurs in a toxin-independent manner. We therefore presume that this first step in CDI is not disrupted by *tsf* mutations.

Next, we considered that the translocation step across the periplasm and inner membrane may be affected by *tsf* mutations. As discussed in Chapter 2, we have recently shown that the N-terminal domain of CdiA-CTs dictates the specific inner membrane protein required for delivery into target cells. Because EF-Ts is essential for translation of proteins, it is possible that mutations in *tsf* affect translation rates, and that this could differentially impact IMP synthesis. In turn, this could alter the levels of IMPs acting as receptors for CdiA-CT toxins, and decreased levels of specific IMPs required for CdiA-CT import could result in increased resistance against particular toxins. To probe whether this hypothesis is feasible, we performed sequence analysis on the CdiA-CTs that interact either genetically or biochemically with EF-Tu and EF-Ts to identify any underlying homology that may be responsible for these co-factor requirements. We compared the N-terminal domains from the set of CdiA-CTs that require wild-type *tsf* for inhibition of target cells and found that they have little to no sequence conservation (Figure 4A). In general, CdiA-CT sequences are bipartite, and N-terminal domains sort independently from C-terminal domains (167, 173, 176). We next looked for *tsf*-independent CdiA-CTs that share an N-terminal domain but not

a C-terminal domain with *tsf*-dependent CdiA-CTs, reasoning that these related toxins would be translocated via the same pathway (based on N-terminal domain similarity) but would have different cytotoxic activities (as dictated by the C-terminal domain). Therefore, if *tsf* mutations disrupted translocation, both toxins with a shared N-terminal domain would be affected. If *tsf* mutations affected activity, then N-terminal domain homology would not be important, and toxins with different C-terminal domains would differentially inhibit *tsf* cells. We chose to use CdiA-CT^{Kp342}, which was identified from our co-culture competition screen, and CdiA-CT^{NC101}, which was previously found to require wild-type *tsf* for inhibition (Allison Jones and David Low, unpublished data).

The N-terminal domain of CdiA-CT^{NC101} is similar to that of a toxin from *Dickeya zeae* (CdiA-CT^{Dzeae}), and the N-terminal domain of CdiA-CT^{Kp342} is similar to the same region of a CdiA-CT from *Yersinia kristensenii* 33638 (CdiA-CT^{Yk33638}) (Figure 4B and C). The C-terminal activity domains of each toxin are distinct regardless of N-terminal domain homology. We compared inhibition data from each toxin against the same set of wild-type and *tsf* cells previously used to identify CdiA-CT^{Kp342}. While CdiA-CT^{NC101} and CdiA-CT^{Kp342} inhibit wild-type but not *tsf* cells, both N-terminal domain partners inhibit all tested genotypes regardless of *tsf* allele (Figure 4D and E). This suggests that *tsf* mutations do not disrupt translocation of these toxins, or inhibition would be linked to N-terminal domain identity. Therefore, it is likely that EF-Ts is directly involved in modulating the activity of these CdiA-CT domains once delivered to the cytoplasm.

If EF-Ts is required for intracellular activity, then toxin molecules directly produced in the cytoplasm (as opposed to delivered from a CDI$^+$ inhibitor cell) should also be inactive in *tsf* mutant backgrounds. Conversely, if *tsf* mutations produce a defect in translocation but do

not affect CdiA-CT activity, cells expressing mutant EF-Ts should still be sensitive to internally-produced toxin. Delivery of CdiA-CTs into a separate target cells can be bypassed using an intracellular expression system. To test whether wild-type *tsf* is needed for intracellular activity, we cloned CdiA-CT/CdiI^{NC101} into a controllable degradation system in which the immunity protein is linked to an *ssrA*(DAS) tag that is degraded by the ClpXP protease (268). We transformed this construct into wild-type cells and cells expressing the EF-Ts Ala202Glu and Δcoiled-coil variants along with an empty plasmid vector or a plasmid expressing untagged CdiI^{NC101} (Figure 5A) and monitored the growth of these strains by measuring OD_{600} values over time (Figure 5B). Expression of CdiA-CT^{NC101} inhibits cells, and inhibition is blocked by co-expression of the immunity protein. Cells with mutated *tsf* alleles are resistant to internal expression of CdiA-CT^{NC101}, indicating that EF-Ts is required for the proper intracellular function of this toxin.

5. CdiA-CT$^{O32:H37}$ co-purifies with EF-Tu

Thus far, we have identified several CdiA-CTs that interact with translation machinery in different ways. CdiA-CT^{Ec869} requires wild-type *tsf* to inhibit target cells and interacts with EF-Tu *in vitro*. CdiA-CT^{NC101} and CdiA-CT$^{96.154}$ both require wild-type *tsf* to inhibit cell growth (Allison Jones and David Low, unpublished data). CdiA-CT^{Kp342} requires wild-type *tsf* for inhibition, but does not interact with EF-Tu or EF-Ts *in vitro*. Therefore, we wondered whether additional CdiA-CTs physically interact with these co-factors *in vitro*, and whether these cofactors were required for activity via the same mechanism as CdiA-CT^{Ec869}. As part of an ongoing structure/function collaboration with Argonne National Laboratory (Darien, Illinois), we discovered that a CdiA-CT from *E. coli* O32:H37 co-purified with a protein migrating at approximately 43 kDa (Figure 6A and B), which is close to the size of

EF-Tu (43.2 kDa). CdiA-CT$^{O32:H37}$ is the toxin domain (predicted size 15.8 kDa) associated with a full-length CdiA protein found in a strain of *E. coli* associated with diseases in dairy cattle (394). Two of these bands correspond to the predicted gel mobility of CdiA-CT$^{O32:H37}$ and CdiI$^{O32:H37}$. The third band is present at an equimolar amount to CdiA-CT$^{O32:H37}$ and CdiI$^{O32:H37}$ and has an apparent size of approximately 43 kDa (Figure 6A). This protein and CdiA-CT$^{O32:H37}$ co-elute under denaturing conditions (Figure 6B), suggesting that it interacts with either CdiA-CT$^{O32:H37}$ or CdiI$^{O32:H37}$. Based on size, abundance, and previously-characterized interactions between CdiA-CTs and translation machinery, we surmised that the third band that co-purifies with CdiA-CT$^{O32:H37}$ could be EF-Tu.

To ascertain whether the EF-Tu is required for activity of CdiA-CT$^{O32:H37}$ in the same manner as CdiA-CT^{Ec869}, we first determined the activity of CdiA-CT$^{O32:H37}$ inside cells. CdiA-CT$^{O32:H37}$ was fused to the structural domain of CdiA^{EC93}, and cells expressing the resulting CDI^{+} cosmid were mixed with targets carrying either an empty plasmid vector or *cdiI*$^{O32:H37}$. After 1 h of co-culture, target cells lacking the immunity were inhibited approximately 100-fold, while cells expressing CdiI$^{O32:H37}$ did not lose viability (Figure 7A). Mutation of a conserved histidine residue to an alanine (His71Ala) ablated toxicity of target cells. We examined RNA from these co-cultures and looked for evidence of degradation using Northern blot probes to tRNA and rRNA species. RNA cleavage products were detected using probes that recognize tRNA$_2^{Thr}$, tRNA^{Gln}, and tRNA$_2^{Arg}$, as well as a probe for 23S ribosomal RNA (Figure 7B). This activity was blocked by expression of CdiI$^{O32:H37}$.

We next purified the CdiA-CT$^{O32:H37}$/EF-Tu complex to examine *in vitro* activity of this toxin. We mixed either 100 nM or 1 μM of this complex with total guanidine isothiocyanate-extracted cellular RNA and examined the reactions using ethidium bromide staining and

Northern blots to observe degradation products. This purified complex was able to degrade RNA *in vitro*, as evidenced by the degradation of high molecular weight bands corresponding to 23S and 16S ribosomal RNA as well as the appearance of additional degraded RNA species (Figure 7C, top panel). *In vitro* activity against $tRNA^{Gln}$ is also evident in the Northern blot analysis (Figure 7C, bottom panel). The inactive CdiA-$CT^{O32:H37}$ H71A/EF-Tu complex did not have *in vitro* activity against RNA. Interestingly, although CdiA-CT^{Ec869} requires EF-Ts for complete cleavage of substrates *in vitro*, the activity of the re-folded EF-Tu/ CdiA-$CT^{O32:H37}$ complex was not enhanced by the addition of EF-Ts (Figure 7C, top panel, compare middle two lanes to two lanes on the right). This suggests that if EF-Tu is required, CdiA-$CT^{O32:H37}$ may utilize this cofactor in a mechanistically-distinct way as compared to CdiA-CT^{EC869}. Additional work on separating CdiA-$CT^{O32:H37}$ from EF-Tu to further elucidate the activity of this toxin is ongoing.

Both CdiA-CT^{Ec869} and CdiA-$CT^{O32:H37}$ interact with EF-Tu in some capacity, but appear to do so in different ways. Therefore, we wished to determine whether CdiA-$CT^{O32:H37}$ had the same genetic interaction with *tsf* as CdiA-CT^{Ec869}. We mixed cells expressing $CDI^{O32:H37}$ with wild-type target cells as well as cells expressing the EF-Ts Ala202Glu and Δcoiled-coil mutations and measured viability of target cells after 3 h of co-culture. All target strains were inhibited approximately 100-fold, indicating that CdiA-$CT^{O32:H37}$ does not require EF-Ts the same way as CdiA-CT^{Ec869} *in vivo* or *in vitro* (Figure 8). The same target cell lines were also co-cultured with CDI^{Ec869} as a positive control, and $CDI_{o11}{}^{EC869}$ (a DNase that does not require *tsf* for *in vitro* or *in vivo* activity (177, 202)) was included as a negative control. As expected, target cells with *tsf* mutations were resistant to inhibition by CDI^{Ec869} and were inhibited to wild-type levels by $CDI_{o11}{}^{EC869}$ (Figure 8).

6. CdiA-CT$^{O32:H37}$ does not interact with EF-Tu or EF-Ts in vitro

CdiA-CT^{Ec869} interacts with EF-Tu when mixed together *in vitro* as purified components. Therefore, we wished to determine whether the CdiA-CT$^{O32:H37}$/EF-Tu complex could be reconstituted outside of cells. We purified an untagged inactive CdiA-CT$^{O32:H37}$ His178Ala mutant and mixed it with purified EF-Tu carrying an N-terminal His6-TrxA fusion. CdiA-CT$^{O32:H37}$ eluted in the unbound fraction (Figure 9A), indicating that this protein was not bound to EF-Tu *in vitro*. We then repeated these experiments in a variety of reaction conditions including Tris and sodium phosphate buffers, varying concentrations of salts, and in the presence of whole-cell lysates to determine whether a molecule like Mg^{2+} or RNA was required for binding (Figure 9). However, we were unable to recapitulate the complex purified from intact cells. We next tried using fusion proteins with different N- or C-terminal tags to decrease the probability that binding was blocked due to steric hindrance from the location of the His6/His6-TrxA epitope (Figure 9B, C, and D). Again, the CdiA-CT$^{O32:H37}$/EF-Tu complex could not be formed under any *in vitro* conditions.

We then considered the differences in experimental conditions that could lead to purification of a complex from whole cells but an inability to reconstitute this complex *in vitro*. One possibility is that the native complex includes CdiA-CT$^{O32:H37}$ and EF-Tu in addition to CdiI$^{O32:H37}$, as the initial CdiA-CT$^{O32:H37}$/EF-Tu complex was isolated from cells expressing both CdiA-CT$^{O32:H37}$ and CdiI$^{O32:H37}$-His6. To test this, we purified all three proteins and repeated *in vitro* binding assays (Figure 10). We first showed that a stable complex forms between CdiA-CT$^{O32:H37}$ and CdiI$^{O32:H37}$-His6 *in vitro* (Figure 10A, left lanes), indicating that these proteins are correctly folded after purification. We then mixed these purified proteins with untagged EF-Tu. All three proteins were present in the bound

fraction, indicating that some ternary complex formed (Figure 10A, right lanes). CdiI$^{O32:H37}$-His6 does not interact with EF-Tu in the absence of CdiA-CT$^{O32:H37}$ (Figure 10B).

A second possibility is that EF-Tu plays some role in protein folding during CDI. The current CDI model posits that CdiA-CTs are unfolded during translocation into target cells, meaning they must refold in the correct confirmation to carry out activity. Chaperone activities have been described for both eukaryotic and prokaryotic EF-Tu (395-398). It is therefore possible that as CdiA-CT domains translocate across the inner membrane into the cytoplasm, an unfolded portion interacts with EF-Tu, facilitating re-folding of the entire delivered toxic peptide into an activity-competent conformation. To test whether EF-Tu acts as a chaperone for CdiA-CT$^{O32:H37}$, we purified tagged His10- and His6-TrxA-CdiA-CT$^{O32:H37}$ constructs under denaturing conditions, ensuring the protein remained unfolded. We then mixed these unfolded samples with a concentrated solution of native EF-Tu and immediately incubated the protein mixtures in dialysis buffer to permit refolding of denatured CdiA- CT$^{O32:H37}$. After dialysis, we performed a pulldown assay using nickel-agarose resin to trap the tagged CdiA-CT$^{O32:H37}$ constructs. After these steps, Ef-Tu was detected in the bound fraction of both CdiA-CT$^{O32:H37}$ constructs (Figure 10C and D). We also re-folded an aliquot of these toxin elutions independently (away from EF-Tu) and tested them in binding assays after dialysis. Neither construct pulled down EF-Tu when dialyzed separately (Figure 10E).

Although this suggests that EF-Tu may chaperone the folding of CdiA-CTO32:H37, enforcing complex formation between these proteins, we observed similar results when we carried out the same experiments with two negative controls. We performed the same dialysis procedure using a tagged variant of CdiA-CT^{Ec536}, which does not require EF-Tu as a

co-factor and instead uses the cysteine biosynthesis pathway enzyme CysK for activity (193). We also included His6-TrxA-CdiA-CT_{o11}^{Ec869}, a tagged form of a DNase toxin that does not require any additional co-factors for activity (177, 202). After the co-dialysis and protein pulldown steps, some EF-Tu was found in the bound fraction of both negative control reactions, indicating that EF-Tu may indiscriminately interact with unfolded proteins (Figure 10F and G). This may be exacerbated by the high concentrations of proteins used in these assays, and this may mask any differences in binding affinity between EF-Tu and various CdiA-CTs.

C. Discussion

The data presented here describe CdiA-CTs from *E. coli* and *Klebsiella pneumoniae* that interact, either genetically or biochemically, with the translation factors EF-Tu and EF-Ts. Interestingly, none of these toxins have strong sequence homology to each other in either the N-terminal or C-terminal domains (Figure 4A). Two hypotheses could explain this observation. The first is that perhaps these toxins share common structural motifs that are involved in interacting with these co-factors. We previously published a study showing that the *E. coli* toxin CdiA-CT_{o11}^{EC869} and the *Burkholderia pseudomallei* toxin CdiA-CT_{II}^{1026b} have unrelated primary sequences (less than 15% identity) but nearly identical core structures (177). Therefore, it is possible that the CdiA-CTs that interact with EF-Tu and EF-Ts share structural homology that is crucial for these interactions but that is simply not definable without crystallographic analysis. Detailed structure-function studies could reveal binding domains or motifs that cannot be identified by primary sequence gazing. A second possibility is that these toxins share no common structural or binding features, but that each evolved the ability and necessity to interact with EF-Tu or EF-Ts in a unique way. All of the EF-Tu/EF-Ts-dependent toxins with characterized activities have been found to be RNases,

and it is interestingly that no known DNase or pore-forming CdiA-CT domains use either of these co-factors for activity. Perhaps this requirement represents a common feature of substrate recognition or activity carried out by toxins that interact with translational machinery. An attractive hypothesis, especially for the tRNase toxins, is that interacting with components of the translational machinery help position these toxins near their tRNA substrates. This interaction between EF-Tu and the specific CdiA-CTs described here could also facilitate substrate recognition, binding, or activity. Because the canonical role of EF-Tu is to bring aminoacylated tRNAs to the ribosome during translation, interacting with EF-Tu might simply be a means by which tRNase domains can localize near their targets. It remains to be empirically determined whether EF-Tu/EF-Ts-dependent toxins interact preferentially with the aminoacylated tRNA form that would be delivered to the ribosome, although *in vitro* activity assays suggest that purified toxin can cleave charged and uncharged substrates.

CdiA-CT^{Kp342} has a genetic interaction with *tsf*, but does not interact with EF-Ts or EF-Tu *in vitro*. It is possible that it requires some other cellular co-factor for binding, but this is unlikely as binding was tested in whole-cell S30 lysates. While it is formally possible that purification and refolding results in an improperly-folded toxin, this is extremely unlikely because CdiA-CT^{Kp342} binds its cognate immunity *in vitro*. Furthermore, all CdiA-CTs tested thus far have been successfully unfolded and refolded during purification (167, 169, 174, 175, 202). An attractive alternate hypothesis is that the lack of *in vitro* interaction is suggestive of the role EF-Ts plays in activity. The physiological function of EF-Ts is to catalyze guanine nucleotide exchange to recycle EF-Tu during delivery of tRNAs to the ribosome during translation (389, 391). While EF-Ts mutants lacking the coiled-coil domain

can still catalyze GDP turnover, its ability to do so is decreased (392). Perhaps the GDP turnover activity performed by EF-Ts is essential for the (yet-to-be-determined) activity of CdiA-CT^{Kp342}. Disrupting this domain could block activity of this toxin yet not be detrimental enough to halt cell growth. However EF-Ts contributes to the activity of CdiA-CT^{Kp342}, we presume that this role is catalytic and not structural based on the lack of strong *in vitro* interactions. Another possibility is that EF-Ts and CdiA-CT^{Kp342} do have a specific binding interaction, but that this binding is weak and not detectable using a crude bait-prey assay approach. Future work could involve cross-linking experiments or more sensitive interaction studies to precisely determine the contribution of EF-Ts to the activity of CdiA-CT^{Kp342}.

While CdiA-CT$^{O32:H37}$ does not share the genetic *tsf* interaction with CdiA-CT^{Kp342} and CdiA-CT^{EC869}, it does co-purify with EF-Tu, thus fitting within the broad classification of toxins that interact with EF-Tu or EF-Ts. These differences may be indicative of different mechanisms of action against cellular substrates. It is interesting to note that the cleavage products produced by CdiA-CT$^{O32:H37}$ are not identical to the fragments produced by CdiA-CT^{EC869} or another CdiA-CT from *E. coli* NC101 that requires both EF-Tu and EF-Ts for activity. Both of these (EF-Tu)-dependent toxins cleave the tRNA acceptor stem near the end of the CCA tail (Fernando Garza-Sanchez, Grant Gucinski, Christopher Hayes, and David Low, unpublished data). However, the cleavage pattern produced by CdiA-CT$^{O32:H37}$ resembles that of CdiA-CT^{Ec536}, which cleaves the anticodon loop of tRNA substrates (174, 193). If EF-Tu is required for activity of CdiA-CT$^{O32:H37}$, perhaps this toxin interacts with EF-Tu using a different interface, contributing to the difference in tRNA cleavage patterns.

An alternative explanation for the relationship between CdiA-CT$^{O32:H37}$ and EF-Tu is that

these do not form a stable complex required for activity, but rather a transient catalytic complex that is stabilized through addition of the immunity protein CdiI$^{O32:H37}$. The co-purification between toxin and EF-Tu was first observed using a construct that also expresses the immunity protein. Ternary complex formation is also observed using purified components *in vitro*. Perhaps a weak interaction occurs between EF-Tu and CdiA-CT$^{O32:H37}$ inside the cell, but CdiI$^{O32:H37}$ stabilizes it as part of the mechanism of immunity protection. This would remove some EF-Tu from the cellular pool available for translation, but given the high intracellular concentration of EF-Tu, the amount bound to CdiA-CT$^{O32:H37}$ would presumably be low enough as to maintain the overall rate of protein synthesis. A number of non-canonical activities have been ascribed to EF-Tu in both prokaryotic and eukaryotic organisms (262, 395-401). Therefore, there is precedence for pools of EF-Tu being used for non-translation purposes. Perhaps by "locking" CdiA-CT$^{O32:H37}$ and EF-Tu together in a stable complex, CdiI$^{O32:H37}$ completely prevents dissociation and thus tRNase activity. CdiI$^{O32:H37}$ is an interesting protein by itself, as it is a small, cysteine-rich peptide (6 of 81 residues) that coordinates an iron atom using 4 cysteines in a well-conserved fold (Argonne National Laboratory, preliminary data). An additional cysteine residue is located in a loop on the opposite face of the protein and could facilitate the formation of disulfide bridges or aid in multimerization. This is apparent during *in vitro* handling of this protein, as it readily forms dimers and multimers that are somewhat resistant to destabilization even in the presence of DTT and under SDS-PAGE gel conditions (Julia Willett and Christopher Hayes, unpublished data).

Regardless of the specific functional relationship between these CdiA-CTs, the toxins described in this chapter comprise a group of diverse proteins that interact with translational

machinery in different ways. Recent studies on type 6 secretion systems show that this interaction extends beyond the scope of CdiA-CT domains to other forms of bacterial inhibition. The type 6 secretion system (T6SS) effector Tse6 from *Pseudomonas aeruginosa* is a glycohydrolase that blocks cell growth by degrading NAD^+ and $NADP^+$ (262). In *P. aeruginosa* cells, Tse6 interacts with other T6SS proteins and, surprisingly, GDP-bound EF-Tu. Through analysis of crystal structures and activity assays, the authors concluded that EF-Tu is required for entry of this toxin into cells (262). This result is surprising, especially considering the syringe-like model of T6SS effector injection into target cells (240, 241, 243, 251). It was previously thought that T6SS toxins acting in the cytoplasm were injected through both membranes and released (240, 402), but the association of Tse6 with EF-Tu suggests that this delivery process may occur with some mechanistic subtleties, and that EF-Tu could help import Tse6 into the cytoplasm during delivery. Though not related to T6SS, another study using *P. aeruginosa* showed that a pool of methylated EF-Tu localizes to the cell membrane of this bacteria, where it is interacts with host epithelial cells during infection of the respiratory system (399).

Additional examples of non-canonical EF-Tu usage have been shown in other bacteria, as well. In the Gram-positive organism *Bacillus subtilis*, EF-Tu localizes to the inner face of the cell wall, where it interacts with the prokaryotic actin homolog MreB and influences the fidelity of cell shape (401). In *Francisella tularensis*, a subset of EF-Tu is found at the external face of the outer cell membrane, where it interacts with host-produced nucleolin during infection (400). Surface-bound EF-Tu from *Streptococcus pneumoniae* interacts with complement proteins, including Factor H and plasminogen, resulting in cleavage of fibrinogen, C3, and C3b and pathogen survival against host immune responses (403).

Involvement in bacterial inhibition systems is yet another example of a moonlighting function outside of the well-characterized functions typically associated with EF-Tu.

What is apparent from our studies is that EF-Tu and EF-Ts do not contribute to the delivery of toxins into the cytoplasm of target cells, based on experiments performed with our current understanding of translocation. This is in opposition to the T6SS effector Tse6, which requires EF-Tu for import into target cells (262). The preliminary data showing connections between a variety of toxins and translational machinery may be indicative of some evolutionary pressure or benefit conferred by these co-factors. This is interesting to consider in terms of toxin evolution, as these toxins have presumably never existed in an environment that contains CDI systems but lacks EF-Tu. Because these CdiA-CTs are tRNases, interacting with EF-Tu or EF-Ts would presumably position them near their substrates. The process of translation is conserved across all domains of life, and EF-Tu proteins are highly conserved throughout bacteria. Therefore, utilizing this protein as a co-factor or chaperone as opposed to a protein specific to *E. coli* or gammaproteobacteria would allow for a greater organismal diversity of theoretical targets. Cells would have virtually no chance to evolve resistance to EF-Tu/EF-Ts-dependent toxins without influencing some aspect of their own translation processes. Considering many elements of CDI systems are linked to horizontal gene transfer through their presence on genomic or pathogenicity islands (170), perhaps using an essential, well-conserved protein co-factor enables them to seamlessly adapt to transfer across species without loss of activity.

Many questions about the specific relationship between CdiA-CTs, EF-Tu, and EF-Ts remain to be answered. However, it can be concluded that a subset of toxins associated with diverse bacterial inhibition systems have evolved to use translational machinery for activity.

These co-factors may help delivered toxins efficiently find their target in the complex cytoplasmic milieu. Future biochemical and structural studies will be needed to precisely delineate the contribution of these translational components to the specific inhibitory activities of CdiA-CTs.

D. Materials and Methods

1. Plasmid construction

All strains, plasmids, and cosmids are listed in Table 2. Oligonucleotide sequences are listed in Table 3. All plasmids and cosmids were verified by sequencing (University of California, Berkeley). Strains containing *tsf* mutations were a gift from Allison Jones and David Low (University of California, Santa Barbara). The pUC57 plasmid constructs used as template DNA for the amplification of CdiA-CT/CdiI modules was graciously provided by Argonne National Laboratory (Darien, IL). Plasmid-borne chimeric CDI systems were constructed by allelic exchange of the counter selectable *pheS** marker from plasmid pCH10163 as described previously (177). The various cdiA-CT/cdiI sequences were amplified by PCR by using the following primer pairs: *Escherichia coli* 97.0246, CH3562/CH3564; *E. coli* DEC9E, CH3562/CH3563; *E. coli* EC1738, CH3565/CH3566; *E. coli* EC869, CDI209/CDI208; *E. coli* EC93 *cdi*2, CH3822/CH3823; *E. coli* STEC_O31, CH3176/CH3569; *E. coli* O32:H37, CH3567/CH3568; *Dickeya dadantii* CT2, CH3513/CH3514; *D. dadantii* CT3, CH3515/CH3516; *Klebsiella pneumoniae* 342, CH3517/CH3518; *Yersinia intermedia*, CH3745/CH3746; *Y. mollaretti*, CH3747/CH3748; and *Providencia alcalifaciens*, CH3743/CH3744. The *E. coli* O32:H37 H71A mutation was constructed by amplifying the N-terminal sequence of CdiA-CT$^{O32:H37}$ with primers CH3567 and CH3897. This fragment was purified and fused to the rest of the CdiA-CT/CdiI coding

sequence via megaprimer PCR using primer CH3568. Each *cdiA-CT*/*cdiI* fragment was fused to upstream and downstream homology regions amplified from the $cdiA^{EC93}$ gene. The $cdiA^{EC93}$ upstream homology fragment was amplified by using primers DL1527/DL2470, and the downstream fragment was amplified with primers DL1663/DL2368. The three products (*cdiA-CT*/*cdiI*, upstream $cdiA^{EC93}$, and downstream $cdiA^{EC93}$) were then fused to each other through overlapping-end PCR (OE-PCR) by using primers DL1527/DL2368. The final DNA product (100 ng) was electroporated together with plasmid pCH10163 (300 ng) into *E. coli* strain DY378 cells as described previously (11). Clones with recombinant plasmids were selected on yeast extract glucose-agar supplemented with 33 μg/mL chloramphenicol and 10 mM d/l-p-chlorophenylalanine. The *Dickeya zeae* 1594 chimera was a gift from Grant Gucinski, the *Yersinia kristensii* 33638 chimera was a gift from Greg Ekberg, and the *E. coli* 536/*Ruminococcus lactaris* chimera was a gift from Christina Beck (University of California, Santa Barbara).

Constructs for overexpression and purification of proteins were constructed as follows. The CdiA-CT/CdiI module from *Klebsiella pneumoniae* 342 was amplified with primers CH3962 and either CH3685 (for construction of His6-tagged pET21 constructs) or CH3570 (for constructs with a native immunity gene). The PCR products were treated with appropriate restriction endonucleases (NcoI/SpeI for the CH3962/CH3685 PCR product and KpnI/XhoI for the CH3962/CH3570 PCR product) and were ligated to pET21 plasmid vectors that had been treated with the same enzymes. $cdiI^{Kp342}$ was amplified using primers CH3965 and CH3685. PCR products were digested with KpnI and SpeI and were ligated to a pET21 backbone treated with the same enzymes. The CdiA-CT/CdiI module from *E. coli* O32:H37 was amplified using primer CH3896 and either CH3898 (for constructs with a C-

terminal His6 tag) or CH3571 (for native immunity sequences). The CH3896/CH3898 PCR product was treated with NcoI and SpeI and was ligated to a pET21b vector treated with the same enzymes. The CH3896/CH3571 PCR product was treated with KpnI/XhoI and ligated to a KpnI/XhoI-treated pET21 vector. $CDI^{O32:H37}$ variants carrying the His71Ala mutation were amplified from pCH12768 and treated with the same restriction endonucleases for cloning. pET21b plasmids were used as vectors for all constructs carrying C-terminal His6 tags or N-terminal His6-TrxA fusions. The kanamycin-resistant pET21db plasmid was used to fuse N-terminal His10 tags, where appropriate. The native $cdiI^{O32:H37}$ construct was amplified using primers CH3603 and CH3571, digested using KpnI/XhoI, and ligated to a pTrc99AKX backbone. The CdiA-CT/$CdiI^{NC101}$ expression construct used for *in vitro* activation growth curves was a gift from Grant Gucinski.

2. Transposon mutagenesis and isolation of mutants

The *mariner* transposon was introduced into *E. coli* CH10229 cells through conjugation with *E. coli* MFDpir donor cells carrying plasmid pSC189. Donor and recipient cells were grown to mid-log phase in lysogeny broth (LB) medium supplemented with 150 µg/mL ampicillin and 30 µM diaminopimelic acid (donors) or 33 µg/mL chloramphenicol (recipients). Donors (~6.0×10^8 cfu) and recipients (~3×10^8 cfu) were mixed and collected by centrifugation for 2 min at 6,000 × g in a microcentrifuge. The supernatant was removed by aspiration and the cell pellet resuspended in 100 µL of 1× M9 salts. Cell mixtures were spotted onto 0.45-µm nitrocellulose membranes, and the filters were then incubated on LB agar (without inversion) for 4 h at 37 °C. The cells were then harvested from the filters by using 2 mL of 1× M9 salts. Transposon insertion mutants were selected by plating 10-fold serial dilution on LB-agar supplemented with 50 µg/mL of kanamycin.

More than 20,000 colonies from each transposon library were collected from the agar plates in 1× M9 salts and inoculated into 50 mL of LB medium in a 250-mL baffled flask. CDI^+ inhibitor strains were grown in a parallel 50 mL LB medium culture. Both cultures were grown at 37 °C until mid-log phase, then mixed at approximately a 10:1 ratio and cultured for 3 h with shaking at 37 °C. Viable target cells from the transposon mutant library were enumerated as cfu counts per milliliter on LB agar supplemented with 50 μg/mL of kanamycin. The survivors of the first round of CDI competition were harvested from the plates with 1× M9 salts and used to inoculate 50 mL LB medium culture for a second round of CDI selection; this process was repeated to yield a third round of competition. Individual clones were then isolated and the CDI^R phenotype confirmed in competition co-cultures. The transposon mutations were then transferred into CDI-sensitive cells by bacteriophage P1-mediated transduction, and the resulting transductants were tested for a CDI^R phenotype.

Transposon insertion locations were identified using a two-step arbitrary PCR procedure. In the first set of reactions, CH2255/CH2020, CH2258/CH2020, CH2255/CH2022, and CH2258/CH2022 were with chromosomal DNA templates isolated from target mutant clones used to amplify the transposon/chromosome junctions. The second set of PCRs used the first PCR products as templates along with primer pairs CH2256/CH2021 (for reactions done with CH2255) and CH2259/CH2021 (for reactions done with CH2258) to selectively amplify only DNA fragments containing the transposon. Sequencing reactions were performed with primers CH2257 (for reactions done with primers CH2255 and CH2256) and CH2270 (for reactions were done with primers CH2258 and CH2259). Nucleotide sequencing reads were mapped to the *E. coli* reference genome using NCBI BLAST to identify genomic locations of transposon insertions.

3. Growth competition assays

Competition co-culture assays were carried out as previously described (175, 177). Briefly, inhibitor cells (*E. coli* EPI100 carrying CDI expression constructs) and target cells (*E. coli* MC4100 carrying pTrc99a derivatives) were grown in LB medium supplemented with appropriate antibiotics overnight at 37 °C. The next day, cells were inoculated into fresh LB medium without antibiotics in baffled flasks. Individual cultures were grown with shaking until early log phase, and then the populations were mixed at a 1:1 ratio in fresh pre-warmed LB in baffled flasks. A sample of each co-culture was taken at initial mixing to enumerate viable target cells as cfu counts per milliliter. The co-cultures were incubated with shaking for 3 h at 37 °C. Viable target cell counts are presented as the average ± SEM of three independent competition experiments.

4. Activation of CdiA-CT toxins inside E. coli *cells*

E. coli MG1655 cells (WT and *tsf* mutants) were co-transformed with an empty pTrc99a vector or a derivative expressing *cdiI*^{NC101} and empty pCH450 or a derivative that expresses the CdiA-CT/CdiI^{NC101}-DAS protein pair. Transformants were selected overnight on LB agar supplemented with 150 µg/mL Amp, 15 µg/mL Tet, and 0.4% glucose. The following day, transformants were inoculated into 25 mL of LB medium supplemented with Amp and Tet, and glucose. Cells were grown to mid-log phase and then diluted to an OD600 of 0.05 in fresh LB supplemented with Amp and Tet to allow low levels of expression from both plasmids. Cell growth was monitored by measuring the OD600 of the culture every 30 min for 5 h. The presented growth curves show the average ± SEM for three independently performed experiments.

5. Protein purification

Cells carrying pET21 derivatives (CH2016 carrying pET21b constructs or CH6247 carrying pET21db constructs) were grown in baffled flasks with shaking at 37 °C in LB medium with 50 μg/mL kanamycin or 150 μg/mL ampicillin until OD_{600} 0.4-0.6, at which point 1.5 mM isopropyl β-D-1-thiogalactopyranoside (IPTG) was added to induce protein expression for ~3 hours before harvesting. Cells were pelleted by centrifugation in a Sorvall RC 5B centrifuge at 6,000 rpm for 15 min at 4 °C, and pellets were stored at -80 °C for future use. Cells overexpressing His6-tagged immunity proteins and CdiA-CT/CdiI complexes with C-terminal His6 tags were resuspended in non-denaturing buffers (20 mM sodium phosphate (pH 7.0), 150 mM NaCl, and 1 mM PMSF or 20 mM Tris-HCl (pH 7.0), 150 mM NaCl, and 1 mM PMSF) and were lysed using a French press (2 passes at 20,000 psi). Lysates were cleared by centrifugation (15,000 × g in a Sorvall RC 5B centrifuge at 4 °C) and were mixed with nickel agarose beads (1 uL Ni^{2+}-NTA resin per 1 mL of original culture volume) for 1 h at 4 °C. Resin was washed with resuspension buffer supplemented with 20 mM imidazole (pH 8.0), and His6-tagged proteins were eluted using resuspension buffer plus 250 mM imidazole (pH 8.0). Elution fractions were immediately dialyzed against 2 liters of resuspension buffer and were quantified after dialysis by measuring absorbance at 280 nm.

Denaturing urea lysis buffer (8 M urea, 150 mM NaCl, 10 mM Tris-HCl (pH 8.0), 1 mM PMSF) was used to resuspend cell pellets from cultures overexpressing constructs with N-terminal His6 or His6-TrxA epitopes fused to CdiA-CTs. Cells were broken with a freeze-thaw cycle at -80 °C. Lysates were cleared and applied to Ni^{2+}-NTA resin as described above. Wash steps were performed with urea lysis buffer supplemented with 20 mM imidazole, and proteins were eluted into urea lysis buffer plus 250 mM imidazole. Proteins

were refolded against 2 liters of non-denaturing resuspension buffer quantified by measuring absorbance at 280 nm.

6. Protein-protein interaction assays

Binding interactions between CdiA-CT domains, CdiI proteins, EF-Tu, and EF-Ts were assessed by bait-prey assays. Proteins fused to His6 or His6-TrxA epitopes were used as "bait" (tagged constructs labeled in all figures). Untagged "prey" proteins were added to a final concentration of 5 uM in reaction buffer for 30 min at 4 °C. An "input" aliquot was removed for analysis via SDS-PAGE, and Ni^{2+}-resin was added for 1 h at 4 °C to trap tagged proteins and any *in vitro* complexes that formed during the incubation. Tubes were centrifuged at 3000 rpm for 5 minutes in a tabletop centrifuge to collect the Ni^{2+}-NTA beads, and the supernatant was removed as the "unbound" fraction. Resin was washed 4 times with reaction buffer plus 20 mM imidazole, and "bound" proteins were eluted into reaction buffer supplemented with 250 mM imidazole. All fractions were analyzed by SDS-PAGE (10% acrylamide at 110 V for 1 h, unless otherwise indicated) and stained with Coomassie brilliant blue dye.

7. RNA isolation and analysis

Cultures of *E. coli* X90 cells in logarithmic phase (OD_{600} 0.4 – 0.6) were flash-fixed in ice-cold methanol, and cells were collected by centrifugation in a Sorvall RC 5B centrifuge at 15,000 × g for 15 min at 4 °C. Cell pellets were frozen at −80 °C, and RNA was isolated by guanidine isothiocyanate-phenol extraction as described previously (379). 10 μg of this total RNA preparation was mixed with the indicated concentrations of purified proteins an reaction buffer for 1 h at 37 °C, and the reactions were once again extracted with guanidine isothiocyanate-phenol to remove protein species before electrophoresis. RNA was resolved

on denaturing 8 M urea/10% (wt/vol) polyacrylamide gels and then electrotransferred onto nylon membrane (Nytran Supercharge). The indicated RNA species were detected by Northern blot hybridization by using radiolabeled oligonucleotides as probes. Blots were visualized on a Bio-Rad PhosphorImager by using Quantity One software.

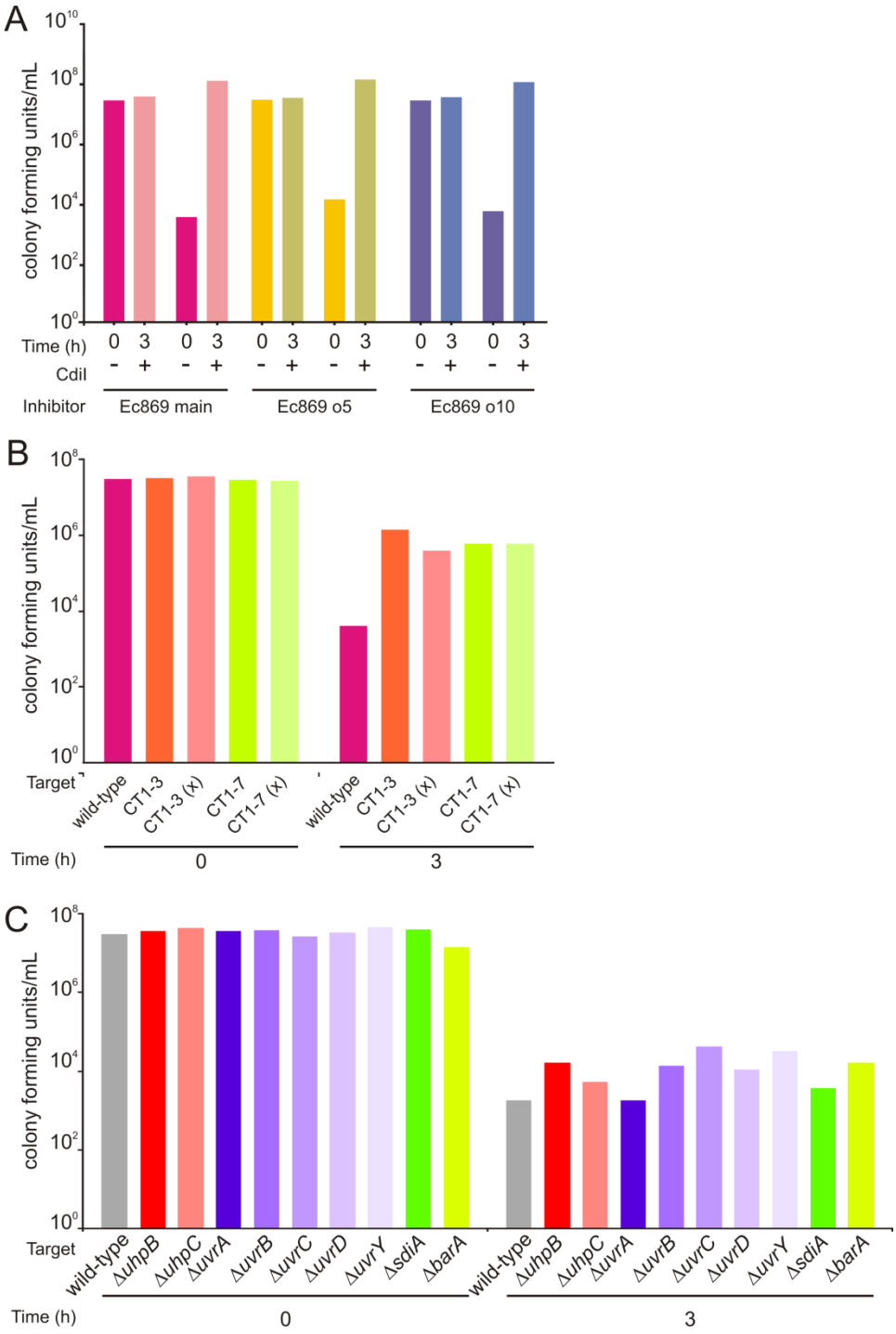

Figure 1. Transposon mutagenesis fails to produce strains resistant to three CdiA-CT toxins from *E. coli* EC869. (A) CDI^{EC869}, CDI_{o5}^{EC869}, and CDI_{o10}^{EC869} and their corresponding CdiI proteins are functional toxin/immunity complexes. Inhibitor cells expressing each cosmid were mixed with wild-type cells or targets expressing the cognate immunity. Viable target cells were scored at 0 and 3 h. (B) Mutants isolated after 3 rounds of enrichment co-cultures with CDI^{EC869} are partially CDI^{R}. Transposons were moved into fresh cell backgrounds to test genetic linkage (targets labeled with "x" are transductants). (C) Clean knockouts of *uhpB*, *uvrY*, and related genes were tested for resistance to CDI^{EC869}. Target cell viability was measured at 0 and 3 h.

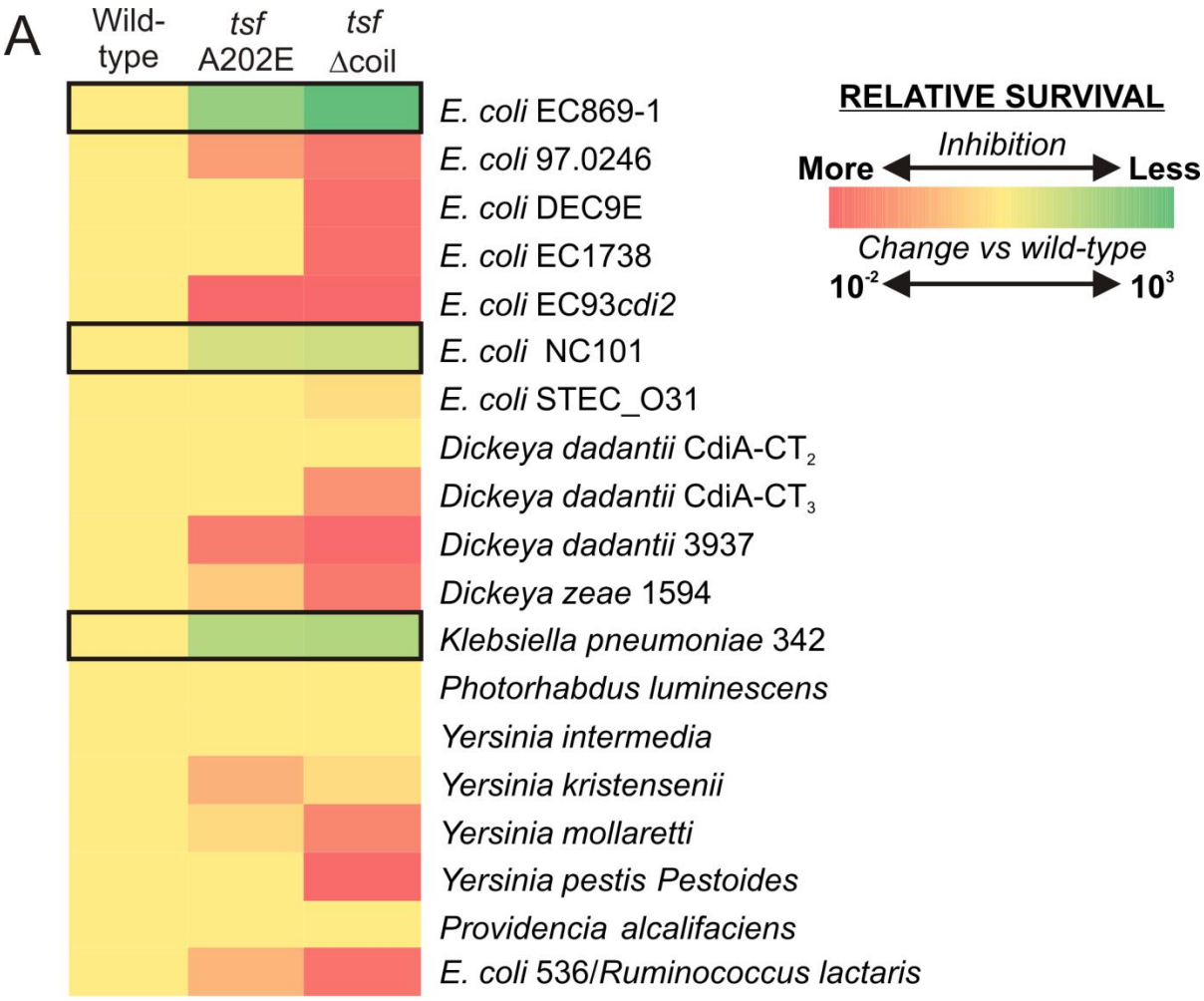

B

EC869	100%			
NC101	8.23%	100%		
96.154	7.79%	7.79%	100%	
Kp342	13.25%	9.09%	4.16%	100%
	EC869	NC101	96.154	Kp342

Figure 2. CDI^{Kp342} does not inhibit *tsf* mutants. (A) For the 19 toxins tested, the relative inhibition of wild-type cells compared to *tsf* mutants (genotypes indicated at the top of the table) were color-coded such that green indicates higher viability and red indicates more inhibition. Wild-type viability values were adjusted to 1 for each set of co-culture assays. (B) Pairwise identity comparisons were performed to determine conservation between toxins that require wild-type EF-Ts for inhibition. Protein sequences were aligned using Clustal Omega, and pairwise comparison values were calculated using the SIAS pairwise alignment server (found at http://imed.med.ucm.es/Tools/sias.html).

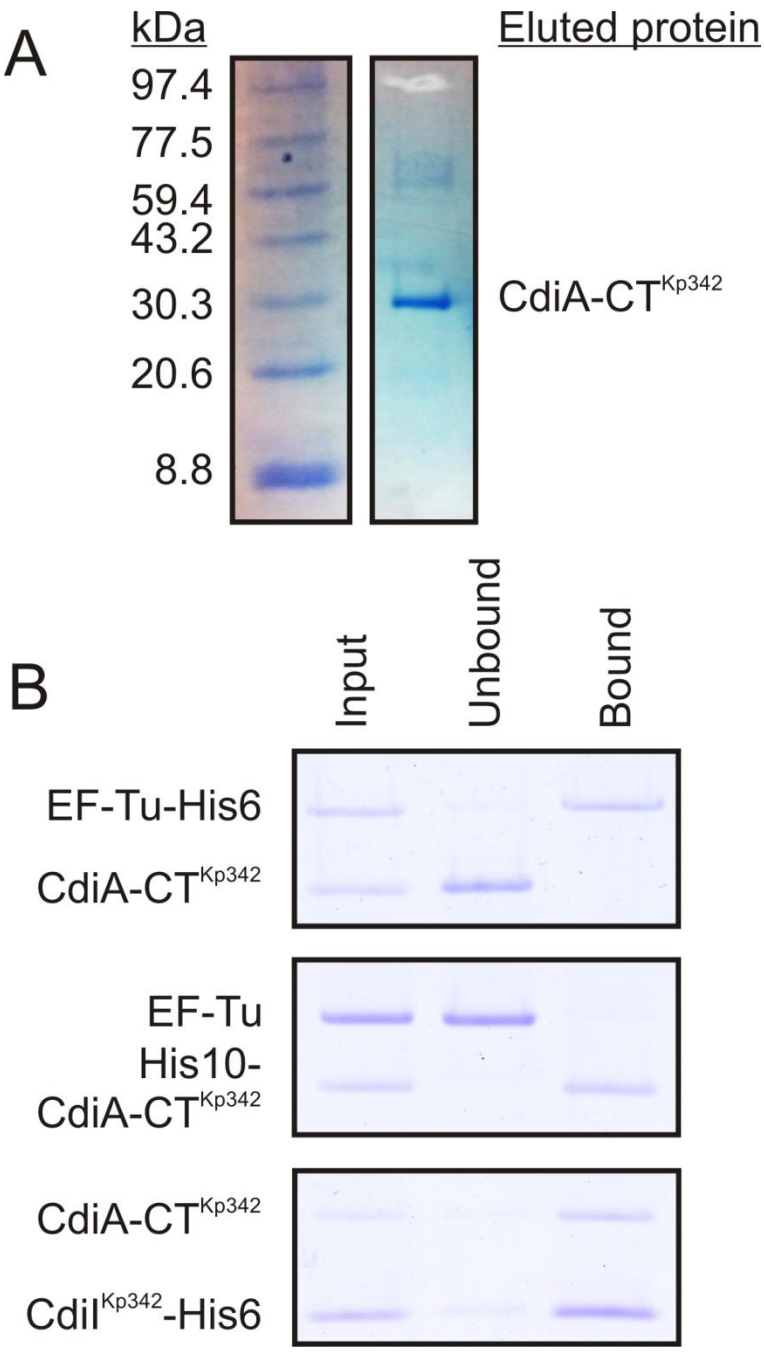

Figure 3. CdiA-CT^{Kp342} does not interact with EF-Tu or EF-Ts *in vitro*. (A) The CdiA-CT/CdiI^{Kp342}-His6 complex was natively purified and bound to nickel agarose beads. CdiA-CT^{Kp342} and any bound co-factors were eluted with denaturing washes and analyzed via SDS-PAGE. (B) Tagged and untagged variants of CdiA-CT^{Kp342} and EF-Tu were used for bait-prey assays. To show proper re-folding of CdiA-CT^{Kp342} after purification, a binding assay with this protein and CdiI^{Kp342}-His6 was performed.

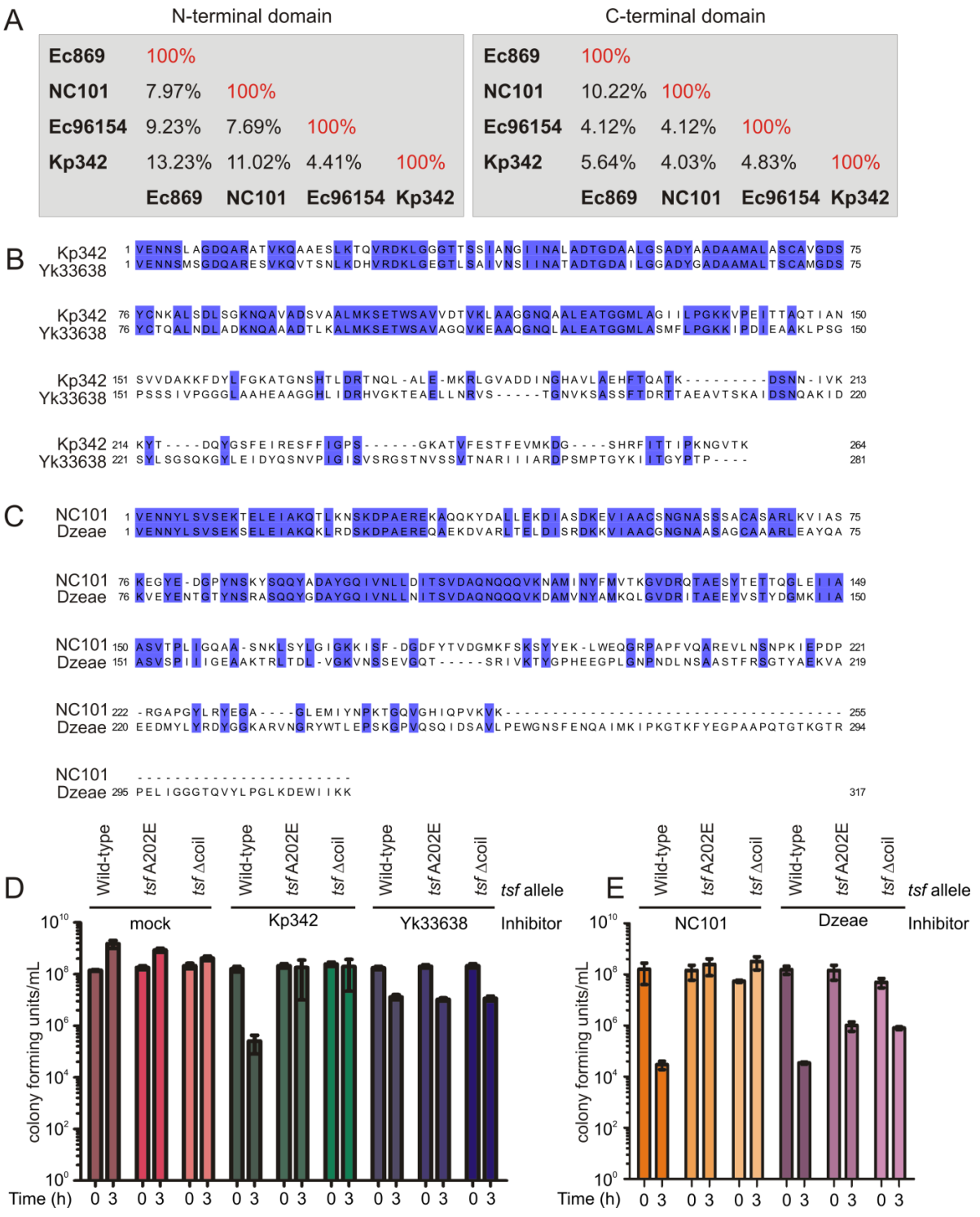

Figure 4. Mutations in *tsf* do not contribute to translocation of CdiA-CTs. (A) Pairwise comparisons of the N- and C-terminal domains of *tsf*-dependent CdiA-CTs reveal little conservation in either region. Sequence alignment of (B) CdiA-CT^{Kp342} and CdiA-CT^{Yk33638} and (C) CdiA-CT^{NC101} and CdiA-CT^{Dzeae} show conservation in the N-terminal translocation domains. The toxin domains aligned in (B) and (D) were fused to CdiA and delivered into the target cells indicated in (D) and (E) during co-culture assays. Target cell viability was measured at 0 and 3 hours. Data represented the mean of three independent experiments ±SEM.

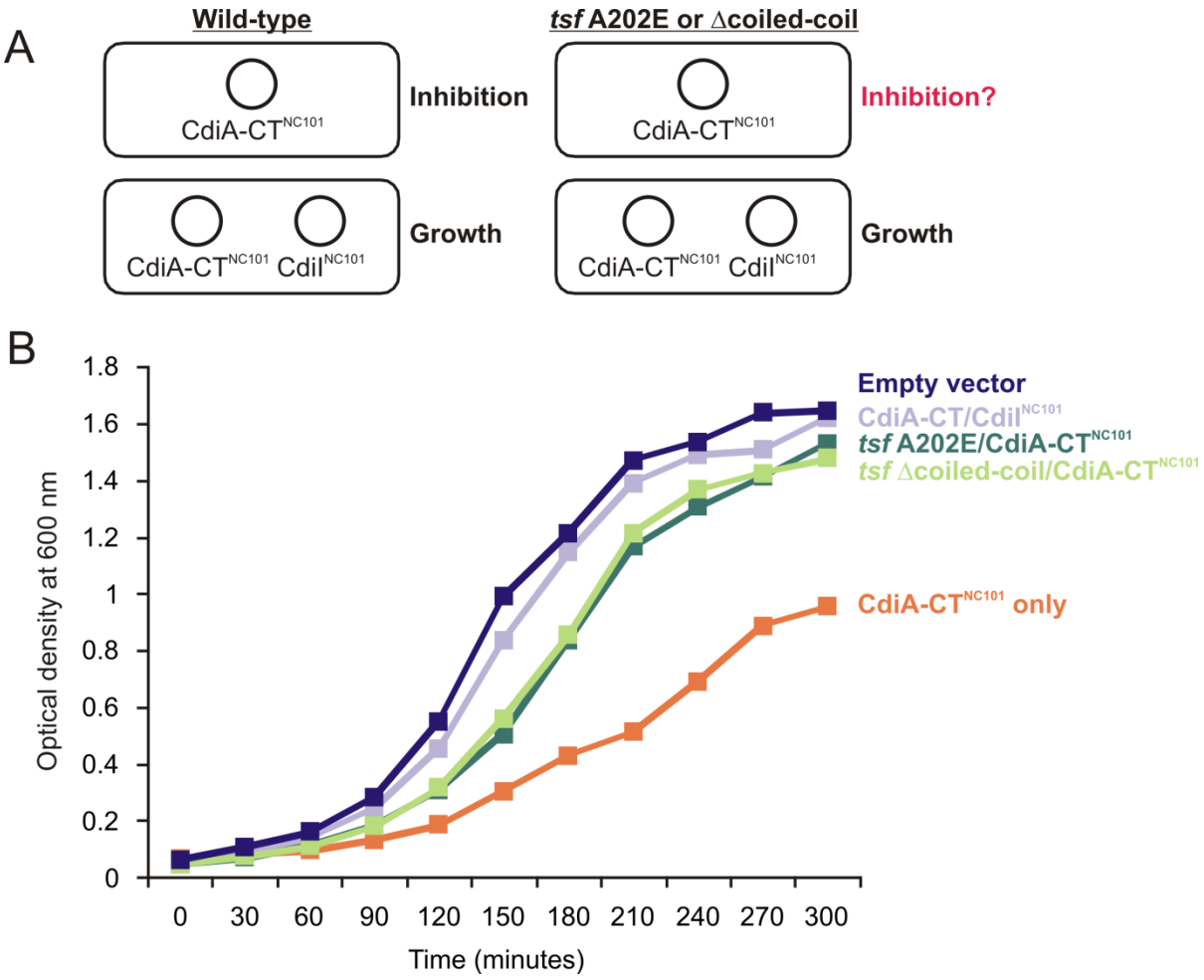

Figure 5. Wild-type EF-Ts is required for intracellular activity of CdiA-CT^{NC101}. (A) Experimental design. Plasmids expressing CdiA-CT^{NC101} or CdiI^{NC101} are expressed inside wild-type and *tsf* mutant *E. coli* background to decouple delivery from activity. (B) Cell densities as measured by OD_{600}. Intracellular expression of CdiA-CT^{NC101} inhibits wild-type *E. coli* (orange line) as compared to growth of a strain carrying empty plasmid vectors (dark purple line, top). Expression of the immunity gene rescues growth (light purple line compared to orange line). Expression of the toxin permits growth in both *tsf* mutant backgrounds (light and dark green lines).

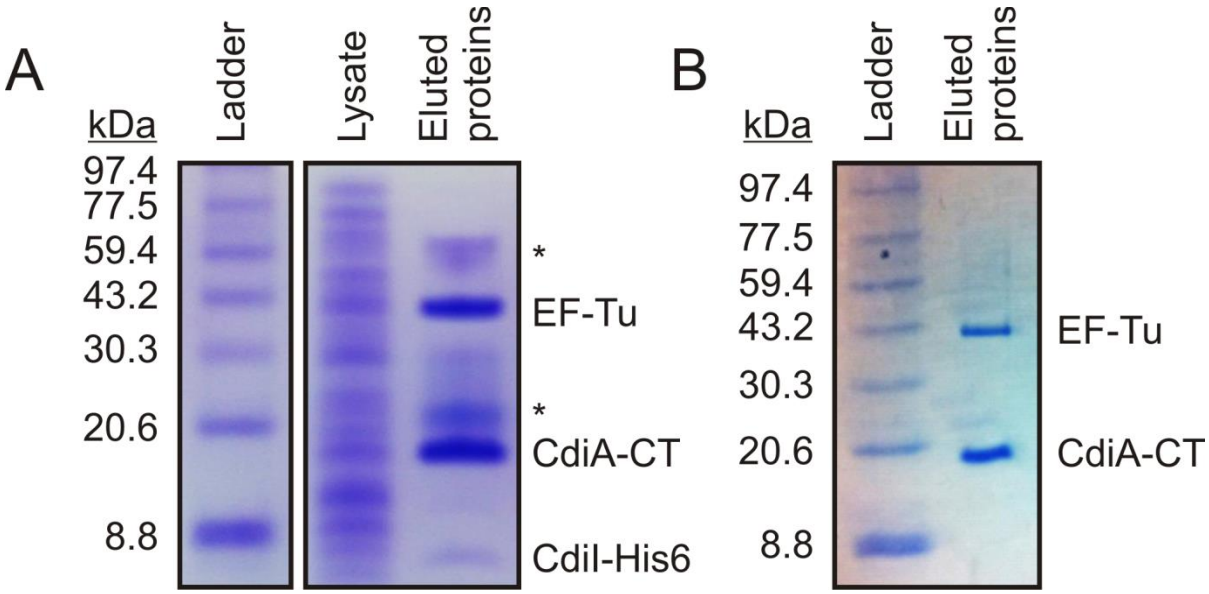

Figure 6. CdiA-CTO32:H37 co-purifies with EF-Tu. (A) The CdiA-CT/CdiI$^{O32:H37}$ module was expressed as a complex inside cells and purified under native conditions using a C-terminal His6 tag fused to CdiI$^{O32:H37}$. An aliquot of the purified fraction was analyzed via SDS-PAGE. The major CdiA-CT, CdiI, and EF-Tu species are labeled. Bands marked with an asterisk (*) are presumably dimers and multimers of CdiI$^{O32:H37}$-His6. In (B), the same CdiA-CT/CdiI$^{O32:H37}$-His6 complex was expressed inside cells and was bound to nickel-agarose beads under native conditions. Denaturing conditions in 6M guanidine buffer were done to denature CdiA-CT$^{O32:H37}$ and any associated proteins.

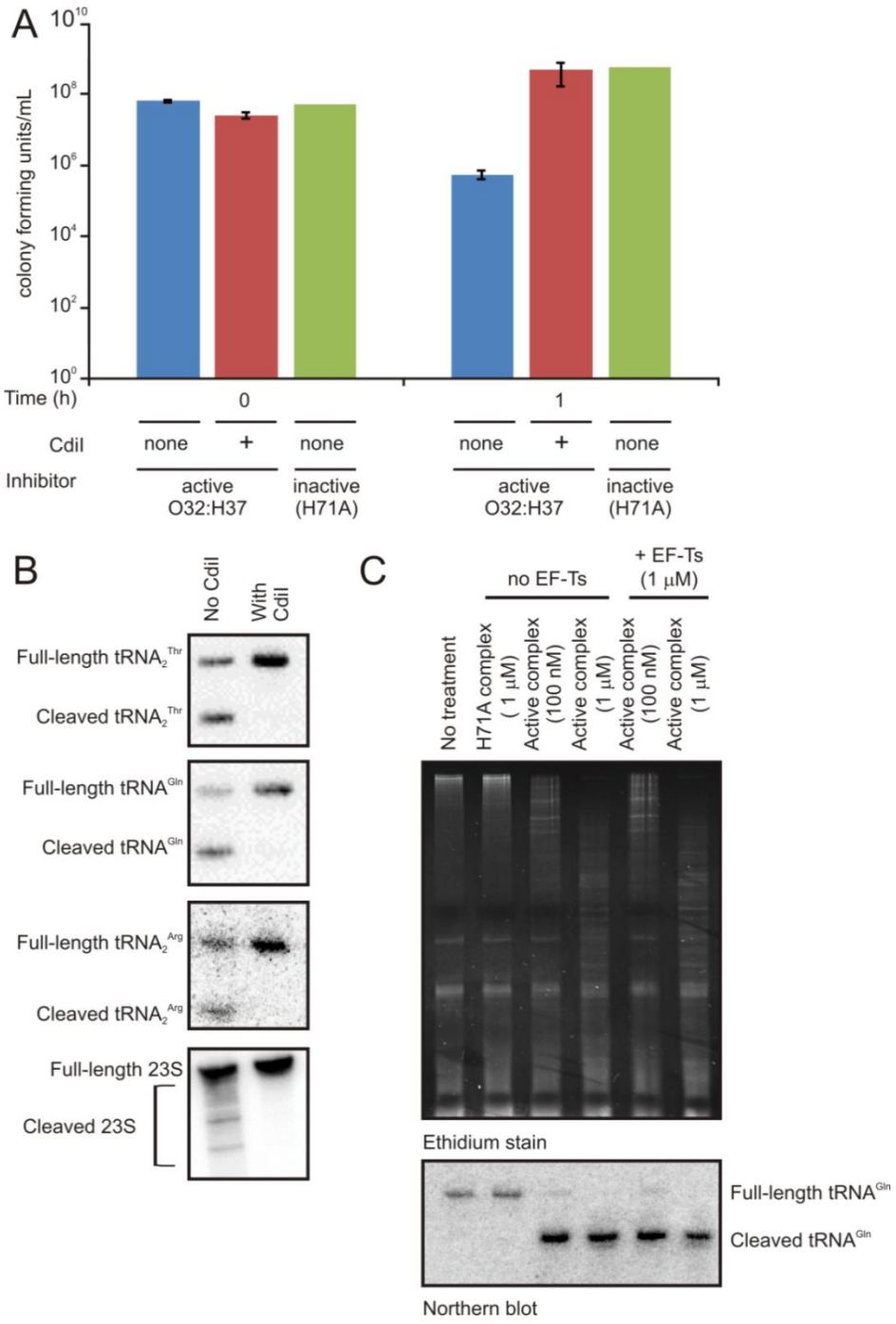

Figure 7. CdiA-CTO32:H37 is an RNase. (A) Cells expressing wild-type CDI$^{O32:H37}$ or a variant at the putative active site residue H71A were used in co-culture assays with target cells carrying the indicated empty vector or *cdiI* constructs. Target cell viability was measured at 0 and 1 h. Disrupting the histidine at position 71 ablates activity. (B) CDI$^{O32:H37}$ cleaves RNA in co-culture assays with target cells. Total RNA was harvested from the competitions shown in (A) and analyzed via Northern blots using probes to the indicated tRNA and rRNA species. The sizes of full-length and cleaved RNA products are indicated. (C) The CdiA-CT$^{O32:H37}$/EF-Tu complex was purified under denaturing conditions and refolded before mixing with total guanidine isothiocyanate-extracted cellular RNA *in vitro.* Samples were split into equal parts for ethidium staining and Northern blot analysis.

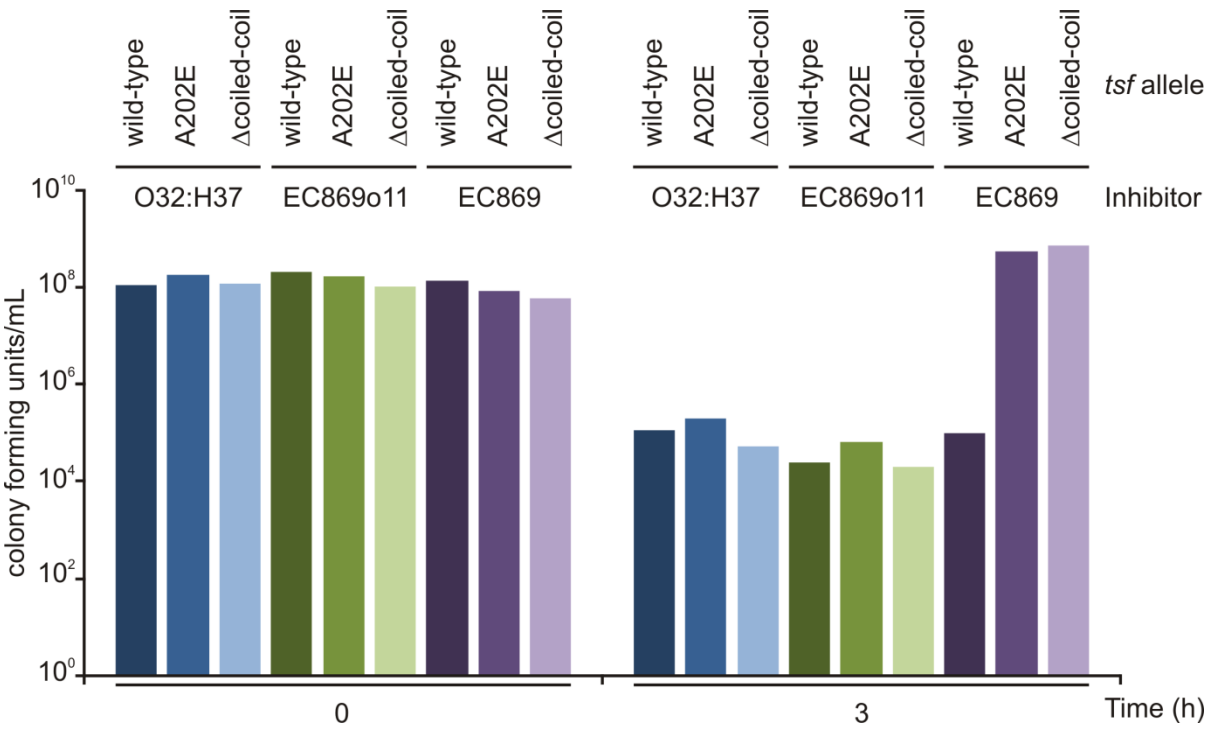

Figure 8. CDI$^{O32:H37}$ inhibition of target cells is not affected by mutations in EF-Ts. Inhibitor cells carrying CDI$_+$ cosmids as labeled were mixed with target cells with the indicated target cells. Viable target cells were measured at 0 and 3 h. Data presented is representative of 2 independent experiments.

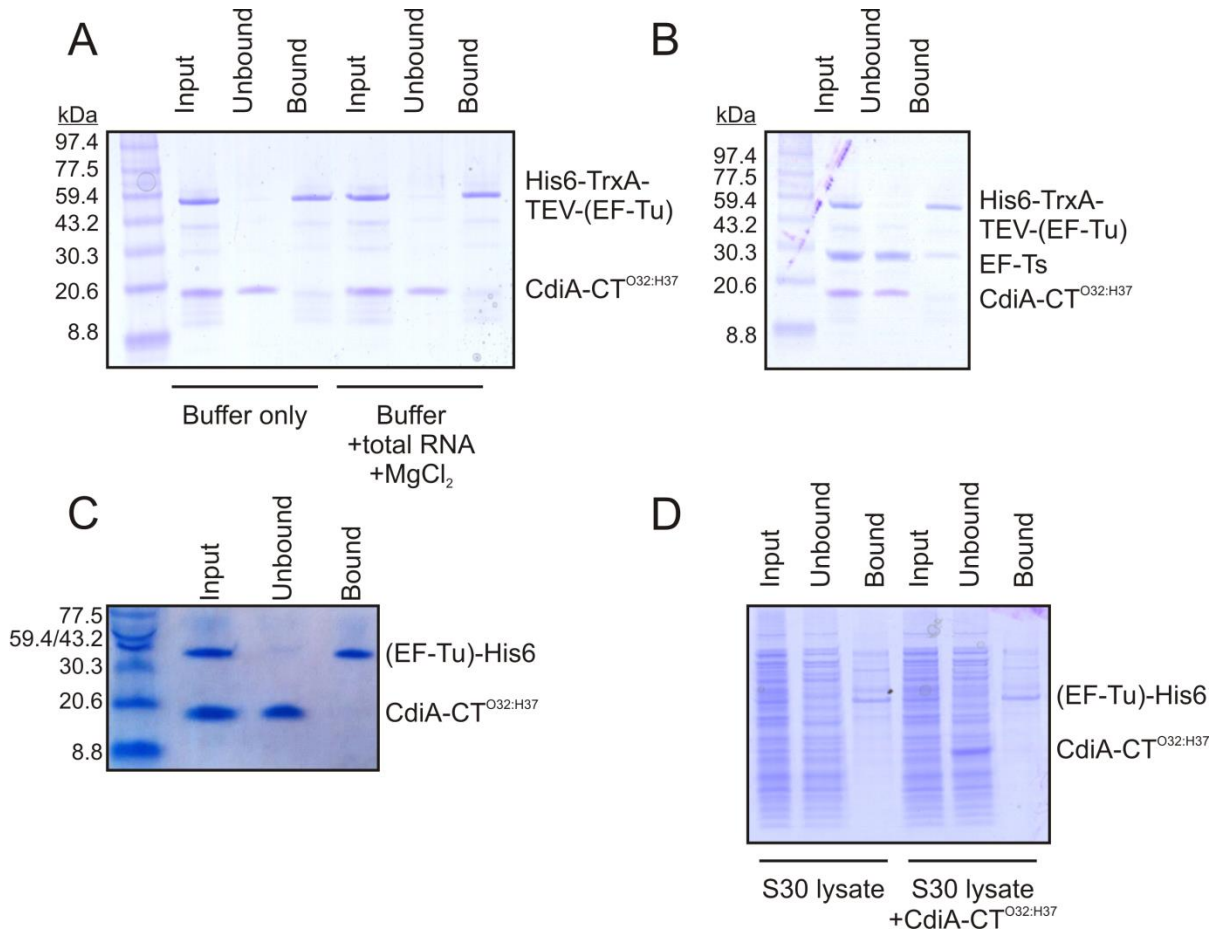

Figure 9. CdiA-CT$^{O32:H37}$ does not interact with EF-Tu or EF-Ts *in vitro*. (A) Purified CdiA-CT$^{O32:H37}$ and His6-TrxA-TEV-(EF-Tu) were mixed together in the absence or presence of $MgCl^{2+}$ and total purified RNA. (B) The protein constructs used in (A) were mixed with EF-Ts to test whether the presence of EF-Ts facilitated complex formation. (C) An EF-Tu construct with a C-terminal His6 tag and no extra N-terminal domain was mixed with purified CdiA-CT$^{O32:H37}$ *in vitro*. (D) A whole-cell S30 lysate from cells expressing a C-terminal His6-tagged EF-Tu construct was mixed with CdiA-CT$^{O32:H37}$, and (EF-Tu)-His6 was selectively removed from the lysate using nickel agarose beads.

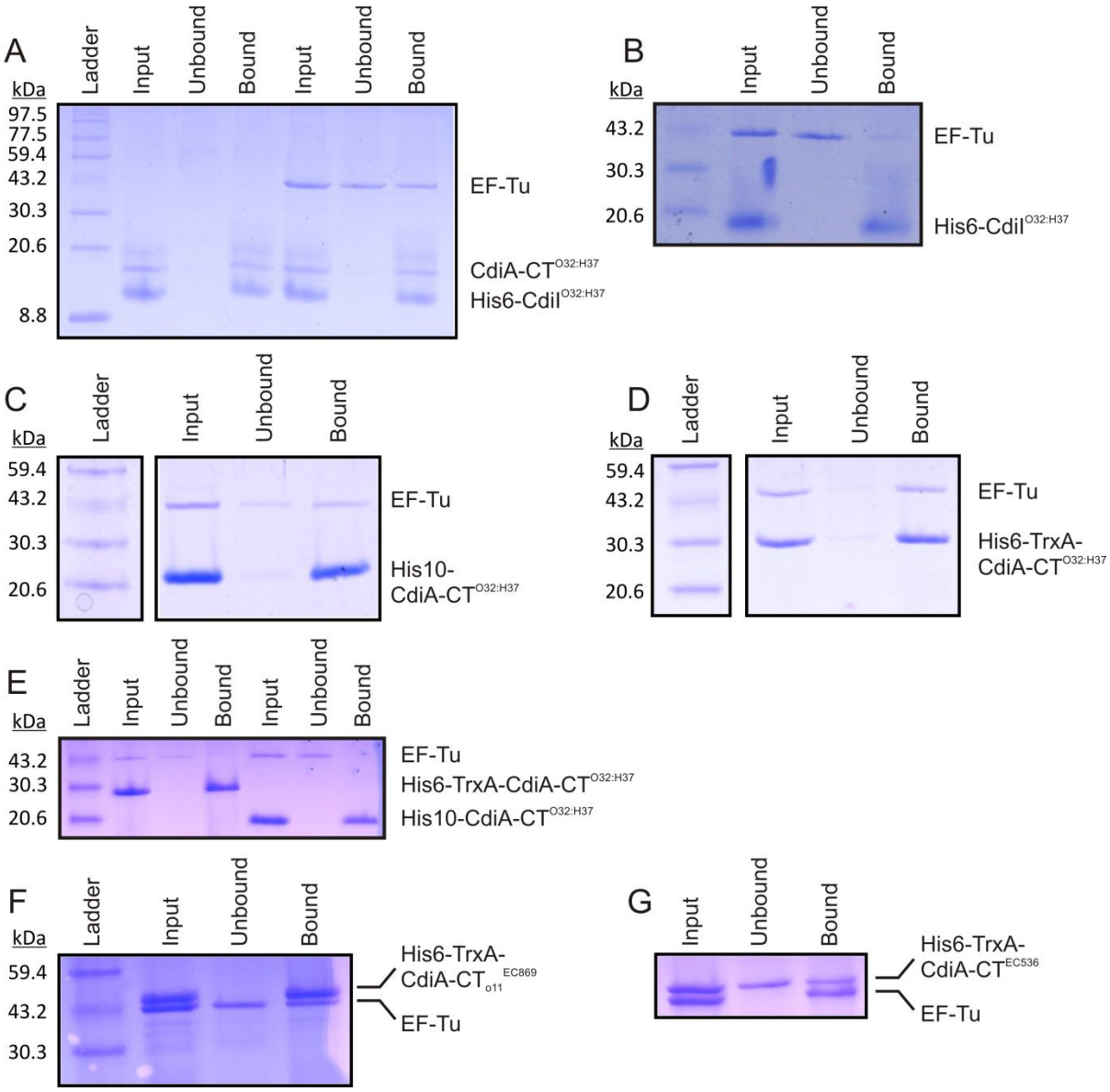

Figure 10. EF-Tu may be involved in binding both CdiA-CT$^{O32:H37}$ and CdiI$^{O32:H37}$ or in chaperoning the folding of CdiA-CT$^{O32:H37}$ upon delivery into cells. (A) CdiA-CT$^{O32:H37}$ and CdiI$^{O32:H37}$ interact *in vitro*, and a ternary complex is formed in the presence of EF-Tu. (B) His6-CdiI$^{O32:H37}$ and EF-Tu do not interact *in vitro* in the absence of CdiA-CT$^{O32:H37}$. Purified His10-CdiA-CT$^{O32:H37}$ (C) and His6-TrxA-TEV-CdiA-CT$^{O32:H37}$ (D) interact with EF-Tu when unfolded and dialyzed in the presence of native EF-Tu. The same denatured protein preparations used in (C) and (D) were folded away from EF-Tu and used in parallel binding assays as shown in (E). As negative controls, CdiA-CT$_{o11}^{EC869}$ (F) and CdiA-CT^{Ec536} (G) – which do not interact genetically with *tsf* nor do they require EF-Tu or EF-Ts for *in vitro* activity – were unfolded and refolded in the presence of EF-Tu before being subjected to a pulldown assay using nickel agarose beads.

Table 1. CdiA-CTs tested for genetic interaction with *tsf*.

Organism	***Activity***
E. coli 97.0246	Unknown
E. coli DEC9E	Unknown
E. coli EC1738	Unknown
E. coli EC869-1	tRNase, specific for $tRNA^{Gln}$ (172)
E. coli EC93*cdi*2	Unknown
E. coli NC101	tRNase (Grant Gucinski and Christopher Hayes, unpublished data)
E. coli STEC_O31	RNase (Julia Willett and Christopher Hayes, unpublished data)
Dickeya dadantii CdiA-CT_2	Unknown
Dickeya dadantii CdiA-CT_3	Unknown
Dickeya dadantii EC3937	DNase (194)
Dickeya zeae 1594	Unknown
Klebsiella pneumoniae 342	Unknown
Photorhabdus luminescens TTO1	DNase (Julia Willett and Christopher Hayes, unpublished data)
Yersinia intermedia	Unknown
Yersinia kristensenii	General RNase (Greg Ekberg, Grant Gucinski, Celia Goulding, and Christopher Hayes, unpublished data)
Yersinia mollaretti	Unknown
Yersinia pestis Pestoides A	Unknown
Providencia alcalifaciens	Unknown
E. coli 536/*Ruminococcus lactaris*	tRNase, general (Christina Beck and Christopher Hayes, unpublished data)

Table 2. Bacterial strains and plasmids used in this study.

Strain	***Description[a]***	***Reference***
X90	F´ *lacI*^{q} *lac´ pro´/ara* Δ*(lac-pro) nal1 argE*(amb) *rif*^{r} *thi-1*, Rif^R	
EPI100	F$^-$ *mcrA* Δ*(mrr-hsdRMS-mcrBC) φ80dlacZ*Δ*M15* Δ*lacXcZ*Δ*M15* Δ*lacX recA1 endA1 araD139* Δ*(ara, leu)7697 galU galK* λ$^-$ *rpsL nupG pir*$^+$*(DHFR)*, Str^R Tp^R	Epicentre
MG1655	F$^-$ λ$^-$ *ilvG*$^-$ *rfb-50 rph-1*	
CH2016	X90 (DE3) Δ*rna* Δ*slyD::kan*, Kan^R	
CH8251	MC4100 rif^r, Rif^R	(173)
DL8705	MG1655 ara::spec, *araBAD* genes replaced by a spectinomycin resistance cassette	Allison Jones and David Low
DL8730	MG1655 ara::spec *tsf* Ala202Glu, *araBAD* genes replaced by a spectinomycin resistance cassette and single point mutation in codon 202 of *tsf* changing alanine to glutamic acid	Allison Jones and David Low
DL8731	MG1655 ara::spec *tsf* Δcoiled-coil, *araBAD* genes replaced by	Allison

	a spectinomycin resistance cassette and clean deletion of the coiled-coil domain (helixes 10 and 11) in *tsf*	Jones and David Low
Plasmid	***Description[a]***	***Reference***
pCH481	pET21b, cloning vector, Amp^R	
pCH1272	pET24db*::relE*, cloning vector, Amp^R	Dan Bolon
pCH1417	Constitutive expression of chimeric *cdiA*^{EC93}-*CT*$^{Y.\ Pestoides\ A}$ and *cdiI*$^{Y.\ Pestoides\ A}$ genes, Cm^R	
pCH2260	Constitutive expression of chimeric *cdiA*^{EC93}-*CT*$^{97.0246}$ and *cdiI*$^{97.0246}$genes, Cm^R	This study
pCH2261	Constitutive expression of chimeric *cdiA*^{EC93}-*CT*^{EC1738} and *cdiI*^{EC1738}, Cm^R	This study
pCH2262	Constitutive expression of chimeric *cdiA*^{EC93}-*CT*$^{O32:H37}$ and *cdiI*$^{O32:H37}$, Cm^R	This study
pCH2274	pTrc99aU2::*cdiI*$^{O32:H37}$, expresses *cdiI*$^{O32:H37}$ under an IPTG-inducible promoter, Amp^R	This study
pCH2275	Constitutive expression of chimeric *cdiA*^{EC93}-*CT*^{DEC9E} and *cdiI*^{DEC9E}, Cm^R	This study
pCH2408	Constitutive expression of chimeric *cdiA*^{EC93}-*CT*$^{STEC\_O31}$ and *cdiI*$^{STEC\_O31}$, Cm^R	This study
pCH6275	pUC57::*cdiA-CT/cdiI*^{DEC9E}, high-copy expression construct containing untagged *cdiA-CT/cdiI*^{DEC9E} alleles, Amp^R	Argonne National Laboratory, this study
pCH6276	pUC57::*cdiA-CT/cdiI*$^{97.0246}$, high-copy expression construct containing untagged *cdiA-CT/cdiI*$^{97.0246}$ alleles, Amp^R	Argonne National Laboratory, this study
pCH6277	pUC57::*cdiA-CT/cdiI*^{EC1738}, high-copy expression construct containing untagged *cdiA-CT/cdiI*^{EC1738} alleles, Amp^R	Argonne National Laboratory, this study
pCH6278	pUC57::*cdiA-CT/cdiI*$^{STEC\_O31}$, high-copy expression construct containing untagged *cdiA-CT/cdiI*$^{STEC\_O31}$ alleles, Amp^R	Argonne National Laboratory, this study
pCH6279	pUC57::*cdiA-CT/cdiI*^{NC101}, high-copy expression construct containing untagged *cdiA-CT/cdiI*^{NC101} alleles, Amp^R	Argonne National Laboratory, this study
pCH6281	pUC57::*cdiA-CT/cdiI*$^{O32:H37}$, high-copy expression construct containing untagged *cdiA-CT/cdiI*$^{O32:H37}$ alleles, Amp^R	Argonne National Laboratory, this study
pCH6286	pUC57::*cdiA-CT/cdiI*$^{P.\ lum\ TTO1}$, high-copy expression construct containing untagged *cdiA-CT/cdiI*$^{P.\ lum\ TTO1}$ alleles from *Photorhabdus luminescens*, Amp^R	Argonne National Laboratory,

		this study
pCH6289	pUC57::*cdiA-CT/cdiI*^{Kp342}, high-copy expression construct containing untagged *cdiA-CT/cdiI*^{Kp342} alleles from *Klebsiella pneumonia* 342, Amp^{R}	Argonne National Laboratory, this study
pCH6290	pUC57::*cdiA-CT/cdiI*^{Ymoll}, high-copy expression construct containing untagged *cdiA-CT/cdiI*^{Ymoll} alleles from *Y. mollaretii* 43969, Amp^{R}	Argonne National Laboratory, this study
pCH6300	pUC57::*cdiA-CT/cdiI*^{Palca}, high-copy expression construct containing untagged *cdiA-CT/cdiI*^{Palca} alleles from *P. alcalifaciens* 30120, Amp^{R}	Argonne National Laboratory, this study
pCH6302	pUC57::*cdiA-CT/cdiI*^{Yint}, high-copy expression construct containing untagged *cdiA-CT/cdiI*^{Yint} alleles from *Y. intermedia*, Amp^{R}	Argonne National Laboratory, this study
pCH6303	pUC57::*cdiA-CT/cdiI*^{Yk33638}, high-copy expression construct containing untagged *cdiA-CT/cdiI*^{Yk33628} alleles from *Y. kristensenii* 33638, Amp^{R}	Argonne National Laboratory, this study
pCH6306	pUC57::*cdiA-CT/cdiI*^{PestA}, high-copy expression construct containing untagged *cdiA-CT/cdiI*^{PestA} alleles from *Y. pestis* Pestoides A, Amp^{R}	Argonne National Laboratory, this study
pCH7445	pWEB-TNC, cosmid vector, Amp^{R} Cm^{R}	This study
pCH10163	Cosmid pCdiA-CT/*pheS** that carries a *kan-pheS** cassette in place of the *E. coli* EC93 *cdiA-CT/cdiI* coding sequence. Used for allelic exchange and counter-selection. Cm^{R} Kan^{R}	
pCH11009	Constitutive expression of chimeric *cdiA*^{EC93}-*CT*^{EC3937} and *cdiI*^{EC3937}, Cm^{R}	This study
pCH11434	Constitutive expression of chimeric *cdiA*^{EC93}-*CT*^{NC101} and *cdiI*^{NC101}, Cm^{R}	This study
pCH11948	Constitutive expression of chimeric *cdiA*^{EC93}-*CT*^{Kp342} and *cdiI*^{Kp342}, Cm^{R}	This study
pCH11949	Constitutive expression of chimeric *cdiA*^{EC93}-*CT*^{Plum} and *cdiI*^{Plum}, Cm^{R}	This study
pCH11950	Constitutive expression of chimeric *cdiA*^{EC93}-*CT*^{DdaCT2} and *cdiI*^{DdaCT2}, Cm^{R}	This study
pCH11951	Constitutive expression of chimeric *cdiA*^{EC93}-*CT*^{DdaCT3} and *cdiI*^{DdaCT3}, Cm^{R}	This study
pCH12241	Constitutive expression of chimeric *cdiA*^{EC93}-*CT*^{Yk33638} and *cdiI*^{Yk33638}, Cm^{R}	This study
pCH12351	Constitutive expression of chimeric *cdiA*^{EC93}-*CT*^{Yint} and *cdiI*^{Yint}, Cm^{R}	This study
pCH12389	Constitutive expression of chimeric *cdiA*^{EC93}-*CT*$^{Ec536\text{-}Rlact}$ and	This study

	cdiI^{Rlact}, Cm^{R}	
pCH12398	Constitutive expression of chimeric *cdiA*^{EC93}-*CT*^{EC93cdi2} and *cdiI*^{EC93cdi2}, Cm^{R}	This study
pCH12491	Constitutive expression of chimeric *cdiA*^{EC93}-*CT*^{Dzeae1594} and *cdiI*^{Dzeae1594}, Cm^{R}	This study
pCH12715	pET21::*cdiA-CT/cdiI*$^{O32:H37}$-His6, overproduces the CdiA-CT/CdiI$^{O32:H37}$-His6 complex under control of the T7 promoter, Amp^{R}	This study
pCH12717	pET21::*cdiA-CT/cdiI*$^{O32:H37\ H71A}$-His6, overproduces the inactive CdiA-CT/CdiI$^{O32:H37\ H71A}$-His6 complex under control of the T7 promoter, Amp^{R}	This study
pCH12721	pET21::His6-*trxA-cdiA-CT/cdiI*$^{O32:H37}$, overproduces the inactive His6-TrxA-CdiA-CT/CdiI$^{O32:H37}$ H71A complex under control of the T7 promoter, Amp^{R}	This study
pCH12750	pET21::*cdiI*$^{O32:H37}$-His6, overproduces the CdiI$^{O32:H37}$ protein under control of the T7 promoter, Amp^{R}	This study
pCH12768	Constitutive expression of chimeric *cdiA*^{EC93}-*CT*$^{O32:H37\ H71A}$ and *cdiI* $^{O32:H37}$, Cm^{R}	This study
pCH12847	Constitutive expression of chimeric *cdiA*^{EC93}-*CT*^{Ymoll} and *cdiI* ^{Ymoll}, Cm^{R}	This study
pCH12848	Constitutive expression of chimeric *cdiA*^{EC93}-*CT*^{Palca} and *cdiI* ^{Palca}, Cm^{R}	This study
pCH12852	pET21db::His10- *cdiA-CT/cdiI*$^{O32:H37\ H71A}$, overproduces the inactive His10-CdiA-CT/CdiI$^{O32:H37}$ H71A complex under control of the T7 promoter, Kan^{R}	This study
pCH12861	pET21::*cdiA-CT/cdiI*^{Kp342}-H6, overproduces the CdiA-CT/CdiI^{Kp342}-His6 complex under control of the T7 promoter, Amp^{R}	This study
pCH12863	pET21::His6-*trxA-cdiA-CT/cdiI*^{Kp342}, overproduces the His10-TrxA-CdiA-CT/CdiI^{Kp342} complex under control of the T7 promoter, Amp^{R}	This study
pCH12898	pET21::*cdiI*^{Kp342}-His6, overproduces the CdiI^{Kp342}-His6 protein under control of the T7 promoter, Amp^{R}	This study
pCH12910	pET21db::His10- *cdiA-CT/cdiI*^{Kp342}, overproduces the His10-CdiA-CT/CdiI^{Kp342} complex under control of the T7 promoter, Kan^{R}	This study

[a]Abbreviations: Amp^{R}, ampicillin-resistant; Apr^{R}, aprimycin-resistant; Cm^{R}, chloramphenicol-resistant; Erm^{R}, erythromycin-resistant; Kan^{R}, kanamycin-resistance; Rif^{R}, rifampicin-resistant; Tet^{R}, tetracycline-resistant; Zeo^{R}, zeocin-resistant.

Table 3. Oligonucleotides used in this study.

Oligonucleotide	***Sequence[a]***	***Reference***
CDI208 (EC869-cdiI-rev)	5' - CTA ACC TAC TGC CTC AAA AAA ACT TTC C - 3'	This study

CDI209 (EC869-CT-for)	5' - TAT CTG AGT AAA GCC CAG AAA GCT C - 3'	This study
CH3176 (NC101-CT(OE)-for)	5'- CAG GTA GGA ACT CGG TTG AGA ATA ATT ACC TGA GCG TGT CTG AAA AGA CAG – 3’	This study
CH3513 (3937CT2-mid-for)	5'- CAG GTA GGA ACT CGG TTG AGA ATA ATT TCC TGA ACA AAG GAA GAC CG – 3’	This study
CH3514 (3937CT2-mid-rev)	5'- GGT CTG GTG TCT AAC CTT TGG GTT AAC TCC ACT TCC ATT TTA TGA TCA AAT – 3’	This study
CH3515 (3937CT3-mid-for)	5'- CAG GTA GGA ACT CGG TTG AGA ATA ATT ATC TGA GCA GTA CGG ACA AGA GC – 3’	This study
CH3516 (3937CT3-mid-rev)	5'- GGT CTG GTG TCT AAC CTT TGG GTT AAG GCT GGT AAT CTT CAT ATT CC – 3’	This study
CH3517 (Kpn342-mid-for)	5'- CAG GTA GGA ACT CGG TTG AGA ATA ATT CGT TGG CGG GCG ATC AG – 3’	This study
CH3518 (Kpn342-mid-rev)	5'- GGT CTG GTG TCT AAC CT TGG GTT ATC TAA TGA CAG AGC TAC TTT TTA TTT – 3’	This study
CH3562 (DEC9E/97.0246-mid-for)	5' - CAG GTA GGA ACT CGG TTG AGA ATA ATA TGC TGA ACG TGA TAG CCA C - 3'	This study
CH3563 (DEC9E-mid-rev)	5' - GGT CTG GTG TCT AAC CTT TGG TTA GGT CCA TCC GAG AGA GCC - 3'	This study
CH3564 (97.0246-mid-rev)	5' - GGT CTG GTG TCT AAC CTT TGG TTA GGC AAG TAG CTC TAA TTT TGC - 3'	This study
CH3565 (EC1738-mid-for)	5' - CAG GTA GGA ACT CGG TTG AGA ATA ATT ATC TGA GCA GTA AGC - 3'	This study
CH3566 (EC1738-mid-rev)	5' - GGT CTG GTG TCT AAC CTT TGG CTA TTT CTT GAT TCC TAA ACG G - 3'	This study
CH3567 (O32:H37-mid-for)	5' - CAG GTA GGA ACT CGG TTG AGA ATA ATG CGC TGG GTA AC - 3'	This study
CH3568 (O32:H37-mid-rev)	5' - GGT CTG GTG TCT AAC CTT TGG TTA CTG TTC GTT AAA TC TCG TTT C - 3'	This study
CH3569 (STEC_O31-mid-rev)	5' - GGT CTG GTG TCT AAC CTT TGG TTA GGA TGG GAT TTT AGA	This study

	CAG TAA TT - 3'	
CH3570 (pUC57-univ-rev-Xho)	5' - AAA CTC GAG GCC TCT GCA GTC G - 3'	This study
CH3571 (pUC57-univ-for-Xho)	5' - AAA CTC GAG TCG CGA ATG CAT C - 3'	This study
CH3603 (O32:H37-cdiI-Kpn-for)	5' - AAA GGT ACC ATG AAT AAT GGT TC - 3'	This study
CH3685 (Kp342-cdiI-Spe-rev)	5'- TGA ACT AGT TCT AAT GAC AGA GC	This study
CH3743 (Palc-mid-for)	5'- CAG GTA GGA ACT CGG TTG AGA ATA ATT TTT TAT CAG CGA CAA AAA ATG A – 3’	This study
CH3744 (Palc-mid-rev)	5'- GGT CTG GTG TCT AAC CTT TGG GTT AAA AAT AAA TTA ATA AAT GAT TTTT GTA CAT TAC C – 3’	This study
CH3745 (Yint-mid-for)	5'- CAG GTA GGA ACT CGG TTG AGA ATA ATT ATC TCA ATG CCA GTG ATA AGA – 3’	This study
CH3746 (Yint-mid-rev)	5'- GGT CTG GTG TCT AAC CTT TGG GCT AAA CCA GCT TTA ATA GCT TCA – 3’	This study
CH3747 (Ymol-mid-for)	5'- CAG GTA GGA ACT CGG TTG AGA ATA ATA ACC TTA GTT TTG GCA AAG G – 3’	This study
CH3748 (Ymol-mid-rev)	5'- GGT CTG GTG TCT AAC CTT TGG GTT AAG CAG GTA ATT TAG TCA GTA AAT C – 3’	This study
CH3822 (EC93-CT2-mid-for)	5'- CAG GTA GGA ACT CGG TTG AGA ATA ATT CAC TCA GTG ATG GCT GGA AC – 3’	This study
CH3823 (EC93-CT2-mid-rev)	5'- GGT CTG GTG TCT AAC CTT TGG GTT AAC GAT AAA AAC GAT TTA ATA TCA ATA TGA TGA – 3’	This study
CH3897 (O32:H37-H71A-rev)	5' - GGA AAC TCT TTT CCA GCT TTT GTC CAA TGC C - 3'	This study
CH3898 (O32:H37-cdiI-Spe-rev)	5' - TTT ACT AGT CTG TTC GTT AAA TGC TCG - 3'	This study
CH3962 (Kp342-CT-Kpn/Nco-for)	5' - TTT GGT ACC ATG GTT GAG AAT AAC TTG GCG G - 3'	This study
CH3965 Kp342-cdiI-Kpn-for	5' - TTT GGT ACC ATG TTC ATA GAA AAT AAG CC - 3'	This study
DL1527	5´ - GAA CAT CCT GGC ATG AGC G	
DL1663	5´ - CCC AAA GGT TAG ACA CCA GAC C	
DL2368	5´ - GTT GGT AGT GGT GGT GCT G	
DL2470	5´ - ATT ATT CTC AAC CGA GTT	

	CCT ACC TG	

VII. CDI systems as synthetic biology tools

This research was conducted in collaboration with Beatrice Ramm and Drew Endy at Stanford University, who performed the reversibility studies and the time-lapse microscopy. I constructed many of the strains used throughout this study, performed the co-culture assays and additional microscopy, and wrote a significant portion of the manuscript.

A. Introduction

The complexity of higher-order organisms often makes it difficult to understand the source of arising patterns in cell populations. A simplified system that is easy to manipulate and quantify can provide valuable information on the underlying design principles of biological pattern formation. To understand higher-order developmental patterns, the field of synthetic biology has taken an interest in programming pattern formation using bacteria. Synthetic biology and computational modeling using bacterial systems have contributed to our knowledge of two and three-dimensional patterning in response to morphogens (404, 405) and physical parameters such as cell shape (406), modeling of multicellular behavior (407, 408), and edge detection (409). In eukaryotic systems, synthetic biology has been utilized to understand how Notch-Delta signaling controls patterning during development (410-412). A goal of synthetic biology is to create well-defined systems that can be precisely manipulated with the end goal of controlling cell growth or gene expression in a multicellular community. Such studies on bacterial interactions can also contribute to our knowledge of complex microbial communities such as biofilms.

As perhaps the best-studied Gram-negative bacterium, *Escherichia coli* is simple to engineer, and formed patterns can be observed in detail using time-lapse microscopy (TLM) (413). As a result, *E. coli* is an ideal unicellular tool for modeling patterning in a population.

Though *E. coli* is genetically tractable and is easy to manipulate under laboratory conditions, natural bacterial environments are much more complex. To navigate this population space, bacteria have evolved myriad ways to compete and communicate with other microbes in their surroundings, some of which have been adapted for use in synthetic biology systems. Quorum sensing is a well-studied form of bacterial communication that uses small molecules like oligopeptides and *N*-acyl homoserine lactones (AHLs) to coordinate group behaviors on a population level by regulating biofilm development, growth of microbial communities, and host-microbe interactions (16, 19, 414). As a synthetic biology tool, quorum sensing has been used to regulate cell growth in a variety of ways, including controlling pattern development (405, 409, 415, 416), encoding genetic oscillators (417), and creating synthetic ecosystems (418, 419). The use of these diffusible molecules simulates developmental morphogen gradients used by eukaryotic organisms to direct cell differentiation and growth. However, building more complex cell-cell communication schemes based on quorum sensing systems is difficult because of cross-talk and overlap between ligand and receptor families (420, 421). Recent efforts to diversify existing communication schemes include the introduction of decoupled DNA messaging (421) or the proposition of a contact-dependent communication form based on conjugation (422).

In addition to communication systems based upon diffusible compounds, bacteria can interact using a variety of contact-dependent systems that require physical interaction between two cells. Bacteria utilize pili, adhesins, and effector secretion systems to interact with other cells or surfaces, and, in some cases, deliver toxic effectors into prokaryotic and eukaryotic targets (130, 243, 245, 248, 402, 423-428). Contact-dependent growth inhibition (CDI) is a type 5 secretion system and a form of bacterial competition by which CDI^+ cells

can inhibit the growth of target cells following physical contact with a receptor and delivery of a toxic peptide (156, 167, 169, 173, 175, 194). CDI was first described in *Escherichia coli* strain EC93, which was isolated from a rat gut and could inhibit the growth of *E. coli* K-12 cells upon physical contact (156). This inhibitory activity was localized to a three-gene locus encoding *cdiBAI*. CdiA and CdiB comprise a two-partner secretion system in which CdiB facilitates the surface display of the large exoprotein CdiA. Upon recognition of a target cell via binding the outer membrane receptor BamA (157), the C-terminal region of CdiA (termed CdiA-CT) presumably undergoes a proteolytic cleavage event and can be delivered to target cells, resulting in inhibition of growth (172, 194, 429). Inhibitory activity of CdiA-CTs is blocked by CdiI, an immunity protein that physically binds and inactivates the toxin (169, 175, 177, 193, 202).

CDI systems are widespread across Gram-negative bacteria, and CDI systems have been identified in a variety of α-, β-, and γ-proteobacteria including plant pathogens (*Dickeya* spp. and *Erwinia pyrifoliae*), animal pathogens (*Moraxella catarrhalis*), and human pathogens (*Klebsiella pneumoniae*, *Yersinia pestis*, and uropathogenic *E.coli* (168, 170). More than 16% of sequenced E. coli genomes contain a CDI gene cluster (213), and CDI systems are remarkably diverse even among closely-related strains. Almost 30 distinct families of CDI toxins have been identified in *E. coli* alone (170). CdiA-CTs characterized include toxins that act as DNases (177, 194), ionophores (158), general tRNases (193), specific tRNases (169, 172), and ribosomal rRNases (175), and a variety of other toxin/immunity pairs have been bioinformatically predicted (199, 200). CDI can influence group behavior of bacterial communities, and expression of CDI systems leads to cell aggregation and enhanced biofilm formation (159, 430).

To our knowledge, the potential of bacterial contact-dependent forms of communication and competition have not been explored for synthetic biology purposes. CDI systems may be an ideal platform for the development of synthetic biology tools because they are modular, can influence the growth of specific target populations, and are capable of delivering cargo to another cell. Previous work demonstrated that cells inhibited by a pore-forming CdiA-CT can resume growth after toxicity is neutralized by expression of CdiI (158). This reversibility may enable long-term experiments with on/off cycles of CDI toxin expression. Additionally, given the vast distribution of *cdi* genes throughout gammaproteobacteria and range of CdiA-CT activities, the array of available CDI systems constitutes a great wealth of potential tools. Here, we sought to determine whether reversibility of inhibition was a feature of other CDI systems and whether these inhibition systems could be used to construct synthetic biology tools to study cell growth and pattern formation in bacterial communities. As CDI activity is dependent on physical contact, these systems could be harnessed as a way to control cell growth and patterning in multicellular populations without the need for diffusible signaling compounds. We present the development of CDI-based synthetic biology tools and show that they can be used to reversibly control cell growth in culture and to influence cellular morphology within a bacterial population.

B. Results

1. Tunable control of cell growth rates by CdiA-CT/CdiI expression

Reversible growth inhibition mediated by CdiA-CT/CdiI pairs could be useful for constructing dynamic growth rate systems to control the growth of cells over time. To achieve this, such a system should have tight control of toxin expression (i.e., no change in growth rate of cells without induction of toxin), a range of changes in growth rate, the ability

to rescue growth defects by expression of the respective immunity gene, and reversibility of growth inhibition. Previous work demonstrated the reversibility of inhibition from a pore-forming toxin (158), so we wanted to test the reversibility of other classes of CdiA-CTs. We reasoned that low levels of RNase activity may be reversible to some degree if protein synthesis can resume after inactivation of the toxin and selected four previously-characterized CdiA-CT/CdiI pairs to evaluate using these criteria: CdiA-CT^{ECL} from *Enterobacter cloacae* (16s rRNase) (175), CdiA-CT^{Ec869} from *E. coli* (tRNase specific for tRNA^{Gln}) (172), CdiA-CT$_{II}^{Bp1026}$ (cleaves tRNA^{Ala}) (169), and CdiA-CT^{Ec536} from *E. coli* (general tRNase) (193). We first asked whether a range of cellular inhibition could be achieved by varying expression of these toxins. To study the effects of these toxins on growth rate, we cloned these four CdiA-CT/CdiI pairs into growth control plasmids in which CdiA-CT is expressed under control of the L-arabinose-inducible P_{BAD} promoter (ara), and CdiI expression is regulated by the anhydrotetracycline-inducible promoter $P_{LtetO-1}$ (atc) (431). We transformed the four resulting pGC::CdiA-CT/CdiI constructs into *E.coli* DH5αZ1 and monitored growth of these strains by measuring the optical density at 600 nanometers (OD_{600}) over time. CdiA-CT and CdiI expression were regulated by varying arabinose (0 – 0.1%) and atc (0 or 200 ng/mL) concentrations in the media. Non-inducing conditions did not result in any growth rate changes as compared to cells carrying a control plasmid.

Of the four CdiA-CT/CdiI pairs tested, three did not meet the criteria for tunable growth control systems (Figure 1). Growth rates of cells expressing CdiA-CT^{Ec536} and CdiA-CT$_{II}^{Bp1026b}$ toxins do not appear to be tunable in this system, as even low levels of arabinose resulted in complete growth inhibition (Figure 1C and E). With high toxin induction,

expression of the respective *cdiI* genes for these systems does not completely block inhibition (Figure 1D and F). Expression of CdiA-CT^{EC869} appears to be leaky, as uninduced cells (no arabinose) show a growth defect at late stages of growth (Figure 1G). Furthermore, CdiI^{EC869} does not fully rescue inhibition at the highest levels of toxin induction (Figure 1H). Previous studies have shown these CdiA-CT/CdiI modules to be functional, and these immunity proteins can neutralize CdiA-CT toxicity in liquid co-culture experiments *and in vitro* (169, 172, 193). We presume that in our system, *cdiI* expression is lower than that of the *cdiA-CT* genes and that full protection from toxicity could be achieved for all CdiA-CT/CdiI pairs by tuning the expression levels of the respective constructs.

We identified the 16S rRNase CdiA-CT^{ECL} as the most promising candidate for controllable growth rate systems (Figure 2). Without toxin induction, *E.coli* DH5αZ1 cells carrying pGC::CdiA-CT/CdiI^{ECL} grow at the same rate as cells harboring the control plasmid (Figure 2B, black and pink lines). Low levels of toxin induction (Figure 2B, blue line) slow cell growth, and higher levels of arabinose lead to an arrest of growth as measured by OD_{600} (Figure 2B, green and brown lines). Full induction of *cdiI*^{ECL} does not affect cell growth in the absence of toxin induction (Figure 2C, black and pink lines). When CdiA-CT^{ECL} is expressed at low levels, CdiI^{ECL} rescues growth almost to control levels (Figure 2C, blue line). With increasing arabinose concentrations, CdiI^{ECL} partially rescues growth, resulting in a lower growth rate but not full attenuation (Figure 2C, green and brown lines).

2. Control of cell growth rates by CdiA-CTs is reversible

To determine if the change in growth rate observed with the induction of pGC::CdiA-CT/CdiI^{ECL} is reversible, we performed a re-growth experiment (Figure 2D). Cells carrying the CdiA-CT/CdiI^{ECL} expression plasmid or a control plasmid vector (Figure 2E) were grown

in media either lacking arabinose or with the lowest inducing condition (0.001% ara). In phase 1, pGC::CdiA-CT/CdiI^{ECL} cells grown in arabinose showed a decrease in growth rate, consistent with our growth curve results shown in Figure 2B (Figure 2D, left panel). After the untreated cells reached stationary phase, both populations were washed to remove inducing agent, and cell density was diluted to an OD_{600} of 0.01 (Figure 2D, transition between left and middle panels). In phase II, each initial population was grown in media either lacking inducer or media with 0.001% ara (Figure 2D, middle panel). The cells supplemented with arabinose showed a similarly suppressed growth as cells in phase I. Cells without inducer recovered growth, eventually reaching the same final OD_{600} of 1.0 as control cells (Figure 2D, middle panel), but showed a significantly longer lag phase than control cells or cells grown without inducer in phase I. The cells which showed recovered growth in the absence of arabinose were washed, diluted, and split into cultures with varying arabinose concentrations (Figure 2D, right panel). Cells that had been previously inhibited by CdiA-CT expression and recovered by CdiI were once again inhibited by expression of CdiA-CT^{ECL}. Cells without inducer grew comparably to phase I and the negative control (Figure 2D, compare left and right panels). The lag phase of cells was shorter again and can be compared to the lag phase of phase I or the negative control. These results demonstrate that growth inhibition of cells can be achieved by inducing expression of CdiA-CT^{ECL}, and that this inhibition is reversible when the cognate CdiI is expressed. Cells inhibited by CdiA-CT^{ECL} are capable of re-growing like untreated cells and can undergo several cycles of reversible inhibition.

3. Homogeneous control of growth inhibition by CdiA-CT^{ECL} at a single-cell level

Expression of the P_{BAD} promoter in a population of *E. coli* DH5αZ1 cells is not

homogeneous, and it is regulated by an all-or-none response to induction in each cell (432). Intermediate expression of the target gene at a population level is not caused by intermediate expression levels in single cells, but instead represents a distribution of high and low expression. However, systems have been developed for homogeneous expression using the P_{BAD} promoter, ensuring that intermediate inducer levels lead to intermediate gene expression in all cells (433). *E. coli* strain BW27786 lacks the high-affinity arabinose transport operon AraFGH, is deficient in arabinose metabolism, and constitutively expresses the low-affinity arabinose transporter AraE from the chromosome. P_{BAD} induction in this strain leads to an even gene expression response from all cells (433). Therefore, we tested whether this strain could control cell growth rates at a single-cell level over a range of inducer concentrations using pGC::CdiA-CT/CdiI^{ECL}. As BW27786 does not contain the *tetR* gene needed for the regulation of $P_{LtetO-1}$, cells were co-transformed with pGC::CdiA-CT/CdiIECL or the empty control plasmid as well as pTS1127, which encodes constitutively-expressed *tetR*. These strains were grown under control and inducing conditions, and growth rates were assessed with OD_{600} measurements. As with DH5αZ1, growth of BW27786 cells carrying the control plasmid were not influenced by different arabinose concentrations or by atc addition (Figure 3C and D). Cells carrying pGC::CdiA-CT/CdiI^{ECL} showed normal growth in the absence of inducer (Figure 3A). Lower arabinose concentrations (1×10^{-6}% and 1×10^{-5}% (w/v)) did not have an effect on growth rate. Intermediate concentrations of arabinose (5×10^{-5}%, 7.5×10^{-5}% and 1×10^{-4}% (w/v)) slowed cell growth considerably (Figure 3A). Cells subjected to high levels of inducer (0.001% and 0.01% (w/v)) stopped growing after 2 hours but seemed to resume growth after 7 hours. Induction of *cdiI* gene expression had no detrimental effect on cell growth (data not shown).

Growth inhibition caused by low levels of CdiA-CT induction could be rescued by co-expression of CdiI, but CdiI does not protect against toxicity at high levels of CdiA-CT expression (Figure 3B). These results suggest that systems which permit homogeneous gene expression are suitable for controlling growth rates at a population and single-cell level.

4. Controlling colony morphology with CDI

We have previously reported the DNase activity of an orphan CdiA-CT from *E. coli* O157:H7 EC869 (CdiA-CT_{o11}^{EC869}), a Shiga toxin-producing strain isolated from cattle (177, 434). Cells that have been inhibited by CdiA-CT_{o11}^{EC869} have damaged nucleoids and are often elongated and filamentous (173, 177, 202). The physical effects of this CDI system are striking, but it is possible that these morphology changes are an artifact of forced contact between inhibitors and targets during growth in shaking broth. Therefore, we wanted to observe the effects of CdiA-CT_{o11}^{EC869} in real time using time-lapse microscopy (TLM) to determine whether these physical changes occur in a more natural environment, such as two cell populations growing towards each other. TLM has previously been used to monitor patterning in bacterial communities and T6SS toxicity between bacteria (402, 427). As a preliminary test, we performed growth competitions in liquid culture using the media conditions used for TLM experiments. GFP-labeled CDI^{+} inhibitor cells carrying a plasmid constitutively expressing CDI_{o11}^{EC869} were mixed with mKate2-labeled target cells transformed with either a plasmid encoding $cdiI_{o11}^{EC869}$ or an empty vector (Figure 4). As previously demonstrated, wild-type target cells lose viability upon mixing with CDI_{o11}^{EC869} inhibitors, and this growth inhibition is blocked by expression of *cdiI* (Figure 4A). Microscopy images reveal that susceptible target cells become elongated and filamentous after competition in liquid media (Figure 4B), consistent with our previously-reported

phenotype. Cells expressing *cdiI*$_{o11}^{EC869}$ retain normal morphology (Figure 4B).

TLM was then used to observe the phenotypic effects of inhibition of these target cells in real time. The same CDI^{+} inhibitor and target strains used for the liquid competitions were applied to an agarose pad at a low density, and image locations were chosen where cells from both populations were positioned close to each other. When CDI$_{o11}^{EC869}$ inhibitor cells collided with susceptible target cells, the targets elongated at the interface of the two colonies, smoothing the collision border with filamentous cells aligned parallel to the inhibitor/target cell interface (Figure 5A). In contrast, contact between CDI$_{o11}^{EC869}$ inhibitor cells and immune targets expressing *cdiI*$_{o11}^{EC869}$ did not induce morphological changes in target cells at the interface (Figure 5B). Examination of the border between CDI^{+} and cells expressing *cdiI*$_{o11}^{EC869}$ shows mixing of the two populations, as evidenced by the intermingling of GFP-labeled CDI^{+} cells and mKate2-labeled target cells (and vice versa). These invaginations lead to a rough, jagged colony interface (Figure 5B). Conversely, filamentation of susceptible target cells after interaction with CDI$_{o11}^{EC869}$ cells leads to a smooth border between the two populations (Figure 5A). Elongated cells exclude CDI^{+} inhibitor cells, preventing them from invading the target cell population. Therefore, we conclude that filamentation of target cells is a relevant physical consequence of inhibition by the CDI$_{o11}^{EC869}$ system, and that morphological changes associated with this system can be harnessed to alter the boundary between growing cell populations.

We next wished to determine whether we could combine reversibility of cell inhibition and morphology changes in a CDI-based synthetic biology system. As we demonstrated earlier, expression of CdiA-CT^{ECL} can be used to modulate cell growth over several cycles (Figures 2 and 3). We performed liquid co-culture competition assays with target cells

expressing *cdiI*^{ECL} and an empty plasmid vector and visualized cellular morphology after mixing to determine whether delivery of this toxin was also associated with changes in target cell morphology. Delivery of CdiA-CT^{ECL} to targets did not change the overall cell morphology during inhibition (Figure 6B), so it is unlikely that using this toxin for reversible inhibition would alter cell morphology during patterning. Taken together, these data suggest that CdiA-CTs have unique properties that can be harnessed for synthetic biology purposes, but that a combinatorial approach using reversible inhibition to create cyclic alterations in cell morphology may not be feasible.

5. An inducible CDI system to control cell growth and colony morphology

CdiA-CTs are delivered rapidly during CDI, and toxin activity can be observed in target cells before a decrease in viable target cells is observed (172). Because of the physical requirements of TLM, cells are incubated together for upwards of 30 minutes before imaging begins. During this time, freely-diffusing target cells can come into contact with CDI^{+} cells and inhibition can occur before the first images are acquired. This is an imperfect setup for studying morphological and physiological changes that accompany delivery of CDI toxins into target cells as well as for precise control of colony growth and patterning. To address this, we utilized an IPTG-inducible CDI$_{o11}$^{EC869} system to enable tighter control of toxin delivery (Figure 7). In the absence of IPTG, *cdiA* is not expressed, and co-culture of these inhibitor cells with susceptible target cells does not result in growth inhibition (Figure 6A) nor in morphological changes of target cells (Figure 7B and C). Upon addition of IPTG, CdiA is expressed, resulting in target cell filamentation (Figure 7B and C) and inhibition (Figure 7A). However, the plasmid encoding the *cdiI*$_{o11}$^{EC869} gene contains an IPTG-inducible promoter, and overexpression of this immunity protein is lethal to cells (Figure 8).

Therefore, we used another CDI^R strain that lacks *yciB*, a gene encoding a putative inner membrane protein required for delivery of CdiA-CT_{o11}^{EC869} into target cells (173). When co-cultured with IPTG added to the media, Δ*yciB* cells are not inhibited (Figure 7A) and do not display any morphological defects (Figure 7B and C). We again performed TLM with mKate2$^+$ wild-type and Δ*yciB* targets (Figure 9) and did not observe filamentation in the CDI-resistant Δ*yciB* cells. As with immune cells and the constitutive CDI_{o11}^{EC869} system, growth of IPTG-CDI_{o11}^{EC869} and *yciB* cells on agarose pads resulted in intercalation of the two populations (Figure 9B). Therefore, cell morphology can be controlled by CDI systems by altering expression of either cognate CdiI proteins or inner membrane proteins required for delivery.

6. The modularity of CDI systems expands potential synthetic biology applications

CDI is a simple process in that inhibition is mediated by a three-gene locus. This is in stark contrast to the elaborate T6SS apparatus, which consists of a dozen or more subunits (133, 240, 243, 256, 402). Delivery of CdiA-CT domains into target cells can be manipulated by altering a single protein at either the outer or inner membrane of target cells. Given the diversity of translocation pathways used by CdiA-CT toxins to enter the cell and the multiple morphological outcomes of inhibition by CdiA-CTs, it is plausible that specific subpopulations of cells in a complex environment could be individually manipulated using CDI systems. As a proof of concept, we carried out tri-population co-culture assays in which GFP$^+$ CDI_{o11}^{EC869} cells were mixed with both mKate2$^+$ wild-type targets and BFP$^+$ targets expressing $cdiI_{o11}^{EC869}$ (Figure 10). As expected, only the CDI-sensitive mKate2$^+$ target cells show the filamentatous phenotype that is a hallmark of inhibition by this toxin. BFP$^+$ cells carrying a plasmid-borne copy of $cdiI_{o11}^{EC869}$ are protected from inhibition, and do not

elongate or change morphology. Thus, CDI systems can be used to selectively influence individual populations within a mixed culture, increasing the applicability of these as synthetic biology tools.

C. Discussion

Controlling colony morphology and cell growth is a necessary step towards engineering complex microbial consortia that mimic the complexity of biofilms and other microbial communities in terms of communication, competition, and species variety. Furthermore, development and maintenance of complex microbial systems requires coordination of activities between many cells, making them attractive candidates for studying principles of multicellular tissues and organisms. Here, we present new methods for reversibly controlling bacterial cell growth and influencing morphology of subpopulations of cells in a microbial community based on principle components of bacterial contact-dependent growth inhibition systems. Manipulating these variables in a contact-dependent way using a single species of bacteria such as *E. coli* could prove useful as a simplified way to model environments of greater complexity (435).

Previously, Aoki *et al*. demonstrated that inhibition by the pore-forming CdiA-CT^{EC93} is reversible when the cognate CdiI immunity protein is expressed (158). Here, we show that growth inhibition of *E. coli* by CdiA-CT^{ECL}, which cuts 16S rRNA (175), is reversible in a similar manner. Growth of *E. coli* DH5αZ1 cells is suppressed by low levels of toxin, and growth could be fully recovered when the inducing agent was removed. The CdiA-CT^{ECL} growth suppression module was still functional and could inhibit growth when seeded into fresh media containing inducing agents. Therefore, the ability of cells to recover from inhibition is likely not due to the accumulation of inactivating mutations in pCdiA-CT^{ECL} and

instead represents a bonafide reversible growth inhibition system.

Of the CdiA-CT/CdiI pairs we tested, CdiA-CT/CdiI^{ECL} was best able to reversibly regulate the growth of *E.coli*. The 16S rRNase activity of CdiA-CT^{ECL} may contribute to its ability to reversibly control growth for two reasons. First, 16S rRNase activity can be imagined to have a "balanced" effect on cell growth; that is, when 16S rRNA is degraded, synthesis of all proteins will be affected equally since this activity affects general translation machinery and not the levels of specific tRNAs. In contrast, the activity of specific tRNases such as CdiA-CT^{EC869}, which cleaves tRNA^{Gln} molecules (172), might result in unbalanced protein production based on amino acid content. General tRNases are, in theory, a good candidate for controllable growth systems, as induction of these toxins would also affect protein synthesis almost homogenously. However, even low expression of the general tRNase CdiA-CT^{Ec536} halted growth in an irreversible manner. This may be because recovery requires synthesis of many tRNAs instead of only 16S rRNA.

A second reason that 16S rRNase activity from CdiA-CT^{ECL} may reversibly control cell growth is that it mimics natural growth regulation in *E. coli*. Cell growth rate is coupled to protein synthesis, with the production of rRNAs as the rate-limiting step (436, 437). In *E. coli*, rRNA transcription occurs from 7 operons and is under the control of multiple regulatory systems (437). 16S rRNA is subject to further processing by cellular RNases during maturation (438), and RNA stability studies show that 16S rRNA levels fluctuate with nutrient availability and growth phase (439, 440). Furthermore, toxins from classical toxin-antitoxin addiction modules interact with 16S rRNA. RelE interacts with 16S rRNA in order to cleave mRNA transcripts, and the Doc toxin binds 16S RNA but does not cleave mRNA (441). Therefore, low expression levels of CdiA-CT^{ECL} may cleave 16S rRNA in a manner

that mimics rRNA processing during starvation conditions, allowing the cell to recover when toxin activity is neutralized by production of the cognate CdiI or removal of an inducing agent from the media.

Previous studies characterizing CDI systems have examined growth inhibition in well-aerated liquid cultures using rich broth (167, 169, 172, 173, 175, 177, 193, 194). Under these conditions, CDI^- target cells are in constant contact with CDI^+ cells by virtue of physical shaking. Analysis of target cell morphology by microscopy after liquid culture with CDI_{o11}^{EC869} reveals that a majority of target cells have damaged nucleoids and display the elongated, filamentous phenotype that is the hallmark of inhibition by this toxin (177, 202). However, this might not be an accurate representation of how this CDI system inhibits targets in a natural system. Using TLM, we were able to examine populations of CDI^+ and CDI^- cells as they collide during surface growth, which is a better spatial representation of natural bacterial environments.

The results from our TLM experiments indicate that inhibition and phenotypic evidence of CDI toxin delivery in stationary environments does not occur throughout the entire population. As CDI^+ and CDI^- cells collide, target cells at the interface elongate. These cells physically block off internal layers of target cells, encapsulating untouched targets and preventing a lethal interaction with invading CDI^+ inhibitors (Figures 5A and 9A). In this way, intoxicated target cells that stretch across the CDI^+/CDI^--cell interface act as a "border patrol" that protects internal cells from inhibition. The spatial constraints of surface growth prevent constant contact between all cells. When CDI^+ cells encounter "self" immune cells, the populations can mix, as evidenced by crossover of GFP^+ cells to the mKate2-labeled target population (Figures 5B and 9B). These results are in agreement with computational

models predicting the emergence of discrete domains created by interactions between CDI^+ and CDI^- cells (442). In the future, analyzing CDI in stationary conditions using TLM as opposed to shaking batch co-cultures may provide a better assessment of CDI function in natural environments.

The microscopy results presented here have important implications for CDI biology. In natural populations, filamentation as a response to CdiA-CT delivery could be a mechanism by which CDI^- cells exclude invading CDI^+ strains to protect their niche. Alternatively, it could be a means by which CDI^+ cells can create a boundary between "self" and "non-self" populations to establish a community. Anderson *et al*. found that CDI systems in *Burkholderia pseudomallei* influenced biofilm structures by excluding "non-self" cells from pillar structures (443), and CDI systems are important to maintain structure during biofilm development in a variety of bacteria (225, 430). Morphological changes can influence the way bacteria communicate, form multicellular structures, or survive potentially lethal stresses (417, 435, 444-447). For example, filamentation can help pathogens like uropathogenic *E. coli* evade host innate immune responses during infection and *Burkholderia pseudomallei* survive antibiotic treatment (445, 448). Previous computational studies have incorporated morphological terms in systems describing bacterial communities composed of multiple cell types (406, 449).

The usefulness of contact-dependent methods for patterning and multicellular computing has been modelled computationally (422, 442). Here, we experimentally demonstrate that a toxin used for contact-dependent growth inhibition can reversibly control growth of cells and that CDI toxins can alter cell morphology upon delivery into targets. The ability to reversibly control bacterial growth using $CdiA\text{-}CT^{ECL}$ could be a useful tool to dynamically

control colony morphologies. CDI systems could be utilized to create defined, self-contained subpopulations within larger synthetic microbial ecologies. The development of reporters to measure delivery of CdiA-CT into target cells could be used to create a precise edge detector within a complex population of bacteria. The ability to control colony growth and morphology using these toxin/immunity pairs could be combined with other patterning tools and algorithms to build complex bacterial networks, engineer biofilms, and study gene expression in multicellular systems.

Using CDI systems to control cell growth and patterning has several advantages. CdiA-CT/CdiI pairs can be separated from the structural domains required for delivery, allowing for intracellular expression. This provides a platform for controlling cell growth independent of interactions with surrounding cells, as these growth control modules can be activated by addition of exogenous inducing agents or by light-regulated gene expression (408, 450). Fine-tuning of gene expression models allows for homogenous control of growth regulators, ensuring equivalent toxin doses across a system. The delivery of CDI toxins is also tunable at several steps, allowing for the construction and control of complex microbial consortia in which subpopulations can be targeted by one CDI system but resistant to another. We have demonstrated that delivery of CdiA-CT domains requires a specific inner membrane protein for each toxin. Therefore, knockout strains that lack the requisite inner membrane protein for delivery of a given toxin is specifically resistant to inhibition by that CDI system, but not other CdiA-CTs (173). Unlike quorum sensing, in which there is cross-talk between AHL receptors, the tight levels of control provided by CDI delivery pathways may provide a better method to engineer complex microbial populations. Given the species-specificity observed with CdiA-receptor interactions (159), contact between subpopulations of cells can be

controlled simply by replacing a target cell receptor with an allele containing polymorphisms that prevent interaction with CdiA. Receptor-independent, homotypic interactions between CdiA proteins, and thus, different subpopulations, can also be controlled by expression of different *cdiA* alleles (225). CdiA-CT/CdiI domains are modular (157), and inhibition by different CdiA-CTs results in a variety of cell morphologies (158, 177) (Figures 4, 5, and 6). Groups of CDI^+ cells within a complex community could be constructed such that delivery of phenotype-altering toxins could occur in specific subpopulations, generating multiple morphologies. Finally, CdiI proteins can be expressed independently of their cognate CdiA-CTs, allowing for creation of groups of cells that are resistant to a particular CDI^+ strain while maintaining susceptibility to other CDI toxins in the community. Because CDI systems are touch-dependent, control of growth or a patterning response is not dependent on the diffusion of an inducing agent, such as AHLs or other small molecules, and can thus be controlled with higher precision. This modularity provides a platform for the construction of expansive bacterial communities in which subpopulations of cells can interact with each other in a tightly-controlled, contact-dependent manner.

CdiA-CTs with RNase and pore-forming activity (158) have the ability to reversibly control toxicity. It is possible that the toxicity of other CdiA-CTs with RNase activity is also reversible. Given the strict cognate/non-cognate interactions between CdiA-CTs and CdiI proteins, using multiple reversible CdiA-CT/CdiI pairs could allow for construction of oscillating cell populations in liquid culture. CDI systems could also be harnessed for delivery of heterologous cargo that regulates gene expression or cell metabolism, leading to changes in patterning or cell morphology. Delivery of such effectors could be controlled at both the outer and inner membranes of target cells, enabling delivery and response in a

specific target population. However, we note that preliminary attempts to deliver heterologous cargo proteins using CdiA scaffolds have been unsuccessful, suggesting that there may be biological constraints on what can be delivered using CDI. Incorporating elements of CDI systems into existing bioengineering platforms will provide a variety of new tools for synthetic biology and modeling.

D. Materials and Methods

1. Plasmid and strain construction

All plasmids, cosmids, and bacterial strains are listed in Table 1. All oligonucleotides are listed in Table 2. All plasmids and cosmids were verified by sequencing (University of California, Berkeley). The four growth control plasmids pGC::CdiA-CT/CdiI express *cdiA-CT* under the control of the promoter P_{BAD} (i0500) and the corresponding antitoxin *cdiI* under the control of $P_{\mathrm{LtetO\text{-}1}}$. Promoter and coding sequences are separated by the ribozyme-based insulator parts RiboJ and SccJ (451) and the bicistronic junctions BCD2 and Gene10_LeuL (452) as translation initiation elements. We separately amplified the *cdiA-CT* and *cdiI* coding regions using the following primer pairs and plasmid templates: *E. coli* 536, BR1/BR2 and BR3/BR4 on pCH10540; ECL, BR15/BR16 and BR17/BR18 on pCH10445; EC869, BR19/BR20 and BR21/BR22 on pCH10525; and Bp1026b, BR23/BR24 and BR25/BR26 on pCH10415. We amplified the J64100 backbone using the primers TS433/TS455 and the promoter region from plasmid TS1465 with the primers TS349/TS460. The four linearized templates (*cdiA-CT*, *cdiI*, J64100 backbone, and TS1465 promoter) were then combined using Golden Gate Assembly [69] to yield the plasmids pGC::CdiA-CT/CdiI$^{\mathrm{Ec536}}$, pGC::CdiA-CT/CdiI$^{\mathrm{ECL}}$, pGC::CdiA-CT/CdiI$^{\mathrm{EC869}}$ and pGC::CdiA-CT/CdiI$_{\mathrm{II}}^{\mathrm{Bp1026b}}$. We obtained the control plasmid pGC by cutting J64100 with XbaI and

SpeI and self-ligating. The cosmid pCH12502 allows for IPTG-inducible expression of CDI_{o11}^{EC869} and was a gift from Zach Ruhe (University of California, Santa Barbara).

The chromosomal insertions in fluorescent strains CH12735 (mKate2) and CH2699 (sfGFP) were constructed using the integration vectors TS1013 and TS1014 and the corresponding helper plasmid pAH69 (453). TS1013 and TS1014 are enhanced versions (454) of the original integration vectors (453), encoding the fluorescent proteins mKate2 and sfGFP under the control of the constitutive promoter J23119 (369), respectively.

2. Growth experiments

We chemically transformed the pGC::CdiA-CT/CdiI constructs or a control plasmid into *E.coli* DH5αZ1. Overnight cultures were grown 12 – 16 hours at 37°C with shaking and were diluted into fresh LB media supplemented with chloramphenicol (25 µg/mL). 200 µL of each dilution was transferred to a clear-bottom 96-well plate (Greiner Bio-One). We prepared fresh serial dilutions of L-arabinose (Calbiochem) and anhydrotetracycline (Sigma-Aldrich) and added 2 µl of the respective dilution where appropriate to reach the final arabinose concentrations of 0.1% - 1×10^{-6}% (w/v) and 200 ng/ml atc. Plates were sealed with a gas-permeable Aeraseal sealing film (Excel Scientific) and incubated at 37 °C, 80 % humidity, and 460 rpm in a LT-X plate shaker. OD_{600} was measured hourly using the Spectramax i3 (Molecular Devices). Each condition was tested in triplicate. All experiments were at least repeated once.

To test reversibility of growth inhibition, we repeated the growth experiments final arabinose concentrations of 0 % and 0.001 % (w/v). When cells grown without arabinose reached stationary phase, we transferred the liquid into Eppendorf tubes. After centrifugation for 3 min at 3000 rpm in a tabletop centrifuge, we resuspended the cells in fresh LB without

inducer. After three washes, the OD_{600} of each sample was measured, and cells were diluted to an OD_{600} of 0.01 in a final volume of 200 µl of fresh LB media. We split the cells that originally received arabinose into two groups. One received the same concentration of arabinose, and the other culture was treated with a buffer control. After another growth cycle, the procedure was repeated, and the cells that did not receive arabinose treatment were split into two groups for subsequent growth. To test the plasmid pGC::CdiA-CT/CdiI^{ECL} in the strain BW27786, we chemically co-transformed pGC::CdiA-CT/CdiI^{ECL} or a vector control with the plasmid pTS1127, which constitutively expresses *tetR*. Growth curves were recorded as described above.

3. Liquid competitions

Overnight cultures of inhibitor cells (EPI100 carrying pWEB-TNC, pCH7874, pCH9305, pCH12502, or pCH10445) and target cells (MC4100 carrying pTrc99a or *cdiI* derivatives or MC4100 Δ*yciB::kan* carrying pTrc99a) were grown overnight in LB media or M9 supplemented media (M9 salts (Sigma), 1 mM thiamine hydrochloride (Sigma), 0.2% casamino acids (Acros Organics), 2 mM $MgSO_4$ (EMD reagents), 0.1 mM $CaCl_2$ (Sigma), and 0.4% glycerol (Fisher Scientific)) with antibiotics. Cells were diluted in fresh media and were grown to mid-log phase at 37 ^{o}C with shaking. For co-culture experiments, cells were mixed at a 1:1 inhibitor:target ratio in fresh pre-warmed media supplemented with 1 mM IPTG where indicated. At various timepoints, aliquots were removed, diluted in M9 salts, and plated onto LB-agar or M9-agar supplemented with 200 ug/mL rifampicin to enumerate viable target cells. Data is represented as viable target cells per milliliter of culture, and values shown are the mean ± SEM from three independent replicates.

For competitions with fluorescently-labeled cells, inhibitors (CH2699 carrying pWEB-

TNC, pCH9305, pCH12502, or pCH10445) and targets (CH2567 or CH1273 carrying pTrc99a derivatives) were grown in either LB or M9 supplemented media at 30 ^{o}C with appropriate antibiotics. Cells were mixed at a 1:1 ratio in pre-warmed LB, and aliquots were removed at various timepoints to assess phenotypes via epifluorescence microscopy. Agarose pads were made using M9 supplemented media (as described above, with 1.5 % (w/v) UltraPure™ Low Melting Point Agarose (Life Technologies)) and were cut into 1 cm^2 pads for imaging. 10 µL of each competition mixture was removed from the shaking flask, mixed with DAPI II plus Fluorogel (EMS), and applied to an agarose pad. A coverslip was added, and the slides were incubated at room temperature for 10 minutes to allow cells to settle before viewing. Images were acquired using an Olympus fluorescent microscope with a 100x oil objective and an Optronics MacroFire digital microscope camera. Lightfield images were taken with a 12 millisecond exposure (gain 2), and DAPI images were acquired with a 47.8 millisecond exposure (gain 2). Fluorescent field images were acquired with a gain of 5 and either a 502 millisecond exposure (sfGFP and BFP) or a 1 second exposure time (mKate2). All images were acquired in grayscale and were false-colored using the FIJI image suite (292). Overlays were cropped to 200x200 pixels using GIMP.

4. Time-lapse Microscopy

Time-lapse microscopy was performed as previously described (455). We prepared agarose pads for imaging with M9 supplemented media plus 100 µg/ml carbenicillin. Time-lapse microscopy of low-density colliding microcolonies was performed as followed. Inhibitors (CH2699 carrying the cosmid pCH9305, which constitutively expresses CDI_{o11}^{EC869} (177)) and targets (CH2567 either carrying empty pTrc99a or pCH9315 ($cdiI_{o11}^{EC869}$)) were grown for 12 – 16 h in LB media at 37°C with shaking. Cultures were

diluted to an OD_{600} of 0.01 in fresh supplemented M9 media, grown to mid-log phase (OD_{600} 0.3-0.5), and diluted again to an OD_{600} of 0.015. 0.5 µl of each diluted strain was spotted onto an agarose pad for imaging. For time-lapse microscopy at higher cell density, we used the inhibitor strain CH2699 carrying pCH12502 (IPTG-inducible expression of CDI_{o11}^{EC869}) and susceptible or immune targets (CH2567 or CH12735 (Δ*yciB::kan*), respectively). Both target strains carried pTrc99a and expressed mKate2 from the chromosome. Overnight cultures were diluted, grown to mid-log phase, and diluted again to an OD_{600} of 0.1. Inhibitors and targets were mixed, and 1 µl was applied to an agarose pad supplemented with 1 mM IPTG. Non-fluorescent control cells (CH8251) were also prepared and imaged for each replicate to correct for autofluorescence of cells.

All images were acquired with a 60x Plan Apo oil immersion objective (NA 1.4) using a Nikon Eclipse TE2000-E inverted microscope equipped with Perfect Focus. The Lambda-XL (Sutter Instruments) served as an epifluorescence light source, and a halogen bulb provided phase contrast illumination. The open-source software µmanager (version 1.3.43) (456) controlled the CoolSnap HQ2 CCD camera (Photometric), the MS 2000 motorized stage (ASI instruments), and shutters. Sample temperature was constantly kept at 37 °C using an environmental chamber with heat control (World Precision Instruments). Fluorescent images were taken using the 89006 filter set from Chroma Technology Corporation. ImageJ (457) was used for image processing. An image series from one position was imported into ImageJ, and the brightness of images as a whole was adjusted such that non-fluorescent cells imaged on a separate pad were not visible. All images from the same day and same imaging channel were set to the same display range. False color images were generated by merging the fluorescent channels and the phase-contrast images.

E. Acknowledgments

We thank Pakpoom Subsoontorn for providing the integration vectors TS1013 and TS1014 and the plasmids pTS1465 and pTS1127. We also thank Jing Xiong and Zach Ruhe for providing the IPTG-inducible cosmid system. We are grateful to Francois St-Pierre, Atri Choksi, and Paul Jaschke for their helpful discussions and technical assistance. JLEW was supported by National Science Foundation Graduate Research Fellowship DGE-1144085.

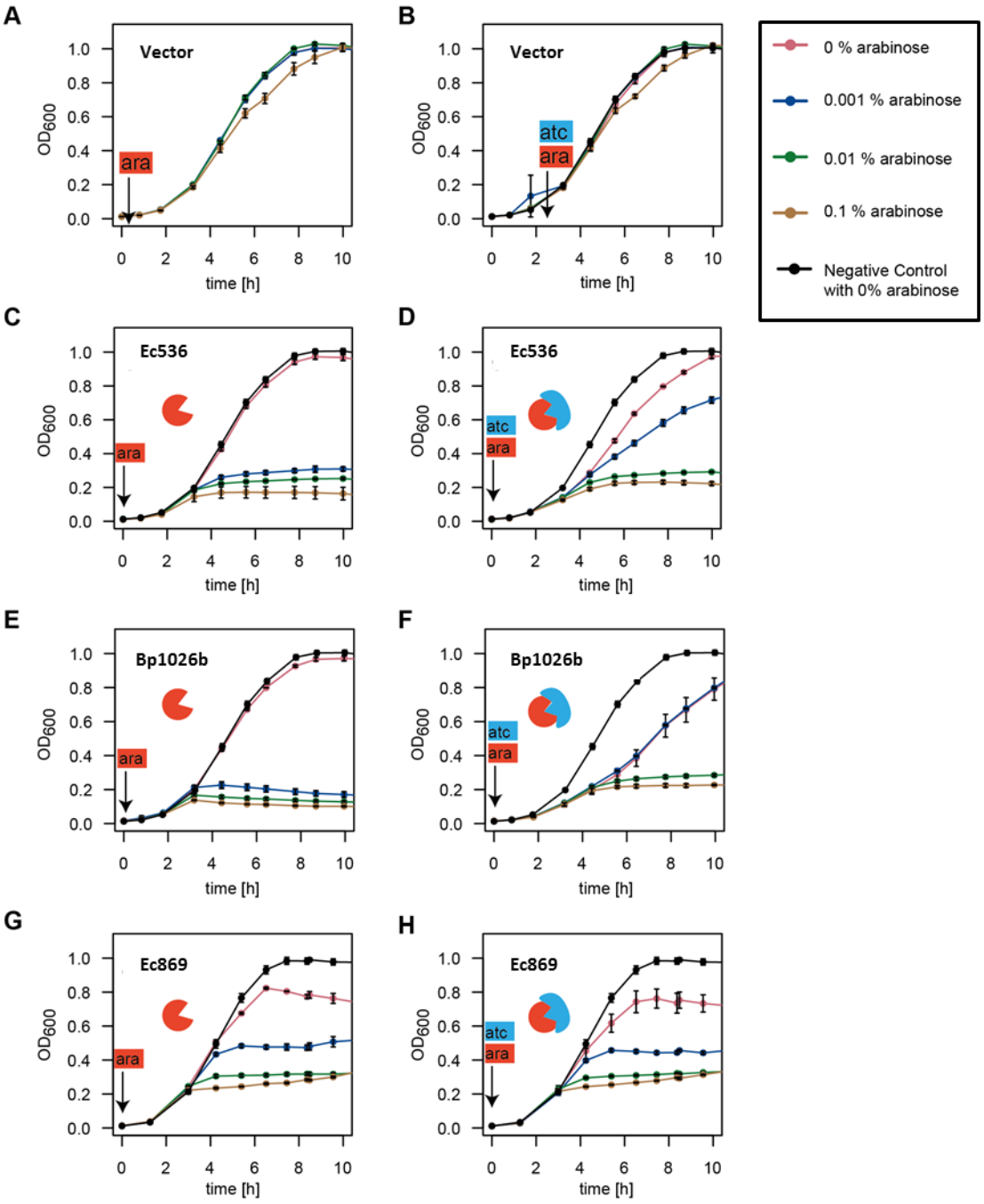

Figure 1. CdiA-CT^{Ec536}, CdiA-CT$_{II}^{Bp1026b}$, and CdiA-CT^{EC869} do not reversibly inhibit cells. *E. coli* DH5αZ1 cells were grown in the presence of (A) arabinose and (B) arabinose and anhydrotetracycline and do not show any growth defect with either treatment. Expression of (C) CdiA-CT^{Ec536}, (E) CdiA-CT$_{II}^{Bp1026b}$, and (G) CdiA-CT^{EC869} inhibit the growth of cells when expressed intracellularly. Of these, only CdiA-CT^{EC869} inhibits cells growth in a titratable manner (compare pink, blue, and green/tan lines. Expression of the cognate CdiI protein partially blocks toxicity of (D) CdiA-CT^{Ec536} and (F) CdiA-CT$_{II}^{Bp1026b}$, but not (H) CdiA-CT^{EC869}. Values are the mean ± SD of three independent samples.

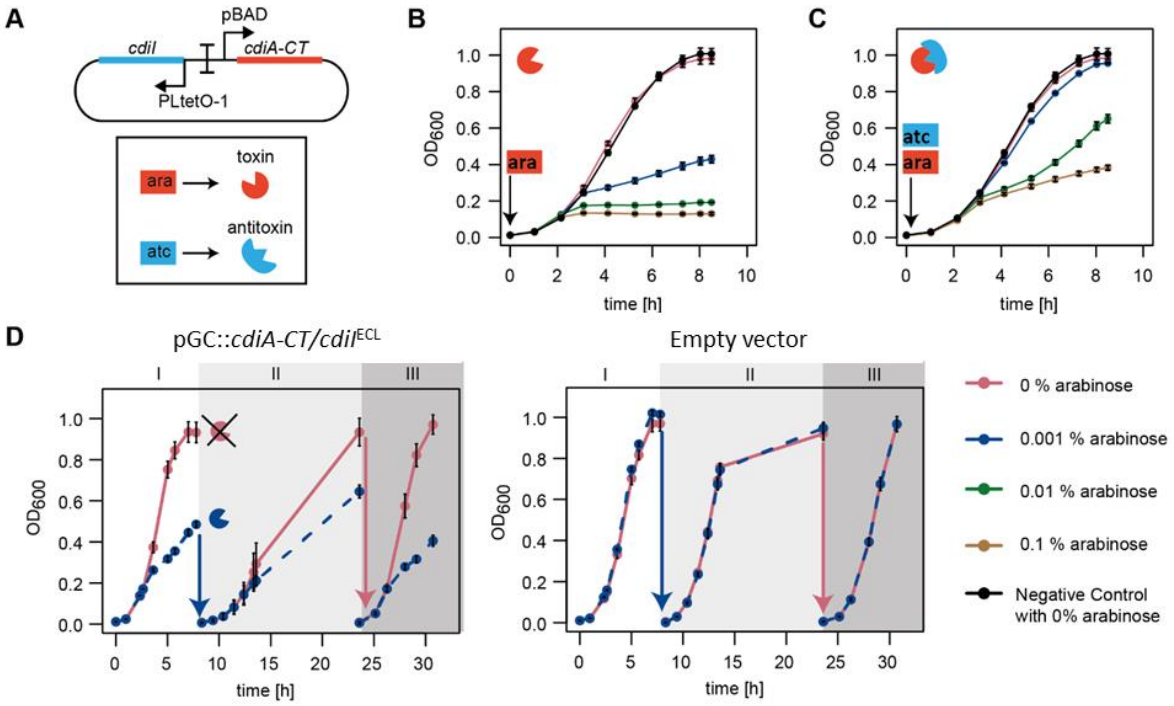

Figure 2. Iterative expression of CdiA-CT^{ECL} can reversibly control cell growth. (A) Schematic of the inducible *cdiA-CT* and *cdiI* modules. CdiA-CT^{ECL} is under control of the arabinose-inducible P_{BAD} promoter, and CdiI^{ECL} is expressed from the anhydrotetracycline-inducible promoter $P_{LtetO-1}$. (B) Inducing CdiA-CT^{ECL} expression by increasing the arabinose concentration slows cell growth as measured by OD_{600}. (C) Expression of CdiI^{ECL} fully rescues inhibition of *E. coli* DH5αZ1caused by low levels of CdiA-CT^{ECL} induction and partially rescues inhibition caused by full induction of CdiA-CT^{ECL}. Values shown are the mean ± SD of three independent samples. (D) Growth inhibition by CdiA-CT^{ECL} is reversible (left panel). *E. coli* DH5αZ1 cells expressing CdiA-CT^{ECL} (induced with 0.001% arabinose, blue lines) are inhibited compared to non-inducing conditions (pink lines). Growth recovers when arabinose is removed (transition from blue line, left panel, phase I to pink line, left panel, phase II) and can be re-suppressed by addition of arabinose (blue line transition from phase I to phase II, left panel). *E. coli* DH5αZ1 grows normally in the presence of arabinose without the CdiA-CT^{ECL} module (right panel). Values are the mean ± SD of three independent samples.

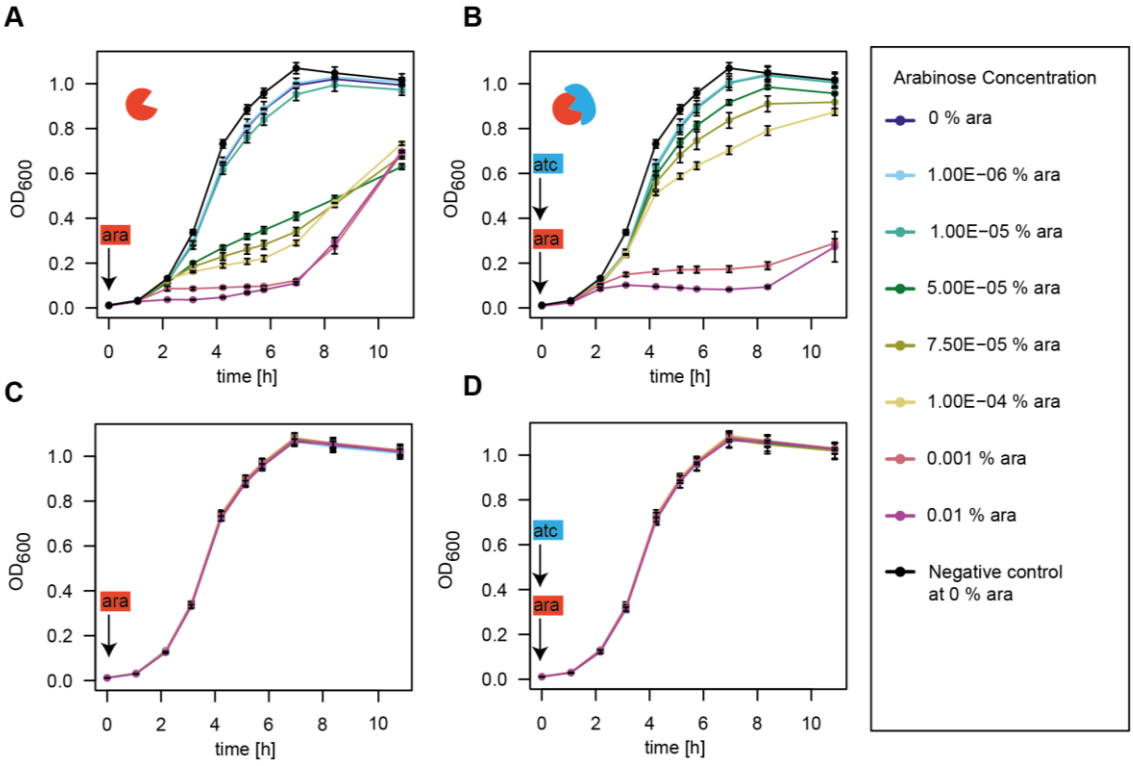

Figure 3. Expression of CdiA-CT^{ECL} inhibits growth when homogenously expressed in strain BW27786. (A) Growth rates of cells expressing CdiA-CT^{ECL} under control of the P_{BAD} promoter were measured using different concentrations of arabinose to induce gene expression. Suppression of the growth inhibition phenotype at the highest inducer concentrations (pink and purple lines) is observed after 7 h of culture. (B) Expression of CdiI^{ECL} by addition of 200 ng/mL anhydrotetracycline reduces toxicity at intermediate arabinose conditions (compare kelly green, olive green, and yellow lines to panel (A)). Growth of BW27786 carrying empty plasmid vectors is not affected by the presence of (C) arabinose or (D) arabinose and anhydrotetracycline in the media. Values are the mean ± SD of three independent samples.

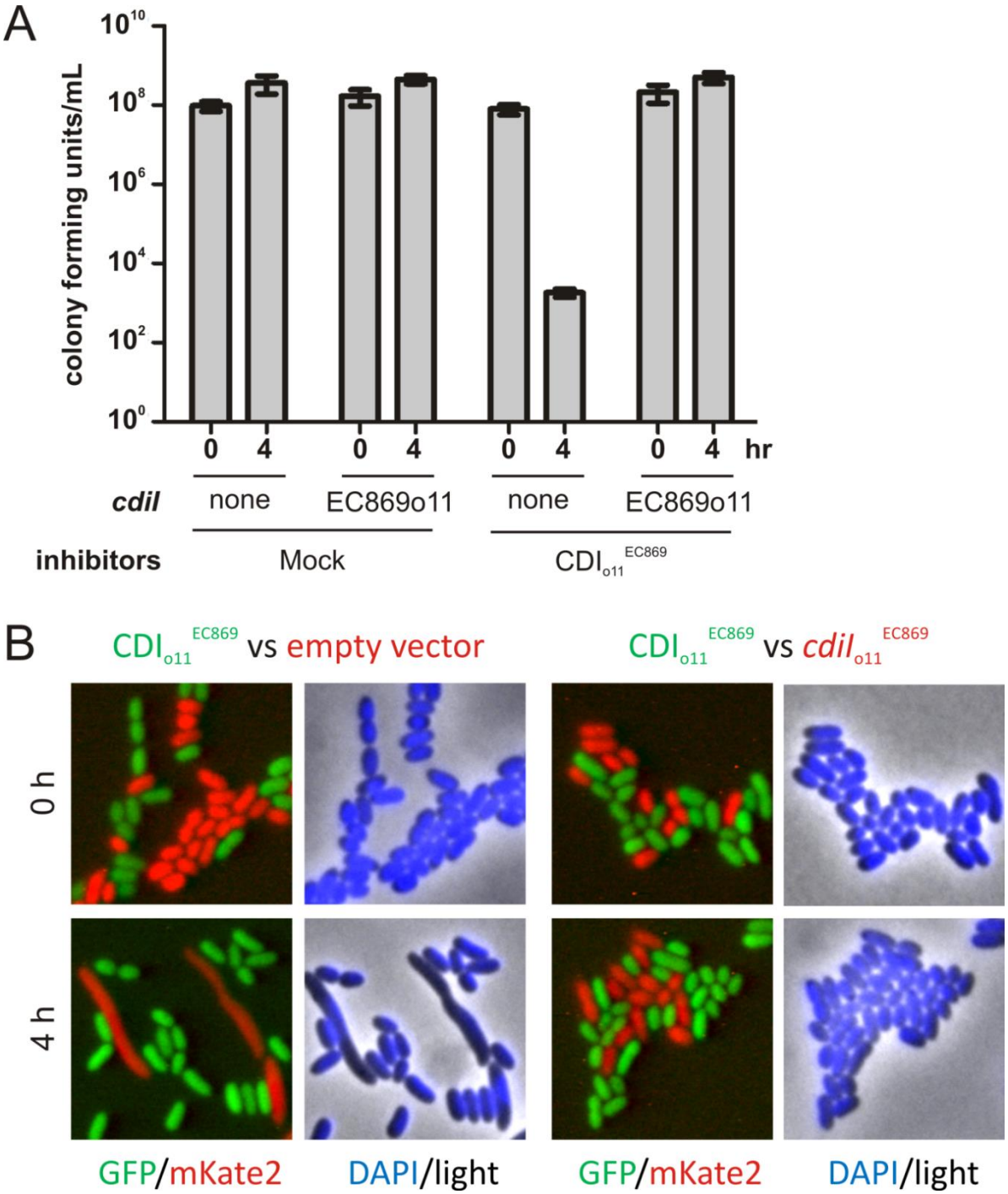

Figure 4. Constitutive expression of CDI_{o11}^{EC869} leads to target cell filamentation. (A) Cells carrying a constitutively-active CDI_{o11}^{EC869} system or a vector control were mixed with wild-type *E. coli* cells or cells carrying a plasmid expressing $cdiI_{o11}^{EC869}$. Viable target cells were measured at 0 and 4 h. (B) GFP-labeled CDI_{o11}^{EC869} cells were mixed with mKate2-labeled target cells in shaking liquid culture. At 0, 3, and 4 h timepoints, aliquots were spotted onto agarose pads and observed using epifluorescence microscopy. CDI-sensitive target cells (left) become filamentous after co-culture with inhibitors, while immune cells (right) do not display any cell morphology defects.

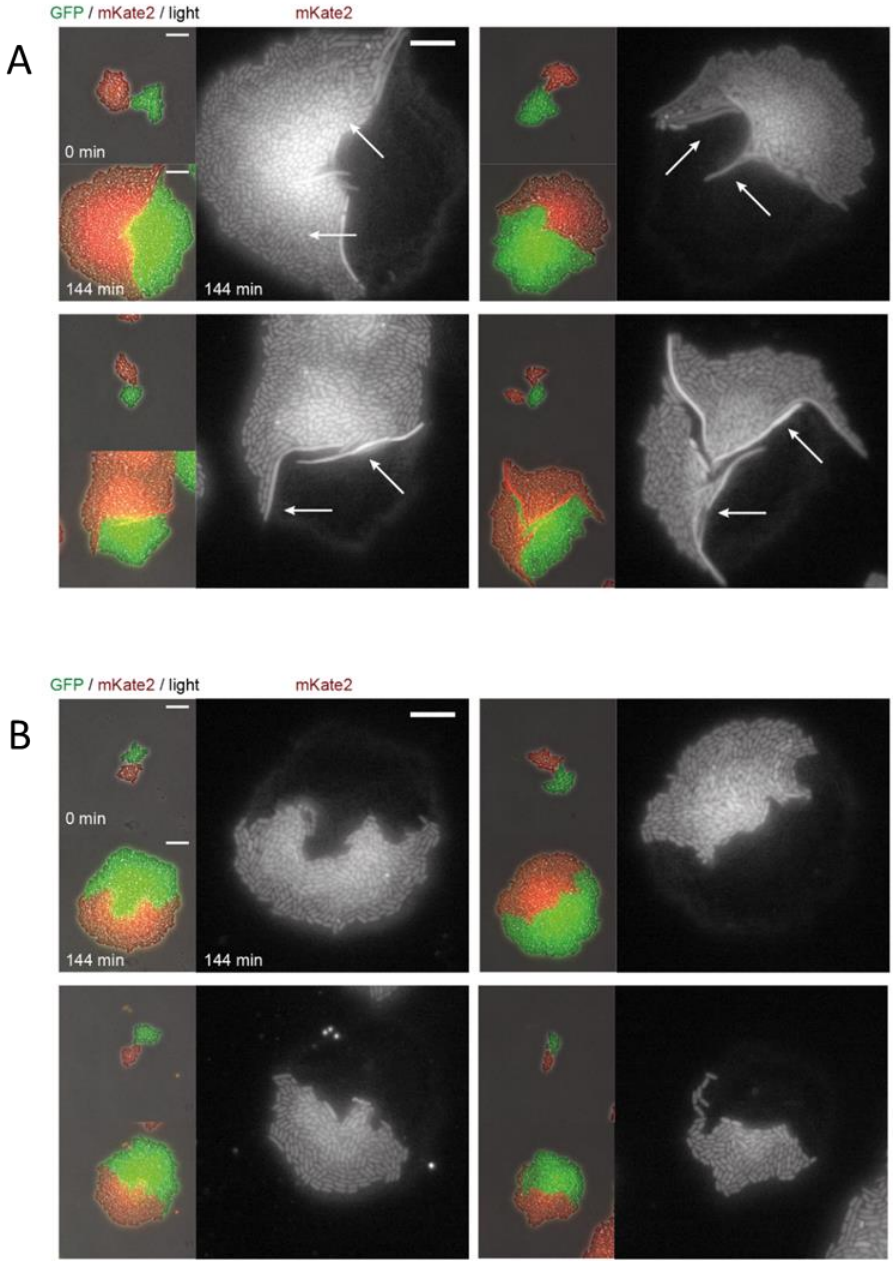

Figure 5. Cells filament in response to inhibition by CDI_{o11}^{EC869}, creating a smooth border between the inhibitor and target populations. (A) GFP-labeled CDI_{o11}^{EC869} inhibitor cells were mixed with mKate2-labeled wild-type *E. coli* target cells carrying a pTrc99a vector control on a stationary agarose pad. Images from initial contact (0 minutes, upper panels) and the result of collision (144 minutes, lower panels) are displayed as a merged GFP/mKate2 field. Target bacteria are independently visualized in the enlarged grayscale images (right panels). Filamentous cells can be observed at the border of the $mKate2^+$ population. (B) The inhibitor strain from (A) was mixed on stationary agarose pads with mKate2-labeled target cells expressing $CdiI^{ECL}$. The merged GFP/mKate2 fields are shown for initial contact (0 minutes, upper panels) and after competition (144 minutes, lower panels). mKate2-labeled cells at 144 minutes are shown in grayscale in the enlarged images. No filamentation or morphological changes are observed. Scale bars are 10 μm.

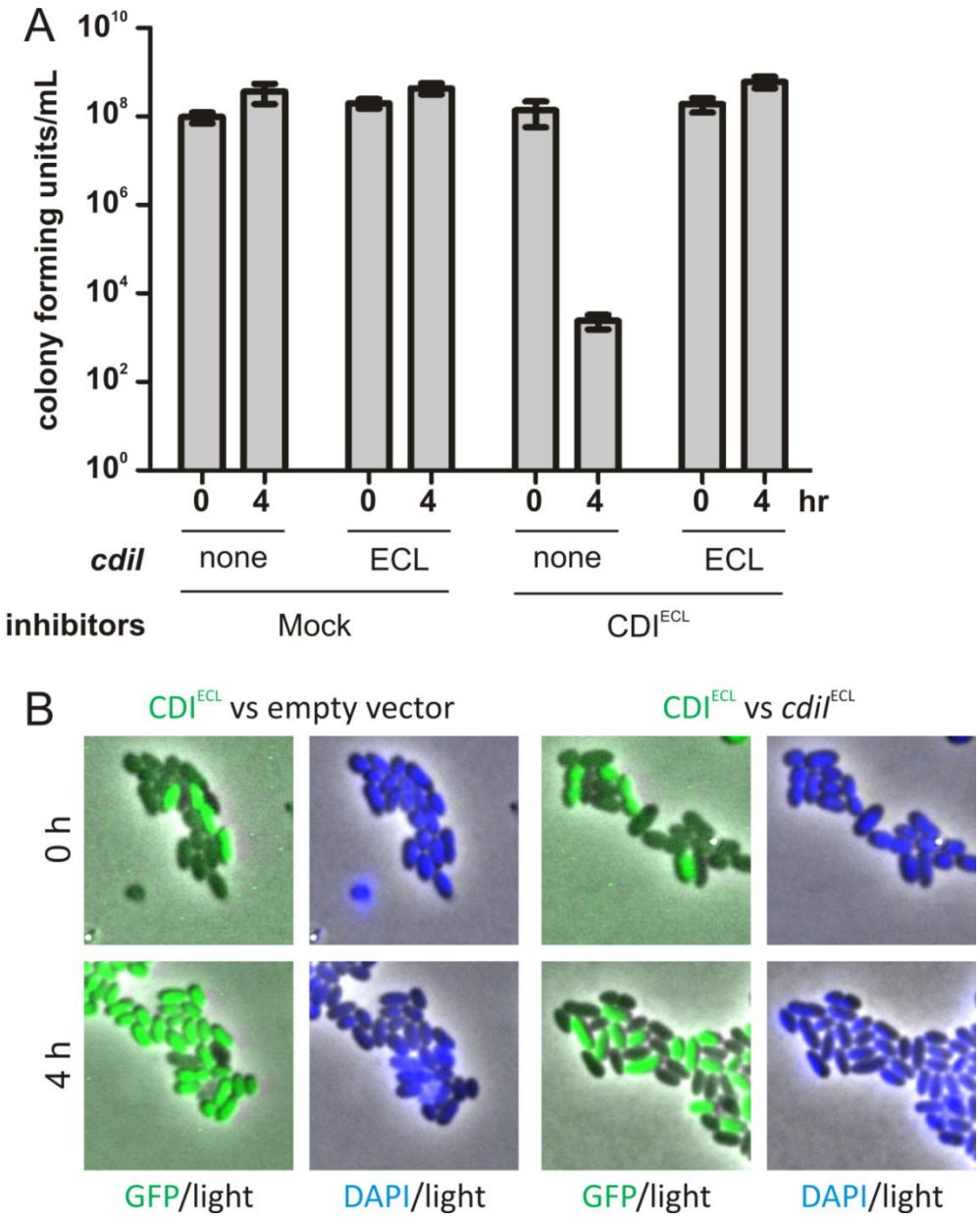

Figure 6. Inhibition of target cells by CDI^{ECL} does not alter target cell morphology. (A) Cells expressing CDI^{ECL} were mixed with targets carrying an empty vector or a plasmid expressing *cdiI*^{ECL} at a 1:1 ratio in M9 supplemented media. Viable target cells were enumerated at 0 and 4 h. Reported values are the average ± SEM for three independent experiments. (B) GFP^{+} CDI^{ECL} cells were mixed with the unlabeled target cells used in the experiments for (A). Cell morphology at 0 and 4 h was visualized via microscopy. CDI^{ECL} does not alter target cell morphology despite decreasing viability by several logs. The morphology of inhibited target cells (left panels) is identical to that of immune target cells (right panels).

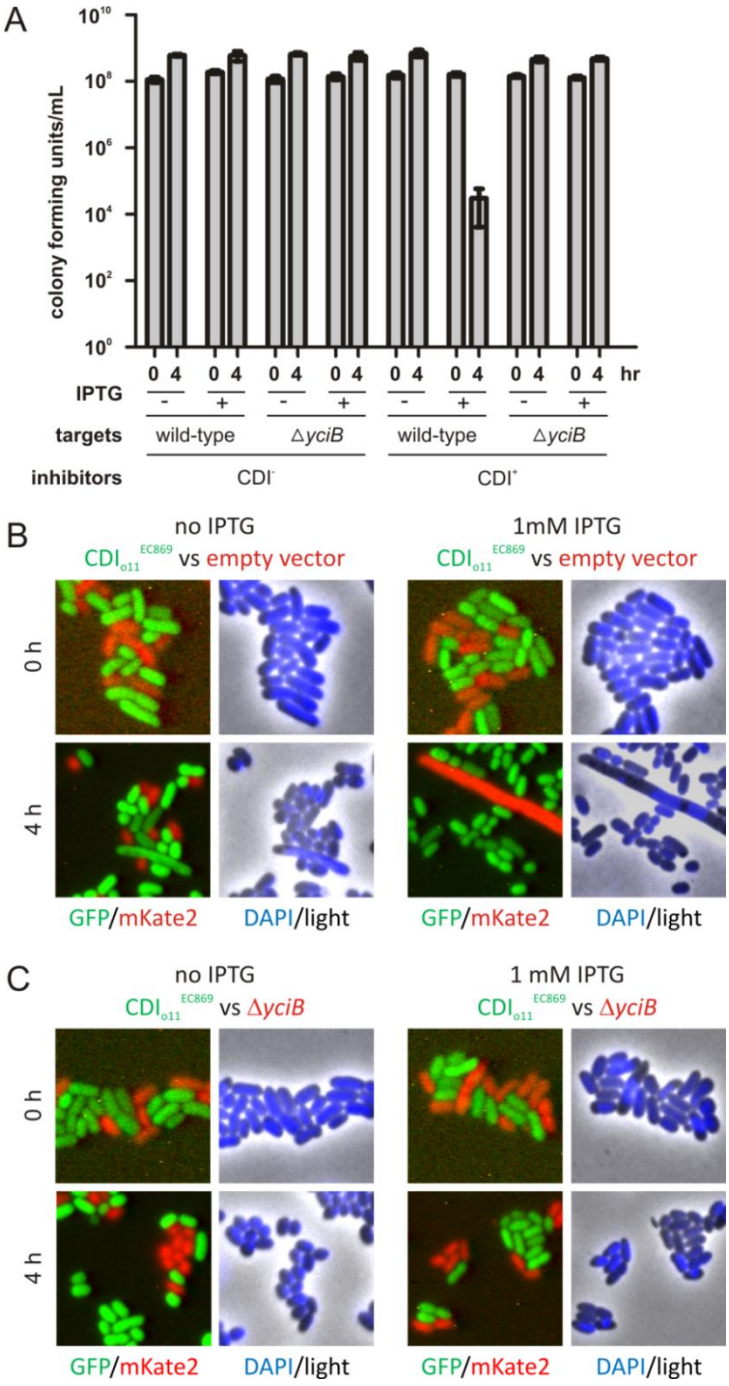

Figure 7. Target cell filamentation can be controlled using IPTG-inducible CDI_{o11}^{EC869}. (A) Inhibitor cells carrying an IPTG-inducible CDI_{o11}^{EC869} system or a control plasmid were mixed with wild-type or Δ*yciB* target strains in the presence and absence of IPTG. Wild-type cells are only inhibited when CDI expression is induced with IPTG. Viable target cells were enumerated at 0 and 4 h. Values reported are the mean ± SEM for three independent experiments. GFP^+ IPTG-CDI_{o11}^{EC869} cells were mixed with mKate2-labeled wild-type target cells (B) or Δ*yciB* target cells (C). Filamentation and DNA degradation is only observed in wild-type cells with induction of CDI_{o11}^{EC869} by IPTG. No filamentation or evidence of cellular damage was observed in Δ*yciB* cells, even in the presence of IPTG.

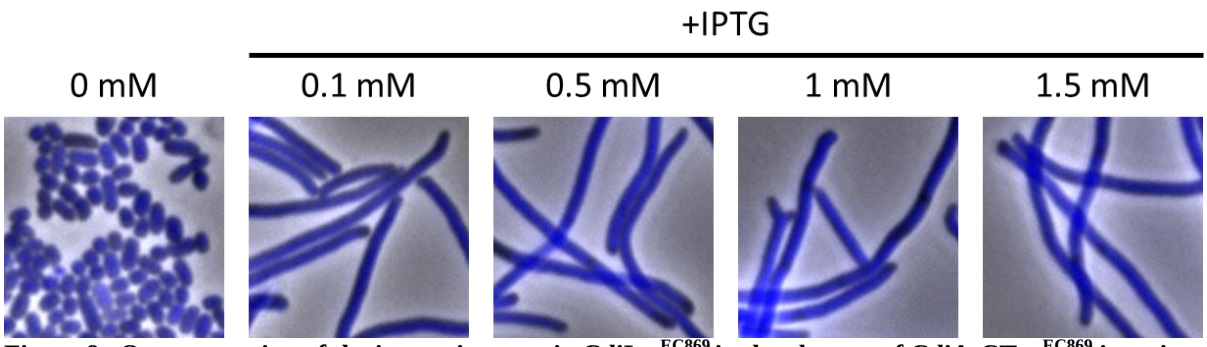

Figure 8. Overexpression of the immunity protein $CdiI_{o11}^{EC869}$ in the absence of $CdiA\text{-}CT_{o11}^{EC869}$ is toxic to cells. Cells carrying the pTrc99a::$cdiI_{o11}^{EC869}$ construct were grown in LB media with the indicated concentration of IPTG. Images were taken after 3 h of growth. Elongated cells are present in all samples except for the untreated culture, but no evidence of DNA degradation is observed. Images are 20x20 μm.

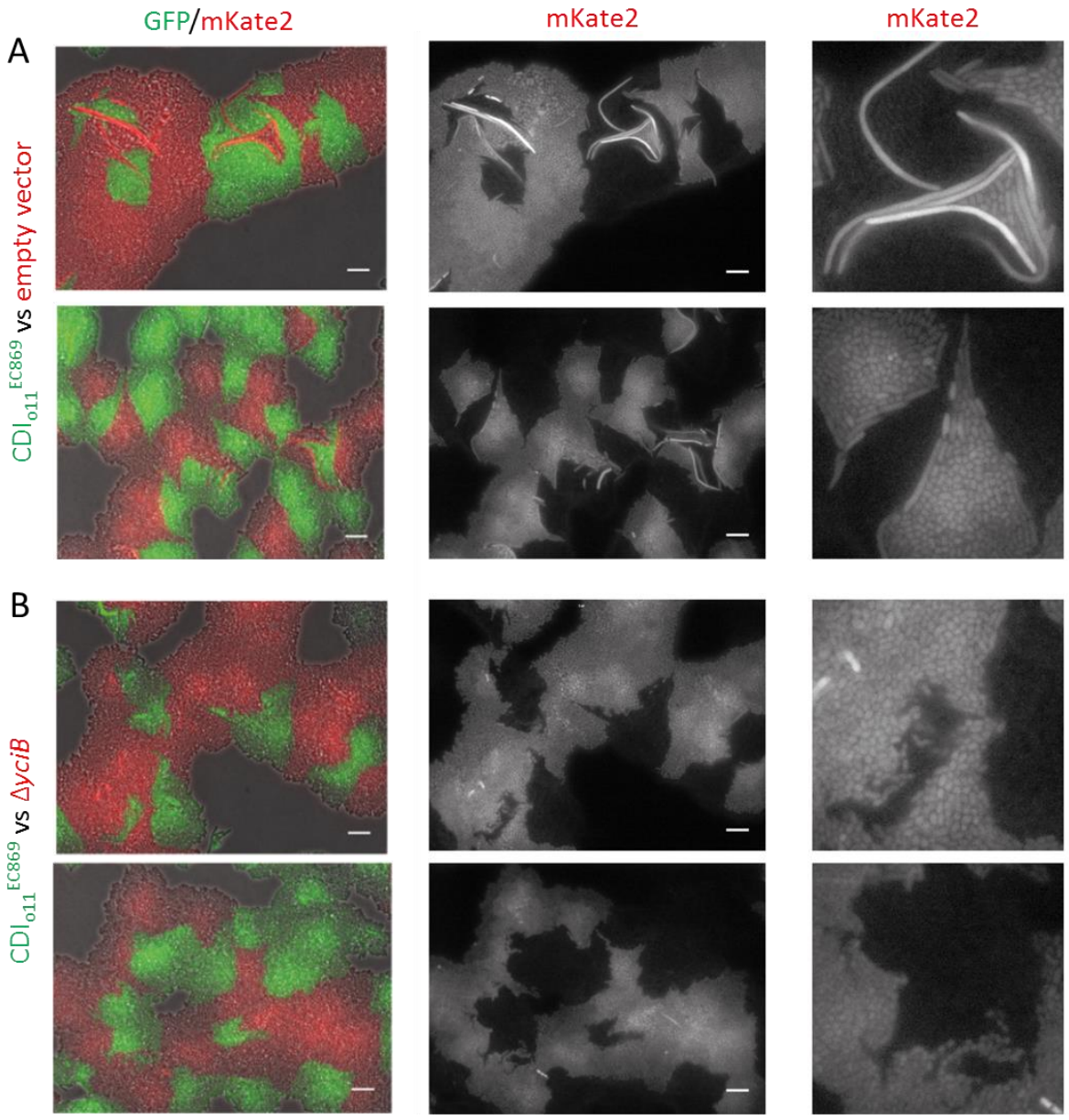

Figure 9. Inner membrane proteins can be utilized to influence population morphology with IPTG-CDI$_{o11}^{EC869}$. (A) GFP$^+$ IPTG-CDI$_{o11}^{EC869}$ cells were mixed with mKate2$^+$ targets and imaged after 240 minutes (4 h). Target cells elongate at the inhibitor/target interface, preventing mixing of the populations and smoothing the interface between the populations. Both populations are shown in the overlaid green/red images (left panels). mKate2-labeled target populations are shown in grayscale (center and right panels). Scale bars are 10 µm. Left panels show a 3x magnification of the full-field (center) images. (B) mKate2$^+$ cells lacking the inner membrane protein required for translocation are not inhibited, and populations intermingle over the course of the 240 minute competition. The border between GFP$^+$ and mKate2$^+$ cells is jagged, as opposed to the smooth interface observed in (A).

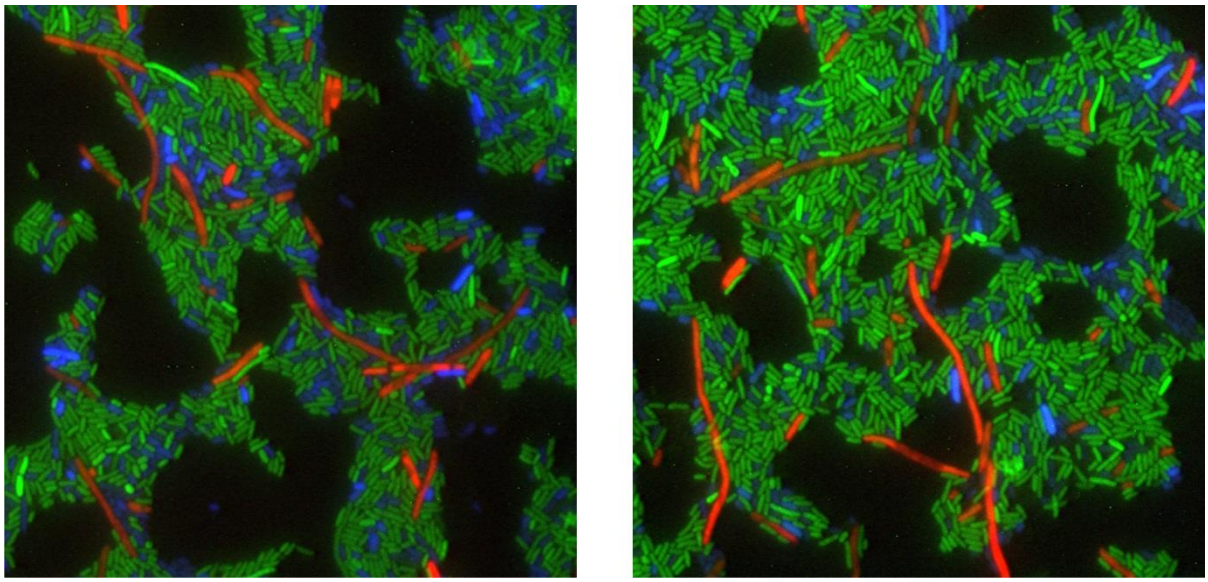

Figure 10. Subpopulations of cells in a complex environment can be targeted using CDI systems. GFP-labeled CDI_{o11}^{EC869} cells were mixed with immune BFP-labeled cells expressing $cdiI_{o11}^{EC869}$ and CDI-sensitive mKate2^{+} target cells in shaking liquid culture and were spotted onto agarose pads for imaging. Only the mKate2-labeled target cells undergo filamentation, while the immune BFP^{+} population remains morphologically unchanged. Representative images from two independent experiments are shown.

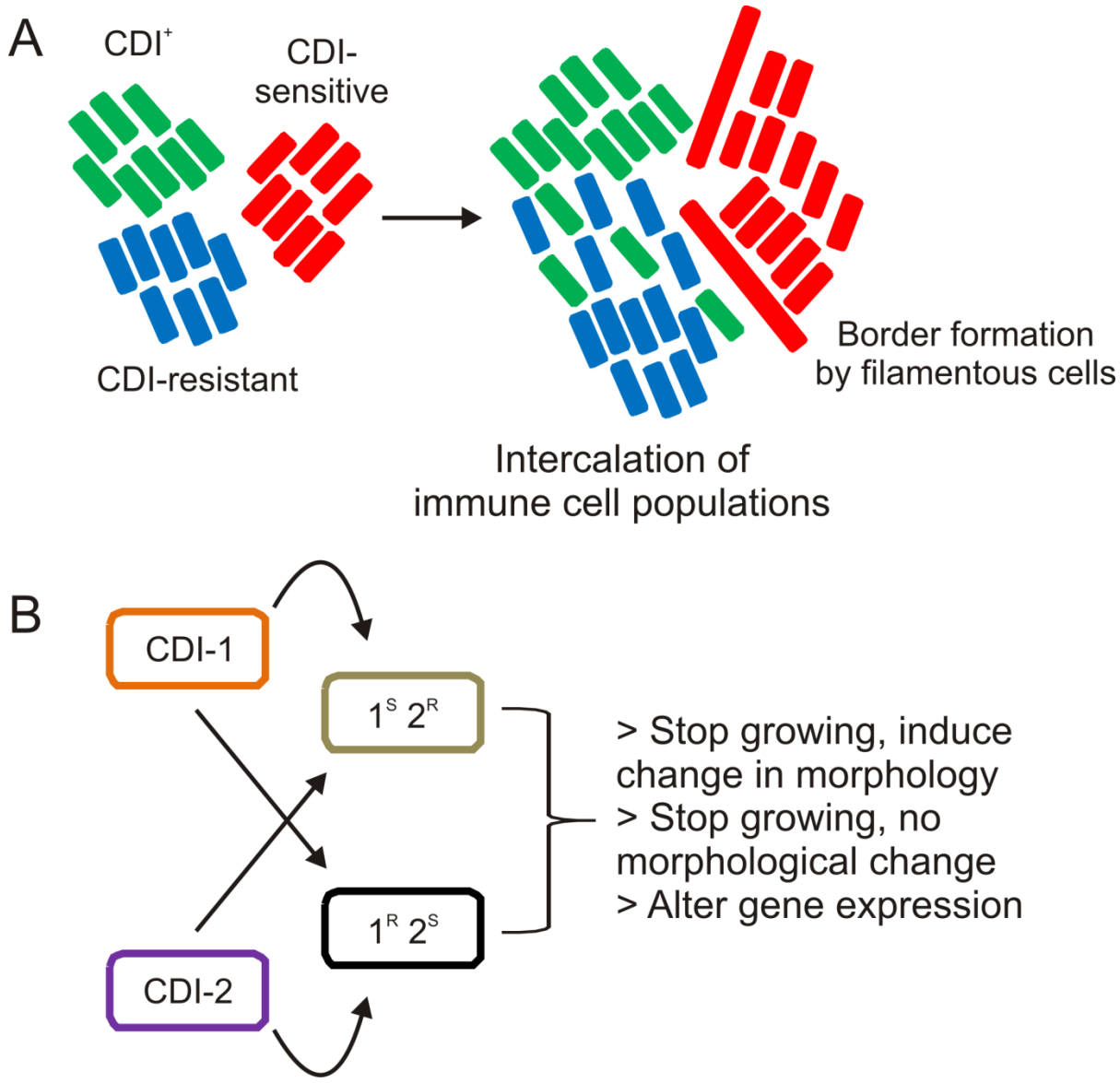

Figure 11. Applications of CDI-based synthetic biology tools. Two possible methods to differentially control subpopulations of cells are diagrammed. As shown in (A), a three-cell system composed of sensitive and immune target cells could be used to make zones of green and blue cells while excluding red cells, which block invading green cells by filamentation after inhibition by CdiA-CTs like CdiA-CT_{o11}^{EC869}. (B) shows how multiple toxins and target cells could be utilized to built synthetic biology tools of increasing complexity.

Table 1. Bacterial strains and plasmids used in this study.

Strains		
DH5αZ1	Δ(argF-lac)169, φ80dlacZ58(M15), ΔphoA8, glnX44(AS), λ-, deoR481, rfbC1, gyrA96(NalR), recA1, endA1, thiE1, hsdR17, laci^{q}, PN25-tetR, Sp^{R}	(431)
BW27786	Δ(araD-araB)567, ΔlacZ4787(::rrnB-3), λ-, Δ(araH-araF)570(::FRT), ΔaraEp-532::FRT, φPcp13araE534, Δ(rhaD-rhaB)568, hsdR514	(433)
MC4100	F- araD139 Δ(argF-lac)U169 rpsL150 relA1 flbB5301 deoC1 ptsF25 rbsR, Str^{R}	(458)
CH2567	MC4100 rif^{R} *mKate2::cat*	(202)
CH2699	MC4100 rif^{R} *GFP::kan*	This study
CH8251	MC4100 rif^{R}	(173)
CH9404	MC4100 rif^{R} Δ*yciB::kan*	(173)
CH12735	MC4100 rif^{R} *ΔyciB::kan mKate2::cat*	This study
DA28102	*galK::mTagBFP2opt-cat*, constitutive expression of BFP at the *gal* locus	Sanna Koskiniemi
Plasmids		
J64100	Regulated ColE1 origin, CmR	Registry of Standard Biological Parts
pSB4A5	Low copy pSC101 origin, AmpR	Registry of Standard Biological Parts
pGCCtrl	Control plasmid, CmR	This study
pGC::CdiA-CT/CdiI^{UPEC536}	Expression of *cdiA-CT*^{UPEC536} under the control of PBAD and *cdiI*^{UPEC536} under the control of $P_{LtetO-1}$, Cm^{R}	This study
pGC::CdiA-CT/CdiI^{ECL}	Expression of *cdiA-CT*^{ECL} under the control of PBAD and *cdiI*^{ECL} under the control of $P_{LtetO-1}$, Cm^{R}	This study
pGC::CdiA-CT/CdiI^{EC869}	Expression of *cdiA-CT*^{EC869} under the control of PBAD and *cdiI*^{EC869} under the control of $P_{LtetO-1}$,	This study

	Cm^R	
pGC::CdiA-CT/CdiI^{Bp1026b}	Expression of *cdiA-CT*^{1026b} under the control of PBAD and *cdiI*^{1026b} under the control of $P_{LtetO-1}$, Cm^R	This study
pTS1127	pSB4A5 expressing *tetR* under the control of the constitutive promoter J23100, Amp^R	Pakpoom Subsoontorn
pTS1465	Expression of superfolder GFP under the control of P_{BAD} and of mKate2 under the control of P_{TET}, Cm^R	Pakpoom Subsoontorn
pTS1013	HK022 integration vector expressing mKate2 under the control of the promoter J23119, Cm^R	Pakpoom Subsoontorn
pTS1014	HK022 integration vector expressing superfolderGFP under the control of the promoter J23119, Cm^R	Pakpoom Subsoontorn
pAH69	CRIM helper plasmid encoding integrase HK022	(453)
pCH9305	Constitutive expression of chimeric *cdiA*^{EC93}-*CT*^{EC869o11} and *cdiI*^{EC869o11} genes, Amp^R	(177)
pCH9433	Constitutive expression of chimeric *cdiA*^{EC93}-*CT*^{Bp1026b} and *cdiI*^{Bp1026b} genes, Cm^R	(172)
pCH10445	Constitutive expression of *cdiA*^{EC93}-*CT*^{ECL} and *cdiI*^{ECL} genes, Cm^R	(175)
pCH10525	Constitutive expression of *cdiA*^{EC93}-*CT*^{EC869o5} and *cdiI*^{EC869o5} genes, Cm^R	(172)
pCH10540	Constitutive expression of *cdiA*^{EC93}-*CT*^{Ec536} and *cdiI*^{UPEC536} genes, Cm^R	(172)
pCH12502	IPTG-inducible expression of *cdiA*^{EC93}-*CT*^{EC869o11} and *cdiI*^{EC869o11}, Amp^R	This study
pTrc99a	IPTG-inducible expression plasmid, Amp^R	GE Healthcare
pCH9315	pTrc99a::*cdiI*^{EC869o11}, Amp^R	(177)
pCH9000	pTrc99a::*cdiI*^{ECL}, Amp^R	(175)
pCH7874	Derivative of pDAL660Δ1-39 in which the *cdiA-CT/cdiI* region has been deleted, Cm^R Amp^R	(194)

Table 2. Oligonucleotide sequences used in this study.

Oligonucleotide	Sequence
TS349	5’ – GCT GAG GGT CTC ATG CGA TAA TGT TTA GTC ATG CTA GCC ATG – 3’
TS433	5’ – TAC AAA GGT CTC TTA ACT CTA GAA GCG GCC GCG AAT TC – 3’
TS455	5’ – AAT TAG GTC TCA CTA GTA GCG GCC GCT GCA G – 3’
TS460	5’ – TAC AAA GGT CTC AGC ATG ATT AAG ATG TTT CAG TAC GAA AAT TGC – 3’
BR1_UPEC536_cdiI_fw	5’ – CCT GAA GGT CTC AGT TAT CAT CAG TGG TGG TGG TGG TGG – 3’
BR2_UPEC536_cdiI_rev	5’ – ATA TAT GGT CTC ACG CAT TCA TCT GGA GCT GAT TTA ATG ATT ACC TTA CGT AAA TTG ATT GGA AAC ATC AAT ATG AC – 3’
BR3_UPEC536_cdiACT_fw	5’ – CGT TAA GGT CTC GAT GCT AAG GAG GTT TTC TAA TGG TTG AGA ATA ATG CGC TGA GTC TGG – 3’
BR4_UPEC536_cdiACT_rev	5’ – ATT AAC GGT CTC GCT AGT ACT CTA GTA TCA TAT TCC ATA TCC TTT CAA GGC TGA TTC TAT TT – 3’
BR15_ECL_cdiI_fw	5’ – AGC GAT GGT CTC AGT TAT CAG TTG TTA AGA CTA TGA TAA AAA TCT AAA ACA CTA TTT – 3’
BR16_ECL_cdiI_rev	5’ – CAT TTC GGT CTC TCG CAT TCA TCT GGA GCT GAT TTA ATG TTT GGA ATA TTC TCT AAA GGT GAA CCA GT – 3’
BR17_ECL_cdiACT_fw	5’ – CAC TCC GGT CTC CAT GCT AAG GAG GTT TTC TAA TGT CGC TGG CAC TGG TTG C – 3’
BR18_ECL_cdiACT_rev	5’ – TCG CAA GGT CTC ACT AGT ACT CTA GTA CTA GTC CTT AAT CCT GTT TAG TCC GC – 3’
BR19_EC869_cdiI_fw	5’ – TAG CTC GGT CTC CGT TAT CAC TAA CCT ACT GCC TCA AAA AAA CTT TCC – 3’
BR20_EC869_cdiI_rev	5’ – GGA GCT GGT CTC ACG CAT TCA TCT GGA GCT GAT TTA ATG AAA TTA ACT GTA GAT AGC GTT

	ATT AAT GAA CC – 3’
BR21_EC869_cdiACT_fw	5’ – CCT TGC GGT CTC TAT GCT AAG GAG GTT TTC TAA TGT ATC TGA GTA AAG CCC AGA AAG CTC – 3’
BR22_EC869_cdiACT_rev	5’ – TAC TGC GGT CTC ACT AGT ACT CTA GTA TTA TTT ATA CAA CGC ATG CTT TAA TAC TGG ATA – 3’
BR23_1026b_cdiI_fw	5’ – GGA TGA GGT CTC CGT TAT CAT CAC CTC CGG TAT TCG TTA TCT TG – 3’
BR24_1026b_cdiI_rev	5’ – CTG AAA GGT CTC ACG CAT TCA TCT GGA GCT GAT TTA ATG GCA ATT GAC TTG TTT TGC TAT CTC TCA – 3’
BR25_1026b_cdiACT_fw	5’ – TGC TCA GGT CTC GAT GCT AAG GAG GTT TTC TAA TGG GCT CTT TAT CAG GCA AGC C – 3’
BR26_1026b_cdiACT_rev	5’ – ACC TGG GGT CTC GCT AGT ACT CTA GTA TTA ATT CCC CTT TGG CTT TAT GAT GGT – 3’

VIII. Conclusion

Bacteria are ubiquitous in nature. The density and complexity of the microscopic world necessitates tools to help these cells acquire nutrients, communicate with neighboring microbes, and fend off direct competitors, all while replicating and establishing a niche in a host organism or another environment. These needs are evidenced by the diversity of inhibition and competition systems that have been discovered in prokaryotic organisms. Both contact-independent and contact-dependent bacterial competition systems have been classically envisioned as a means by which an inhibitor cell (or population of inhibitor cells) can gain an advantage over nearby susceptible cells, thus promoting their own growth or the growth of sibling cells over surrounding microbes.

This thesis has explored aspects of contact-dependent growth inhibition (CDI) systems in *E. coli* in an effort to understand the process by which these systems deliver CdiA-CT toxin domains into neighboring cells, how these effector domains exert toxicity, and how these systems are involved in general bacterial physiology. Chapter II presented genetic evidence towards the mechanism by which CdiA-CT toxins translocate across the inner membrane of target cells during delivery. Chapter III illustrated a physiological role for one such inner membrane protein, YciB, which we demonstrate is required for metal tolerance in *E. coli* in addition to CdiA-CT delivery. In Chapter IV, we examined CDI from the viewpoint of a target cell and discussed insertion element transposition as a way to confer transient resistance to certain toxins. This type of target cell stress response may contribute to the physiology of these systems in natural environments. Chapter V presented work investigating the basis of CdiA-CT diversification across bacterial genomes, specifically focusing on a family of toxins related to the DNase toxin CdiA-CT_{o11}^{EC869}. This work shows

how CdiA-CT/CdiI pairs evolve at the toxin-immunity interface while retaining a conserved core structure. In Chapter VI, we discussed new data on a co-factor involved in the activity of two CDI toxins. This protein, EF-Tu, is a well-characterized translation factor that has recently been implicated in the delivery of a type 6 secretion system toxin in *Pseudomonas aeruginosa*. Finally, in Chapter VII, we stepped outside the physiological role of CDI to use these modular toxin-immunity domains as synthetic biology tools. Taken together, this thesis highlights how a seemingly-simple three gene locus encodes an inhibition system of remarkably complexity.

Future research will continue to investigate how these bacterial competition systems interact with and inhibit other cells, and this work will refine our understanding of the biological role of CDI in microbial environments. In this concluding chapter, we discuss some research questions of significant interest in the field of CDI. A notable observation regarding is that every facet of CDI studied thus far has had implications not only for these inhibition systems, but for fundamental aspects of bacterial physiology. The processes required for biogenesis and surface display of CdiA, delivery of toxins, and carrying out inhibitory activity is inherently intertwined with research areas such as protein translocation across membranes, translation, metabolism, microbial stress responses, and evolution. A deeper understanding of the mechanisms involved in CDI will undoubtedly provide a fresh, interesting perspective on well-studied principles of microbiology.

A. Outlook on the mechanisms of CdiA-CT delivery

1. Rethinking the model of CdiA biogenesis

The current understanding of the biogenesis of CdiA is based on the model of FHA protein orientation in *Bordatella pertussis*, which proposes that the C-terminus of the protein

projects away from the cell surface, while the N-terminal region anchors the protein to the cell surface (148). However, this model has several logistical flaws. First, CdiA and FHA proteins are exceptionally large (200-600 kDa), and the C-terminal toxin domains of CdiA are relatively small (20-30 kDa) (167, 170). Therefore, presenting the "business end" of this protein into extracellular space is a bold, somewhat risky option given the possibility of degradation by extracellular proteases. However, it is possible that the native conformation of CdiA is such that the C-terminal toxic domain is protected from the extracellular milieu by the folding of another yet-uncharacterized domain upstream in CdiA into a pseudo-chaperone domain that shields CdiA-CT until delivery, much like how the RHS repeat domains in ABC-type toxins form a "cage" around the delivered effector domain (233). Additionally, the receptor binding region of CdiA lies in the middle of the primary sequence (157, 159, 225). It is not immediately obvious why this would be the optimal domain localization if the C-terminus is secreted from the cell first, considering that receptor binding must occur for toxin delivery.

Perhaps a more parsimonious explanation is that the current model of CdiA presentation is inverted. CdiA requires the Sec machinery for co-translational secretion into the periplasm of CDI^+ cells, and the N-terminus is transported into the periplasm before the C-terminus. If the N-terminus of CdiA is also secreted via CdiB before the C-terminus, this could conceivably be a mechanism by which the extracellular portion of CdiA, presumably containing the receptor-binding domain, could sample the surface of nearby cells to ensure that there is an appropriate target in the vicinity that can receive the CdiA-CT domain. This orientation could also protect CdiA-CT from extracellular degradation by selectively releasing this domain from the periplasm of producing cells after receptor binding occurs,

ensuring its immediate delivering into an awaiting cell. A number of periplasmic chaperones are required to keep domains in other T5SSs unfolded in the periplasm before export out of the cell (459, 460), so it is plausible that a similar system could protect CdiA-CT from the activity of periplasmic peptidases or retain the effector in a delivery-competent state until delivery into a target cell can occur. This model could also rationalize the lack of periplasmic-acting CdiA-CT toxins identified thus far. It is interesting to considering that in contrast to T6SS effector domains and colicins, no known CdiA-CTs degrade periplasmic components like peptidoglycan. CdiI proteins are produced in the cytoplasm and have no signal peptides or export signals to localize them to the periplasm for protection against incoming toxins.

2. Target cell recognition

The first outer membrane receptor identified for CDI systems was BamA, an essential outer membrane protein involved in outer membrane protein biogenesis (157, 190). Detailed studies revealed that CdiA makes contact with the surface-exposed extracellular loops of BamA, which have little sequence homology across species (159). The CdiA/BamA interaction is species-specific; only BamA protein from *E. coli* supports binding of *E. coli* EC93 CdiA and subsequent delivery of CdiA-CTs and target cell inhibition (159). This specificity profile dictates potential CDI interactions and restricts the inhibitory potential of the *E. coli* EC93 CDI system to other *E. coli* strains, thereby constraining the range of target bacteria that are susceptible to attack by *E. coli* CDI systems. This raises the question of what benefit is derived from only targeting sibling cells instead of different species that may be competing for space and nutrients in the same niche.

Preliminary data suggests that distinct classes of CdiA protein may utilize different outer

membrane receptors (Zach Ruhe, Christina Beck, David Low, and Christopher Hayes, unpublished data). The ability of CDI systems to target different outer membrane proteins or structures increases the number of ways that CDI^+ cells can interact with surrounding targets. This interplay may be complicated by expression patterns of proteins that serve as CDI receptors, as outer membrane proteins are known to be regulated by a variety of factors (461-464). Outer membrane proteins are targeted by phage (191), colicins (23), and host immune systems and are under constant selective pressure (465, 466). CDI systems that target specific outer membrane proteins or cell surface structures are conceivably another form of selective pressure that can shape the content of surface-exposed residues of outer membrane proteins. Interestingly, cell surface modifications such as production capsule can block CDI (157), suggesting that the inhibitory or communication potentials of these systems are subject to regulation on multiple levels at the outer membrane.

3. Processing and delivery across the inner membrane

For the nuclease CdiA-CT toxins, delivery into the cytoplasm of target cells is a requirement for target cell inhibition. The work presented in Chapter II sheds light on unique toxin/inner membrane protein relationships involved in this process. However, the precise mechanistic details of moving these proteinaceous cargoes across the lipid bilayer inner membrane are far from clear. DNase colicins are predicted to interact with the anionic lipid head groups via positively-charged residues (81, 85). Colicin D and related klebicins require LepB, an inner membrane peptidase, for translocation, and this interaction presumably brings the toxins close enough to the inner membrane to facilitate transport through FtsH or another pathway (91, 101, 103, 467). Therefore, it is plausible that CdiA-CT domains could translocate across the inner membrane via similar mechanisms. The inner membrane proteins we identified may take the place of LepB, bringing these toxins close enough to the

lipid face to initiate the final translocation steps. One model for translocation is that after CdiA-CT domains gain proximity to the inner membrane by binding or interacting with a membrane receptor, they transverse through the inner membrane at the protein/lipid interface.

Evidence of another aspect of toxin translocation across the inner membrane comes from the T6SS in *Pseudomonas aeruginosa*. Tse6, a toxin with cytotoxic $NAD(P)^+$-ase activity. This toxin requires the translation elongation factor EF-Tu for delivery into the cytoplasm, presumably via a ratchet-like mechanism in which EF-Tu interacts with an exposed hydrophobic patch of Tse6 and pulls the toxin across the inner membrane (262). Like colicins, Tse6 is predicted to interact to with the inner membrane via positively-charged residues. It is known that the proton motive force is required for CdiA-CT translocation, regardless of the intracellular activity of the toxin (172). A fragment of CdiA containing the CdiA-CT is delivered to the periplasm after the initial BamA recognition event occurs at the outer membrane. This fragment can be stably retained in this compartment in the absence of pmf, but complete translocation across the inner membrane into the cytoplasm requires pmf (172). Perhaps CdiA-CT movement across the inner membrane shares commonalities with both colicin import and T6SS delivery, and intrinsic association of CdiA-CTs with the inner membrane recruits other cellular factors that harness pmf to complete the delivery process.

Though we have been unable to demonstrate direct binding between CdiA-CTs and the inner membrane proteins required for delivery of these toxic domains, what is known is a genetic link between the N-terminal half of CdiA-CTs and their inner membrane translocation pathway. It is clear from our study presented in Chapter II that the CdiA-CT N-terminal domain dictates the delivery of these toxins across the inner membrane. These N-

terminal regions are typically poorly resolved in crystal structures of CdiA-CTs (175, 177) and are presumably more labile than their attached cytotoxic domains. Current studies using NMR and membrane-association techniques are underway in an effort to determine whether these N-terminal domains have affinity for their required inner membrane proteins or the inner membrane itself. A combinatorial approach using structural, genetic, and biochemical approaches will be required to fully understand the role of CdiA-CT N-terminal domains in toxin translocation during CDI as well as the biochemical rules that govern the "mixing and matching" of N-terminal translocation domains and C-terminal cytotoxic domains in CdiA-CTs. We note that while we have been able to swap translocation and cytotoxic domains between some CdiA-CT toxins, not all constructs have yielded a functional CDI system. A better understanding of the interactions between the N- and C-terminal domains as well as between the N-terminal domain and translocation pathway components will allow us to understand why some, but not all, N-terminal/C-terminal combinations support CDI.

In addition to the mechanistic details of membrane translocation during delivery, another aspect of CdiA-CT translocation that is poorly understood is the processing of CdiA that occurs during these steps. CdiA proteins are highly conserved up until the VENN tetrapeptide that demarcates the start of the CdiA-CT domain (167). One scenario that explains the conservation of this motif is that these residues are involved in a critical step of CdiA-CT delivery. If a processing event that liberates the toxin domain is required for inhibition, then the VENN residues might facilitate this chemistry. Preliminary experiments show that mutation of the terminal asparagines to alanine residues results in a loss of inhibition, suggesting that they are indeed important for the overall process of CDI (Julia Webb, Grant Gucinski, David Low, and Christopher Hayes, unpublished data). CdiA-CT

domains found in *Burkholderia pseudomallei* are demarcated by a SNVELYN motif instead of the VENN tetrapeptide commonly found in gammaproteobacterial CDI systems. Though not identical, the residues in the *Burkholderia* motif could still presumably support autoproteolytic activity during delivery. Several questions about the precise mechanism of delivery remain to be answered. What is the specific role of the VENN motif, and is it catalytic? Are cleavage mechanisms involved in delivery of CdiA-CT domains conserved across all CDI systems?

Identifying the delivered domain of CdiA-CT could aid in the clarification of processing steps that occur during delivery. However, attempts to "fish out" a delivered CdiA-CT fragment from inside target cells has been ongoing and unsuccessful, presumably in no small part affected by the small number of CdiA-CT molecules that are delivered to a single target cell. Also compounding identification of this domain is the experimental requirement of a two-cell system; it has so far not been possible to inhibit cells using purified extracellular doses of CdiA. This distinguishes CDI from colicins and other related secreted toxins, which can be readily purified and added exogenously to cells. A possible solution would be the use of two-dimensional gels to increase resolution and identify delivered fragments. Another option would be to utilize an alternative delivery method based on technology used for vaccine development, where "ghost" cells are made by expressing low levels of phage lysis proteins (468). These cells are devoid of DNA and RNA but retain the overall cell rigidity and shape. This allows for the surface display of high molecular weight antigens, such as those used for vaccine development. If these "cells" could display CdiA and facilitate delivery to target cells, this might remove some of the protein background from experiments aimed at identifying the delivered cytotoxic CdiA-CT fragment.

B. The role of CDI in bacterial environments

1. Regulation of cdi *loci*

The strain in which CDI was first identified, *E. coli* EC93, was initially of interest because it was the dominant intestinal isolate from a rat colony. Its characterized CDI system is constitutively active and presumably contributed to the outgrowth of this strain over other gut microbes. Interestingly, sequencing data revealed that this strain carries a second *cdi* locus that is genetically intact but not active under laboratory conditions (Stephen Poole, David Low, and Christopher Hayes, unpublished data). This suggests that some level of regulatory control governs the differential expression of these systems. We have examined *cdi* loci from a number of other bacteria, including *Dickeya dadantii*, Enterobacter *cloacae*, and clinical isolates of *E. coli*, and have found that expression of these systems is typically repressed under laboratory conditions, necessitating the construction of inducible promoters to enable the study of these operons.

Little is known about what regulates the expression of CDI systems. In *Burkholderia*, quorum sensing systems regulate expression of *cdi* loci (469-471). Perhaps other CDI loci are also negatively or positively regulated by quorum sensing or small signaling molecules produced by other bacteria. A regulatory role for quorum sensing in expression of CDI genes would ensure that these large genes and gene products are not produced until neighboring cells are near enough to be targeted. Given the metabolic load required to produce CdiA proteins (which range from 300-600 kDa across species), this could be a clever way to conserve cellular resources until the activity of CDI systems is needed.

The relationship between CDI regulation and other microbial communication or competition systems is also unknown. Work from the T6SS field shows that these systems

can be activated by attack from T6SS systems produced by other cells or membrane perturbations from T4SS pili and antibiotics (260). However, in these examples, the T6SS machinery is already assembled and fires in response to signals from other cells. Given the receptor-mediated process of CdiA/target cell recognition, it is unlikely that a signal from a neighboring cell would trigger this process. Expression of type 3 secretion systems (T3SS) in enteropathogenic *E. coli* is intertwined with non-ribosomal peptide production by *Streptomyces* species (472). T3SS effectors are can be chimeric, like CDI toxins, and these systems are thought to diversify by recombination mechanisms similar to Rhs-CT or CdiA-CT domain swapping (473). CDI systems are commonly found in bacteria with quorum sensing systems, additional secretion systems for effector delivery, pili and other surface adhesins, and the ability to produce compounds that inhibit other cells, so it is possible that *cdi* expression is co-regulated along with these other communication and competition systems. In some uropathogenic *E. coli*, the *cdi* genes are encoded on pathogenicity island 2 (PAI-2), which contains a number of other virulence factors such as iron-uptake systems, toxin secretion systems, and pili (474). These genes are differentially regulated during various stages of host colonization or infection to optimize virulence. Therefore, it is likely that the expression of CDI systems on these mobile islands would be controlled in a similar fashion. Similarly, it is well known that plant pathogens regulate a variety of adhesion and virulence factors upon association with a host (475). HecA, an adhesin from *Dickeya dadantii* that we now know to be a CdiA protein (175, 476), is essential for aggregation and host cell death during *Dickeya* infections. It is likely that CDI systems in pathogens with complex virulence factor arrays or pathogenicity islands is highly regulated and linked to the expression of other genes essential for virulence.

2. CdiA-CT activities can alter target cell morphology

While the canonical CDI model presents this system as a "killing" mechanism utilized by bacteria, it is interesting to consider a more subtle role for these genes in light of the work presented in Chapters IV and VII. We demonstrated in Chapter IV that spontaneous CDI-resistant mutants can arise in a population subjected to selective pressure from a CdiA-CT with DNase activity, CdiA-CT_{o11}^{EC869}. This resistance was in large part due to the transposition of insertion elements into *yciB*, a gene encoding an inner membrane protein required for the delivery of this toxin. Additional nonsense mutations and small deletions in *yciB* also conferred resistance to this toxin. The diversity of IS element insertions in *yciB* in each pool of resistant target cells cannot be explained simply by a basal level of stochastic movement of these mobile elements, as the normal transposition rates of these sequences is extremely low (348). Furthermore, the large-scale transposition of IS elements into *yciB* was not observed in mutants resistant to a tRNase toxin delivered through the same inner membrane protein, suggesting that these transposition events are directly linked to the DNA damage induced by delivery of CdiA-CT_{o11}^{EC869}. Together, this suggests that although the delivery of CdiA-CT_{o11}^{EC869} into target bacteria is eventually lethal for a vast majority of the population, the kinetics of this toxicity allow for some behavioral response by target cells. Interestingly, we observed increased transposition of IS elements even in cell backgrounds lacking RecA, the ssDNA-binding protease that activates the SOS pathway in response to DNA damage by inactiving LexA, a transcriptional repressor (41). This suggests that mobilization of IS elements in response to DNA damage mediated by CdiA-CT_{o11}^{EC869} may be stimulated via a RecA-independent mechanism.

Co-culture experiments have shown that sublethal amounts of tRNA cleavage products

accumulate in target cells before a loss in viability can be measured (172). The laboratory conditions in which these experiments are carried out is severe, with target and inhibitor cells growing together in a confined space with constant mixing and aeration. This forces interactions between these two populations that may not be representative of CDI in a natural environment. While this provides a rich environment to study the activities of CdiA-CTs and the genetics required for CDI import by target cells, this may not be ideal for understanding the subtle consequences of low levels of toxin delivery.

The response to CDI by target cells seems markedly different than that of the outcome of inhibition by T6SSs. Many T6SS effectors are periplasmic-acting effectors that, when delivered into neighboring bacteria, result in a dramatic rounded phenotype and subsequent cell lysis – an obviously irreversible event. Conversely, many CdiA-CTs act in the cytoplasm and cleave nucleic acid targets. The work in Chapter VII shows that the activity of at least one CdiA-CT, a 16S RNase from *Enterobacter cloacae*, is irreversible. A previous study showed that the toxicity associated with the pore-forming CdiA-CT^{EC93} could be reversed by expression of the cognate immunity protein. Taken together, these data suggest that cells can recover from a small amount of CdiA-CT activity (for a subset of toxins, at least), but there exists some threshold past which cell death is inevitable. Sub-inhibitory concentrations of antibiotics and other toxic molecules can influence gene expression (448, 477, 478). Specific cellular responses, including induction of the SOS response pathway, are associated with low levels of DNA damage (41). During the SOS response, cells halt growth and repair DNA breaks before dividing. This cascade of events is possible because the cell is able to detect DNA damage events that are not immediately lethal, giving the cell time to respond. Perhaps sub-lethal amounts damage induced by CdiA-CTs have physiological roles

outside of eventual lethality.

As shown in Chapters II and V, the activity of some CdiA-CTs, like CdiA-CT_{o11}^{EC869}, results in the filamentation of target cells (177, 202). Cell elongation to a lesser degree has also been observed after delivery of CdiA-CT^{EC93} (158). These morphological changes suggest that gene expression changes take place after delivery of a toxin. Given the importance of atypical phenotypes in protection from host immune response during some bacterial infections (445), it is intriguing to hypothesize that CDI systems can perhaps influence the phenotype of surrounding cells (and survival of the community as a whole) by delivering low doses of toxins to invoke a physiological stress response. Perhaps these morphological responses are less important in our well-aerated shaking laboratory co-culture conditions but are more relevant to natural populations. Dynamic control of phenotypes and *sulA*-mediated filamentation of uropathogenic *E. coli* are essential for virulence in a host (445). During infection, UPEC can undergo multiple rounds of differentiation into filaments, which help evade the host immune system and protect the bacteria from phagocytosis (445-447). Furthermore, bacterial filaments contribute to evolution of antibiotic resistance in sub-MIC conditions (446, 479). Filamentation can be triggered by a variety of environmental factors, including host and predator signals, quorum sensing, and low doses of antimicrobial compounds (446).

3. Kin selection and the influence of CDI on bacterial populations

Given the importance of atypical phenotypes to bacterial survival, it is intriguing to hypothesize that CDI systems can influence survival of the entire bacterial community by delivering low doses of toxins to invoke a physiological stress response. As shown in Chapter VII, filamentation of target cells upon contact with a CDI_{o11}^{EC869} inhibitor creates

pockets of target cells physically shielded from inhibitors by elongated cells. In a mixed population, perhaps this elongation response helps promote the survival of bacterial communities during scenarios in which filamentation is advantageous. In a urinary tract infection, this could be coupled to kin selection – by delivering toxins to neighboring *E. coli* cells, a filamentation response could help UPEC cells survive while also removing non-self cells from the population. This may be a dual role for CDI that promotes fitness in a given environment.

Computational modeling suggests that CDI may be important for establishing niches or zones of CDI^+ bacteria in natural environments. Blanchard *et al*. showed that in simulations of CDI^+ and CDI^- populations in liquid culture, one group of cells will "win" over time (442). If inhibition from CDI systems is strong enough, then this provides a growth advantage, and CDI^+ cells will outgrow the susceptible target cells. However, if the fitness effect of expressing CDI systems is too great, then CDI^- cells will overtake the niche despite delivery of toxic peptides by CDI^+ cells. In models of stationary environments, distinct zones of CDI^+ and CDI^- cells are created, and patches of CDI^- cells can survive even in the presence of cells expressing CDI. Perhaps the morphology changes described above contribute to this patterning and niche development during bacterial growth. These stationary simulations may be a good proxy for how CDI systems influence naturally-occurring bacterial populations. The time-lapse microscopy presented in Chapter VII shows that target cells in contact with a growing population of CDI_{o11}^{EC869} inhibitors filament, but that this event forms a border between the invading CDI^+ cells and the rest of the susceptible population. One could imagine that in a natural bacterial environment, the sacrifice of this outer border of cells would enable survival of the shielded internal cells.

CDI systems can be involved policing the composition of bacterial communities on multiple levels. First, at the outer-most level of the surface receptor, CdiA proteins discriminate between cells expressing the correct receptor. CdiA is sensitive to both different species (the extracellular loops in BamA vary across species (159), and *Burkholderia* LPS moieties are different than those displayed in other species (192)) and outer membrane proteins within the same species (based on recognition of different outer membrane proteins by different classes of CdiA). Once identity has been established at the outer membrane, translocation initiation can occur. After toxin delivery, a second level of control occurs at the level of the immunity protein. *E. coli* cells may carry the correct outer membrane receptor but lack an immunity gene, and would therefore be inhibited. This could help winnow a complex environment down to the most dominant strain by direct cell inhibition and killing, or delivery of specific toxins could influence the population through gene expression and morphological changes. Additionally, it is possible that CdiA-CT/CdiI complexes could exert their own secondary effects in immune cells. The CdiA-CT/$CdiI_{o11}^{EC869}$ complex binds DNA (177), and in a cell, this could influence gene expression upon delivery and formation of this complex. An interesting question to ask from the perspective of immunity protection is what happens when two cells of the same species, both expressing CDI systems with different toxins, deliver into one another but do not carry the immunity gene required for protection? Perhaps the benefits the community as a whole gains from CDI systems would allow subsets of cells to persist instead of the end result being death of both populations. CdiA is also involved in intercellular adhesion between sibling cells via a domain that is distinct from the receptor-binding domain. These activities may help form beneficial bacterial networks or biofilms in a toxin-independent manner, increasing their fitness. Both

the receptor-mediated and CdiA-mediated, receptor-independent abilities of CdiA may allow CDI^+ cells to detect "self" or sibling cells in a mixed environment (225). Similar mechanisms of kin selection are known to increase fitness in a population (480).

C. Structural and biochemical features of CdiA-CTs

Apart from elucidating the regulatory features of CDI systems, another focus of future research will be on the precise mechanism of CdiA-CT activities inside the cell. Evidence from the CDI system in uropathogenic *E. coli* strain 536 combined with the data presented in Chapter VI indicate that some CdiA-CTs require a co-factor or permissive factor for activity (193). Our data suggests that multiple toxins utilize EF-Tu and EF-Ts, but perhaps for different purposes. Taken together, the data on $CdiA\text{-}CT^{O32:H37}$ and $CdiA\text{-}CT^{Kp342}$ suggests that a variety of CdiA-CTs have some biochemical or genetic interaction with EF-Tu and/or EF-Ts, but that these individual relationships may be unique. Targeting a well-conserved protein as a co-factor makes some amount of evolutionary sense. Because EF-Tu and EF-Ts are highly conserved across bacteria, a toxin requiring these for delivery or activity would have to undergo a minimal amount of evolution if transferred into the genome of another organism. The usage of conserved co-factors may allow for greater spread of toxin/immunity modules throughout bacteria while retaining the ability to rapidly inhibit neighboring bacteria. To date, all characterized CdiA-CTs are pore formers, DNases, or RNases. However, extensive bioinformatic analysis by Zhang and Aravind predict many more functions for CdiA-CTs, including deaminases and peptidases (199, 200, 232, 481). Given the vast array of CdiA-CTs (more than 20 distinct families of toxins in E. coli alone (170)), it is likely that examination of additional crystal structures will reveal novel features about CDI biology.

Structural analysis and molecular modeling will also elucidate how inactivation by immunity proteins specifically blocks toxic activity. Thus far, we have discovered examples of CdiI proteins that neutralize their cognate toxins by directly occluding the active site residues as well as CdiI proteins that bind an exosite away from where the catalytic activity occurs (175, 177). While active site occlusion is a readily-interpretable form of inactivation via immunity proteins, it is more difficult to understand the mechanisms of exosite inactivation. Structural studies have also revealed unique prokaryotic folds, such as the β-complementation that forms between CdiA-CTs and CdiI proteins in the EC869 superfamily of DNase toxins (177, 202). This toxin/immunity interface provides a rich surface to study the evolution of CdiA-CT/CdiI modules as they spread throughout bacteria. Riley and other colicin biologists have proposed that diversification of bacteriocins occurs at the toxin/immunity interface, where mutations in the immunity that retain high-affinity binding to the colicin are matched by mutations in the toxin (38, 39, 212). Similar evolutionary forces likely contribute to the diversity of CdiA-CT/CdiI pairs.

While many aspects of the mechanisms involved in CDI remain unclear, what is increasingly apparent is that CDI and related systems are important in a variety of cellular processes in bacteria, from kin selection to biofilm formation to gene regulation in host organisms. Future work will not only reveal fine mechanistic detail regarding the delivery and activity of these systems, but will also contextualize them in the big-picture scope of bacterial physiology within complex communities. That every "answer" obtained in this work raises more questions speaks to the rich future of research on contact-dependent growth inhibition systems in bacteria.

1. Sogin ML, *et al.* (2006) Microbial diversity in the deep sea and the underexplored "rare biosphere". *Proc Natl Acad Sci U S A* 103(32):12115-12120.
2. Engel P & Moran NA (2013) The gut microbiota of insects - diversity in structure and function. *FEMS Microbiol Rev* 37(5):699-735.
3. Chu H & Mazmanian SK (2013) Innate immune recognition of the microbiota promotes host-microbial symbiosis. *Nat Immunol* 14(7):668-675.
4. Sommer F & Bäckhed F (2013) The gut microbiota--masters of host development and physiology. *Nat Rev Microbiol* 11(4):227-238.
5. Koropatnick TA, *et al.* (2004) Microbial factor-mediated development in a host-bacterial mutualism. *Science* 306(5699):1186-1188.
6. McFall-Ngai M (2008) Host-microbe symbiosis: the squid-Vibrio association--a naturally occurring, experimental model of animal/bacterial partnerships. *Adv Exp Med Biol* 635:102-112.
7. Reinhardt C, *et al.* (2012) Tissue factor and PAR1 promote microbiota-induced intestinal vascular remodelling. *Nature* 483(7391):627-631.
8. Stappenbeck TS, Hooper LV, & Gordon JI (2002) Developmental regulation of intestinal angiogenesis by indigenous microbes via Paneth cells. *Proc Natl Acad Sci U S A* 99(24):15451-15455.
9. Sandrini S, Aldriwesh M, Alruways M, & Freestone P (2015) Microbial endocrinology: host-bacteria communication within the gut microbiome. *J Endocrinol* 225(2):R21-34.
10. Hsiao EY, *et al.* (2013) Microbiota modulate behavioral and physiological abnormalities associated with neurodevelopmental disorders. *Cell* 155(7):1451-1463.
11. Diaz Heijtz R, *et al.* (2011) Normal gut microbiota modulates brain development and behavior. *Proc Natl Acad Sci U S A* 108(7):3047-3052.
12. Diamond B, Huerta PT, Tracey K, & Volpe BT (2011) It takes guts to grow a brain: Increasing evidence of the important role of the intestinal microflora in neuro- and immune-modulatory functions during development and adulthood. *Bioessays* 33(8):588-591.
13. Collins SM, Surette M, & Bercik P (2012) The interplay between the intestinal microbiota and the brain. *Nat Rev Microbiol* 10(11):735-742.
14. Sharon G, *et al.* (2010) Commensal bacteria play a role in mating preference of Drosophila melanogaster. *Proc Natl Acad Sci U S A* 107(46):20051-20056.
15. Le KY & Otto M (2015) Quorum-sensing regulation in staphylococci-an overview. *Front Microbiol* 6:1174.
16. Keller L & Surette MG (2006) Communication in bacteria: an ecological and evolutionary perspective. *Nat Rev Microbiol* 4(4):249-258.
17. Henke JM & Bassler BL (2004) Bacterial social engagements. *Trends Cell Biol* 14(11):648-656.
18. Lyon GJ & Novick RP (2004) Peptide signaling in Staphylococcus aureus and other Gram-positive bacteria. *Peptides* 25(9):1389-1403.
19. Ng WL & Bassler BL (2009) Bacterial quorum-sensing network architectures. *Annu Rev Genet* 43:197-222.
20. Saha R, Saha N, Donofrio RS, & Bestervelt LL (2013) Microbial siderophores: a mini review. *J Basic Microbiol* 53(4):303-317.
21. Fatima U & Senthil-Kumar M (2015) Plant and pathogen nutrient acquisition strategies. *Front Plant Sci* 6:750.
22. Koh EI & Henderson JP (2015) Microbial Copper-binding Siderophores at the Host-Pathogen Interface. *J Biol Chem* 290(31):18967-18974.
23. Cascales E, *et al.* (2007) Colicin biology. *Microbiol Mol Biol Rev* 71(1):158-229.
24. Ghequire MG & De Mot R (2014) Ribosomally encoded antibacterial proteins and peptides from Pseudomonas. *FEMS Microbiol Rev* 38(4):523-568.
25. Rebuffat S (2012) Microcins in action: amazing defence strategies of Enterobacteria. *Biochem Soc Trans* 40(6):1456-1462.
26. Duquesne S, Petit V, Peduzzi J, & Rebuffat S (2007) Structural and functional diversity of microcins, gene-encoded antibacterial peptides from enterobacteria. *J Mol Microbiol Biotechnol* 13(4):200-209.
27. Eckburg PB, *et al.* (2005) Diversity of the human intestinal microbial flora. *Science* 308(5728):1635-1638.
28. Hardy KG, Meynell GG, Dowman JE, & Spratt BG (1973) Two major groups of colicin factors: their evolutionary significance. *Mol Gen Genet* 125(3):217-230.

29. Herschman HR & Helinski DR (1967) Comparative study of the events associated with colicin induction. *J Bacteriol* 94(3):691-699.
30. Herschman HR & Helinski DR (1967) Purification and characterization of colicin E2 and colicin E3. *J Biol Chem* 242(22):5360-5368.
31. Konisky J & Richards FM (1970) Characterization of colicin Ia and colicin Ib. Purification and some physical properties. *J Biol Chem* 245(11):2972-2978.
32. Akutsu A, Masaki H, & Ohta T (1989) Molecular structure and immunity specificity of colicin E6, an evolutionary intermediate between E-group colicins and cloacin DF13. *J Bacteriol* 171(12):6430-6436.
33. Chak KF & James R (1986) Characterization of the ColE9-J plasmid and analysis of its genetic organization. *J Gen Microbiol* 132(1):61-70.
34. Chak KF, Kuo WS, Lu FM, & James R (1991) Cloning and characterization of the ColE7 plasmid. *J Gen Microbiol* 137(1):91-100.
35. Cole ST, Saint-Joanis B, & Pugsley AP (1985) Molecular characterisation of the colicin E2 operon and identification of its products. *Mol Gen Genet* 198(3):465-472.
36. Curtis MD, James R, & Coddington A (1989) An evolutionary relationship between the ColE5-099 and the ColE9-J plasmids revealed by nucleotide sequencing. *J Gen Microbiol* 135(10):2783-2788.
37. Jakes KS & Zinder ND (1984) Plasmid ColE3 specifies a lysis protein. *J Bacteriol* 157(2):582-590.
38. Riley MA (1993) Molecular mechanisms of colicin evolution. *Mol Biol Evol* 10(6):1380-1395.
39. Riley MA (1993) Positive selection for colicin diversity in bacteria. *Mol Biol Evol* 10(5):1048-1059.
40. Lau PC & Condie JA (1989) Nucleotide sequences from the colicin E5, E6 and E9 operons: presence of a degenerate transposon-like structure in the ColE9-J plasmid. *Mol Gen Genet* 217(2-3):269-277.
41. Little JW & Mount DW (1982) The SOS regulatory system of Escherichia coli. *Cell* 29(1):11-22.
42. Masaki H & Ohta T (1985) Colicin E3 and its immunity genes. *J Mol Biol* 182(2):217-227.
43. Kanoh S, Masaki H, Yajima S, Ohta T, & Uozumi T (1991) Signal peptide of the colicin E2 lysis protein causes host cell death. *Agric Biol Chem* 55(6):1607-1614.
44. Spangler R, Zhang SP, Krueger J, & Zubay G (1985) Colicin synthesis and cell death. *J Bacteriol* 163(1):167-173.
45. Di Masi DR, White JC, Schnaitman CA, & Bradbeer C (1973) Transport of vitamin B12 in Escherichia coli: common receptor sites for vitamin B12 and the E colicins on the outer membrane of the cell envelope. *J Bacteriol* 115(2):506-513.
46. Wayne R, Frick K, & Neilands JB (1976) Siderophore protection against colicins M, B, V, and Ia in Escherichia coli. *J Bacteriol* 126(1):7-12.
47. Zakharov SD, Zhalnina MV, Sharma O, & Cramer WA (2006) The colicin E3 outer membrane translocon: immunity protein release allows interaction of the cytotoxic domain with OmpF porin. *Biochemistry* 45(34):10199-10207.
48. Zakharov SD, Sharma O, Zhalnina M, Yamashita E, & Cramer WA (2012) Pathways of colicin import: utilization of BtuB, OmpF porin and the TolC drug-export protein. *Biochem Soc Trans* 40(6):1463-1468.
49. Loftus SR, *et al.* (2006) Competitive recruitment of the periplasmic translocation portal TolB by a natively disordered domain of colicin E9. *Proc Natl Acad Sci U S A* 103(33):12353-12358.
50. Housden NG, *et al.* (2010) Directed epitope delivery across the Escherichia coli outer membrane through the porin OmpF. *Proc Natl Acad Sci U S A* 107(50):21412-21417.
51. Housden NG & Kleanthous C (2012) Colicin translocation across the Escherichia coli outer membrane. *Biochem Soc Trans* 40(6):1475-1479.
52. Benedetti H, Lazdunski C, & Lloubès R (1991) Protein import into Escherichia coli: colicins A and E1 interact with a component of their translocation system. *EMBO J* 10(8):1989-1995.
53. Journet L, *et al.* (2001) Import of colicins across the outer membrane of Escherichia coli involves multiple protein interactions in the periplasm. *Mol Microbiol* 42(2):331-344.
54. Shultis DD, Purdy MD, Banchs CN, & Wiener MC (2006) Outer membrane active transport: structure of the BtuB:TonB complex. *Science* 312(5778):1396-1399.
55. Pawelek PD, *et al.* (2006) Structure of TonB in complex with FhuA, E. coli outer membrane receptor. *Science* 312(5778):1399-1402.
56. El Ghachi M, *et al.* (2006) Colicin M exerts its bacteriolytic effect via enzymatic degradation of undecaprenyl phosphate-linked peptidoglycan precursors. *J Biol Chem* 281(32):22761-22772.
57. Vetter IR, *et al.* (1998) Crystal structure of a colicin N fragment suggests a model for toxicity. *Structure* 6(7):863-874.

58. Wiener M, Freymann D, Ghosh P, & Stroud RM (1997) Crystal structure of colicin Ia. *Nature* 385(6615):461-464.
59. Schein SJ, Kagan BL, & Finkelstein A (1978) Colicin K acts by forming voltage-dependent channels in phospholipid bilayer membranes. *Nature* 276(5684):159-163.
60. Hilsenbeck JL, *et al.* (2004) Crystal structure of the cytotoxic bacterial protein colicin B at 2.5 A resolution. *Mol Microbiol* 51(3):711-720.
61. Elkins P, Bunker A, Cramer WA, & Stauffacher CV (1997) A mechanism for toxin insertion into membranes is suggested by the crystal structure of the channel-forming domain of colicin E1. *Structure* 5(3):443-458.
62. Cavard D, *et al.* (1988) Hydrodynamic properties of colicin A. Existence of a high-affinity lipid-binding site and oligomerization at acid pH. *Eur J Biochem* 172(2):507-512.
63. Cooper PC & James R (1984) Two new E colicins, E8 and E9, produced by a strain of Escherichia coli. *J Gen Microbiol* 130(1):209-215.
64. James R, Penfold CN, Moore GR, & Kleanthous C (2002) Killing of E coli cells by E group nuclease colicins. *Biochimie* 84(5-6):381-389.
65. Schaller K & Nomura M (1976) Colicin E2 is DNA endonuclease. *Proc Natl Acad Sci U S A* 73(11):3989-3993.
66. Bowman CM, Dahlberg JE, Ikemura T, Konisky J, & Nomura M (1971) Specific inactivation of 16S ribosomal RNA induced by colicin E3 in vivo. *Proc Natl Acad Sci U S A* 68(5):964-968.
67. Boon T (1972) Inactivation of ribosomes in vitro by colicin E 3 and its mechanism of action. *Proc Natl Acad Sci U S A* 69(3):549-552.
68. Ogawa T, *et al.* (1999) A cytotoxic ribonuclease targeting specific transfer RNA anticodons. *Science* 283(5410):2097-2100.
69. Ogle JM, Carter AP, & Ramakrishnan V (2003) Insights into the decoding mechanism from recent ribosome structures. *Trends Biochem Sci* 28(5):259-266.
70. Tomita K, Ogawa T, Uozumi T, Watanabe K, & Masaki H (2000) A cytotoxic ribonuclease which specifically cleaves four isoaccepting arginine tRNAs at their anticodon loops. *Proc Natl Acad Sci U S A* 97(15):8278-8283.
71. Kleanthous C, *et al.* (1999) Structural and mechanistic basis of immunity toward endonuclease colicins. *Nat Struct Biol* 6(3):243-252.
72. Ko TP, Liao CC, Ku WY, Chak KF, & Yuan HS (1999) The crystal structure of the DNase domain of colicin E7 in complex with its inhibitor Im7 protein. *Structure* 7(1):91-102.
73. Keeble AH, Hemmings AM, James R, Moore GR, & Kleanthous C (2002) Multistep binding of transition metals to the H-N-H endonuclease toxin colicin E9. *Biochemistry* 41(32):10234-10244.
74. Pommer AJ, *et al.* (1999) Homing in on the role of transition metals in the HNH motif of colicin endonucleases. *J Biol Chem* 274(38):27153-27160.
75. Pommer AJ, *et al.* (2001) Mechanism and cleavage specificity of the H-N-H endonuclease colicin E9. *J Mol Biol* 314(4):735-749.
76. Graille M, Mora L, Buckingham RH, van Tilbeurgh H, & de Zamaroczy M (2004) Structural inhibition of the colicin D tRNase by the tRNA-mimicking immunity protein. *EMBO J* 23(7):1474-1482.
77. Luna-Chávez C, Lin YL, & Huang RH (2006) Molecular basis of inhibition of the ribonuclease activity in colicin E5 by its cognate immunity protein. *J Mol Biol* 358(2):571-579.
78. Kleanthous C & Walker D (2001) Immunity proteins: enzyme inhibitors that avoid the active site. *Trends Biochem Sci* 26(10):624-631.
79. Soelaiman S, Jakes K, Wu N, Li C, & Shoham M (2001) Crystal structure of colicin E3: implications for cell entry and ribosome inactivation. *Mol Cell* 8(5):1053-1062.
80. Mosbahi K, *et al.* (2002) The cytotoxic domain of colicin E9 is a channel-forming endonuclease. *Nat Struct Biol* 9(6):476-484.
81. Mosbahi K, *et al.* (2004) Destabilization of the colicin E9 Endonuclease domain by interaction with negatively charged phospholipids: implications for colicin translocation into bacteria. *J Biol Chem* 279(21):22145-22151.
82. Mosbahi K, Walker D, James R, Moore GR, & Kleanthous C (2006) Global structural rearrangement of the cell penetrating ribonuclease colicin E3 on interaction with phospholipid membranes. *Protein Sci* 15(3):620-627.

83. Escuyer V, Boquet P, Perrin D, Montecucco C, & Mock M (1986) A pH-induced increase in hydrophobicity as a possible step in the penetration of colicin E3 through bacterial membranes. *J Biol Chem* 261(23):10891-10898.
84. van der Goot FG, González-Mañas JM, Lakey JH, & Pattus F (1991) A 'molten-globule' membrane-insertion intermediate of the pore-forming domain of colicin A. *Nature* 354(6352):408-410.
85. Walker D, Mosbahi K, Vankemmelbeke M, James R, & Kleanthous C (2007) The role of electrostatics in colicin nuclease domain translocation into bacterial cells. *J Biol Chem* 282(43):31389-31397.
86. Kurisu G, *et al.* (2003) The structure of BtuB with bound colicin E3 R-domain implies a translocon. *Nat Struct Biol* 10(11):948-954.
87. Housden NG, Loftus SR, Moore GR, James R, & Kleanthous C (2005) Cell entry mechanism of enzymatic bacterial colicins: porin recruitment and the thermodynamics of receptor binding. *Proc Natl Acad Sci U S A* 102(39):13849-13854.
88. Penfold CN, *et al.* (2004) Flexibility in the receptor-binding domain of the enzymatic colicin E9 is required for toxicity against Escherichia coli cells. *J Bacteriol* 186(14):4520-4527.
89. Walker D, Moore GR, James R, & Kleanthous C (2003) Thermodynamic consequences of bipartite immunity protein binding to the ribosomal ribonuclease colicin E3. *Biochemistry* 42(14):4161-4171.
90. Duché D, Frenkian A, Prima V, & Lloubès R (2006) Release of immunity protein requires functional endonuclease colicin import machinery. *J Bacteriol* 188(24):8593-8600.
91. Chauleau M, Mora L, Serba J, & de Zamaroczy M (2011) FtsH-dependent processing of RNase colicins D and E3 means that only the cytotoxic domains are imported into the cytoplasm. *J Biol Chem* 286(33):29397-29407.
92. Mora L & de Zamaroczy M (2014) In vivo processing of DNase colicins E2 and E7 is required for their import into the cytoplasm of target cells. *PLoS One* 9(5):e96549.
93. Bowles LK & Konisky J (1981) Cleavage of colicin Ia by the Escherichia coli K-12 outer membrane is not mediated by the colicin Ia receptor. *J Bacteriol* 145(1):668-671.
94. Brey RN (1982) Fragmentation of colicins A and E1 by cell surface proteases. *J Bacteriol* 149(1):306-315.
95. Cavard D & Lazdunski C (1979) Interaction of colicin E4 with specific receptor sites mediates its cleavage into two fragments inactive towards whole cells. *Eur J Biochem* 96(3):525-533.
96. Cavard D & Lazdunski C (1990) Colicin cleavage by OmpT protease during both entry into and release from Escherichia coli cells. *J Bacteriol* 172(2):648-652.
97. Masi M, Vuong P, Humbard M, Malone K, & Misra R (2007) Initial steps of colicin E1 import across the outer membrane of Escherichia coli. *J Bacteriol* 189(7):2667-2676.
98. Leytus SP, Bowles LK, Konisky J, & Mangel WF (1981) Activation of plasminogen to plasmin by a protease associated with the outer membrane of Escherichia coli. *Proc Natl Acad Sci U S A* 78(3):1485-1489.
99. Sugimura K & Higashi N (1988) A novel outer-membrane-associated protease in Escherichia coli. *J Bacteriol* 170(8):3650-3654.
100. Duché D, Issouf M, & Lloubès R (2009) Immunity protein protects colicin E2 from OmpT protease. *J Biochem* 145(1):95-101.
101. de Zamaroczy M, Mora L, Lecuyer A, Géli V, & Buckingham RH (2001) Cleavage of colicin D is necessary for cell killing and requires the inner membrane peptidase LepB. *Mol Cell* 8(1):159-168.
102. Dalbey RE & Wickner W (1985) Leader peptidase catalyzes the release of exported proteins from the outer surface of the Escherichia coli plasma membrane. *J Biol Chem* 260(29):15925-15931.
103. Mora L, Moncoq K, England P, Oberto J, & de Zamaroczy M (2015) The Stable Interaction Between Signal Peptidase LepB of Escherichia coli and Nuclease Bacteriocins Promotes Toxin Entry into the Cytoplasm. *J Biol Chem* 290(52):30783-30796.
104. Matsuzawa H, Ushiyama S, Koyama Y, & Ohta T (1984) Escherichia coli K-12 tolZ mutants tolerant to colicins E2, E3, D, Ia, and Ib: defect in generation of the electrochemical proton gradient. *J Bacteriol* 160(2):733-739.
105. Qu JN, *et al.* (1996) The tolZ gene of Escherichia coli is identified as the ftsH gene. *J Bacteriol* 178(12):3457-3461.
106. Makino S, *et al.* (1997) A silent mutation in the ftsH gene of Escherichia coli that affects FtsH protein production and colicin tolerance. *Mol Gen Genet* 254(5):578-583.

107. Teff D, Koby S, Shotland Y, Ogura T, & Oppenheim AB (2000) A colicin-tolerant Escherichia coli mutant that confers hfl phenotype carries two mutations in the region coding for the C-terminal domain of FtsH (HflB). *FEMS Microbiol Lett* 183(1):115-117.
108. Asahara Y, *et al.* (2000) FtsH recognizes proteins with unfolded structure and hydrolyzes the carboxyl side of hydrophobic residues. *J Biochem* 127(5):931-937.
109. Bertani D, Oppenheim AB, & Narberhaus F (2001) An internal region of the RpoH heat shock transcription factor is critical for rapid degradation by the FtsH protease. *FEBS Lett* 493(1):17-20.
110. Herman C, Thévenet D, Bouloc P, Walker GC, & D'Ari R (1998) Degradation of carboxy-terminal-tagged cytoplasmic proteins by the Escherichia coli protease HflB (FtsH). *Genes Dev* 12(9):1348-1355.
111. Ito K & Akiyama Y (2005) Cellular functions, mechanism of action, and regulation of FtsH protease. *Annu Rev Microbiol* 59:211-231.
112. Bhakdi S, *et al.* (1988) The hemolysin of Escherichia coli. *Eur J Epidemiol* 4(2):135-143.
113. Linhartová I, *et al.* (2010) RTX proteins: a highly diverse family secreted by a common mechanism. *FEMS Microbiol Rev* 34(6):1076-1112.
114. Gilson L, Mahanty HK, & Kolter R (1990) Genetic analysis of an MDR-like export system: the secretion of colicin V. *EMBO J* 9(12):3875-3884.
115. Thomas S, Holland IB, & Schmitt L (2014) The Type 1 secretion pathway - the hemolysin system and beyond. *Biochim Biophys Acta* 1843(8):1629-1641.
116. Kanonenberg K, Schwarz CK, & Schmitt L (2013) Type I secretion systems - a story of appendices. *Res Microbiol* 164(6):596-604.
117. Holland IB, Schmitt L, & Young J (2005) Type 1 protein secretion in bacteria, the ABC-transporter dependent pathway (review). *Mol Membr Biol* 22(1-2):29-39.
118. Gerken H & Misra R (2004) Genetic evidence for functional interactions between TolC and AcrA proteins of a major antibiotic efflux pump of Escherichia coli. *Mol Microbiol* 54(3):620-631.
119. Pos KM (2009) Drug transport mechanism of the AcrB efflux pump. *Biochim Biophys Acta* 1794(5):782-793.
120. Delepelaire P (2004) Type I secretion in gram-negative bacteria. *Biochim Biophys Acta* 1694(1-3):149-161.
121. Cornelis GR (2006) The type III secretion injectisome. *Nat Rev Microbiol* 4(11):811-825.
122. Mota LJ & Cornelis GR (2005) The bacterial injection kit: type III secretion systems. *Ann Med* 37(4):234-249.
123. Jin Q & He SY (2001) Role of the Hrp pilus in type III protein secretion in Pseudomonas syringae. *Science* 294(5551):2556-2558.
124. Daniell SJ, *et al.* (2001) The filamentous type III secretion translocon of enteropathogenic Escherichia coli. *Cell Microbiol* 3(12):865-871.
125. Grant SR, Fisher EJ, Chang JH, Mole BM, & Dangl JL (2006) Subterfuge and manipulation: type III effector proteins of phytopathogenic bacteria. *Annu Rev Microbiol* 60:425-449.
126. Alfano JR & Collmer A (2004) Type III secretion system effector proteins: double agents in bacterial disease and plant defense. *Annu Rev Phytopathol* 42:385-414.
127. Hayes CS, Aoki SK, & Low DA (2010) Bacterial contact-dependent delivery systems. *Annu Rev Genet* 44:71-90.
128. Alvarez-Martinez CE & Christie PJ (2009) Biological diversity of prokaryotic type IV secretion systems. *Microbiol Mol Biol Rev* 73(4):775-808.
129. Wallden K, Rivera-Calzada A, & Waksman G (2010) Type IV secretion systems: versatility and diversity in function. *Cell Microbiol* 12(9):1203-1212.
130. Christie PJ, Whitaker N, & González-Rivera C (2014) Mechanism and structure of the bacterial type IV secretion systems. *Biochim Biophys Acta* 1843(8):1578-1591.
131. Anonymous (!!! INVALID CITATION !!!).
132. Ilangovan A, Connery S, & Waksman G (2015) Structural biology of the Gram-negative bacterial conjugation systems. *Trends Microbiol* 23(5):301-310.
133. Bhatty M, Laverde Gomez JA, & Christie PJ (2013) The expanding bacterial type IV secretion lexicon. *Res Microbiol* 164(6):620-639.
134. Costa TR, *et al.* (2015) Secretion systems in Gram-negative bacteria: structural and mechanistic insights. *Nat Rev Microbiol* 13(6):343-359.

135. Zhang W, Rong C, Chen C, & Gao GF (2012) Type-IVC secretion system: a novel subclass of type IV secretion system (T4SS) common existing in gram-positive genus Streptococcus. *PLoS One* 7(10):e46390.
136. Goessweiner-Mohr N, Arends K, Keller W, & Grohmann E (2013) Conjugative type IV secretion systems in Gram-positive bacteria. *Plasmid* 70(3):289-302.
137. Waters CM & Dunny GM (2001) Analysis of functional domains of the Enterococcus faecalis pheromone-induced surface protein aggregation substance. *J Bacteriol* 183(19):5659-5667.
138. Chen Y, *et al.* (2008) Enterococcus faecalis PcfC, a spatially localized substrate receptor for type IV secretion of the pCF10 transfer intermediate. *J Bacteriol* 190(10):3632-3645.
139. Korotkov KV, Sandkvist M, & Hol WG (2012) The type II secretion system: biogenesis, molecular architecture and mechanism. *Nat Rev Microbiol* 10(5):336-351.
140. Douzi B, Filloux A, & Voulhoux R (2012) On the path to uncover the bacterial type II secretion system. *Philos Trans R Soc Lond B Biol Sci* 367(1592):1059-1072.
141. Nivaskumar M & Francetic O (2014) Type II secretion system: a magic beanstalk or a protein escalator. *Biochim Biophys Acta* 1843(8):1568-1577.
142. Filloux A (2010) Secretion signal and protein targeting in bacteria: a biological puzzle. *J Bacteriol* 192(15):3847-3849.
143. Leo JC, Grin I, & Linke D (2012) Type V secretion: mechanism(s) of autotransport through the bacterial outer membrane. *Philos Trans R Soc Lond B Biol Sci* 367(1592):1088-1101.
144. van Ulsen P, Rahman S, Jong WS, Daleke-Schermerhorn MH, & Luirink J (2014) Type V secretion: from biogenesis to biotechnology. *Biochim Biophys Acta* 1843(8):1592-1611.
145. Szabady RL, Peterson JH, Skillman KM, & Bernstein HD (2005) An unusual signal peptide facilitates late steps in the biogenesis of a bacterial autotransporter. *Proc Natl Acad Sci U S A* 102(1):221-226.
146. Provence DL & Curtiss R (1994) Isolation and characterization of a gene involved in hemagglutination by an avian pathogenic Escherichia coli strain. *Infect Immun* 62(4):1369-1380.
147. Yen YT, Kostakioti M, Henderson IR, & Stathopoulos C (2008) Common themes and variations in serine protease autotransporters. *Trends Microbiol* 16(8):370-379.
148. Mazar J & Cotter PA (2006) Topology and maturation of filamentous haemagglutinin suggest a new model for two-partner secretion. *Mol Microbiol* 62(3):641-654.
149. Buscher AZ, Grass S, Heuser J, Roth R, & St Geme JW (2006) Surface anchoring of a bacterial adhesin secreted by the two-partner secretion pathway. *Mol Microbiol* 61(2):470-483.
150. Oberhettinger P, Leo JC, Linke D, Autenrieth IB, & Schütz MS (2015) The inverse autotransporter intimin exports its passenger domain via a hairpin intermediate. *J Biol Chem* 290(3):1837-1849.
151. Hoiczyk E, Roggenkamp A, Reichenbecher M, Lupas A, & Heesemann J (2000) Structure and sequence analysis of Yersinia YadA and Moraxella UspAs reveal a novel class of adhesins. *EMBO J* 19(22):5989-5999.
152. Oberhettinger P, *et al.* (2012) Intimin and invasin export their C-terminus to the bacterial cell surface using an inverse mechanism compared to classical autotransport. *PLoS One* 7(10):e47069.
153. Tsai JC, *et al.* (2010) The bacterial intimins and invasins: a large and novel family of secreted proteins. *PLoS One* 5(12):e14403.
154. Abdallah AM, *et al.* (2007) Type VII secretion--mycobacteria show the way. *Nat Rev Microbiol* 5(11):883-891.
155. Holberger LE, Garza-Sánchez F, Lamoureux J, Low DA, & Hayes CS (2012) A novel family of toxin/antitoxin proteins in Bacillus species. *FEBS Lett* 586(2):132-136.
156. Aoki SK, *et al.* (2005) Contact-dependent inhibition of growth in Escherichia coli. *Science* 309(5738):1245-1248.
157. Aoki SK, *et al.* (2008) Contact-dependent growth inhibition requires the essential outer membrane protein BamA (YaeT) as the receptor and the inner membrane transport protein AcrB. *Mol Microbiol* 70(2):323-340.
158. Aoki SK, Webb JS, Braaten BA, & Low DA (2009) Contact-dependent growth inhibition causes reversible metabolic downregulation in Escherichia coli. *J Bacteriol* 191(6):1777-1786.
159. Ruhe ZC, Wallace AB, Low DA, & Hayes CS (2013) Receptor polymorphism restricts contact-dependent growth inhibition to members of the same species. *MBio* 4(4).
160. Cotter PA, *et al.* (1998) Filamentous hemagglutinin of Bordetella bronchiseptica is required for efficient establishment of tracheal colonization. *Infect Immun* 66(12):5921-5929.

161. Ishibashi Y, Claus S, & Relman DA (1994) Bordetella pertussis filamentous hemagglutinin interacts with a leukocyte signal transduction complex and stimulates bacterial adherence to monocyte CR3 (CD11b/CD18). *J Exp Med* 180(4):1225-1233.
162. Relman D, *et al.* (1990) Recognition of a bacterial adhesion by an integrin: macrophage CR3 (alpha M beta 2, CD11b/CD18) binds filamentous hemagglutinin of Bordetella pertussis. *Cell* 61(7):1375-1382.
163. Noel GJ, Love DC, & Mosser DM (1994) High-molecular-weight proteins of nontypeable Haemophilus influenzae mediate bacterial adhesion to cellular proteoglycans. *Infect Immun* 62(9):4028-4033.
164. Noel GJ, Barenkamp SJ, St Geme JW, Haining WN, & Mosser DM (1994) High-molecular-weight surface-exposed proteins of Haemophilus influenzae mediate binding to macrophages. *J Infect Dis* 169(2):425-429.
165. Makhov AM, *et al.* (1994) Filamentous hemagglutinin of Bordetella pertussis. A bacterial adhesin formed as a 50-nm monomeric rigid rod based on a 19-residue repeat motif rich in beta strands and turns. *J Mol Biol* 241(1):110-124.
166. Clantin B, *et al.* (2007) Structure of the membrane protein FhaC: a member of the Omp85-TpsB transporter superfamily. *Science* 317(5840):957-961.
167. Aoki SK, *et al.* (2010) A widespread family of polymorphic contact-dependent toxin delivery systems in bacteria. *Nature* 468(7322):439-442.
168. Aoki SK, Poole SJ, Hayes CS, & Low DA (2011) Toxin on a stick: modular CDI toxin delivery systems play roles in bacterial competition. *Virulence* 2(4):356-359.
169. Nikolakakis K, *et al.* (2012) The toxin/immunity network of Burkholderia pseudomallei contact-dependent growth inhibition (CDI) systems. *Mol Microbiol* 84(3):516-529.
170. Willett JL, Ruhe ZC, Goulding CW, Low DA, & Hayes CS (2015) Contact-Dependent Growth Inhibition (CDI) and CdiB/CdiA Two-Partner Secretion Proteins. *J Mol Biol* 427(23):3754-3765.
171. Delattre AS, *et al.* (2011) Substrate recognition by the POTRA domains of TpsB transporter FhaC. *Mol Microbiol* 81(1):99-112.
172. Ruhe ZC, Nguyen JY, Beck CM, Low DA, & Hayes CS (2014) The proton-motive force is required for translocation of CDI toxins across the inner membrane of target bacteria. *Mol Microbiol* 94(2):466-481.
173. Willett JL, Gucinski GC, Fatherree JP, Low DA, & Hayes CS (2015) Contact-dependent growth inhibition toxins exploit multiple independent cell-entry pathways. *Proc Natl Acad Sci U S A* 112(36):11341-11346.
174. Beck CM, Diner EJ, Kim JJ, Low DA, & Hayes CS (2014) The F pilus mediates a novel pathway of CDI toxin import. *Mol Microbiol* 93(2):276-290.
175. Beck CM, *et al.* (2014) CdiA from Enterobacter cloacae delivers a toxic ribosomal RNase into target bacteria. *Structure* 22(5):707-718.
176. Poole SJ, *et al.* (2011) Identification of functional toxin/immunity genes linked to contact-dependent growth inhibition (CDI) and rearrangement hotspot (Rhs) systems. *PLoS Genet* 7(8):e1002217.
177. Morse RP, *et al.* (2012) Structural basis of toxicity and immunity in contact-dependent growth inhibition (CDI) systems. *Proc Natl Acad Sci U S A* 109(52):21480-21485.
178. Dobrindt U, *et al.* (2002) Genetic structure and distribution of four pathogenicity islands (PAI I(536) to PAI IV(536)) of uropathogenic Escherichia coli strain 536. *Infect Immun* 70(11):6365-6372.
179. Hochhut B, *et al.* (2006) Role of pathogenicity island-associated integrases in the genome plasticity of uropathogenic Escherichia coli strain 536. *Mol Microbiol* 61(3):584-595.
180. Tumapa S, *et al.* (2008) Burkholderia pseudomallei genome plasticity associated with genomic island variation. *BMC Genomics* 9:190.
181. Tuanyok A, *et al.* (2008) Genomic islands from five strains of Burkholderia pseudomallei. *BMC Genomics* 9:566.
182. Anderson MS, Garcia EC, & Cotter PA (2012) The Burkholderia bcpAIOB genes define unique classes of two-partner secretion and contact dependent growth inhibition systems. *PLoS Genet* 8(8):e1002877.
183. Gentle I, Gabriel K, Beech P, Waller R, & Lithgow T (2004) The Omp85 family of proteins is essential for outer membrane biogenesis in mitochondria and bacteria. *J Cell Biol* 164(1):19-24.
184. Gentle IE, Burri L, & Lithgow T (2005) Molecular architecture and function of the Omp85 family of proteins. *Mol Microbiol* 58(5):1216-1225.

185. Sklar JG, *et al.* (2007) Lipoprotein SmpA is a component of the YaeT complex that assembles outer membrane proteins in Escherichia coli. *Proc Natl Acad Sci U S A* 104(15):6400-6405.
186. Wu T, *et al.* (2005) Identification of a multicomponent complex required for outer membrane biogenesis in Escherichia coli. *Cell* 121(2):235-245.
187. Jain S & Goldberg MB (2007) Requirement for YaeT in the outer membrane assembly of autotransporter proteins. *J Bacteriol* 189(14):5393-5398.
188. Kim S, *et al.* (2007) Structure and function of an essential component of the outer membrane protein assembly machine. *Science* 317(5840):961-964.
189. Malinverni JC, *et al.* (2006) YfiO stabilizes the YaeT complex and is essential for outer membrane protein assembly in Escherichia coli. *Mol Microbiol* 61(1):151-164.
190. Werner J & Misra R (2005) YaeT (Omp85) affects the assembly of lipid-dependent and lipid-independent outer membrane proteins of Escherichia coli. *Mol Microbiol* 57(5):1450-1459.
191. Smith DL, *et al.* (2007) Short-tailed stx phages exploit the conserved YaeT protein to disseminate Shiga toxin genes among enterobacteria. *J Bacteriol* 189(20):7223-7233.
192. Koskiniemi S, *et al.* (2015) Genetic analysis of the CDI pathway from Burkholderia pseudomallei 1026b. *PLoS One* 10(3):e0120265.
193. Diner EJ, Beck CM, Webb JS, Low DA, & Hayes CS (2012) Identification of a target cell permissive factor required for contact-dependent growth inhibition (CDI). *Genes Dev* 26(5):515-525.
194. Webb JS, *et al.* (2013) Delivery of CdiA nuclease toxins into target cells during contact-dependent growth inhibition. *PLoS One* 8(2):e57609.
195. Gabel CV & Berg HC (2003) The speed of the flagellar rotary motor of Escherichia coli varies linearly with protonmotive force. *Proc Natl Acad Sci U S A* 100(15):8748-8751.
196. Vankemmelbeke M, *et al.* (2009) Energy-dependent immunity protein release during tol-dependent nuclease colicin translocation. *J Biol Chem* 284(28):18932-18941.
197. Skare JT & Postle K (1991) Evidence for a TonB-dependent energy transduction complex in Escherichia coli. *Mol Microbiol* 5(12):2883-2890.
198. Skare JT, Ahmer BM, Seachord CL, Darveau RP, & Postle K (1993) Energy transduction between membranes. TonB, a cytoplasmic membrane protein, can be chemically cross-linked in vivo to the outer membrane receptor FepA. *J Biol Chem* 268(22):16302-16308.
199. Zhang D, Iyer LM, & Aravind L (2011) A novel immunity system for bacterial nucleic acid degrading toxins and its recruitment in various eukaryotic and DNA viral systems. *Nucleic Acids Res* 39(11):4532-4552.
200. Zhang D, de Souza RF, Anantharaman V, Iyer LM, & Aravind L (2012) Polymorphic toxin systems: Comprehensive characterization of trafficking modes, processing, mechanisms of action, immunity and ecology using comparative genomics. *Biol Direct* 7:18.
201. Hwang WC, *et al.* (2014) Site-specific recombination of nitrogen-fixation genes in cyanobacteria by XisF-XisH-XisI complex: Structures and models. *Proteins*.
202. Morse RP, *et al.* (2015) Diversification of β-Augmentation Interactions between CDI Toxin/Immunity Proteins. *J Mol Biol* 427(23):3766-3784.
203. Walker D, Lancaster L, James R, & Kleanthous C (2004) Identification of the catalytic motif of the microbial ribosome inactivating cytotoxin colicin E3. *Protein Sci* 13(6):1603-1611.
204. Hillier BJ, Christopherson KS, Prehoda KE, Bredt DS, & Lim WA (1999) Unexpected modes of PDZ domain scaffolding revealed by structure of nNOS-syntrophin complex. *Science* 284(5415):812-815.
205. Gronenborn AM (2009) Protein acrobatics in pairs--dimerization via domain swapping. *Curr Opin Struct Biol* 19(1):39-49.
206. Fan B, Grass G, Rensing C, & Rosen BP (2001) Escherichia coli CopA N-terminal Cys(X)(2)Cys motifs are not required for copper resistance or transport. *Biochem Biophys Res Commun* 286(2):414-418.
207. Carr S, Walker D, James R, Kleanthous C, & Hemmings AM (2000) Inhibition of a ribosome-inactivating ribonuclease: the crystal structure of the cytotoxic domain of colicin E3 in complex with its immunity protein. *Structure* 8(9):949-960.
208. Tan K, *et al.* (2015) The structure of a contact-dependent growth-inhibition (CDI) immunity protein from Neisseria meningitidis MC58. *Acta Crystallogr F Struct Biol Commun* 71(Pt 6):702-709.
209. Cappadocia L, Parent JS, Sygusch J, & Brisson N (2013) A family portrait: structural comparison of the Whirly proteins from Arabidopsis thaliana and Solanum tuberosum. *Acta Crystallogr Sect F Struct Biol Cryst Commun* 69(Pt 11):1207-1211.

210. Schumacher MA, Karamooz E, Zíková A, Trantírek L, & Lukes J (2006) Crystal structures of T. brucei MRP1/MRP2 guide-RNA binding complex reveal RNA matchmaking mechanism. *Cell* 126(4):701-711.
211. Jamet A, *et al.* (2015) A new family of secreted toxins in pathogenic Neisseria species. *PLoS Pathog* 11(1):e1004592.
212. Tan Y & Riley MA (1997) Positive selection and recombination: major molecular mechanisms in colicin diversification. *Trends Ecol Evol* 12(9):348-351.
213. Ruhe ZC, Low DA, & Hayes CS (2013) Bacterial contact-dependent growth inhibition. *Trends Microbiol* 21(5):230-237.
214. Kredich NM, Becker MA, & Tomkins GM (1969) Purification and characterization of cysteine synthetase, a bifunctional protein complex, from Salmonella typhimurium. *J Biol Chem* 244(9):2428-2439.
215. Fimmel AL & Loughlin RE (1977) Isolation and characterization of cysK mutants of Escherichia coli K12. *J Gen Microbiol* 103(1):37-43.
216. Tai CH, Nalabolu SR, Jacobson TM, Minter DE, & Cook PF (1993) Kinetic mechanisms of the A and B isozymes of O-acetylserine sulfhydrylase from Salmonella typhimurium LT-2 using the natural and alternative reactants. *Biochemistry* 32(25):6433-6442.
217. Rabeh WM & Cook PF (2004) Structure and mechanism of O-acetylserine sulfhydrylase. *J Biol Chem* 279(26):26803-26806.
218. Mino K, *et al.* (2000) Characteristics of serine acetyltransferase from Escherichia coli deleting different lengths of amino acid residues from the C-terminus. *Biosci Biotechnol Biochem* 64(9):1874-1880.
219. Huang B, Vetting MW, & Roderick SL (2005) The active site of O-acetylserine sulfhydrylase is the anchor point for bienzyme complex formation with serine acetyltransferase. *J Bacteriol* 187(9):3201-3205.
220. Zhao C, *et al.* (2006) On the interaction site of serine acetyltransferase in the cysteine synthase complex from Escherichia coli. *Biochem Biophys Res Commun* 341(4):911-916.
221. Campanini B, *et al.* (2015) Moonlighting O-acetylserine sulfhydrylase: New functions for an old protein. *Biochim Biophys Acta* 1854(9):1184-1193.
222. Foster SJ (1993) Molecular analysis of three major wall-associated proteins of Bacillus subtilis 168: evidence for processing of the product of a gene encoding a 258 kDa precursor two-domain ligand-binding protein. *Mol Microbiol* 8(2):299-310.
223. Antelmann H, Yamamoto H, Sekiguchi J, & Hecker M (2002) Stabilization of cell wall proteins in Bacillus subtilis: a proteomic approach. *Proteomics* 2(5):591-602.
224. Koskiniemi S, *et al.* (2013) Rhs proteins from diverse bacteria mediate intercellular competition. *Proc Natl Acad Sci U S A* 110(17):7032-7037.
225. Ruhe ZC, *et al.* (2015) CdiA promotes receptor-independent intercellular adhesion. *Mol Microbiol* 98(1):175-192.
226. Lin RJ, Capage M, & Hill CW (1984) A repetitive DNA sequence, rhs, responsible for duplications within the Escherichia coli K-12 chromosome. *J Mol Biol* 177(1):1-18.
227. Jackson AP, Thomas GH, Parkhill J, & Thomson NR (2009) Evolutionary diversification of an ancient gene family (rhs) through C-terminal displacement. *BMC Genomics* 10:584.
228. Hill CW, Sandt CH, & Vlazny DA (1994) Rhs elements of Escherichia coli: a family of genetic composites each encoding a large mosaic protein. *Mol Microbiol* 12(6):865-871.
229. Wang YD, Zhao S, & Hill CW (1998) Rhs elements comprise three subfamilies which diverged prior to acquisition by Escherichia coli. *J Bacteriol* 180(16):4102-4110.
230. Koskiniemi S, *et al.* (2014) Selection of orphan Rhs toxin expression in evolved Salmonella enterica serovar Typhimurium. *PLoS Genet* 10(3):e1004255.
231. Aggarwal K & Lee KH (2011) Overexpression of cloned RhsA sequences perturbs the cellular translational machinery in Escherichia coli. *J Bacteriol* 193(18):4869-4880.
232. Iyer LM, Zhang D, Rogozin IB, & Aravind L (2011) Evolution of the deaminase fold and multiple origins of eukaryotic editing and mutagenic nucleic acid deaminases from bacterial toxin systems. *Nucleic Acids Res* 39(22):9473-9497.
233. Busby JN, Panjikar S, Landsberg MJ, Hurst MR, & Lott JS (2013) The BC component of ABC toxins is an RHS-repeat-containing protein encapsulation device. *Nature* 501(7468):547-550.

234. Minet AD, Rubin BP, Tucker RP, Baumgartner S, & Chiquet-Ehrismann R (1999) Teneurin-1, a vertebrate homologue of the Drosophila pair-rule gene ten-m, is a neuronal protein with a novel type of heparin-binding domain. *J Cell Sci* 112 (Pt 12):2019-2032.
235. Sisto A, *et al.* (2010) An Rhs-like genetic element is involved in bacteriocin production by Pseudomonas savastanoi pv. savastanoi. *Antonie Van Leeuwenhoek* 98(4):505-517.
236. Kung VL, *et al.* (2012) An rhs gene of Pseudomonas aeruginosa encodes a virulence protein that activates the inflammasome. *Proc Natl Acad Sci U S A* 109(4):1275-1280.
237. Lim YW, *et al.* (2013) Mechanistic model of Rothia mucilaginosa adaptation toward persistence in the CF lung, based on a genome reconstructed from metagenomic data. *PLoS One* 8(5):e64285.
238. Hill CW, *et al.* (1995) Correlation of Rhs elements with Escherichia coli population structure. *Genetics* 141(1):15-24.
239. Youderian P & Hartzell PL (2007) Triple mutants uncover three new genes required for social motility in Myxococcus xanthus. *Genetics* 177(1):557-566.
240. Russell AB, *et al.* (2011) Type VI secretion delivers bacteriolytic effectors to target cells. *Nature* 475(7356):343-347.
241. Pukatzki S, *et al.* (2006) Identification of a conserved bacterial protein secretion system in Vibrio cholerae using the Dictyostelium host model system. *Proc Natl Acad Sci U S A* 103(5):1528-1533.
242. Ma AT, McAuley S, Pukatzki S, & Mekalanos JJ (2009) Translocation of a Vibrio cholerae type VI secretion effector requires bacterial endocytosis by host cells. *Cell Host Microbe* 5(3):234-243.
243. Silverman JM, Brunet YR, Cascales E, & Mougous JD (2012) Structure and regulation of the type VI secretion system. *Annu Rev Microbiol* 66:453-472.
244. Whitney JC, *et al.* (2014) Genetically distinct pathways guide effector export through the type VI secretion system. *Mol Microbiol* 92(3):529-542.
245. Mougous JD, *et al.* (2006) A virulence locus of Pseudomonas aeruginosa encodes a protein secretion apparatus. *Science* 312(5779):1526-1530.
246. Hood RD, *et al.* (2010) A type VI secretion system of Pseudomonas aeruginosa targets a toxin to bacteria. *Cell Host Microbe* 7(1):25-37.
247. Boyer F, Fichant G, Berthod J, Vandenbrouck Y, & Attree I (2009) Dissecting the bacterial type VI secretion system by a genome wide in silico analysis: what can be learned from available microbial genomic resources? *BMC Genomics* 10:104.
248. Leiman PG, *et al.* (2009) Type VI secretion apparatus and phage tail-associated protein complexes share a common evolutionary origin. *Proc Natl Acad Sci U S A* 106(11):4154-4159.
249. Lossi NS, *et al.* (2013) The HsiB1C1 (TssB-TssC) complex of the Pseudomonas aeruginosa type VI secretion system forms a bacteriophage tail sheathlike structure. *J Biol Chem* 288(11):7536-7548.
250. Pell LG, Kanelis V, Donaldson LW, Howell PL, & Davidson AR (2009) The phage lambda major tail protein structure reveals a common evolution for long-tailed phages and the type VI bacterial secretion system. *Proc Natl Acad Sci U S A* 106(11):4160-4165.
251. Pukatzki S, Ma AT, Revel AT, Sturtevant D, & Mekalanos JJ (2007) Type VI secretion system translocates a phage tail spike-like protein into target cells where it cross-links actin. *Proc Natl Acad Sci U S A* 104(39):15508-15513.
252. Basler M, Pilhofer M, Henderson GP, Jensen GJ, & Mekalanos JJ (2012) Type VI secretion requires a dynamic contractile phage tail-like structure. *Nature* 483(7388):182-186.
253. Silverman JM, *et al.* (2013) Haemolysin coregulated protein is an exported receptor and chaperone of type VI secretion substrates. *Mol Cell* 51(5):584-593.
254. Brunet YR, Hénin J, Celia H, & Cascales E (2014) Type VI secretion and bacteriophage tail tubes share a common assembly pathway. *EMBO Rep* 15(3):315-321.
255. Mesyanzhinov VV (2004) Bacteriophage T4: structure, assembly, and initiation infection studied in three dimensions. *Adv Virus Res* 63:287-352.
256. Durand E, *et al.* (2015) Biogenesis and structure of a type VI secretion membrane core complex. *Nature* 523(7562):555-560.
257. Zoued A, *et al.* (2014) Architecture and assembly of the Type VI secretion system. *Biochim Biophys Acta* 1843(8):1664-1673.
258. Kapitein N, *et al.* (2013) ClpV recycles VipA/VipB tubules and prevents non-productive tubule formation to ensure efficient type VI protein secretion. *Mol Microbiol* 87(5):1013-1028.
259. Pietrosiuk A, *et al.* (2011) Molecular basis for the unique role of the AAA+ chaperone ClpV in type VI protein secretion. *J Biol Chem* 286(34):30010-30021.

260. Basler M, Ho BT, & Mekalanos JJ (2013) Tit-for-tat: type VI secretion system counterattack during bacterial cell-cell interactions. *Cell* 152(4):884-894.
261. Ho BT, Basler M, & Mekalanos JJ (2013) Type 6 secretion system-mediated immunity to type 4 secretion system-mediated gene transfer. *Science* 342(6155):250-253.
262. Whitney JC, *et al.* (2015) An interbacterial NAD(P)(+) glycohydrolase toxin requires elongation factor Tu for delivery to target cells. *Cell* 163(3):607-619.
263. Kajava AV, *et al.* (2001) Beta-helix model for the filamentous haemagglutinin adhesin of Bordetella pertussis and related bacterial secretory proteins. *Mol Microbiol* 42(2):279-292.
264. Gál J, Szvetnik A, Schnell R, & Kálmán M (2002) The metD D-methionine transporter locus of Escherichia coli is an ABC transporter gene cluster. *J Bacteriol* 184(17):4930-4932.
265. Merlin C, Gardiner G, Durand S, & Masters M (2002) The Escherichia coli metD locus encodes an ABC transporter which includes Abc (MetN), YaeE (MetI), and YaeC (MetQ). *J Bacteriol* 184(19):5513-5517.
266. Stewart JB & Hermodson MA (2003) Topology of RbsC, the membrane component of the Escherichia coli ribose transporter. *J Bacteriol* 185(17):5234-5239.
267. Buhr A, Flükiger K, & Erni B (1994) The glucose transporter of Escherichia coli. Overexpression, purification, and characterization of functional domains. *J Biol Chem* 269(38):23437-23443.
268. McGinness KE, Baker TA, & Sauer RT (2006) Engineering controllable protein degradation. *Mol Cell* 22(5):701-707.
269. Meins M, *et al.* (1993) Cysteine phosphorylation of the glucose transporter of Escherichia coli. *J Biol Chem* 268(16):11604-11609.
270. Akiyama Y, Kihara A, Mori H, Ogura T, & Ito K (1998) Roles of the periplasmic domain of Escherichia coli FtsH (HflB) in protein interactions and activity modulation. *J Biol Chem* 273(35):22326-22333.
271. Tomoyasu T, *et al.* (1993) Topology and subcellular localization of FtsH protein in Escherichia coli. *J Bacteriol* 175(5):1352-1357.
272. Yamada-Inagawa T, Okuno T, Karata K, Yamanaka K, & Ogura T (2003) Conserved pore residues in the AAA protease FtsH are important for proteolysis and its coupling to ATP hydrolysis. *J Biol Chem* 278(50):50182-50187.
273. Karata K, Verma CS, Wilkinson AJ, & Ogura T (2001) Probing the mechanism of ATP hydrolysis and substrate translocation in the AAA protease FtsH by modelling and mutagenesis. *Mol Microbiol* 39(4):890-903.
274. Karata K, Inagawa T, Wilkinson AJ, Tatsuta T, & Ogura T (1999) Dissecting the role of a conserved motif (the second region of homology) in the AAA family of ATPases. Site-directed mutagenesis of the ATP-dependent protease FtsH. *J Biol Chem* 274(37):26225-26232.
275. Law CJ, Maloney PC, & Wang DN (2008) Ins and outs of major facilitator superfamily antiporters. *Annu Rev Microbiol* 62:289-305.
276. Narberhaus F, Obrist M, Führer F, & Langklotz S (2009) Degradation of cytoplasmic substrates by FtsH, a membrane-anchored protease with many talents. *Res Microbiol* 160(9):652-659.
277. Akiyama Y & Ito K (2000) Roles of multimerization and membrane association in the proteolytic functions of FtsH (HflB). *EMBO J* 19(15):3888-3895.
278. Kihara A, Akiyama Y, & Ito K (1998) Different pathways for protein degradation by the FtsH/HflKC membrane-embedded protease complex: an implication from the interference by a mutant form of a new substrate protein, YccA. *J Mol Biol* 279(1):175-188.
279. Akiyama Y, Kihara A, Tokuda H, & Ito K (1996) FtsH (HflB) is an ATP-dependent protease selectively acting on SecY and some other membrane proteins. *J Biol Chem* 271(49):31196-31201.
280. Shotland Y, *et al.* (1997) Proteolysis of the phage lambda CII regulatory protein by FtsH (HflB) of Escherichia coli. *Mol Microbiol* 24(6):1303-1310.
281. Kihara A, Akiyama Y, & Ito K (1996) A protease complex in the Escherichia coli plasma membrane: HflKC (HflA) forms a complex with FtsH (HflB), regulating its proteolytic activity against SecY. *EMBO J* 15(22):6122-6131.
282. Saikawa N, Akiyama Y, & Ito K (2004) FtsH exists as an exceptionally large complex containing HflKC in the plasma membrane of Escherichia coli. *J Struct Biol* 146(1-2):123-129.
283. Shotland Y, *et al.* (2000) Proteolysis of bacteriophage lambda CII by Escherichia coli FtsH (HflB). *J Bacteriol* 182(11):3111-3116.

284. Hoskins JR, Yanagihara K, Mizuuchi K, & Wickner S (2002) ClpAP and ClpXP degrade proteins with tags located in the interior of the primary sequence. *Proc Natl Acad Sci U S A* 99(17):11037-11042.
285. Sharma O, *et al.* (2009) Genome-wide screens: novel mechanisms in colicin import and cytotoxicity. *Mol Microbiol* 73(4):571-585.
286. Williams N, Fox DK, Shea C, & Roseman S (1986) Pel, the protein that permits lambda DNA penetration of Escherichia coli, is encoded by a gene in ptsM and is required for mannose utilization by the phosphotransferase system. *Proc Natl Acad Sci U S A* 83(23):8934-8938.
287. Cumby N, Reimer K, Mengin-Lecreulx D, Davidson AR, & Maxwell KL (2015) The phage tail tape measure protein, an inner membrane protein and a periplasmic chaperone play connected roles in the genome injection process of E. coli phage HK97. *Mol Microbiol* 96(3):437-447.
288. Chiang SL & Rubin EJ (2002) Construction of a mariner-based transposon for epitope-tagging and genomic targeting. *Gene* 296(1-2):179-185.
289. Baba T, *et al.* (2006) Construction of Escherichia coli K-12 in-frame, single-gene knockout mutants: the Keio collection. *Mol Syst Biol* 2:2006.0008.
290. Garza-Sánchez F, Janssen BD, & Hayes CS (2006) Prolyl-tRNA(Pro) in the A-site of SecM-arrested ribosomes inhibits the recruitment of transfer-messenger RNA. *J Biol Chem* 281(45):34258-34268.
291. Datta S, Costantino N, & Court DL (2006) A set of recombineering plasmids for gram-negative bacteria. *Gene* 379:109-115.
292. Schindelin J, *et al.* (2012) Fiji: an open-source platform for biological-image analysis. *Nat Methods* 9(7):676-682.
293. Ferrières L, *et al.* (2010) Silent mischief: bacteriophage Mu insertions contaminate products of Escherichia coli random mutagenesis performed using suicidal transposon delivery plasmids mobilized by broad-host-range RP4 conjugative machinery. *J Bacteriol* 192(24):6418-6427.
294. Akiyama Y, Shirai Y, & Ito K (1994) Involvement of FtsH in protein assembly into and through the membrane. II. Dominant mutations affecting FtsH functions. *J Biol Chem* 269(7):5225-5229.
295. Yamazaki Y, Niki H, & Kato J (2008) Profiling of Escherichia coli Chromosome database. *Methods Mol Biol* 416:385-389.
296. Keseler IM, *et al.* (2013) EcoCyc: fusing model organism databases with systems biology. *Nucleic Acids Res* 41(Database issue):D605-612.
297. Riley M, *et al.* (2006) Escherichia coli K-12: a cooperatively developed annotation snapshot--2005. *Nucleic Acids Res* 34(1):1-9.
298. Hu P, *et al.* (2009) Global functional atlas of Escherichia coli encompassing previously uncharacterized proteins. *PLoS Biol* 7(4):e96.
299. Leong JM, *et al.* (1985) The phi 80 and P22 attachment sites. Primary structure and interaction with Escherichia coli integration host factor. *J Biol Chem* 260(7):4468-4477.
300. Andrews JC & Short SA (1985) Genetic analysis of Escherichia coli oligopeptide transport mutants. *J Bacteriol* 161(2):484-492.
301. Somerville RL & Yanofsky C (1965) Studies on the regulation of tryptophan biosynthesis in *Escherichia coli*. *J Mol Biol* 11:747-759.
302. Hong M, Gleason Y, Wyckoff EE, & Payne SM (1998) Identification of two Shigella flexneri chromosomal loci involved in intercellular spreading. *Infect Immun* 66(10):4700-4710.
303. Mac Síomóin RA, *et al.* (1996) Identification and characterization of ispA, a Shigella flexneri chromosomal gene essential for normal in vivo cell division and intracellular spreading. *Mol Microbiol* 19(3):599-609.
304. Badaluddin NA & Kitakawa M (2015) Escherichia coli inner membrane protein YciB interacts with ZipA that is important for cell division. *Genes Cells* 20(11):956-965.
305. Li G, Badaluddin NA, & Kitakawa M (2015) Characterization of inner membrane protein YciB in Escherichia coli: YciB interacts with cell elongation and division proteins. *Microbiol Immunol* 59(11):700-704.
306. Krogh A, Larsson B, von Heijne G, & Sonnhammer EL (2001) Predicting transmembrane protein topology with a hidden Markov model: application to complete genomes. *J Mol Biol* 305(3):567-580.
307. Johns SJ (TOPO2, Transmembrane protein display software. (http://www.sacs.ucsf.edu/TOPO2/).
308. Altschul SF, Gish W, Miller W, Myers EW, & Lipman DJ (1990) Basic local alignment search tool. *J Mol Biol* 215(3):403-410.
309. Crooks GE, Hon G, Chandonia JM, & Brenner SE (2004) WebLogo: a sequence logo generator. *Genome Res* 14(6):1188-1190.

310. Nichols RJ, *et al.* (2011) Phenotypic landscape of a bacterial cell. *Cell* 144(1):143-156.
311. Outten FW, Outten CE, Hale J, & O'Halloran TV (2000) Transcriptional activation of an Escherichia coli copper efflux regulon by the chromosomal MerR homologue, cueR. *J Biol Chem* 275(40):31024-31029.
312. Outten FW, Huffman DL, Hale JA, & O'Halloran TV (2001) The independent cue and cus systems confer copper tolerance during aerobic and anaerobic growth in Escherichia coli. *J Biol Chem* 276(33):30670-30677.
313. Rademacher C & Masepohl B (2012) Copper-responsive gene regulation in bacteria. *Microbiology* 158(Pt 10):2451-2464.
314. Stoyanov JV, Hobman JL, & Brown NL (2001) CueR (YbbI) of Escherichia coli is a MerR family regulator controlling expression of the copper exporter CopA. *Mol Microbiol* 39(2):502-511.
315. Franke S, Grass G, Rensing C, & Nies DH (2003) Molecular analysis of the copper-transporting efflux system CusCFBA of Escherichia coli. *J Bacteriol* 185(13):3804-3812.
316. Munson GP, Lam DL, Outten FW, & O'Halloran TV (2000) Identification of a copper-responsive two-component system on the chromosome of Escherichia coli K-12. *J Bacteriol* 182(20):5864-5871.
317. Ochman H & Selander RK (1984) Standard reference strains of Escherichia coli from natural populations. *J Bacteriol* 157(2):690-693.
318. Benov LT & Fridovich I (1994) Escherichia coli expresses a copper- and zinc-containing superoxide dismutase. *J Biol Chem* 269(41):25310-25314.
319. Rensing C & Grass G (2003) Escherichia coli mechanisms of copper homeostasis in a changing environment. *FEMS Microbiol Rev* 27(2-3):197-213.
320. Macomber L, Rensing C, & Imlay JA (2007) Intracellular copper does not catalyze the formation of oxidative DNA damage in Escherichia coli. *J Bacteriol* 189(5):1616-1626.
321. Macomber L & Imlay JA (2009) The iron-sulfur clusters of dehydratases are primary intracellular targets of copper toxicity. *Proc Natl Acad Sci U S A* 106(20):8344-8349.
322. Chaturvedi KS & Henderson JP (2014) Pathogenic adaptations to host-derived antibacterial copper. *Front Cell Infect Microbiol* 4:3.
323. Festa RA & Thiele DJ (2012) Copper at the front line of the host-pathogen battle. *PLoS Pathog* 8(9):e1002887.
324. Babu U & Failla ML (1990) Copper status and function of neutrophils are reversibly depressed in marginally and severely copper-deficient rats. *J Nutr* 120(12):1700-1709.
325. White C, Lee J, Kambe T, Fritsche K, & Petris MJ (2009) A role for the ATP7A copper-transporting ATPase in macrophage bactericidal activity. *J Biol Chem* 284(49):33949-33956.
326. Paauw A, Leverstein-van Hall MA, van Kessel KP, Verhoef J, & Fluit AC (2009) Yersiniabactin reduces the respiratory oxidative stress response of innate immune cells. *PLoS One* 4(12):e8240.
327. Petersen C & Møller LB (2000) Control of copper homeostasis in Escherichia coli by a P-type ATPase, CopA, and a MerR-like transcriptional activator, CopR. *Gene* 261(2):289-298.
328. Grass G, *et al.* (2004) Linkage between catecholate siderophores and the multicopper oxidase CueO in Escherichia coli. *J Bacteriol* 186(17):5826-5833.
329. Pontel LB & Soncini FC (2009) Alternative periplasmic copper-resistance mechanisms in Gram negative bacteria. *Mol Microbiol* 73(2):212-225.
330. Lee SM, *et al.* (2002) The Pco proteins are involved in periplasmic copper handling in Escherichia coli. *Biochem Biophys Res Commun* 295(3):616-620.
331. Kittleson JT, *et al.* (2006) Periplasmic metal-resistance protein CusF exhibits high affinity and specificity for both CuI and AgI. *Biochemistry* 45(37):11096-11102.
332. Loftin IR, *et al.* (2005) A novel copper-binding fold for the periplasmic copper resistance protein CusF. *Biochemistry* 44(31):10533-10540.
333. Loftin IR, Franke S, Blackburn NJ, & McEvoy MM (2007) Unusual Cu(I)/Ag(I) coordination of Escherichia coli CusF as revealed by atomic resolution crystallography and X-ray absorption spectroscopy. *Protein Sci* 16(10):2287-2293.
334. Yamamoto K & Ishihama A (2005) Transcriptional response of Escherichia coli to external copper. *Mol Microbiol* 56(1):215-227.
335. Yamamoto K & Ishihama A (2005) Transcriptional response of Escherichia coli to external zinc. *J Bacteriol* 187(18):6333-6340.
336. Babu U & Failla ML (1990) Respiratory burst and candidacidal activity of peritoneal macrophages are impaired in copper-deficient rats. *J Nutr* 120(12):1692-1699.

337. Fong C, Rohmer L, Radey M, Wasnick M, & Brittnacher MJ (2008) PSAT: a web tool to compare genomic neighborhoods of multiple prokaryotic genomes. *BMC Bioinformatics* 9:170.
338. Imamovic L, *et al.* (2010) OI-57, a genomic island of Escherichia coli O157, is present in other seropathotypes of Shiga toxin-producing E. coli associated with severe human disease. *Infect Immun* 78(11):4697-4704.
339. Perna NT, *et al.* (2001) Genome sequence of enterohaemorrhagic Escherichia coli O157:H7. *Nature* 409(6819):529-533.
340. Peters NT, Dinh T, & Bernhardt TG (2011) A fail-safe mechanism in the septal ring assembly pathway generated by the sequential recruitment of cell separation amidases and their activators. *J Bacteriol* 193(18):4973-4983.
341. Nasoff MS, Baker HV, & Wolf RE (1984) DNA sequence of the Escherichia coli gene, gnd, for 6-phosphogluconate dehydrogenase. *Gene* 27(3):253-264.
342. Verhamme DT, Arents JC, Postma PW, Crielaard W, & Hellingwerf KJ (2001) Glucose-6-phosphate-dependent phosphoryl flow through the Uhp two-component regulatory system. *Microbiology* 147(Pt 12):3345-3352.
343. Ooka T, *et al.* (2009) Inference of the impact of insertion sequence (IS) elements on bacterial genome diversification through analysis of small-size structural polymorphisms in Escherichia coli O157 genomes. *Genome Res* 19(10):1809-1816.
344. Kichenaradja P, Siguier P, Pérochon J, & Chandler M (2010) ISbrowser: an extension of ISfinder for visualizing insertion sequences in prokaryotic genomes. *Nucleic Acids Res* 38(Database issue):D62-68.
345. Siguier P, Perochon J, Lestrade L, Mahillon J, & Chandler M (2006) ISfinder: the reference centre for bacterial insertion sequences. *Nucleic Acids Res* 34(Database issue):D32-36.
346. Siguier P, Varani A, Perochon J, & Chandler M (2012) Exploring bacterial insertion sequences with ISfinder: objectives, uses, and future developments. *Methods Mol Biol* 859:91-103.
347. Kleckner N (1990) Regulation of transposition in bacteria. *Annu Rev Cell Biol* 6:297-327.
348. Sousa A, Bourgard C, Wahl LM, & Gordo I (2013) Rates of transposition in Escherichia coli. *Biol Lett* 9(6):20130838.
349. Eichenbaum Z & Livneh Z (1998) UV light induces IS10 transposition in Escherichia coli. *Genetics* 149(3):1173-1181.
350. Bradshaw VA & McEntee K (1989) DNA damage activates transcription and transposition of yeast Ty retrotransposons. *Mol Gen Genet* 218(3):465-474.
351. Halling SM & Kleckner N (1982) A symmetrical six-base-pair target site sequence determines Tn10 insertion specificity. *Cell* 28(1):155-163.
352. Gioia U, *et al.* (2005) Functional characterization of XendoU, the endoribonuclease involved in small nucleolar RNA biosynthesis. *J Biol Chem* 280(19):18996-19002.
353. Renzi F, *et al.* (2006) The structure of the endoribonuclease XendoU: From small nucleolar RNA processing to severe acute respiratory syndrome coronavirus replication. *Proc Natl Acad Sci U S A* 103(33):12365-12370.
354. Woods RJ, *et al.* (2007) Cyclic modular beta-sheets. *J Am Chem Soc* 129(9):2548-2558.
355. Nowick JS & Brower JO (2003) A new turn structure for the formation of beta-hairpins in peptides. *J Am Chem Soc* 125(4):876-877.
356. Watson R, Rowsome W, Tsao J, & Visentin LP (1981) Identification and characterization of Col plasmids from classical colicin E-producing strains. *J Bacteriol* 147(2):569-577.
357. Wojdyla JA, Fleishman SJ, Baker D, & Kleanthous C (2012) Structure of the ultra-high-affinity colicin E2 DNase--Im2 complex. *J Mol Biol* 417(1-2):79-94.
358. Li W, *et al.* (2004) Highly discriminating protein-protein interaction specificities in the context of a conserved binding energy hotspot. *J Mol Biol* 337(3):743-759.
359. Masaki H, Akutsu A, Uozumi T, & Ohta T (1991) Identification of a unique specificity determinant of the colicin E3 immunity protein. *Gene* 107(1):133-138.
360. Li W, *et al.* (1998) Dual recognition and the role of specificity-determining residues in colicin E9 DNase-immunity protein interactions. *Biochemistry* 37(34):11771-11779.
361. Wallis R, *et al.* (1995) Protein-protein interactions in colicin E9 DNase-immunity protein complexes. 2. Cognate and noncognate interactions that span the millimolar to femtomolar affinity range. *Biochemistry* 34(42):13751-13759.
362. Levin KB, *et al.* (2009) Following evolutionary paths to protein-protein interactions with high affinity and selectivity. *Nat Struct Mol Biol* 16(10):1049-1055.

363. Loughlin WA, Tyndall JD, Glenn MP, & Fairlie DP (2004) Beta-strand mimetics. *Chem Rev* 104(12):6085-6117.
364. Fasan R, *et al.* (2004) Using a beta-hairpin to mimic an alpha-helix: cyclic peptidomimetic inhibitors of the p53-HDM2 protein-protein interaction. *Angew Chem Int Ed Engl* 43(16):2109-2112.
365. Cheng PN, Liu C, Zhao M, Eisenberg D, & Nowick JS (2012) Amyloid β-sheet mimics that antagonize protein aggregation and reduce amyloid toxicity. *Nat Chem* 4(11):927-933.
366. Pham JD, Chim N, Goulding CW, & Nowick JS (2013) Structures of oligomers of a peptide from β-amyloid. *J Am Chem Soc* 135(33):12460-12467.
367. Hayes CS, Bose B, & Sauer RT (2002) Proline residues at the C terminus of nascent chains induce SsrA tagging during translation termination. *J Biol Chem* 277(37):33825-33832.
368. Thomason L, *et al.* (2007) Recombineering: genetic engineering in bacteria using homologous recombination. *Curr Protoc Mol Biol* Chapter 1:Unit 1.16.
369. Bonnet J, Subsoontorn P, & Endy D (2012) Rewritable digital data storage in live cells via engineered control of recombination directionality. *Proc Natl Acad Sci U S A* 109(23):8884-8889.
370. Aiyar A, Xiang Y, & Leis J (1996) Site-directed mutagenesis using overlap extension PCR. *Methods Mol Biol* 57:177-191.
371. Battye TG, Kontogiannis L, Johnson O, Powell HR, & Leslie AG (2011) iMOSFLM: a new graphical interface for diffraction-image processing with MOSFLM. *Acta Crystallogr D Biol Crystallogr* 67(Pt 4):271-281.
372. Otwinowski Z & Minor W (1997) [20] Processing of X-ray diffraction data collected in oscillation mode. *Methods in Enzymology*, (Academic Press), Vol Volume 276, pp 307-326.
373. DeLano WD (2010) The PyMOL Molecular Graphics System, 1.3. (Schroedinger, LLC).
374. Cheng PN & Nowick JS (2011) Giant macrolactams based on β-sheet peptides. *J Org Chem* 76(9):3166-3173.
375. Spencer RK, Li H, & Nowick JS (2014) X-ray crystallographic structures of trimers and higher-order oligomeric assemblies of a peptide derived from Aβ(17-36). *J Am Chem Soc* 136(15):5595-5598.
376. Bergfors T (2003) Seeds to crystals. *J Struct Biol* 142(1):66-76.
377. Beckwith JR & Signer ER (1966) Transposition of the lac region of *Escherichia coli*. I. Inversion of the *lac* operon and transduction of *lac* by phi80. *J Mol Biol* 19(2):254-265.
378. Thomason L, *et al.* (2007) Recombineering: genetic engineering in bacteria using homologous recombination. *Curr Protoc Mol Biol* Chapter 1:Unit 1 16.
379. Garza-Sanchez F, Janssen BD, & Hayes CS (2006) Prolyl-tRNA(Pro) in the A-site of SecM-arrested ribosomes inhibits the recruitment of transfer-messenger RNA. *J Biol Chem* 281(45):34258-34268.
380. Koskiniemi S, *et al.* (2014) Selection of orphan Rhs toxin expression in evolved *Salmonella enterica* serovar Typhimurium. *PLoS Genet* 10(3):e1004255.
381. Hayes CS & Sauer RT (2003) Cleavage of the A site mRNA codon during ribosome pausing provides a mechanism for translational quality control. *Mol Cell* 12(4):903-911.
382. Island MD, Wei BY, & Kadner RJ (1992) Structure and function of the uhp genes for the sugar phosphate transport system in Escherichia coli and Salmonella typhimurium. *J Bacteriol* 174(9):2754-2762.
383. Pernestig AK, *et al.* (2003) The Escherichia coli BarA-UvrY two-component system is needed for efficient switching between glycolytic and gluconeogenic carbon sources. *J Bacteriol* 185(3):843-853.
384. Pernestig AK, Melefors O, & Georgellis D (2001) Identification of UvrY as the cognate response regulator for the BarA sensor kinase in Escherichia coli. *J Biol Chem* 276(1):225-231.
385. Palaniyandi S, *et al.* (2012) BarA-UvrY two-component system regulates virulence of uropathogenic E. coli CFT073. *PLoS One* 7(2):e31348.
386. Suzuki K, *et al.* (2002) Regulatory circuitry of the CsrA/CsrB and BarA/UvrY systems of Escherichia coli. *J Bacteriol* 184(18):5130-5140.
387. Wei BL, *et al.* (2001) Positive regulation of motility and flhDC expression by the RNA-binding protein CsrA of Escherichia coli. *Mol Microbiol* 40(1):245-256.
388. Jackson DW, *et al.* (2002) Biofilm formation and dispersal under the influence of the global regulator CsrA of Escherichia coli. *J Bacteriol* 184(1):290-301.
389. Thirup SS, Van LB, Nielsen TK, & Knudsen CR (2015) Structural outline of the detailed mechanism for elongation factor Ts-mediated guanine nucleotide exchange on elongation factor Tu. *J Struct Biol* 191(1):10-21.

390. Zhang Y, Yu NJ, & Spremulli LL (1998) Mutational analysis of the roles of residues in Escherichia coli elongation factor Ts in the interaction with elongation factor Tu. *J Biol Chem* 273(8):4556-4562.
391. Burnett BJ, *et al.* (2013) Elongation factor Ts directly facilitates the formation and disassembly of the Escherichia coli elongation factor Tu·GTP·aminoacyl-tRNA ternary complex. *J Biol Chem* 288(19):13917-13928.
392. Karring H, Björnsson A, Thirup S, Clark BF, & Knudsen CR (2003) Functional effects of deleting the coiled-coil motif in Escherichia coli elongation factor Ts. *Eur J Biochem* 270(21):4294-4305.
393. Kawashima T, Berthet-Colominas C, Wulff M, Cusack S, & Leberman R (1996) The structure of the Escherichia coli EF-Tu.EF-Ts complex at 2.5 A resolution. (Nature), pp 511-518.
394. Blum S, Sela N, Heller ED, Sela S, & Leitner G (2012) Genome analysis of bovine-mastitis-associated Escherichia coli O32:H37 strain P4. *J Bacteriol* 194(14):3732.
395. Rao D, Momcilovic I, Kobayashi S, Callegari E, & Ristic Z (2004) Chaperone activity of recombinant maize chloroplast protein synthesis elongation factor, EF-Tu. *Eur J Biochem* 271(18):3684-3692.
396. Kudlicki W, Coffman A, Kramer G, & Hardesty B (1997) Renaturation of rhodanese by translational elongation factor (EF) Tu. Protein refolding by EF-Tu flexing. *J Biol Chem* 272(51):32206-32210.
397. Suzuki H, Ueda T, Taguchi H, & Takeuchi N (2007) Chaperone properties of mammalian mitochondrial translation elongation factor Tu. *J Biol Chem* 282(6):4076-4084.
398. Caldas TD, El Yaagoubi A, & Richarme G (1998) Chaperone properties of bacterial elongation factor EF-Tu. *J Biol Chem* 273(19):11478-11482.
399. Barbier M, *et al.* (2013) Lysine trimethylation of EF-Tu mimics platelet-activating factor to initiate Pseudomonas aeruginosa pneumonia. *MBio* 4(3):e00207-00213.
400. Barel M, *et al.* (2008) A novel receptor - ligand pathway for entry of Francisella tularensis in monocyte-like THP-1 cells: interaction between surface nucleolin and bacterial elongation factor Tu. *BMC Microbiol* 8:145.
401. Defeu Soufo HJ, *et al.* (2010) Bacterial translation elongation factor EF-Tu interacts and colocalizes with actin-like MreB protein. *Proc Natl Acad Sci U S A* 107(7):3163-3168.
402. Basler M & Mekalanos JJ (2012) Type 6 secretion dynamics within and between bacterial cells. *Science* 337(6096):815.
403. Mohan S, *et al.* (2014) Tuf of Streptococcus pneumoniae is a surface displayed human complement regulator binding protein. *Mol Immunol* 62(1):249-264.
404. Sohka T, Heins RA, & Ostermeier M (2009) Morphogen-defined patterning of Escherichia coli enabled by an externally tunable band-pass filter. *J Biol Eng* 3:10.
405. Basu S, Gerchman Y, Collins CH, Arnold FH, & Weiss R (2005) A synthetic multicellular system for programmed pattern formation. *Nature* 434(7037):1130-1134.
406. Rudge TJ, Federici F, Steiner PJ, Kan A, & Haseloff J (2013) Cell polarity-driven instability generates self-organized, fractal patterning of cell layers. *ACS Synth Biol* 2(12):705-714.
407. Jang SS, Oishi KT, Egbert RG, & Klavins E (2012) Specification and simulation of synthetic multicelled behaviors. *ACS Synth Biol* 1(8):365-374.
408. Rudge TJ, Steiner PJ, Phillips A, & Haseloff J (2012) Computational modeling of synthetic microbial biofilms. *ACS Synth Biol* 1(8):345-352.
409. Tabor JJ, *et al.* (2009) A synthetic genetic edge detection program. *Cell* 137(7):1272-1281.
410. LeBon L, Lee TV, Sprinzak D, Jafar-Nejad H, & Elowitz MB (2014) Fringe proteins modulate Notch-ligand cis and trans interactions to specify signaling states. *Elife* 3:e02950.
411. Matsuda M, Koga M, Nishida E, & Ebisuya M (2012) Synthetic signal propagation through direct cell-cell interaction. *Sci Signal* 5(220):ra31.
412. Sprinzak D, *et al.* (2010) Cis-interactions between Notch and Delta generate mutually exclusive signalling states. *Nature* 465(7294):86-90.
413. Locke JC & Elowitz MB (2009) Using movies to analyse gene circuit dynamics in single cells. *Nat Rev Microbiol* 7(5):383-392.
414. LaSarre B & Federle MJ (2013) Exploiting quorum sensing to confuse bacterial pathogens. *Microbiol Mol Biol Rev* 77(1):73-111.
415. Payne S, *et al.* (2013) Temporal control of self-organized pattern formation without morphogen gradients in bacteria. *Mol Syst Biol* 9:697.
416. Liu C, *et al.* (2011) Sequential establishment of stripe patterns in an expanding cell population. *Science* 334(6053):238-241.
417. Young KD (2006) The selective value of bacterial shape. *Microbiol Mol Biol Rev* 70(3):660-703.

418. Balagaddé FK, *et al.* (2008) A synthetic Escherichia coli predator-prey ecosystem. *Mol Syst Biol* 4:187.
419. You L, Cox RS, Weiss R, & Arnold FH (2004) Programmed population control by cell-cell communication and regulated killing. *Nature* 428(6985):868-871.
420. Davis RM, Muller RY, & Haynes KA (2015) Can the natural diversity of quorum-sensing advance synthetic biology? *Front Bioeng Biotechnol* 3:30.
421. Ortiz ME & Endy D (2012) Engineered cell-cell communication via DNA messaging. *J Biol Eng* 6(1):16.
422. Goñi-Moreno A, Amos M, & de la Cruz F (2013) Multicellular computing using conjugation for wiring. *PLoS One* 8(6):e65986.
423. Trokter M, Felisberto-Rodrigues C, Christie PJ, & Waksman G (2014) Recent advances in the structural and molecular biology of type IV secretion systems. *Curr Opin Struct Biol* 27:16-23.
424. Craig L, Pique ME, & Tainer JA (2004) Type IV pilus structure and bacterial pathogenicity. *Nat Rev Microbiol* 2(5):363-378.
425. Proft T & Baker EN (2009) Pili in Gram-negative and Gram-positive bacteria - structure, assembly and their role in disease. *Cell Mol Life Sci* 66(4):613-635.
426. Kline KA, Fälker S, Dahlberg S, Normark S, & Henriques-Normark B (2009) Bacterial adhesins in host-microbe interactions. *Cell Host Microbe* 5(6):580-592.
427. LeRoux M, *et al.* (2012) Quantitative single-cell characterization of bacterial interactions reveals type VI secretion is a double-edged sword. *Proc Natl Acad Sci U S A* 109(48):19804-19809.
428. Pizarro-Cerdá J & Cossart P (2006) Bacterial adhesion and entry into host cells. *Cell* 124(4):715-727.
429. Hayes CS, Koskiniemi S, Ruhe ZC, Poole SJ, & Low DA (2014) Mechanisms and biological roles of contact-dependent growth inhibition systems. *Cold Spring Harb Perspect Med* 4(2).
430. Garcia EC, Anderson MS, Hagar JA, & Cotter PA (2013) Burkholderia BcpA mediates biofilm formation independently of interbacterial contact-dependent growth inhibition. *Mol Microbiol* 89(6):1213-1225.
431. Lutz R & Bujard H (1997) Independent and tight regulation of transcriptional units in Escherichia coli via the LacR/O, the TetR/O and AraC/I1-I2 regulatory elements. *Nucleic Acids Res* 25(6):1203-1210.
432. Siegele DA & Hu JC (1997) Gene expression from plasmids containing the araBAD promoter at subsaturating inducer concentrations represents mixed populations. *Proc Natl Acad Sci U S A* 94(15):8168-8172.
433. Khlebnikov A, Datsenko KA, Skaug T, Wanner BL, & Keasling JD (2001) Homogeneous expression of the P(BAD) promoter in Escherichia coli by constitutive expression of the low-affinity high-capacity AraE transporter. *Microbiology* 147(Pt 12):3241-3247.
434. Eppinger M, Mammel MK, Leclerc JE, Ravel J, & Cebula TA (2011) Genome signatures of Escherichia coli O157:H7 isolates from the bovine host reservoir. *Appl Environ Microbiol* 77(9):2916-2925.
435. Kolenbrander PE (2000) Oral microbial communities: biofilms, interactions, and genetic systems. *Annu Rev Microbiol* 54:413-437.
436. Gourse RL, Gaal T, Bartlett MS, Appleman JA, & Ross W (1996) rRNA transcription and growth rate-dependent regulation of ribosome synthesis in Escherichia coli. *Annu Rev Microbiol* 50:645-677.
437. Schneider DA, Ross W, & Gourse RL (2003) Control of rRNA expression in Escherichia coli. *Curr Opin Microbiol* 6(2):151-156.
438. Condon C (2007) Maturation and degradation of RNA in bacteria. *Curr Opin Microbiol* 10(3):271-278.
439. Cangelosi GA & Brabant WH (1997) Depletion of pre-16S rRNA in starved Escherichia coli cells. *J Bacteriol* 179(14):4457-4463.
440. Basturea GN, Zundel MA, & Deutscher MP (2011) Degradation of ribosomal RNA during starvation: comparison to quality control during steady-state growth and a role for RNase PH. *RNA* 17(2):338-345.
441. Yamaguchi Y, Park JH, & Inouye M (2011) Toxin-antitoxin systems in bacteria and archaea. *Annu Rev Genet* 45:61-79.
442. Blanchard AE, Celik V, & Lu T (2014) Extinction, coexistence, and localized patterns of a bacterial population with contact-dependent inhibition. *BMC Syst Biol* 8:23.

443. Anderson MS, Garcia EC, & Cotter PA (2014) Kind discrimination and competitive exclusion mediated by contact-dependent growth inhibition systems shape biofilm community structure. *PLoS Pathog* 10(4):e1004076.
444. Pfeffer C, *et al.* (2012) Filamentous bacteria transport electrons over centimetre distances. *Nature* 491(7423):218-221.
445. Justice SS, Hunstad DA, Seed PC, & Hultgren SJ (2006) Filamentation by Escherichia coli subverts innate defenses during urinary tract infection. *Proc Natl Acad Sci U S A* 103(52):19884-19889.
446. Justice SS, Hunstad DA, Cegelski L, & Hultgren SJ (2008) Morphological plasticity as a bacterial survival strategy. *Nat Rev Microbiol* 6(2):162-168.
447. Horvath DJ, *et al.* (2011) Morphological plasticity promotes resistance to phagocyte killing of uropathogenic Escherichia coli. *Microbes Infect* 13(5):426-437.
448. Chen K, Sun GW, Chua KL, & Gan YH (2005) Modified virulence of antibiotic-induced Burkholderia pseudomallei filaments. *Antimicrob Agents Chemother* 49(3):1002-1009.
449. Storck T, Picioreanu C, Virdis B, & Batstone DJ (2014) Variable cell morphology approach for individual-based modeling of microbial communities. *Biophys J* 106(9):2037-2048.
450. Tabor JJ, Levskaya A, & Voigt CA (2011) Multichromatic control of gene expression in Escherichia coli. *J Mol Biol* 405(2):315-324.
451. Lou C, Stanton B, Chen YJ, Munsky B, & Voigt CA (2012) Ribozyme-based insulator parts buffer synthetic circuits from genetic context. *Nat Biotechnol* 30(11):1137-1142.
452. Mutalik VK, *et al.* (2013) Precise and reliable gene expression via standard transcription and translation initiation elements. *Nat Methods* 10(4):354-360.
453. Haldimann A & Wanner BL (2001) Conditional-replication, integration, excision, and retrieval plasmid-host systems for gene structure-function studies of bacteria. *J Bacteriol* 183(21):6384-6393.
454. St-Pierre F, *et al.* (2013) One-step cloning and chromosomal integration of DNA. *ACS Synth Biol* 2(9):537-541.
455. Young JW, *et al.* (2012) Measuring single-cell gene expression dynamics in bacteria using fluorescence time-lapse microscopy. *Nat Protoc* 7(1):80-88.
456. Edelstein A, Amodaj N, Hoover K, Vale R, & Stuurman N (2010) Computer control of microscopes using μManager. *Curr Protoc Mol Biol* Chapter 14:Unit14.20.
457. Schneider CA, Rasband WS, & Eliceiri KW (2012) NIH Image to ImageJ: 25 years of image analysis. *Nat Methods* 9(7):671-675.
458. Casadaban MJ (1976) Transposition and fusion of the lac genes to selected promoters in Escherichia coli using bacteriophage lambda and Mu. *J Mol Biol* 104(3):541-555.
459. Bodelón G, Marín E, & Fernández LA (2009) Role of periplasmic chaperones and BamA (YaeT/Omp85) in folding and secretion of intimin from enteropathogenic Escherichia coli strains. *J Bacteriol* 191(16):5169-5179.
460. Bodelón G, Marín E, & Fernández L (2015) Analyzing the Role of Periplasmic Folding Factors in the Biogenesis of OMPs and Members of the Type V Secretion System. *Methods Mol Biol* 1329:77-110.
461. Beher MG & Schnaitman CA (1981) Regulation of the OmpA outer membrane protein of Escherichia coli. *J Bacteriol* 147(3):972-985.
462. Guillier M & Gottesman S (2006) Remodelling of the Escherichia coli outer membrane by two small regulatory RNAs. *Mol Microbiol* 59(1):231-247.
463. Forst S & Inouye M (1988) Environmentally regulated gene expression for membrane proteins in Escherichia coli. *Annu Rev Cell Biol* 4:21-42.
464. Forst S, Delgado J, Ramakrishnan G, & Inouye M (1988) Regulation of ompC and ompF expression in Escherichia coli in the absence of envZ. *J Bacteriol* 170(11):5080-5085.
465. Padhi A, Verghese B, & Otta SK (2009) Detecting the form of selection in the outer membrane protein C of Enterobacter aerogenes strains and Salmonella species. *Microbiol Res* 164(3):282-289.
466. Petersen L, Bollback JP, Dimmic M, Hubisz M, & Nielsen R (2007) Genes under positive selection in Escherichia coli. *Genome Res* 17(9):1336-1343.
467. de Zamaroczy M & Buckingham RH (2002) Importation of nuclease colicins into E coli cells: endoproteolytic cleavage and its prevention by the immunity protein. *Biochimie* 84(5-6):423-432.
468. Haidinger W, Mayr UB, Szostak MP, Resch S, & Lubitz W (2003) Escherichia coli ghost production by expression of lysis gene E and Staphylococcal nuclease. *Appl Environ Microbiol* 69(10):6106-6113.
469. Fuqua WC, Winans SC, & Greenberg EP (1994) Quorum sensing in bacteria: the LuxR-LuxI family of cell density-responsive transcriptional regulators. *J Bacteriol* 176(2):269-275.

470. Majerczyk CD, *et al.* (2014) Cross-species comparison of the Burkholderia pseudomallei, Burkholderia thailandensis, and Burkholderia mallei quorum-sensing regulons. *J Bacteriol* 196(22):3862-3871.
471. Majerczyk C, *et al.* (2014) Global analysis of the Burkholderia thailandensis quorum sensing-controlled regulon. *J Bacteriol* 196(7):1412-1424.
472. Iwatsuki M, *et al.* (2008) Guadinomines, Type III secretion system inhibitors, produced by Streptomyces sp. K01-0509. I: taxonomy, fermentation, isolation and biological properties. *J Antibiot (Tokyo)* 61(4):222-229.
473. Stavrinides J, Ma W, & Guttman DS (2006) Terminal reassortment drives the quantum evolution of type III effectors in bacterial pathogens. *PLoS Pathog* 2(10):e104.
474. Lloyd AL, Henderson TA, Vigil PD, & Mobley HL (2009) Genomic islands of uropathogenic Escherichia coli contribute to virulence. *J Bacteriol* 191(11):3469-3481.
475. Reverchon S & Nasser W (2013) Dickeya ecology, environment sensing and regulation of virulence programme. *Environ Microbiol Rep* 5(5):622-636.
476. Rojas CM, Ham JH, Deng WL, Doyle JJ, & Collmer A (2002) HecA, a member of a class of adhesins produced by diverse pathogenic bacteria, contributes to the attachment, aggregation, epidermal cell killing, and virulence phenotypes of Erwinia chrysanthemi EC16 on Nicotiana clevelandii seedlings. *Proc Natl Acad Sci U S A* 99(20):13142-13147.
477. Knudsen GM, Holch A, & Gram L (2012) Subinhibitory concentrations of antibiotics affect stress and virulence gene expression in Listeria monocytogenes and cause enhanced stress sensitivity but do not affect Caco-2 cell invasion. *J Appl Microbiol* 113(5):1273-1286.
478. Goh EB, *et al.* (2002) Transcriptional modulation of bacterial gene expression by subinhibitory concentrations of antibiotics. *Proc Natl Acad Sci U S A* 99(26):17025-17030.
479. Bos J, *et al.* (2015) Emergence of antibiotic resistance from multinucleated bacterial filaments. *Proc Natl Acad Sci U S A* 112(1):178-183.
480. West SA & Gardner A (2010) Altruism, spite, and greenbeards. *Science* 327(5971):1341-1344.
481. Zhang D, Iyer LM, Burroughs AM, & Aravind L (2014) Resilience of biochemical activity in protein domains in the face of structural divergence. *Curr Opin Struct Biol* 26:92-103.